Alkali Activated Natural Pozzolans
for Geopolymer Cement

vorgelegt von

M.Sc.

Rafia Firdous

an der Fakultät VI – Planen Bauen Umwelt

der Technischen Universität Berlin

zur Erlangung des akademischen Grades

Doktor der Ingenieurwissenschaften

- Dr.-Ing. -

genehmigte Dissertation

Promotionsausschuss:

Vorsitzende: Prof. Dr. rer. nat. Sabine Kruschwitz

Gutachter: Prof. Dr. rer. nat. habil. Dietmar Stephan

Gutachter: Prof. Dr.-Ing. Frank Dehn

Tag der wissenschaftlichen Aussprache: 03. Dezember 2020

Berlin 2021

Für meinen größten Unterstützer

Acknowledgements

I would like to extend my deepest, grateful, and sincere thanks to Univ.-Prof. Dr. rer. nat. habil. Dietmar Stephan, for giving me this opportunity, for supervising this thesis as well as for his continuous support, understanding and guidance throughout this research work. He encouraged me to think out of the box and carry out new experiments. He supported me at every step of research work and taught me how to grow as an independent scientist. Without his constant encouragement, expert advice, valuable suggestions and critical reviews, this work would not have been possible.

Many thanks to Higher Education Commission of Pakistan (HEC) and German Academic Exchange Service (DAAD) for funding the whole duration of my PhD studies from 2016 to 2020.

I would like to say sincere thanks to my committee members, Prof. Dr.-Ing. Frank Dehn and Prof. Dr. rer. nat. Sabine Kruschwitz, for their support and invaluable advice.

I express my sincere thanks to Prof. Lars Wadsö and Dr. Yury Andrés Villagrán-Zaccardi for few but fruitful discussions. Special thanks to Prof. Dr. Barbara Lothenbach for supervising the thermodynamic calculations and careful review of the work related to calcium carbonates. Many thanks to Dr. rer. nat. habil. Detlef Klimm for his support in performing experiments of thermal analysis and review of the work related to calcium carbonates. I am grateful to Dr.-Ing. Christian Lehmann for his support in carrying out the experiments of SEM. I also wish to thank the members of Kiwa GmbH, for helping me to use the needed facilities for my research. Special thanks to Dr. Susanne Herting-Agthe and Mineralogische Sammlungen at TU Berlin for providing mineral samples.

I am thankful to all my colleagues at TU Berlin particularly my colleagues from research group building materials and construction chemistry for their help and cooperation during time of this research work. Special thanks to Dr.-Ing. Yu Jin and Dr.-Ing. Mohamed Abd Elrahman for their support.

I would like to extend my appreciation to my friend Dr. Eva Luber for her support and motivation during this journey that made my stay in Germany fulfilling. Many thanks to my friends in Pakistan who encouraged me throughout this time. My deepest appreciation goes to my friend and colleague, M.Sc. Tamino Hirsch, for his endless support, affection, and encouragement.

Many thanks to my sister Samia and brother-in-law Irfan for their help in my early days in Germany. Many thanks to my sister Hafsa and brothers Muzammil and Mudassir for their moral support and wishes. Special gratitude goes to my parents, Jamila and Nazir, for their wishes and support.

Abstract

This thesis deals with the use of six natural pozzolans from Germany and Italy for geopolymer production. As the first part, a detailed study was conducted on the effect of silica modulus of sodium silicate solution and mineralogical composition of natural pozzolans on the extend of geopolymer reaction, reaction kinetics, mechanical properties, and composition of the binder gel. Sixteen solutions of silica moduli in range of 0.4 – 1.7 were used for geopolymer synthesis at ambient temperature. Higher compressive strength was achieved within an optimum range of silica modulus, where this range depended on the mineralogical and chemical composition of pozzolans. On either side of this optimum range the strength achieved in reasonable time was marginal or even drop in strength with time was observed. The extend of geopolymer reaction and reaction constant determined by pseudo-first order kinetics both decreased with increase of silica modulus. However, a faster reaction at early time depended on the SiO_2 and Na_2O content of alkaline solution. The reduction in compressive strength for lower silica moduli was found to be related to the degree of polymerization. Moreover, it was observed that not only X-ray amorphous phase but also the crystalline mineral phases partially participate in the geopolymer reaction.

As the second part of the study, the reactivity enhancement methods (heat curing, calcination and mechanical activation) applied on low reactive pozzolans showed that calcination is an effective method to improve reactivity of Bavarian trass and to reduce the formation of sodium carbonate. Moreover, it revealed that the second exothermic peak observed in calorimetric study of Bavarian trass was related to its calcite content. The effectiveness of each method was studied, and comparisons were drawn.

Based on the findings of these parts, the third part of the study focussed on the reactivity of fifteen minerals in sodium hydroxide and six crystalline minerals in sodium silicate solution. The silicate minerals containing sodium or potassium mostly resulted in formation of hydrosodalite in sodium hydroxide solution. Whereas calcium-containing silicate minerals which exhibited higher reactivity resulted in formation of clinotobermorite, indicating possible formation of calcium-containing binder gel in pozzolan containing these phases. Calcium carbonate exhibited distinct behaviour especially in sodium silicate solution and was therefore studied in detail. The reaction mechanism and reaction products were identified using in-situ and ex-situ methods. This reaction resulted in formation of sodium-containing C-S-H and sodium-calcium carbonates. Consequently, the presence of calcium carbonate minerals in natural pozzolans promotes the availability of calcium for gel phase. Whereas the carbonate can result in formation of sodium carbonate which can indirectly impact compressive strength development as observed in Bavarian trass geopolymers. The outcomes of this part of thesis can be used to predict the behaviour of natural pozzolans containing the examined crystalline phases under similar conditions.

Zusammenfassung

Diese Arbeit beschäftigt sich mit der Verwendung von sechs natürlichen Puzzolanen aus Deutschland und Italien für die Geopolymerherstellung. Als erster Teil wurde eine detaillierte Studie über die Auswirkungen des Silika-Moduls der Natriumsilikatlösung und der Mineralogie des Puzzolans auf Ausmaß der Geopolymerreaktion, Reaktionskinetik, mechanische Eigenschaften und Zusammensetzung des Gels durchgeführt. Geopolymere wurden mit 16 Lösungen von Silika-Modulen zwischen 0,4 – 1,7 bei Umgebungstemperatur hergestellt. Eine höhere Druckfestigkeit wurde innerhalb eines optimalen Bereichs des Silika-Moduls erreicht, wobei dieser Bereich von der Mineralogie und Chemie des Puzzolans abhängt. Die zu beiden Seiten des Optimus in angemessener Zeit erreichte Festigkeit war nur marginal oder es wurde sogar ein Festigkeitsabfall mit der Zeit beobachtet. Sowohl das Ausmaß der Geopolymerreaktion als auch die Reaktionskonstante pseudoerster Ordnung nehmen mit zunehmendem Silika-Modul ab. Dennoch hängt eine schnellere frühe Reaktion mit den Gehalten von SiO_2 and Na_2O der alkalinen Lösung zusammen. Die geringere Druckfestigkeit für niedrige Silika-Module ist durch den Polymerisationsgrad bedingt. Weiterhin nimmt nicht nur die röntgenamorphe Phase, sondern auch teilweise die kristallinen Mineralphasen an der Geopolymerreaktion teil.

In einem zweiten Teil der Studie wurden Wärmebehandlung, Kalzinierung und mechanische Aktivierung als Methoden zur Verbesserung der Reaktivität von niedrig reaktiven natürlichen Puzzolanen angewendet. Kalzinierung war die effektivste Methode zur Reaktivitätsverbesserung von Bayrischem Trass und zur Reduzierung von Natriumkarbonat. Weiterhin, wurde herausgefunden, dass der zweite exotherme Peak von Bayrischem Trass in der Kalorimetrie mit seinem Kalzitgehalt zusammenhängt. Die Wirksamkeit jeder Methode wurde untersucht, und es wurden Vergleiche angestellt.

Auf Basis der Ergebnisse dieser beiden Teile wurde im dritten Teil der Arbeit die Reaktivität von 15 Mineralen in Natriumhydroxid- und 6 in Natriumsilikatlösung untersucht. Silikate reich an Kalium und Natrium formten mit Natriumhydroxidlösung zumeist Hydrosodalith. Bei reaktiveren kalziumhaltigen Silikaten konnte die Bildung Klinotobermorit beobachtet werden, was die Möglichkeit der Formung kalziumhaltiger Gele in Puzzolanen mit diesen Phasen anzeigt. Kalziumkarbonat wies ein spezielles Verhalten insbesondere mit Natriumsilikatlösung auf und wurde daher im Detail untersucht. Der Reaktionsmechanismus und die Reaktionsprodukte wurden mit in-situ- und ex-situ-Methoden identifiziert. Die Reaktion resultierte in natriumhaltiges C-S-H und Natriumkalziumsilikate. Somit fördern Kalziumkarbonatminerale in Puzzolanen die Verfügbarkeit von Kalzium für die Gelphase. Das Karbonat kann zur Bildung von Natriumkarbonat beitragen und somit die Druckfestigkeitsentwicklung beeinflussen, was für die Geopolymere von Bayrischem Trass beobachtet wurde. Diese Resultate können genutzt werden, um das Verhalten von natürlichen Puzzolanen mit diesen Mineralen unter vergleichbaren Bedingungen vorherzusagen.

Table of contents

Chapter 1

Introduction

This chapter presents the background about ecological footprints of traditional cement industry and the necessity for development of alternative binders such as geopolymers/alkali activated materials. A brief introduction about geopolymers, alkali activated binders and available raw materials for their synthesis is also presented. Moreover, the objectives of this research, research outline and introduction to materials used is also part of this chapter.

1.1. General

In thrive of global development involving the development of infrastructure, the statistics for cement production and its effects are astonishing. The easy use and outstanding performance of Portland cement (PC) based construction materials (mortar and concrete) are the reasons that it is the most extensively used synthetic construction material on earth [1,2]. The global cement production was appreciably increasing from year 2006 (2.55 billion metric tons) till 2016 (4.2 billion metric tons) [1]. Production of cement is associated with 5 – 8 % of anthropogenic carbon dioxide (CO_2) emissions where the production of 1 ton of cement produces 1 ton of CO_2 [3–5]. Fig. 1.1 shows the drastic increase in the global CO_2 emission from carbonate decomposition during cement production per year [5]. Current concrete consumption has been reported as 1 ton/year per living human being [6]. Moreover, production of cement is an energy extensive process with almost 5% of total global industrial energy consumption [4]. Such an extensive production and use of cement is one of the major reasons of global warming and usage of energy [7].

Several actions have been taken and goals have been set in order to control and cutdown the CO_2 emissions from cement industry. European committee for carbon footprint reduction aims at reducing the CO_2 emission in European union till 2050 by 80% of the value recorded in 1990 [8]. The cement technology roadmap explained various approaches to reduce the CO_2 emissions at every step of cement production [9]. These include use of alternative fuel in clinker production, increasing the thermal efficiency of kilns, replacement

of clinker, use of alternative cements and carbon capture. It is estimated that by the implementation of these steps the CO_2 emission by PC manufacture and use can be reduced by up to 17% [2,10].
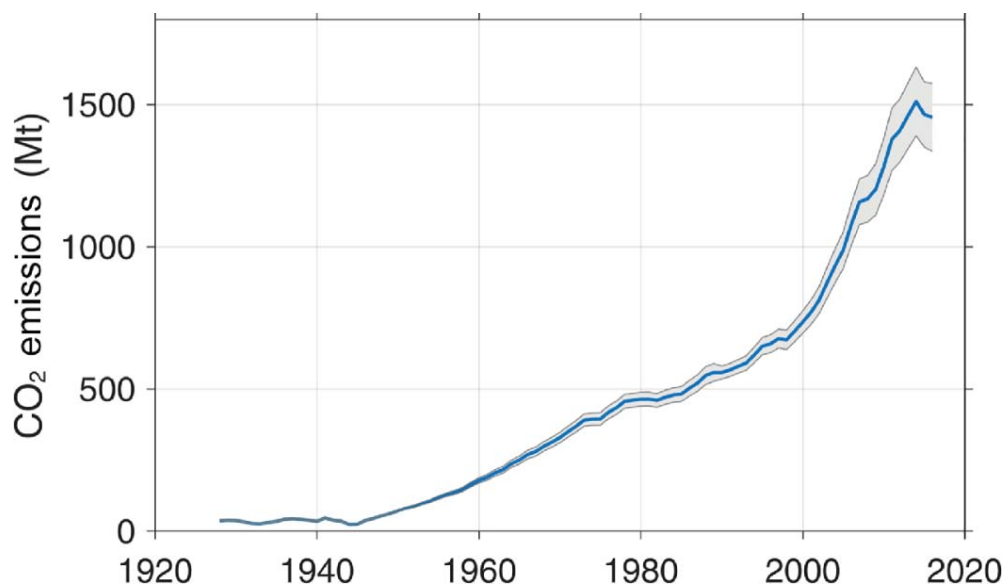
Fig. 1.1. Global CO_2 process emission from cement production, from [5]. (CO_2 emission resulting from burning process of calcium carbonate is known as process emission).

In the process of cement production, 60% of the CO_2 is emitted by calcination of calcium carbonate ($CaCO_3$), while the rest (40%) is emitted by burning of fuel for kiln process [9]. By use of alternative fuel for kiln process, the advantages for reduction in CO_2 emission are marginal. Moreover, improving the thermal efficiency of the in use kiln requires a huge investment, while the latest kilns already operate at 80% of their theoretically possible thermal efficiency [1]. Subsequently, the substitution of clinker and use of alternative binders have gained a lot of interest for some decades. This includes partial replacement of Portland cement with secondary cementitious materials (SCMs) and cements such as CEM-II, CEM-III, CEM-IV and CEM-V have been standardized [11]. However, the most commonly used SCMs, ground granulated blast furnace slag (GGBFS) and fly ash (FA), are not enough available to meet the needs of cement industry particularly in developed countries [1,2]. For more than a decade, several European countries utilise 100% of fly ash, bottom ash and boiler slags in producing blended cement-based concretes and in other ways [2,12]. Additionally, the increasing awareness for environment protection led to the establishment of new environmentally friendly policies in many countries in the world. Germany plans to close all coal power plants by year 2038, which means that there will be no fly ash available from local source in Germany [13]. Moreover, the use of reclaimed

resources is economically not viable because of the re-processing required before use [1]. The use of natural resources and alternative binders is a favourable solution as investigated by several researchers [14,15]. Natural pozzolans are abundant available around the globe and have been used as SCM in cements [16].

In the perspective of environmentally friendly binders in construction sector, alkali activated materials (AAM) and/or geopolymers (GP) have gained a lot of attention in recent years. The key factor in reduction of CO_2 emission is the absence of the high temperature calcination step in AAM and GP, as these binders can be solely synthesised from the natural or artificial pozzolans/secondary cementitious materials by their reaction with alkaline solutions including alkali hydroxide or alkali silicate solutions [2,17]. The contribution of the activating solution in production of greenhouse gases should be optimized to obtain a truly environmentally friendly binder. Comparing alkali activated binder with Portland cement binder, CO_2 reduction of up to 80% has been reported while considering the environmental impact of activating solutions [2,18,19].

Considering the lack of most used resources (fly ash, ground granulated blast furnace slag) and the increasing demand of greenhouse gas reduction, a possible opportunity for development of the environmentally friendly binder could be production of alkali activated binders based on natural pozzolans. The utilization of naturally occurring raw materials such as natural pozzolans for alkali activated binders/geopolymers is not only an ecologically but also an economically viable solution. This is of prime importance in the developed countries where the traditional SCMs are already fully utilized. For their lower CO_2 emission and the possibility of synthesis at ambient conditions, alkali activated materials can be a potential binder particularly for specific applications. Therefore, this thesis focuses on development of alkali activated natural pozzolans; or in other words natural pozzolan-based geopolymers.

1.2. Alkali activated materials and geopolymers

Alkali activated materials (AAM) and geopolymers (GP) are inorganic binders produced by reaction of aluminosilicate raw material with concentrated alkaline solution. Most commonly used alkaline solutions include alkali hydroxide or alkali silicate solution. Other activating solutions include alkali carbonate or alkali sulphate solutions [20,21]. Sodium (Na) and potassium (K) are the most common alkali cations used in the activating solutions, other possible cations are lithium (Li), rubidium (Rb) and caesium (Cs). However, the cost and

relative scarcity of Li, Rb and Cs are the reasons that mostly Na- and K-based alkaline solutions are used [17].

AAM and GP can provide comparable properties to the PC-based binders with the added advantage of lower greenhouse gas emissions. Their wide range of characteristics depend on the precursor selection, processing conditions and mixture design. These properties include high compressive strength, low shrinkage, fast or slow setting, acid resistance, fire resistance and low thermal conductivity [22]. The enhanced properties of these binders are not essential for all formulations. Rather these binders are a careful solution adapted by correct mix and processing design to optimize the properties for the particular use and/or additionally to reduce the cost and environmental footprints for a given application [22].

From more than a decade, there is an increasing interest in the AAM and GP. Number of publications to the topic "geopolymer" and "alkali activated" have progressively increased every year as shown in Fig. 1.2. Intense affords are made for development of standards to scale up the production of alkali activated and geopolymer binders [23,24]. Several companies around the globe work on the industrialization of these binders and these binders are used for several construction projects around the globe.
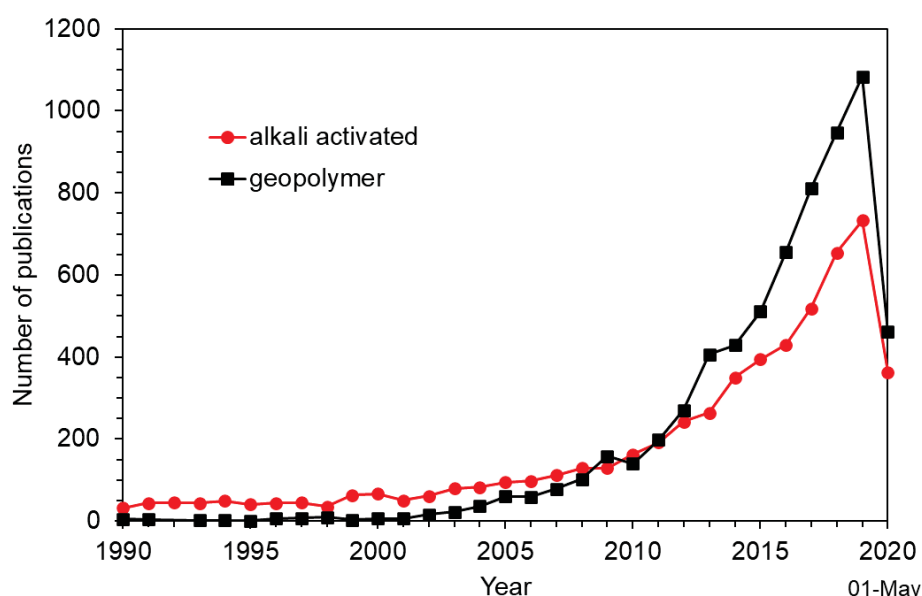
Fig. 1.2. Number of publications each year since 1990. Search results of Scopus for topic "alkali activated" and "geopolymer". (Accessed on 01.05.2020).

The differences in the composition of SCM's effect the composition of resultant binder [25]. Fig. 1.3 shows the composition of various supplementary cementitious materials in respect to the CaO-Al_2O_3-SiO_2 ternary diagram. GGBFS are lower in calcium content in comparison

to PC. Natural pozzolans have a wide range of composition but contain lower CaO content in comparison to GGBFS, PC and FA. Their relatively higher variety of composition is mainly due to variation of SiO_2 and Al_2O_3 content. The composition of FA is diverse as indicated by the large area in Fig. 1.3 and are therefore characterised as calcium-rich FA (class C) and calcium-poor FA (class F).
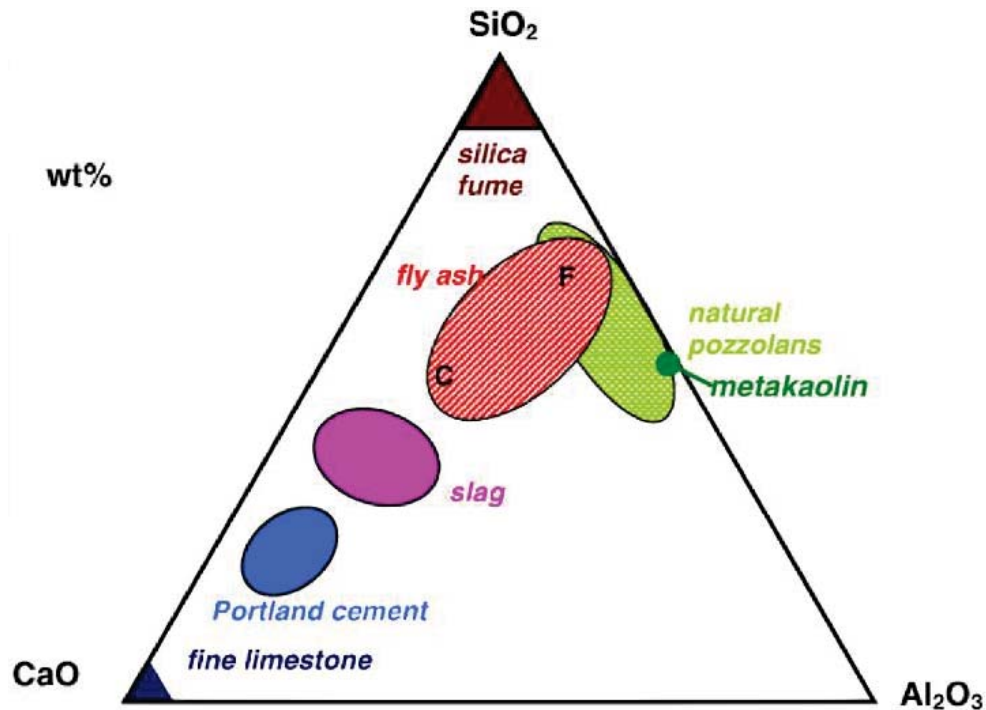
Fig. 1.3. CaO-Al_2O_3-SiO_2 ternary diagram with composition areas of Portland cement and various supplementary cementitious materials, from [25].

Alkali activated materials and geopolymers are differentiated based on the composition of the raw material (calcium content of the precursor) and chemistry of the resultant binder. A precursor rich in calcium upon its reaction with alkaline solution tends to form reaction products similar to PC systems including C-S-H (calcium silicate hydrate) gel which are generally illustrated as C-A-S-H (calcium aluminosilicate hydrate) gels to highlight the high Al content of these gels compared to PC hydration products [7,26]. While the precursors poor in calcium result in formation of N-A-S-H (sodium aluminosilicate hydrate) type gel structure [7,26]. Therefore, an alkali activated binder is considered as a high calcium system, while the system with less calcium is known as geopolymer. In a work by Hermann et al. the classification between Portland cement binders, alkali activated binders and geopolymers have been described [7]. In this work the limiting CaO content of the binder has been designated to be 10 wt.-% after EN 450-1 [7,27]. Fig. 1.4 taken from [7]

summaries the classification of various binders, precursor used for their synthesis and potential reaction products.
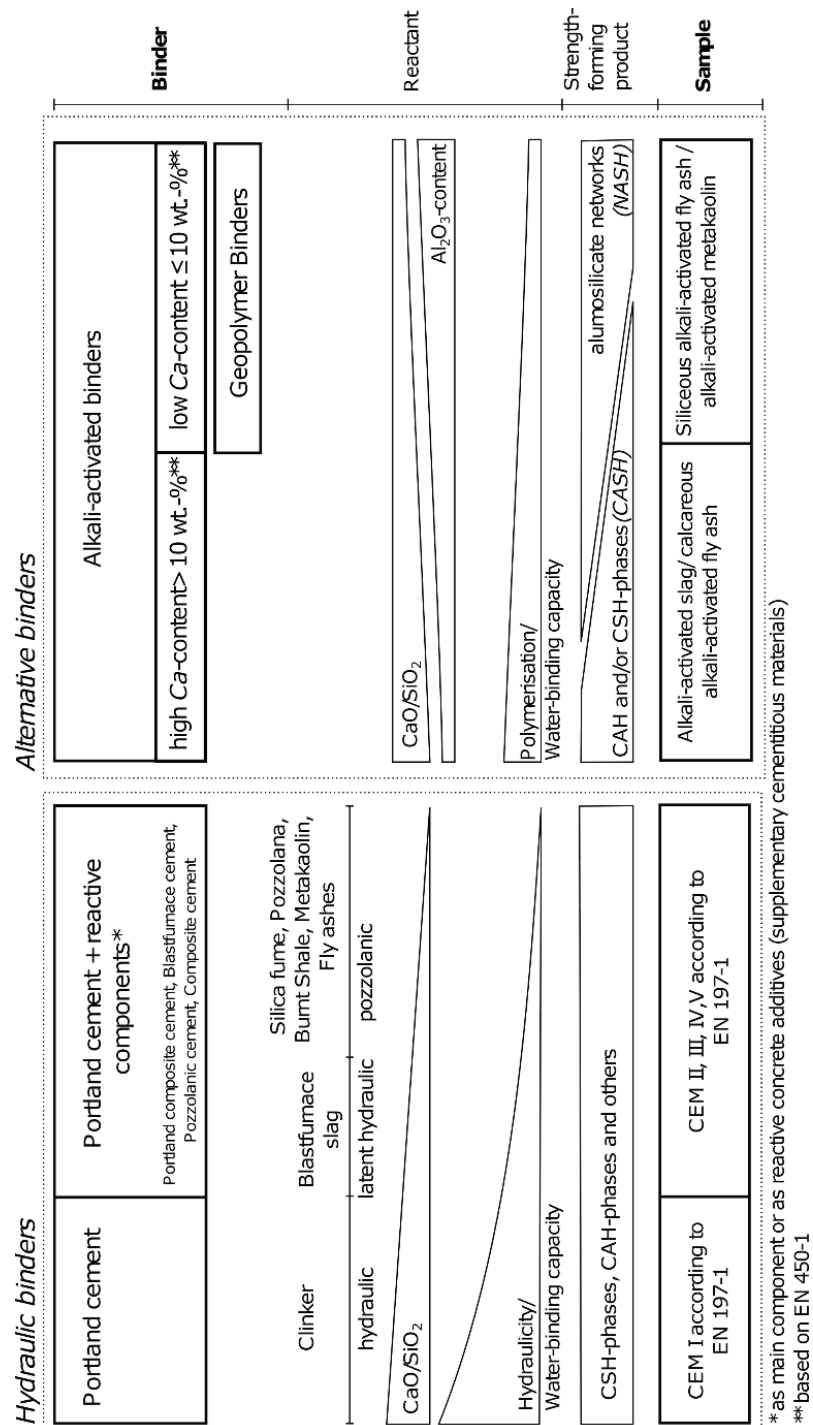
Fig. 1.4. Classification and boundaries of various binders including Portland cement and alkali activated materials, from [7].

A third alkali activated alternative binder system known as blended or hybrid alkaline system is also described in literature [20,26]. This system is a combination of low and high calcium system. Such systems can be achieved by alkali activation of minor amount of Portland cement with high proportion of supplementary cementitious material or alkali activated blends of GGBFS, FA, MK or others. The reaction products precipitating in these systems are complex and can be a mixture of cementitious gels, C-A-S-H incorporating sodium, high calcium N-A-S-H gels [20,26].

Fig. 1.5 shows the binder gel formed as result of reaction of sodium silicate solution with 100 wt.-% FA, 50 wt.-% FA & 50 wt.-% GGBFS and 100 wt.-% GGBFS after 28 d of reaction, as measured by SEM-EDX. The results show visually the effect of composition of raw material on the composition of resultant binder gel. The 100 wt.-% FA binder resulted in N-A-S-H gels belonging to geopolymers. In 100 wt.-% GGBFS C-A-S-H gel formed belonging to alkali activated binders. While in a hybrid system containing both FA and GGBFS, formation of C-(N)-A-S-H is observed [26].
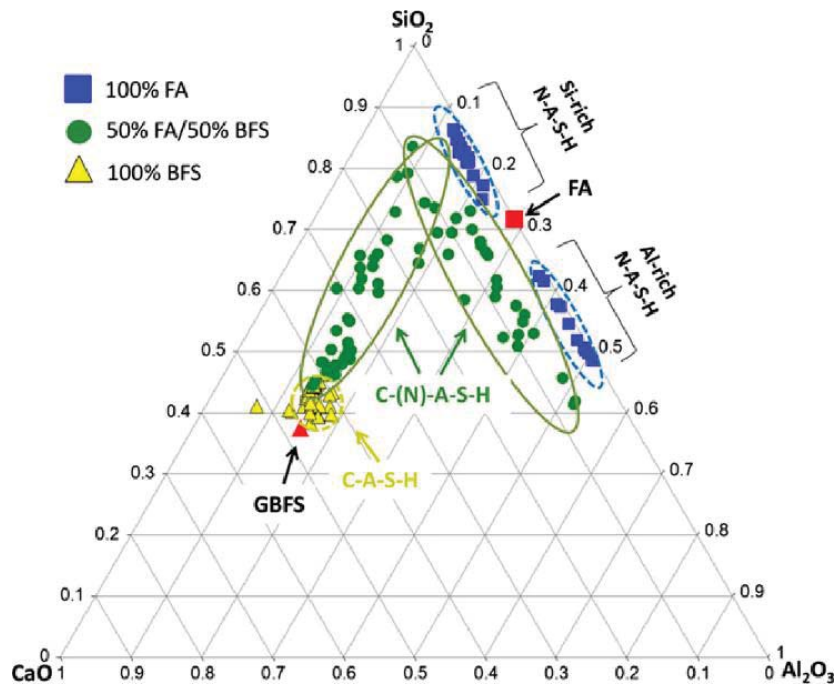
Fig. 1.5. Ternary diagram of alkali activated binder gel composition with various precursors, from [26]. (GBFS and BFS stand for granulated blast furnace slag and is abbreviated as GGBFS in this work).

- Geopolymers

The term geopolymer was first introduced by Davidovits [28]. This category of the binders is also described as soil cements [29,30], geocements [31], low-temperature aluminosilicate glass [32], alkali activated cement [33], inorganic polymers [34], zeocements [35], zeoceramics [35] and several more. A brief history of geopolymer is provided in the chapter 2, section 2.1. Geopolymers are inorganic, X-ray amorphous to semi-crystalline three-dimensional aluminosilicate polymers. They are composed of silicate and aluminate tetrahedrons which are linked by sharing oxygen atoms. The negative charge on the IV-fold coordination of Al^{3+}-ions is balanced by the positive charged alkali ions (e.g. Na^+, K^+ etc) as shown in Fig. 1.6 [22,28].
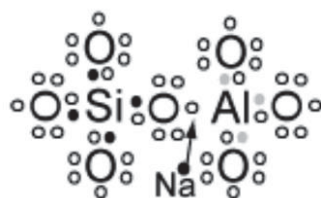
Fig. 1.6. A part of geopolymer structure, from [28].

A schematic diagram of the geopolymer structure is shown in Fig. 1.7 as published by [36]. Geopolymer gels are structurally disordered but show similarity to zeolite on atomic to nanometer level [17]. Unreacted particles and pore network containing the water are embedded within the geopolymer gel phase. Water from the alkaline solution acts as the reaction medium and resides within the pores of gel [17]. Taking in account the theories about the chemistry of silica described by Iler in 1955, Glukhovsky suggested the general model to describe the mechanism of alkali activation [17]. His model was divided in three stages named as Dissolution – Coagulation, Coagulation – Condensation, Condensation – Polymerization [17]. The detailed reaction mechanism of geopolymerization is described in chapter 2, section 2.1. The main reaction product in this type of systems is a N-A-S-H gel as presented above. However, the secondary reaction products in this type of systems has been reported as zeolites such as hydroxysodalite, zeolite P, Na-chabazite and zeolite Y / faujasite [20]. The available literature indicates that the surface area, curing temperature and type of activator significantly controls the reactions kinetics [37]. It is reported that the nature of reaction product changes with increasing age of the geopolymer reaction, where the long curing periods lead to formation of silica-rich products which give rise to mechanical strength [20].
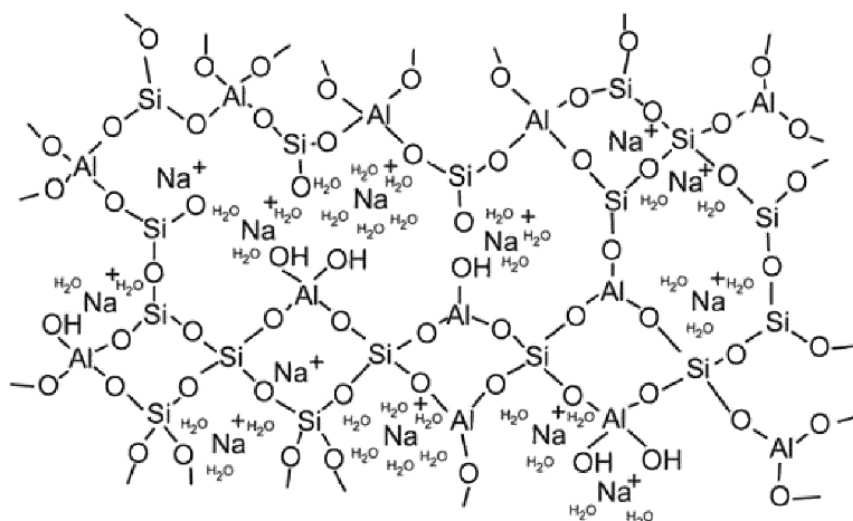
Fig. 1.7. Schematic diagrams of the three-dimensional geopolymer structure, from [36].

The properties of each binder are determined by the micro-structure, chemical structure and chemistry of raw materials. A mathematical model presented by [38,39] considered the impact of several parameters such as amount of water, Si/Al ratio, temperature, and surface area on the alkali activation of low calcium aluminosilicate precursors such as fly ash and metakaolin. According to this mathematical model as presented in Fig. 1.8, geopolymerization can be described by several steps [38,39]. First step is dissolution of the precursor forming silicate and aluminate monomers. This step is in principal comparable to weathering of minerals, but in case of geopolymerization the pH and the solid-to-liquid ratio is higher, and therefore the reaction is much faster [38,39]. Because of the high concentrations in activator solution, silicate oligomers (in the Fig. 1.8 mentioned as polymerized silicate species) exist which persist over the whole time of reaction [38,39]. There is an equilibrium between silicate monomers and oligomers. Silicate oligomers participate only very less in the condensation step [38,39]. Silicate monomers and aluminate monomers built up aluminosilicate oligomers. From the aluminosilicate oligomers, two different reaction paths can be taken [38,39]:

1. Formation of amorphous aluminosilicate which results via further incorporation of silicate monomers in amorphous aluminosilicate gel
2. Quasi- or nano-crystalline aluminosilicate nuclei which develop crystalline zeolitic phases by consuming aluminate from the solution

Consequently, the zeolitic reaction product is richer in Al than the amorphous gel and the over-all system [38,39]. In this model, the reaction stoichiometry with respect to water is

designed such that all the water used in the dissolution of the aluminosilicate source would be released by the end of geopolymerization, if all reactions achieve completion [38,39].

Structure

		Structure
Metakaolin or fly ash		*Layered or glassy aluminosilicate*

Silicate monomer / Aluminate monomer — *Dissolved (Q^0)*

Polymerised silicate species — *Dissolved (Q^1/Q^2)*

Aluminosilicate oligomers — *Dissolved (Q^1/Q^2)*

Aluminosilicate polymer (amorphous) / Aluminosilicate 'nuclei' (quasi- or nano-crystalline) — *Initial gel formation (Q^3)*

Aluminosilicate gel (amorphous) / 'Zeolitic' phase (nanocrystalline) — *Final gel formation (Q^4)*

Fig. 1.8. Layout of the mathematical model for alkaline activation of low Ca-aluminosilicate precursors, taken from [38].

The inclusion of calcium in the structure results in a higher complexity of the structure of the reaction product. Consequently, the reaction mechanisms for alkali activated materials with high calcium content are not described so far [38]. The alkali activation of GGBFS results majorly in formation of C-A-S-H, whereas layered double hydroxides are also observed as secondary reaction product in Mg-rich systems [40]. C-A-S-H gel in structure is comparable to C-S-H gels [41] and have been reported to contain disorder tobermorite-like structure [40]. The structure of C-A-S-H as presented by [40] is shown in Fig. 1.9. C-A-S-H gel contains layers of tetrahedrally coordinated silicate chains with dreierketten structure and the interlayer region contains Ca^{2+} cations, alkalis and water of hydration chemically incorporated into the gel structure. The silicate tetrahedron can be replaced by aluminate tetrahedron especially on the bridging side, whereby the charge balance is maintained by incorporation of alkali cation in the interlayer [40]. The C-A-S-H gels are reported to have lower Ca content than hydrated PC systems [40].
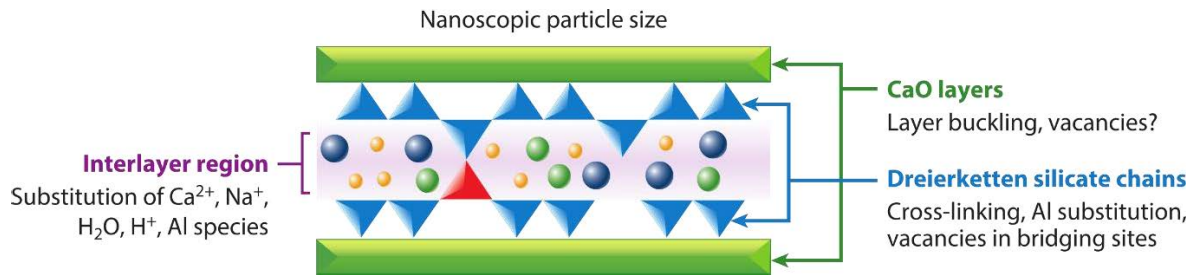
Fig. 1.9. C-A-S-H gel structure, taken from [40]. Blue triangles are Si tetrahedra, red triangle is Al tetrahedra, green rectangles are CaO layers, circles donate various interlayer species.

On contrary the hydration reaction of PC is driven by the addition of water and this can be divided in several periods/phases named as: initial period of high heat development, induction/dormant period of low heat development, acceleration and deceleration phase [42]. A conceptual diagram of cement hydration after [43] is shown in Fig. 1.10.
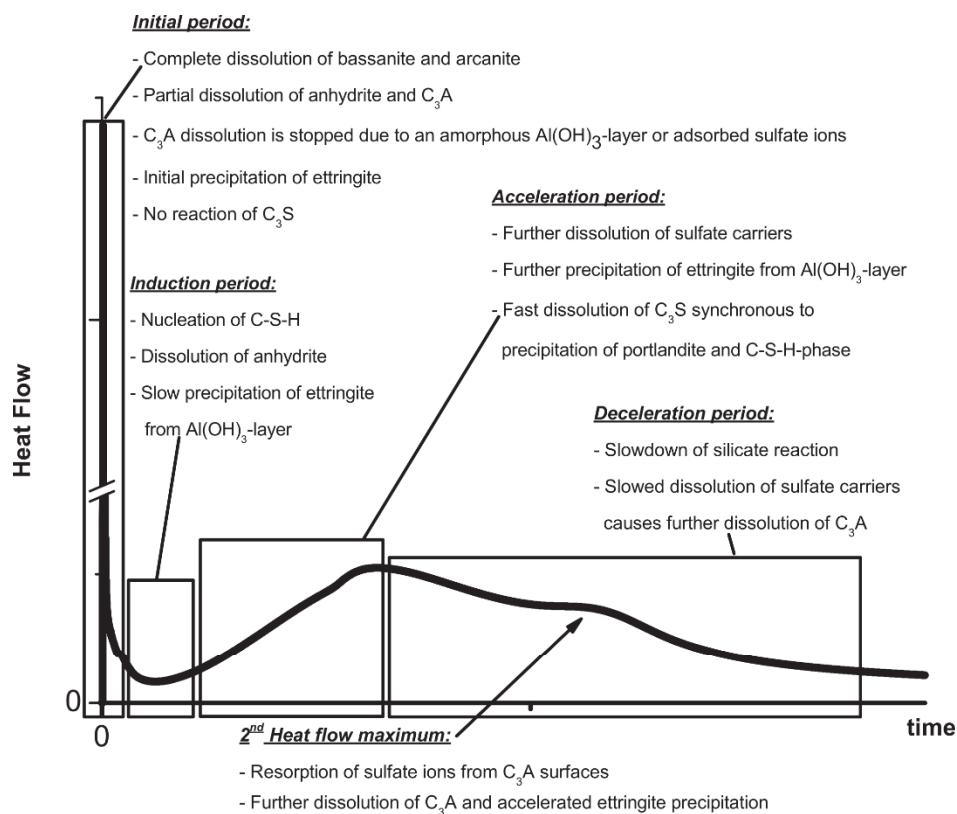
Fig. 1.10. Conceptual diagram of cement hydration, taken from [43]. Sulfate depletion peak is labelled as 2nd heat flow maximum in this picture.

In the initial period, majorly C$_3$A (tricalcium aluminate) and calcium sulfates dissolve and ettringite (Ca$_6$Al$_2$(SO$_4$)$_3$(OH)$_{12}$·26H$_2$O) precipitates [42,43]. In the induction period, calcium sulfate dissolution and ettringite precipitation proceeds, while the nucleation of C-S-H also starts [42,43]. In acceleration phase, reactions of induction period continue but C$_3$S (tricalcium silicate) starts to dissolve strongly, consequently, C-S-H and portlandite (Ca(OH)$_2$) form in large quantity. The exact time point at which the C$_3$S dissolution starts is still under discussion in the scientific community [42,43]. In deceleration phase, C$_3$S dissolution and C-S-H as well as portlandite precipitation slow down [42,43]. On the sulfate depletion peak, sulfate exhausts and the C$_3$A starts to dissolve again. In this phase, ettringite is also consumed and AFm (Al$_2$O$_3$-Fe$_2$O$_3$-mono) phases forms from C$_3$A and ettringite [42,43]. The structure of C-S-H as described by [41,44] is based on silicate chains which shows structural similarity to minerals jennite (Ca$_9$((OH)$_4$|Si$_3$O$_8$OH)$_2$·6H$_2$O) and especially tobermorite (Ca$_5$(Si$_3$O$_8$OH)$_2$·2H$_2$O) and is majorly X-ray amorphous.

1.3. Raw materials for geopolymer synthesis

The term supplementary cementitious material (SCM) is referred to all the materials which possess (latent) hydraulic or pozzolanic properties. These materials can be a suitable precursor for geopolymers/alkali activated binders. They are classified as natural or artificial, where natural SCMs or natural pozzolans are abundant available around the globe and are being used as cementing material from ancient times. Fig. 1.11 shows the global distribution of volcanic rocks and occurrences of reported natural supplementary cementitious material taken from [15]. Historically, the use of man-made binders dates back to 2000 – 1500 BC in Minoan civilization on Crete, where a mixture of slaked lime and finely ground potsherds was used as binder. The Santorin earth has been long used as a pozzolan in Eastern Mediterranean. The first intentional use of pozzolanic volcanic materials by ancient Greeks dates back to 500 – 400 BC. Alternatively, Romans used volcanic pumices or tuffs from mostly renowned sources found in Pozzuoli as binding component for construction binders and there the name pozzolan came into being [15]. Pozzolan is an aluminosilicate raw material which in itself contains little or no cementitious properties but when finely ground and in the presence of moisture reacts chemically with calcium hydroxide at ambient conditions to form cementitious composites exhibiting binding characteristics [45]. The excellent famous examples of Roman buildings constructed with the pozzolan-lime concretes and mortars include the Pantheon and the Pont du Gard, which substantiate the durability and excellent performance of these binders.

Fig. 1.11. Distribution of volcanic rocks (grey areas) and deposits of reported natural supplementary cementitious materials (black dots) around the globe, from [15].

Natural pozzolans often belong to rocks of volcanic or sedimentary origin [15]. They vary greatly in their composition as shown by the ternary diagram in Fig. 1.3 and the composition largely depends on the magmatic or diagenetic processes. The materials of volcanic origin can partially alter to zeolites or clays, while unaltered rocks are vitreous pumices and ashes etc. The materials of sedimentary origin can be further subdivided in chemical sediments and detrital sediments [15,46]. While a special case also includes naturally burnt clays. Moreover, another type of pozzolan can be the materials formed by meteorite impact, known as impactites. The high temperature and pressure due to meteorite impact can partially melt the rock on earth's surface and due to rapid cooling pieces of the melt can form glass. An example of such a pozzolan includes Bavarian trass found in Germany [46]. A detailed literature survey about the use of natural pozzolans as geopolymer precursor is presented in chapter 2, section 2.1.

Artificial pozzolans include burnt clays, industrial and agricultural waste products, municipal solid waste ash, waste glass etc. The most common low calcium artificial pozzolans used for geopolymer synthesis are fly ash (FA) and metakaolin (MK). Metakaolin is produced by burning of kaolin clay, while fly ash is the by-product of coal power plants. The work conducted on the FA- and MK-based geopolymers shows that the composition of raw material, its particle size distribution, curing conditions, concentration and type of alkaline solution influence their geopolymerization potential. The higher surface area of MK results in a higher water demand of the mixture thus resulting in high drying shrinkage and high porosity. The spherical shape of fly ash particles helps in reducing the water demand and

reducing the porosity [47]. Moreover, fly ashes are varying in their composition depending firstly on the impurities present in the coal before burning and secondly on the combustion parameters and quenching process [47]. Therefore, different fly ashes can exhibit diverse behaviour in geopolymer synthesis [48]. The strength development in geopolymers is controlled by particle size distribution as in Portland cements [47].

However, as explained earlier the strong need of alternative binder development and lack of most common artificial pozzolans lead to the need of using other abundant available resources for geopolymer synthesis such as natural pozzolans. The use of local available raw material in natural state is not only environmentally but also economically viable and sustainable solution. Therefore, this work will focus on the determination of geopolymeric potential of various natural pozzolans for geopolymer synthesis and factors that affect their properties. The originality of this work is the determination of geopolymeric potential of several natural pozzolans which are not tested till to date. As the composition of pozzolans varies with origin depending on the condition at their formation, it is necessary to explore the potential of several natural pozzolans. Moreover, determination of the behaviour of mineralogical phases of natural pozzolans in the geopolymer reaction is also a part of this research study which is not done before.

1.4. Research objectives

The work on natural pozzolan-based geopolymers presented in literature does not discuss the potential of European pozzolans for geopolymer synthesis. However, there are several natural pozzolan resources available in Europe including Germany and Italy. Therefore, the main objectives of this work include to study the potential of six natural pozzolans from Germany and Italy for development of geopolymers at ambient synthesis conditions and to examine the role of various minerals in geopolymer reaction. The preliminary investigations showed that the geopolymeric potential of these precursors is depended on the type and concentration of alkaline solutions. Therefore, as a first part of the research work, these natural pozzolans with different mineralogical composition were used to study the effect of silica modulus of sodium silicate solution and age of sample on the properties of the geopolymers. The degree of reaction and phase composition are determined by several methods at various ages. The second goal includes to study the effect of reactivity enhancement methods for a low-reactive natural pozzolan to achieve better performance. Based on the results of the first two parts, the third part of the study was designed which involved to study the role of minerals, as found in studied natural pozzolans, in geopolymer reaction. For this study, fifteen mineral phases were used to examine their reactivity in

sodium hydroxide and sodium silicate solutions. Additionally, the reactivity of calcium carbonate minerals was determined in further detail for eight calcium carbonate samples. The reaction mechanism and reaction products were investigated.

1.5. Research outline

The experimental research is presented in six scientific publications: two published peer-reviewed journal articles, two submitted articles in peer-reviewed journals, two published conference articles (one peer-reviewed). Moreover, further work which is not submitted and not published is also part of this thesis. Accordingly, this thesis is structured in five main sections, as follows:

Chapter 1 contains general information about the ecological impact of cement industry and the need of development of new binders such as geopolymers/alkali activated materials. Furthermore, it presents a short background about geopolymers, alkali activated binders and precursors for their synthesis, objectives of this research, research outline and brief information about the natural pozzolans used in this study.

Chapter 2 and 3 present the main body of the thesis where the peer-reviewed publications and major work is included. **Chapter 2** contains all the scientific publications. The <u>first peer-reviewed publication</u> in a journal is a literature overview on the state of the art for natural pozzolan-based geopolymers. In this regard, the mechanical, durability and microstructural characteristics of natural pozzolan-based geopolymers such as mechanical strength, curing conditions, concentration of alkaline solution, setting time, water absorption, bulk density and apparent porosity have been discussed. Moreover, reaction kinetics and phase composition of hardened geopolymers have been given. Furthermore, the publication presents the overview on the durability characteristics including sulphate resistance, acid resistance, permeability, shrinkage, wetting and drying cycle and applications of natural pozzolan-based geopolymers.

The <u>second peer-reviewed publication</u> focuses on the potential of six natural pozzolans for geopolymer synthesis and determines the effect of silica modulus on mechanical and microstructural properties of these binders. Geopolymer samples have been prepared by using different natural pozzolans and sodium silicate solution of sixteen different silica moduli. Isothermal conduction calorimetry has been used to draw relation between silica modulus and reaction kinetics. While selective dissolution and thermogravimetry have been used to evaluate the relation between degree of reaction and silica modulus at 28 d of geopolymer reaction. To the best of our knowledge, this was the first publication dealing

with determination of degree of reaction by selective dissolution for natural pozzolan-based geopolymers. Moreover, the phase composition at 28 d for samples with various silica moduli has been determined by X-ray diffraction analysis.

The third publication submitted in a peer-reviewed journal presents the impact of mineralogical composition of natural pozzolans on the properties of selected silica modulus samples at various ages. The influence of mineralogy on the formation of sodium carbonate / efflorescence, compressive strength and degree of reaction has been shown. The phase composition as studied by X-ray diffraction analysis showed changes occurring in X-ray amorphous and crystalline phases which helped to explore the impact of mineralogy on the properties of geopolymers. A brief study about the reactivity of calcite in such systems has also been included in this publication.

The fourth peer-reviewed conference paper focuses on a comparative study between the effect of two reactivity enhancement methods on properties of derived geopolymers. A low reactive natural pozzolan prone to development of efflorescence was subjected to heat treatment and mechanical activation. The potential reason for the effectiveness of each method has been explained. The fifth conference paper focuses on implementation of heat curing regime on two low reactive natural pozzolans for geopolymer synthesis. The compressive strength of samples prepared with various types and concentrations of alkaline solution has been determined at 7, 28 and 90 d of age while using two curing methodologies which include curing at room temperature and heat curing. Reaction kinetics have been studied for geopolymers based on both pozzolans at 20 °C.

The results presented till this part of the work laid foundation for the investigations related to reactivity of minerals in sodium hydroxide and sodium silicate solutions. Fifteen mineral phases were chosen based on the mineralogical composition of the used natural pozzolans. Out of all the tested minerals, calcium carbonate exhibited distinct behaviour and was therefore studied in further detail as part of sixth publication. For a better comparison all the mineral phases were ground in laboratory to comparable Blaine fineness values.

The sixth publication submitted in a peer-reviewed journal discusses the reactivity of calcium carbonate minerals in sodium silicate solution. Eight calcium carbonate samples with two polymorphs of calcium carbonate, calcite and aragonite, were used. The samples were reacted with sodium silicate solution of silica modulus 1.061 (≈ 1.1). The reaction mechanism, reaction kinetics, the early and late age reaction products were determined using in- and ex-situ X-ray diffraction analysis, in-situ Fourier transform infrared

spectroscopy, isothermal conduction calorimetry, thermogravimetric analysis coupled with mass spectrometry, differential scanning calorimetry and thermodynamic modelling.

Chapter 3 presents the unpublished work conducted about the reactivity of fifteen mineral phases in sodium hydroxide solution and six minerals in sodium silicate solution. Their reactivity in sodium hydroxide solution (16 mol/kg) and sodium silicate solution (silica modulus 1.061 ≈ 1.1) was determined by thermogravimetric analysis and X-ray diffraction analysis at 8, 28 and 90 d age. While the reaction kinetics were determined by isothermal conduction calorimetry for first 5 d.

In **Chapter 4** all the results and achievements presented in this work are collected and summarized. **Chapter 5** presents the general conclusions drawn from this thesis and some recommendations for the future research.

1.6. Used natural pozzolans

For the purpose, six European natural pozzolans collected from Germany and Italy were used for geopolymer production including Rhenish trass (RT), Bavarian trass (BT1 and BT2/BT), pozzolan Laziale "Red" (PLR), pozzolan Laziale "Black" (PLB) and pozzolan Flegrea (PF). Rhenish trass (RT) is a natural pozzolan of volcanic origin which was formed by the eruption of Laacher See volcano and about 100 other volcanos in the eastern Eifel, Germany that were active until about 13,000 years ago. Bavarian trass (BT1 and BT2/BT) also referred as Suevit was formed approximately 14.5 million years ago, when a meteorite hit the earth in a region later called the Nördlinger Ries, Germany. Initially, it was assumed that Ries was formed because of volcanic eruption. However in 1960, it was shown that the depression in the landscape was caused by meteorite impact [46]. (Note: It is worth to mention here that BT2 in section 2.2 and BT in section 2.3 & 2.4 are two different abbreviations used for same material. However, in chapter 4 abbreviation BT will be used.) Pozzolan Laziale "Red" (PLR) and pozzolan Laziale "Black" (PLB) have been mined at Ponte Lucano quarry, Tivoli (approx. 30 km from Rome, Italy) and was formed in volcanic complex of volcano Laziale some million years ago. PLR occurs in the outcrops of Ponte Lucano quarry, Italy and its red colour is because of oxidation process. Pozzolan Flegrea (PF) is also a volcanic ash and has been obtained from area Campi Flegrei at north of Naples, Italy.

References

[1] Juenger MCG. Low CO_2 cement for sustainable concrete. In: Gardoni P, editor. Routledge Handbook of Sustainable and Resilient Infrastructure. Abingdon, Oxon, New York, NY: Routledge; 2018, p. 377–386.

[2] Provis JL, van Deventer JSJ. Alkali Activated Materials, State-of-the-Art Report, RILEM TC 224-AAM. Springer, Dordrecht, Heidelberg, New York, London; 2014.

[3] Rehan R, Nehdi M. Carbon dioxide emissions and climate change: Policy implications for the cement industry. Environ. Sci. Policy 2005;8(2):105–14. https://doi.org/10.1016/j.envsci.2004.12.006.

[4] Worrell E, Price L, Martin N, Hendriks C, Meida LO. Carbon dioxide emissions from the global cement industry. Annu. Rev. Energy. Environ. 2001;26(1):303–29. https://doi.org/10.1146/annurev.energy.26.1.303.

[5] Andrew RM. Global CO_2 emissions from cement production. Earth Syst. Sci. Data 2018;10(1):195–217. https://doi.org/10.5194/essd-10-195-2018.

[6] Flower DJM, Sanjayan JG. Greenhouse Gas Emissions Due to Concrete Manufacture. In: Flower DJM, Sanjayan JG, editors. Handbook of Low Carbon Concrete: Chapter 1. Elsevier Inc; 2017, p. 1–16.

[7] Herrmann A, Koenig A, Dehn F. Structural concrete based on alkali-activated binders: Terminology, reaction mechanisms, mix designs and performance. Struct. Concr. 2017;130(1-2):213. https://doi.org/10.1002/suco.201700016.

[8] European Commission. A Clean Planet for all - A European strategic long-term vision for a prosperous, modern, competitive and climate neutral economy. Brussels; 2018.

[9] International Energy Agency, World Business Council for Sustainable Development, Cement Sustainability Initiative. Technology Roadmap - Low-Carbon Transition in the Cement Industry. France; 2018.

[10] Damtoft JS, Lukasik J, Herfort D, Sorrentino D, Gartner EM. Sustainable development and climate change initiatives. Cem. Concr. Res. 2008;38(2):115–27. https://doi.org/10.1016/j.cemconres.2007.09.008.

[11] EN 197-1. Cement – Part 1: Composition, specifications and conformity criteria for common cements; 2014.

[12] Manz OE. Worldwide production of coal ash and utilization in concrete and other products. Fuel 1997;76(8):691–6.

[13] Guess M. It'll cost $45 billion, but Germany proposes to eliminate coal in 19 years. [February 19, 2020]; Available from: https://arstechnica.com/tech-policy/2019/01/itll-

cost-45-billion-but-germany-proposes-to-eliminate-coal-in-19-years/?comments=1&post=36745919.

[14] Snellings R. Assessing, Understanding and Unlocking Supplementary Cementitious Materials. RILEM Tech. Lett. 2016;1:50–5. https://doi.org/10.21809/rilemtechlett.2016.12.

[15] Snellings R, Mertens G, Elsen J. Supplementary Cementitious Materials. Rev. Mineral. Geochem. 2012;74(1):211–78. https://doi.org/10.2138/rmg.2012.74.6.

[16] Siddique R. Effect of volcanic ash on the properties of cement paste and mortar. Resour. Conserv. Recycl. 2011;56(1):66–70. https://doi.org/10.1016/j.resconrec.2011.09.005.

[17] Provis JL, van Deventer JSJ (eds.). Geopolymers: Structure, processing, properties and industrial applications. Boca Raton, Fla.: CRC; Oxford Woodhead; 2009.

[18] van Deventer JSJ, Provis JL, Duxson P, Brice DG. Chemical Research and Climate Change as Drivers in the Commercial Adoption of Alkali Activated Materials. Waste Biomass Valor. 2010;1(1):145–55. https://doi.org/10.1007/s12649-010-9015-9.

[19] van Deventer JSJ. Progress in the Adoption of Geopolymer Cement. In: Handbook of Low Carbon Concrete. Elsevier; 2017, p. 217–262.

[20] Pacheco-Torgal F, Labrincha JA, Leonelli C, Palomo A, Chindaprasirt P (eds.). Handbook of Alkali-activated Cements, Mortars and Concretes. Cambridge, Philadelphia, PA: Woodhead Publishing; 2012.

[21] Shi C, Krivenko PV, Roy D. Alkali-Activated Cements and Concretes. London, New York: Taylor & Francis; 2006.

[22] Duxson P, Fernández-Jiménez A, Provis JL, Lukey GC, Palomo A, van Deventer JSJ. Geopolymer technology: The current state of the art. J. Mater. Sci. 2007;42(9):2917–33. https://doi.org/10.1007/s10853-006-0637-z.

[23] Ko LS-C, Beleña I, Duxson P, Kavalerova E, Krivenko PV, Ordoñez L-M et al. AAM Concretes: Standards for Mix Design/Formulation and Early-Age Properties. In: Provis JL, van Deventer JSJ, editors. Alkali Activated Materials. Dordrecht: Springer Netherlands; 2014, p. 157–176.

[24] BSI Standards Publication. PAS 8820-2016 Construction materials – Alkali-activated cementitious material and concrete – Specification;91.100.10: BSI Standards Limited; 2016.

[25] Lothenbach B, Scrivener K, Hooton RD. Supplementary cementitious materials. Cem. Concr. Res. 2011;41(12):1244–56. https://doi.org/10.1016/j.cemconres.2010.12.001.

[26] Bernal SA, Provis JL, Green DJ. Durability of Alkali-Activated Materials: Progress and Perspectives. J. Am. Ceram. Soc. 2014;97(4):997–1008. https://doi.org/10.1111/jace.12831.

[27] EN 450-1. Fly ash for concrete - Part 1: Definition, specifications and conformity criteria 2012.

[28] Davidovits J. Geopolymer Chemistry and Applications. Saint-Quentin, France: Institut Géopolymère; 2008.

[29] Glukhovsky VD. Soil Silicates (Gruntosilikaty). Kiev, USSR Budivelnik Publisher; 1959.

[30] Glukhovsky VD. Soil Silicates, their properties, technology of manufacturing and field of application [Doct. Tech. Sc. Degree Thesis]. Kiev Civil Engineering Institute, Kiev, USSR; 1965.

[31] Krivenko PV. Alkaline cement. Proceeding of the first internation conference on alkaline cements and concrete, VIPOL Stock Company, Kiev, Ukrain 1994:11–129.

[32] Rahier H, van Mele B, Biesemans M, Wastiels J, Wu X. Low-temperature synthesized aluminosilicate glasses: Part I Low-temperature reaction stoichiometry and structure of a model compound. J. Mater. Sci. 1996;31(1):71–9. https://doi.org/10.1007/BF00355128.

[33] Palomo A, López de la Fuente, J. I. Alkali-activated cementitous materials: Alternative matrices for the immobilisation of hazardous wastes. Cem. Concr. Res. 2003;33(2):281–8. https://doi.org/10.1016/S0008-8846(02)00963-8.

[34] van Deventer JSJ, Provis JL, Duxson P, Lukey GC. Reaction mechanisms in the geopolymeric conversion of inorganic waste to useful products. J. Hazard. Mater. 2007;139(3):506–13. https://doi.org/10.1016/j.jhazmat.2006.02.044.

[35] Fernández-Jiménez A, Monzó M, Vicent M, Barba A, Palomo A. Alkaline activation of metakaolin–fly ash mixtures: Obtain of Zeoceramics and Zeocements. Microporous Mesoporous Mater. 2008;108(1-3):41–9. https://doi.org/10.1016/j.micromeso.2007.03.024.

[36] Rowles MR, Hanna JV, Pike KJ, Smith ME, O'Connor BH. ^{29}Si, ^{27}Al, ^{1}H and ^{23}Na MAS NMR Study of the Bonding Character in Aluminosilicate Inorganic Polymers. Appl. Magn. Reson. 2007;32(4):663–89. https://doi.org/10.1007/s00723-007-0043-y.

[37] Bondar D, Lynsdale CJ, Milestone NB, Hassani N, Ramezanianpour AA. Effect of type, form, and dosage of activators on strength of alkali-activated natural pozzolans. Cem. Concr. Compos. 2011;33(2):251–60. https://doi.org/10.1016/j.cemconcomp.2010.10.021.

[38] Provis JL. Geopolymers and other alkali activated materials: Why, how, and what? Mater. Struct. 2014;47(1-2):11–25. https://doi.org/10.1617/s11527-013-0211-5.

[39] Provis JL, van Deventer JSJ. Geopolymerisation kinetics. 2. Reaction kinetic modelling. Chem. Eng. Sci 2007;62(9):2318–29. https://doi.org/10.1016/j.ces.2007.01.028.

[40] Provis JL, Bernal SA. Geopolymers and Related Alkali-Activated Materials. Annu. Rev. Mater. Res. 2014;44(1):299–327. https://doi.org/10.1146/annurev-matsci-070813-113515.

[41] Richardson IG. Model structures for C-(A)-S-H(I). Acta Crystallogr. B Struct. Sci. Cryst. Eng. Mater. 2014;70(Pt 6):903–23. https://doi.org/10.1107/S2052520614021982.

[42] Hesse C, Goetz-Neunhoeffer F, Neubauer J. A new approach in quantitative in-situ XRD of cement pastes: Correlation of heat flow curves with early hydration reactions. Cem. Concr. Res. 2011;41(1):123–8. https://doi.org/10.1016/j.cemconres.2010.09.014.

[43] Jansen D, Goetz-Neunhoeffer F, Stabler C, Neubauer J. A remastered external standard method applied to the quantification of early OPC hydration. Cem. Concr. Res. 2011;41(6):602–8. https://doi.org/10.1016/j.cemconres.2011.03.004.

[44] Richardson IG. The calcium silicate hydrates. Cem. Concr. Res. 2008;38(2):137–58. https://doi.org/10.1016/j.cemconres.2007.11.005.

[45] ASTM C 618 – 01. Standard Specification for Coal Fly Ash and Raw or Calcined Natural Pozzolan for Use as a Mineral Admixture in Concrete(C 618 – 01). 100 Barr Harbor Drive, West Conshohocken, PA 19428-2959, United States: American Society for Testing and Materials; 2001.

[46] Hewlett PC, Lea FM (eds.). Lea's chemistry of cement and concrete. 4th ed. Oxford: Elsevier Butterworth-Heinemann; 2004.

[47] Duxson P, Provis JL. Designing Precursors for Geopolymer Cements. J. Am. Ceram. Soc. 2008;91(12):3864–9. https://doi.org/10.1111/j.1551-2916.2008.02787.x.

[48] Winnefeld F, Leemann A, Lucuk M, Svoboda P, Neuroth M. Assessment of phase formation in alkali activated low and high calcium fly ashes in building materials. Constr. Build. Mater. 2010;24(6):1086–93. https://doi.org/10.1016/j.conbuildmat.2009.11.007.

Chapter 2

Publications

2.1. Natural pozzolan based geopolymers: A review on mechanical, microstructural and durability characteristics

Authors: Rafia Firdous, Dietmar Stephan, Jean Noël Yankwa Djobo
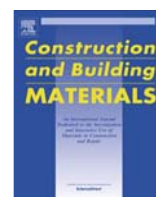
Review

Natural pozzolan based geopolymers: A review on mechanical, microstructural and durability characteristics

Rafia Firdous [a], Dietmar Stephan [a,*], Jean Noël Yankwa Djobo [b]

[a] Technische Universität Berlin, Department of Civil Engineering, Building Materials and Construction Chemistry, Gustav-Meyer-Allee 25, 13355 Berlin, Germany
[b] Local Materials Promotion Authority/MIPROMALO, 2396, Nkolbikok, Yaoundé, Cameroon

HIGHLIGHTS

- Use of natural pozzolans in development of geopolymers.
- Properties of natural pozzolan based geopolymers.
- Factors influencing the geopolymerization of natural pozzolan.
- Durability & microstructural characteristics of natural pozzolan based geopolymers.
- Applications of natural pozzolan based geopolymers.

ARTICLE INFO

ABSTRACT

Natural pozzolans are tremendous source of reactive silica and alumina required for geopolymer synthesis as an alternative binder for ordinary Portland cement. They are available at a comparatively low cost and generate a low ecological footprint through their simple extraction. Following review paper summarizes the mechanical and durability characteristics as well as the microstructural properties of natural pozzolan based geopolymers and their potential as binding material. The microstructural characteristics are based on the advanced analytical techniques used so far to understand geopolymerization, the phase composition, mechanical and durability properties evolution. From this review is obvious that significant analytical techniques have been successfully carried out on fresh and hardened natural pozzolan based geopolymer obtained in alkaline medium, which helped to understand underlying chemical reaction and external factors affecting final properties. These analyses have shown that natural pozzolan based geopolymer has potential to be used as sustainable building materials. But, for its large scale utilisation there is need to upscale the manufacturing process at a pilot-plant in order to address the macroscopic challenges that may arise at that level.

© 2018 Elsevier Ltd. All rights reserved.

Contents

---

* Corresponding author.
   E-mail address: stephan@tu-berlin.de (D. Stephan).

1. Introduction

Natural pozzolan is a type of aluminosilicate generally from volcanic origin, that can react with lime at ambient temperature to form a solid rock [1]. The term pozzolan refers to the city of Pozzuoli in Italy where it has been first discovered by Romans. The latter observed that those natural pozzolan have cementing properties and started using them for making building blocks [2]. The cementitious characteristics are known as pozzolanic properties which depends on the amount of reactive SiO_2 and Al_2O_3 available in the aluminosilicate [2,3]. Because of the pozzolanic properties natural pozzolan have been widely used as supplementary cementitious material (SCM) in Portland cement industry [1].

The use of natural pozzolan for making various types of cement have been reviewed in recent time. The first one was made by Siddique et al. in 2011 who summarized the effects of using volcanic ash as SCM in cement paste and mortar [4]. The microstructure, physical, mechanical and durability properties of cement paste and mortar were thus reviewed. The authors reported that the addition of volcanic ash had beneficial effect on long term physical and mechanical properties, electrical resistivity of resulting cement paste and mortar. The second review authored by Cai et al. in 2016 reported the fresh properties, microstructural, mechanical, and durability properties of concretes using volcano-related materials as SCM and lightweight aggregate [5]. That review highlighted that volcano-related materials can be used to develop the concretes with moderate properties. Their use as SCM significantly improved the durability properties of cement paste and mortar. More recently another comprehensive review dealing this time with the use of volcanic ash for developing alternative cement-based materials named alkali activated materials and geopolymer was successfully reported [6]. The main contribution of that paper was the summary of the existing literature addressing the relationship between the inherent properties of volcanic ash and the synthesis parameters as well as their potential use as raw material for geopolymer synthesis.

The present paper reviews and discusses mechanical, microstructural and durability characteristics of natural pozzolan based geopolymer obtained with alkaline solution as hardener or activator. Since, the mechanical and durability characteristics of geopolymer cement and concretes depend on their properties at nano-structural level this review also aims at giving better understanding of the microstructural analysis results used so far to elucidate the nanometric characteristics of geopolymer materials from natural pozzolan.

1.1. Overview on geopolymers

Geopolymers are inorganic aluminosilicate binders that have polymeric silicon-oxygen-aluminium framework structures. Geopolymers binders result from reaction of solid aluminosilicate from source material (natural pozzolans, industrial and agricultural waste products) with highly concentrated aqueous alkali hydroxide or alkali silicate solution. The alkaline source supplies alkali metal cations thus raising the pH of solution it accelerates the dissolution of solid precursors [7]. The available calcium content of reacting components should be low to enable the formation of three-dimensional polymeric chain and ring structure consisting of Si-O-Al-O bonds [7,8]. As studied by Davidovits, the network of the silico-aluminate based geopolymers consists of SiO_4 and AlO_4 tetrahedra linked alternately by sharing all the oxygens. The positive ions present in framework of cavities balances the negative charge of Al^{3+} in IV-fold coordination [8,9]. The basic empirical formula for geopolymer chain is as given in Eq. (1).

$$M_n\left[-(SiO_2)_z - AlO_2\right]_n \cdot wH_2O \tag{1}$$

where M is the monovalent alkali metal or cation such as K^+, Na^+, Ca^{2+}, Li^+; the symbol '-' indicates the presence of bond, n is the degree of polycondensation or polymerisation; z is 1, 2, 3, or higher.

Geopolymers are considered as environmental friendly binder, since they harden at ambient temperatures and therefore, their synthesis demands less energy, and depending on the activator up to 80 % less CO_2 is emitted in comparison to ordinary Portland cement [10–12]. In 1908 for the first time, a German scientist Hans Kühl investigated the setting properties of ground granulated blast furnace slag (GGBFS) with caustic potash (KOH) solution [1,7,13,14]. In 1937, Chassevent observed the reactivity of slags using caustic potash and caustic soda solution [1,13,15]. However, in 1940 the first extensive experimental study on clinker less cements was done by Purdon [16,17]. His work focused on the reaction of GGBFS with caustic soda or caustic alkalis. In 1957, Glukhovsky discovered the possibilities of producing the binder using low basic calcium or calcium free aluminosilicate and solutions of alkali metal known as soil cements and corresponding concretes as soil silicates [18,19]. Later in 1981, Davidovits produced binders by

mixing alkalis with a burnt mixture of kaolinite, lime stone and dolomite named as geopolymer since they have a polymeric structure. These types of materials belong to the alkaline binding system as discovered by Glukhovsky [1,13].

1.1.1. Mechanism of geopolymerization

The general mechanism of geopolymerization consists in a three-stage reaction: Dissolution – Coagulation, Coagulation – Condensation, Condensation – Polymerization [20]. The reaction starts with the breakage of siloxane (Si–O–Si) ions with OH^- ions from alkali activating solution yielding silanol (–Si–OH) and sialate (-Si-O$^-$) species. The presence of alkali cations normalizes the negative charge while the formation of Si–O$^-$–Na$^+$ bond hinders the reversion to siloxane [13]. The OH^- ions also impacts the Si–O–Al bond in the same way and forms complex species, majorly Al $(OH)_4^-$ anions [8]. The dissolution step depends on the temperature, pH of mixture and possible treatments of the source materials. Higher fineness and higher pH favours the dissolution step and monomeric aluminate and silicate units are formed [21]. In the 2nd stage, the assemblage of ionic species helps to generate contact between the disaggregated products and polycondensation starts causing an increase in the coagulated structure. The silica monomers inter-react to form dimers and then polymers. In the last stage, the further reaction products precipitate because the particles present in the initial solid phase are forming three-dimensional polymeric chain and ring structures consisting of Si–O–Al–O bonds. However, these three steps can overlap with each other and occur almost simultaneously, thus making it difficult to isolate and examine each of them separately [7,8,13,21–23].

1.2. Raw materials for geopolymer synthesis

The raw materials for geopolymer synthesis could be natural pozzolanic materials like volcanic ash (tuff), diatomaceous earth, opaline cherts, shales and pumicites etc. or naturally tempered pozzolanic materials like zeolite, kaolinite, phonolite etc. Artificial raw materials for geopolymers include pozzolanic materials from industrial or agricultural waste such as low calcium fly ash, silica fume, brick powder, granulated blast furnace slag, sugarcane bagasse ash, rice husk ash etc. [3,24–28]. Since recent decades, geopolymers are being used as an alternative to conventional binders with a lot of work carried out on metakaolin or fly ash based geopolymers, however, only little has been done on the use of natural pozzolans for geopolymer synthesis. Since industrial by-products such as fly ash and slag are available only to the extent that they arise in the production of the main product, their use is limited. In addition, decarbonisation will continue to reduce the burning of coal, which is already leading to a shortage of fly ash for concrete production in some countries. This makes the use of alternative binders with a low ecological footprint increasingly important.

1.2.1. Production of natural pozzolans

Pyroclastic rocks resulting from the explosive volcanic eruptions are considered as wide category of natural pozzolans. The explosive volcanic eruption projects minute particles of melted magma into the atmosphere while the rapid pressure decrease results in formation of microporous structure by release of gases dissolved in particles of the magma. Simultaneously, quenching process results for their glassy state. On contrary, non-explosive eruption results in crystallisation of molten magma (little or no pozzolanic activity) due to insufficient quenching [2].

The deposits of volcanic pozzolans exposed to weathering and cementation of loose particles through diagenetic or other natural processes form compact layers (tuffs). Weathering can cause either zeolitisation or argillation resulting in zeolitic minerals or clay minerals respectively, therefore, zeolitisation enhances the pozzolanic properties [2,29]. Fragments of rocks, minerals and volcanic glass produced during the volcanic eruption having sizes less than 2 mm are characterized as volcanic ashes [5,6,29]. The size of the volcanic ashes reduces with the distance from the volcano and can be as small as 0.034 μm for 621 km distance from the volcano [5]. Based on the chemical composition and degree of vesicularity, extrusive volcanic eruptions can form four different types of volcanic ashes named as: felsic, intermediate, mafic and ultramafic. Felsic rocks are acidic and result from explosive eruptions while mafic are basaltic and are result of non-explosive eruption [6,30].

1.2.2. Reactivity of natural pozzolans

The capacity of aluminosilicate material to dissolve in alkaline medium defines its reactivity [31]. The latter depends on fineness / specific surface area of particles, chemical and mineralogical composition of materials [32,33]. Table 1 presents the chemical composition of various natural pozzolans used by researchers for

Table 1
Chemical composition of various volcanic ashes.

Source	SiO$_2$	Al$_2$O$_3$	CaO	Fe$_2$O$_3$	K$_2$O	Na$_2$O	MgO	TiO$_2$	MnO	P$_2$O$_5$	LOI	Total
Mt. Shinmoe, Southern, Japan [38]	54.9	16.4	8.8	10.9	1.7	2.8	3.3	0.8	0.2			99.9
South East, Iran [39–40]	61.7	15.9	8.0	4.3	2.1	3.2	2.0	0.4			1.9	97.7
North West, Iran [39–40]	70.1	11.1	2.5	1.3	2.3	1.0	0.9	0.1			10.3	89.4
North West, Iran [41]	64.7	11.9	6.8	3.0	4.3	2.3	1.1	0.5			5.2	94.5
South East, Iran [41]	68.5	11.8	2.9	3.7	3.2	1.6	1.4	0.4			6.1	93.6
South East, Iran [41]	68.3	12.6	3.9	2.7	3.3	2.4	1.4	0.3			4.4	94.8
Chihuahua, Mexico [11]	59.5	9.4	8.0	2.3							14.3	79.3
Foumbot West Region, Cameroon* [42]	44.2	14.1	10.4	13.2	1.5	3.7	9.7	2.7	0.2	0.6	−0.6	100.3
Foumbot West Region, Cameroon [43]	43.4	15.3	11.1	12.5	1.7	4.5	6.8	2.9	0.2	0.9		99.3
Djoungo, Littoral Region, Cameroon* [44]	46.3	15.4	9.1	13.3	–	3.9	6.7	2.8	0.2	0.6	−0.4	98.4
Djoungo, Littoral Region, Cameroon [45]	44.0	15.3	9.3	12.8	1.4	5.6	7.0	2.9	0.2	0.5	1.1	98.9
Loum, Littoral Region, Cameroon [32]	47.7	15.4	8.3	12.9	1.1	3.6	6.5	2.8	0.2	0.5	0.7	98.9
Galim, West Region, Cameroon [45–48]	41.4	15.4	7.9	12.9	1.0	2.2	6.5	3.0	0.2	0.5	9.3	90.9
Jordan cement factories Lafarge, Jordan [49]	40.2	13.9	9.7	15.2	1.5	3.7	9.6				4.8	93.7
Bayburt Stone waste, Turkey [50]	68.9	12.0	3.9	0.3	2.4	0.2	1.3				10.1	89.2
Rhine Land, Germany [51]	58.6	17.7	4.7	6.2	5.1	3.4	2.4					98.0
Yellow Tuff, Italy [2]	54.7	17.7	3.7	3.8	6.4	3.4	0.9				9.1	99.7
Bacoli, Italy [2]	53.1	17.9	9.0	4.3	7.6	3.1	1.2	0.3			3.0	99.5
Barile, Italy [2]	44.1	19.2	9.0	4.3	7.6	3.1	1.2	0.3			3.0	91.8
Coastal Region, Ecuador [52]	68.2	11.5	3.7	4.1			1.0					88.5
Coastal Region, Ecuador [52]	66.0	11.0	4.7	3.9			1.5					87.1

* The negative value of loss on ignition presents that there was a gain in mass after heating the sample till 1000 °C which could be possibly because of the oxidization [44].

Table 2
Mineralogical composition of volcanic ashes [25,32–33,35–37,41–48,50–51,53–64].

Group	Common Minerals	Probability of Occurrence
Feldspar Group	Alkali feldspar including Albite ((Na,Ca)[(Si,Al)$_4$O$_8$]) (now as Plagiclase classified), Anorthoclase ((Na,K)[AlSi$_3$O$_8$]), Sanidine ((K,Na)[(Si,Al)$_4$O$_8$]), Microcline (K[AlSi$_3$O$_8$])	High
	Plagioclase feldspars including Anorthite ((Ca,Na)[(Si,Al)$_4$O$_8$]), Oligoclase ((Na, Ca)[(Si,Al)$_4$O$_8$])	Average
Olivine Group	Forsterite (Mg$_2$[SiO$_4$])	Average
	Fayalite (Fe$_2$[SiO$_4$])	Low
Foids	Nepheline ((Na,K)[AlSiO$_4$])	Average
	Leucite (K[AlSi$_2$O$_6$])	Low
Pyroxene Group	Augite (Ca,Fe)(Mg,Fe)[Si$_2$O$_6$], Diopside (CaMg[Si$_2$O$_6$])	Low
Mica Group	Muscovite (KAl$_2$[(OH)$_2$|AlSi$_3$O$_{10}$]), Biotite (K(Mg,Fe^{2+})$_3$[(OH,F)$_2$] (Si,Al)$_4$O$_{10}$])	Low
Oxide minerals	Quartz (SiO$_2$), Hematite (Fe$_2$O$_3$), Anatase (TiO$_2$)	Average
	Maghemite (γ-Fe$_2$O$_3$)	Low
Minerals formed by alteration		
Zeolite Group	Heulandite ((Ca,Na,K)$_9$[(Si,Al)$_{36}$O$_{72}$]·26H$_2$O, Analcime (Na[AlSi$_2$O$_6$]·H$_2$O), Phillipsite ((K,Na,Ca)$_4$[(Si,Al)$_{16}$O$_{32}$]·12H$_2$O), Chabazite ((Ca,Na)$_4$[(Si,Al)$_{12}$O$_{24}$]· 13H$_2$O), Mordenite ((Na,Ca,K)$_6$[AlSi$_5$O$_{12}$]$_8$·28H$_2$O)	Low
Sulphates	Anhydrite (CaSO$_4$)	Low
Carbonates	Calcite (CaCO$_3$), Manganocalcite (MnCO$_3$)	Low
Amphibole Group	Ferrohornblende (Na$_{<0.5}$Ca$_2$(Fe^{2+},Mg)$_4$(Al,Fe^{3+},Fe^{2+})[(OH)|(Si,Al)$_4$O$_{11}$]$_2$), Magnesiohornblende (Na$_{<0.5}$Ca$_2$(Mg,Fe^{2+})$_4$ (Al,Fe^{3+},Fe^{2+})[(OH)|(Si,Al)$_4$O$_{11}$]$_2$)	Low
Clay Minerals	Montmorillonite ((Al$_{1·67}$Mg$_{0·33}$)[(OH)$_2$|Si$_4$O$_{10}$]·Na$_{0·33}$(H$_2$O)$_4$), Illite ((K,H$_3$O) Al$_2$[(H$_2$O,OH)$_2$|(Si,Al)$_4$O$_{10}$])	Low
Chlorite Group	Chlorite ((Mg,Fe^{2+},Al)$_3$[(OH)$_2$|AlSi$_3$O$_{10}$]·(Mg,Fe^{2+},Al)$_3$(OH)$_6$)	Low

geopolymer synthesis. This indicates the presence of a fair amount of silica and alumina indicating the suitability of these raw materials for geopolymer synthesis. Higher amount of loss on ignition in some of the materials indicate the presence of dissolved gasses such as CO_2 and water in glassy form, showing the presence of carbonates and clay minerals respectively [6]. The difference in the chemical composition observed in that table depends upon factors like composition of magma, temperature and humidity conditions, nature of eruption, crystal content and dissolved gasses of erupting magma [4,34]. Mineralogical compositions of various volcanic ashes determined by X-ray diffraction (XRD) analysis in various studies are presented in Table 2. Weathering of volcanic glass with time due to climatic condition can produce minerals as mica and clay [6]. It must recall that it is not easy to distinguish between highly and lowly reactive natural pozzolan based only on the chemical and mineralogical composition of the whole sample. This is because only the chemical composition of the glassy phase can determine the degree of reactivity of natural pozzolan. The determination of the reactivity of natural pozzolan has been performed by using the chemical method [35–37]. This involves the dissolution of natural pozzolan in concentrated NaOH or KOH solution at different temperatures and the analysis of the leachate by ICP-OES. The tests showed that roughly, natural pozzolan has a lower reactivity compared to other aluminosilicates, and the glassy phase is mainly constituted of Si, Al, Fe, Ca and Mg with Si as the major component [35–37]. Finally, a total amount of at least 20 wt-% reactive phases are require in natural pozzolan to be suitable for geopolymer synthesis [37].

2. Characteristics of geopolymer pastes

2.1. Calorimetry

Various calorimetry techniques were used to assess the reactivity and geopolymerization of natural pozzolan by measuring heat released during reaction. The two techniques used were Differential Scanning Calorimetry (Isothermal and non-Isothermal DSC) which measures the heat released when temperature rises and Isothermal Conduction Calorimetry (ICC) which measures the heat

flow at a constant temperature. The non-Isothermal DSC of four volcanic ashes carried out by Lemougna et al. highlight that when temperature rises the maximum heats released were reached between 131 and 166 °C; whereas, the Isothermal DSC at 90 °C showed that the maximum heats released were very low compared to the one of metakaolin for example [56]. The authors thus, concluded that volcanic ash is less reactive than calcined clay. This was later on confirmed by the investigation of Djobo et al. who studied the heat released during geopolymerization of Cameroonian volcanic ash at 27 °C by ICC [35]. The latter stressed that the calorimetric curve of geopolymerization of volcanic ash is characterized by a single exothermic peak whose maximum is reached in less than 1 h. This peak which is associated with sorption of alkaline activator solution on the surface of ash particles and dissolution of the ash particles. This demonstrates that the maximum dissolution rate and the maximum amount of dissolved species is achieved within 1 h. Fig. 1 shows the ICC curve depicting the stages of geopolymerization reaction and the effect of fineness on the rate of heat evolution. The fast retardation after the first peak attributes to the wetting process and later stage dissolution and polymerization reaction continues in apparently thermally steady state with lower rate of heat evolution [65].

According to a research study of Kani et al., during geopolymerization of natural pozzolan the reaction time (time at which no further heat is released, and the rate of heat evolution fell to zero) ranges from 21 to 29 h, and the apparent activation energy varies between 49.6 and 64.8 kJ/mol. These data allowed to understand that depending on the temperature at which the reaction takes place and the synthesis conditions, the geopolymerization of natural pozzolan ends within 21–29 h [65]. It is worth pointing out that the activation energy translates the minimum energy that should be applied to the system to undergo a chemical reaction. So, the higher activation energy observed means that higher temperature is required for the geopolymerization and indicates the low reactivity of natural pozzolan compared to fly ash or metakaolin.

2.2. Setting time

Setting time of geopolymer mixtures depends upon the specific surface area and content of free CaO available in the mixture. The
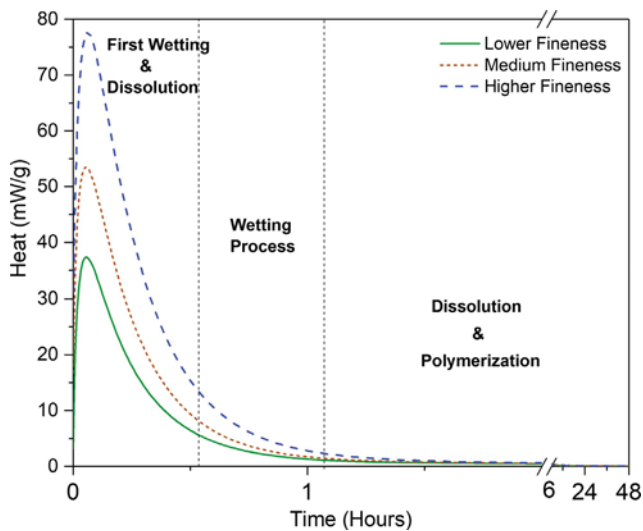
Fig. 1. Heat evolution on different stages of geopolymerization reaction and effect of fineness on heat evolution [32,65].

lower the specific surface area and lower the content of free CaO in the source material leads to higher setting time of geopolymer mixtures. Setting time of geopolymer mixtures can also be controlled with the amount and modulus of the activator sodium silicate; the higher the SiO_2/Na_2O molar ratio the lower is the setting time [37]. Tchakoute et al. studied the compressive strength and setting time of two Cameroonian volcanic ashes originating from Djoungo and Galim named as Z_D and Z_G respectively [37]. Alkaline activating solutions with SiO_2/Na_2O molar ratio of 0.7, 0.9, 1.1, 1.3 and 1.4 were prepared with NaOH (12 M) and Na_2SiO_3 (28.7 % SiO_2, 8.9 % Na_2O). Liquid to solid mass ratio for Z_G was kept constant at 0.49 and for Z_D at 0.37. Low specific surface area (2.3 m^2/g) and low free CaO (3.23 wt.-%) content of Z_D resulted in a setting time longer than 14 days and low compressive strength. Whereas, for Z_G (specific surface area of 15.7 m^2/g and free CaO of 5.11 wt.-%) based geopolymers it was shown that the setting time was reduced with the increase of SiO_2/Na_2O ratio, from 490 min to 180 min, hence higher compressive strength was achieved, as shown in Fig. 2 [37,66,67]. Similar trend was also observed for volcanic ash based geopolymer partially replaced with metakaolin. With increase of SiO_2/Na_2O content in alkaline solution and increased content of metakaolin in the mixture, the initial setting time decreased from 500 min to 160 min for Z_D-metakaolin mixtures,

Fig. 2. Effect of SiO_2/Na_2O molar ratio of alkaline solution on setting time and 28 day compressive strength of Z_D and Z_G based geopolymer; after Tchakoute et al. [37].

while for Z_G-metakaolin geopolymer initial setting time decreased from 220 min to 125 min [45].

Tchakoute et al. studied the setting time of fused soda-volcanic ash based geopolymer. Fused soda-volcanic ash with varying overall Al_2O_3/Na_2O molar ratio was prepared by calcination of mixture at 550 °C for 1 h [53]. Results of setting time indicated that with decrease of Al_2O_3/Na_2O from 0.29 till 0.13, setting time decreased by 40 % (from 25 to 15 min), while with further decrease of Al_2O_3/Na_2O from 0.10 till 0.06 the setting time increased from 16 min to 20 min. The authors reported that these results were found to be in correlation with amount of amorphous phase calculated for each sample and compressive strength, furthermore, it was reported that excess of fused soda hindered the geopolymer synthesis process [48,68].

Influence of the particle size of volcanic ashes on the setting time of geopolymer paste was studied for volcanic ash samples milled for 30, 60, 90 and 120 min and it was reported that with increase of milling duration the initial setting time of geopolymer paste samples firstly decreased from 600< minutes for 30 min milling time to 150 min for 60 min milling time. With further increase of milling time to 90 min the initial setting time decreased to 15 min. However, with further increase of milling time to 120 min the setting time increased slightly to 22 min. The increase of milling time increases the fineness of particles and thus the dissolution rate increases. However, with excessive milling causes agglomeration of particles and recrystallization or polycondensation of glassy phase forms quartz, thus reducing the reactivity of pozzolan sample [32].

3. Physical and mechanical properties

3.1. Water absorption, bulk density and apparent porosity

Water absorption, bulk density and apparent porosity are the primary physical characteristics of the geopolymers. Many influencing factors for these three parameters were investigated. Effect of particle size, Na_2O/SiO_2 molar ratio, curing temperature and age of sample on water absorption, bulk density and apparent porosity have been studied.

Djobo et al. varied the milling time for Cameroonian volcanic ash samples between 30 and 120 min and reported that in most cases minimum bulk density and maximum water absorption and apparent porosity for the paste sample prepared with volcanic ash milled for 90 min was found at 28 days of age. No direct relationship between particle size and physical properties was examined. However, it was seen that with increasing curing temperature (27 °C, 45 °C and 60 °C) water absorption increased from 8.7 % to 11.4 %, apparent porosity increased from 17.5 % to 19.8 %, while bulk density decreased from 2105.6 kg/m^3 to 1798.5 kg/m^3 for Cameroonian volcanic ash based samples at 28 days of age [32]. However, the relation is not consistent with the results presented in [44], where with increase of curing temperature from 27 °C to 80 °C, decrease in water absorption and apparent porosity and increase in bulk density has been observed at 28 days of age. This apparent discrepancy could be due to different examined temperatures and different nature of tested samples. In later study, the temperature between 27 °C and 80 °C has not been studied. It can be assumed that with increase of curing temperature, initially water absorption and apparent porosity increases while bulk density decreases. However, with further increase of curing temperature the trend becomes opposite. It should also be noted that in [32] authors used paste samples while in [44] mortar samples were used. Nevertheless, detailed investigation is necessary to fill the gap of knowledge for paste and mortar samples.
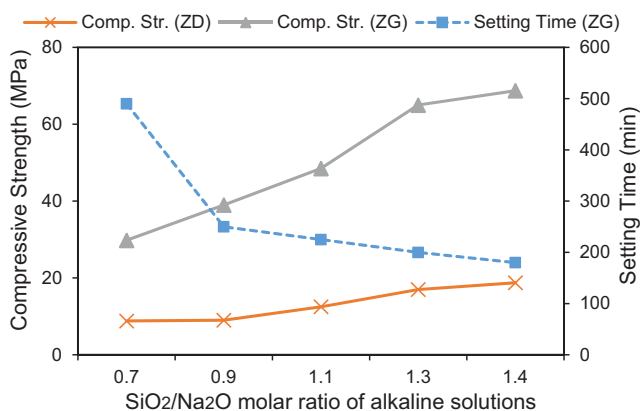
27

Influence of curing period was examined between 7 days and 180 days for mortar samples [44]. With increase of curing period from 7 days to 28 days, a gain in water absorption and apparent porosity was found. However, from 28 to 180 days the values of these two properties changed slightly. However, reverse trend for bulk density had been recorded. With increasing age of sample, bulk density decreased for samples cured at 27 °C, while no uniform trend has been seen for samples cured at 80 °C [44]. No clear influence of water to binder ratio on water absorption of geopolymer samples has been observed [58].

Silica modulus of activator solution has been found to effect the physical properties of geopolymer paste samples. Lemougna et al. studied the effect of Na_2O/SiO_2 molar ratio on the water absorption and bulk density of geopolymer paste samples. It has been reported that with increase or decrease of Na_2O/SiO_2 beyond optimum, the water absorption increases, while bulk density doesn't change appreciably with change of Na_2O/SiO_2 ratio. For optimum Na_2O/SiO_2 molar ratio of 0.25, minimum water absorption of 14.08 % and maximum bulk density of 1910 kg/m^3 was recorded [42].

Inclusion of aluminium and calcium by partial replacement of volcanic ash by bauxite or calcined oyster shell (both 0 to 30 %) respectively, leaded to a progressive increase of apparent porosity of the paste [47].

3.2. Compressive strength and indirect tensile strength

Factors affecting the degree of geopolymerization are particle size, type and concentration of alkali activator, pre-treatment of raw material and curing conditions [32,36,69]. Primary findings from different authors using volcanic ashes for geopolymerization are summarized in Table 3. It is seen that raw volcanic ash without any pre-treatment have poor reactivity due to low dissolution of volcanic ash in alkaline medium, therefore, pre-treatment of volcanic ashes like calcination, alkali fusion, mechanical activation and partial replacement with secondary cementitious materials is suggested [32,40,41,45,47,48,52–54,70]. Sodium hydroxide, sodium silicate, potassium hydroxide and potassium silicate are the majorly used alkali activator solutions [41].

Higher concentration of the activator improves the dissolution of the aluminosilicate and therefore, improves the mechanical properties. However, depending upon the type of activator, curing conditions and mineral type after reaching a certain content of alkali no significant increase in strength can be observed as shown in Fig. 3 [36,38].

The optimum concentration of alkalis should be determined from properties and economic point of view. Bondar et al. studied the effect of using various concentration of NaOH and KOH for Taftan pozzolan based geopolymer paste samples and found out that longer time or higher temperature is required for the sample with higher concentration of alkaline solution beyond 7.5 M concentration and unfavourable properties such as efflorescence and brittleness can enhance due to increased free alkali content in the binding system [36,71].
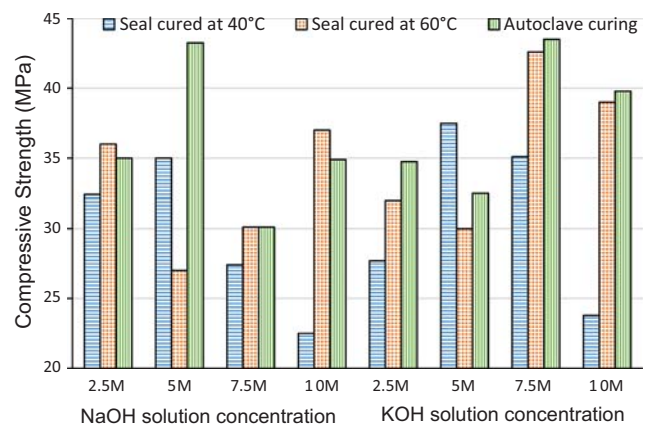

Fig. 3. Effect of type and concentration of activator on geopolymer compressive strength seal and cured at 40 °C, seal and cured at 60 °C and autoclave cured at 2 MPa pressure & 150 °C for 3 h; after Bondar et al. [36].

Table 3
Summary of primary findings and synthesis parameters studied on natural pozzolan based geopolymer.

Author	Raw material & Activation	Alkaline Solution Used	Curing Condition	Compressive Strength
Djobo et al. [32]	Mechanical activation of volcanic ash in ball mill	Na_2SiO_3/NaOH = 2.4, SiO_2/Na_2O = 1.4, Liquid/ash (mass) = 0.4	27, 45 and 60 °C for 24 h afterwards cured at room temperature in a plastic bag	0–37.4 MPa at 28 days 6.6–53.6 MPa at 90 days
Tchakoute et al. [37]	Volcanic ash of particle size 80 μm	SiO_2/Na_2O = 0.7, 0.9, 1.1, 1.3 and 1.4 liquid/solid = 0.49, 0.37, Na_2SiO_3 and NaOH	24 ± 3 °C	23–50 MPa at
Tekin [50]	Marble, travertine and volcanic ash waste crushed and grinded	NaOH 1, 5 and 10 M	22 ± 2 °C & 40 ± 5% R.H. 45 °C for 24 h after demoulding 75 °C for 24 h	46 MPa at 90 days
Bondar et al. [41]	Heat treated dacite and andesite ashes at 700 and 800 °C and ground to <75 μm	NaOH, KOH, Na_2SiO_3	20, 40, 60, and 80 °C	0–81 MPa at 28 days
Takedan et al. [38]	Volcanic ash with particle size <200 μm	8.5–16.5 M NaOH, Na_2SiO_3	50 °C and 80% relative humidity for 72 h.	80.1 MPa at 3 days
Villa et al. [11]	Homogenized zeolite sample	Na_2SiO_3/NaOH = 0.4, 1.5, 5, 10 and 15 ratios using 7 M NaOH, activator/ligand = 0.6	40, 60, and 80 °C	8–35 MPa at 90 days
Lemougna et al. [42]	Volcanic ash ground and sieved through a 400 μm mesh	Volcanic ash mixed with NaOH with Na_2O/SiO_2 = 0.15–0.35, water/ash = 0.21	Seal cured at 40 °C for 24 h, then unsealed cured at 40 °C for 24 h. Afterwards, samples were cured for 5 days in water and open air at 40, 70 and 90 °C	55 MPa at 7 days
Haddad & Alshbuol [49]	Basaltic Tuff of fineness in excess of 700 m^2/kg	Na_2SiO_3, NaOH (10, 12, 14 M)	40, 80 and 120 °C.	30 MPa at 28 days
Vogt et al. [51]	Volcanic tuff of Blaine fineness = 6000 cm^2/g	Na_2SiO_3 and 50% NaOH.	80 °C	22.7 MPa at 7 days

The modulus of sodium silicate (SiO_2/Na_2O) is an important parameter influencing the properties. Keeping the alkali content constant, the higher modulus of water glass promotes development of higher strength within a specific range due to greater contribution of silica. In other way, if the solid sodium silicate content is kept constant in a mixture then the effect of alkali activation is higher than silica. Therefore, it is necessary that an optimum modulus of sodium silicate is selected depending upon the raw material and curing condition. In general, a higher modulus is preferred; a lower modulus should be used only if the alkali activation is insufficient [36,51].

Curing conditions have been found to affect the geopolymerization as well. Higher curing temperature improves the mechanical properties by increasing the rate of dissolution at early ages but does not have much effect on final strength [11,32,72]. However, higher temperature curing also causes fast evaporation of water and propagation of shrinkage cracks, therefore, extended curing should be avoided [38,49,50]. Wet curing causes efflorescence in the samples [50].

The addition of reactive Al_2O_3 helps to improve the mechanical properties of the material by increasing the geopolymeric phase of the material which imprisons the unreacted/partially reacted crystalline phase of the starting material and thereafter, helping to reduce the efflorescence [54,73,74].

At early ages, alkali activated natural pozzolan concrete have lower static modulus of elasticity (SME) compared to OPC concrete. However, long term results indicated 5–20% higher SME for alkali activated natural pozzolan concrete than OPC concrete. SME for geopolymers is also affected by the curing temperature; higher curing temperature at early ages improves SME to a limit depending upon water to binder ratio. The higher curing temperature can cause evaporation of water, therefore, causing loss of strength due to incomplete geopolymerization and hence, lower SME [59]. SME has been found to increase with increased concentration of alkaline activator and the results have been found to be comparable to results of compressive strength [75]. For natural pozzolan based geopolymer mortar synthesised with varying concentration of NaOH, modulus of rupture of have been recorded between 0.732 MPa and 8.490 MPa, ultimate strain between 200 μe and 795 μe and modulus of elasticity between 3481 MPa and 21554 MPa [75].

Indirect tensile strength of geopolymer specimens have been found directly proportional to their compressive strength [59]. In comparison to ordinary Portland cement (OPC) concrete specimens, natural pozzolan based geopolymer concrete exhibit higher indirect tensile strength at later ages. At 7 days, the indirect tensile strength of natural pozzolan based geopolymer was 16.25% less in comparison to 7 days old OPC samples, while at 28 days it increased by 33.7% in comparison to OPC sample of same age [59]. The indirect tensile strength of natural pozzolan based geopolymer is greatly influenced by the curing temperature, as the tensile strength majorly depends on the bond between aggregate and gel. The higher temperature curing improves the strength of geopolymeric gel itself while it may not necessarily increase the interface between aggregate and gel, as at higher temperature and in sealed curing condition, water cannot reabsorb to enhance the matrix bonding properties particularly at the interface of matrix and aggregate [59].

4. Microstructural characteristics of hardened products

4.1. X-ray diffractometry (XRD)

Roughly after geopolymerization or alkaline activation reaction there is the possibility of formation of new crystalline phases and the disappearance of some minerals initially present in the alumi-

nosilicate. It is worth recalling that during geopolymerization or alkaline activation reaction the amorphous phase reacts preferentially to the crystalline phase. The mineralogical changes observed depend upon the type and composition of the alkaline solution, the type and content of calcium source in the mix design. One of the main change is the shift of the 2theta range characteristic of the glassy phase of natural pozzolan. In the case of natural pozzolan based geopolymer, which are obtained with high silica modulus (molar ratio $SiO_2/Na_2O > 1.4$) the changes observed are generally the decrease of peaks intensity and often the disappearance of minerals. For example, it was reported that nepheline and clay mineral-like muscovite, initially present in volcanic ash had taken part to the geopolymerization, while, for the other minerals only the peak intensity was affected [45]. The formation of new crystalline phases (generally hydrated minerals) occurs in the alkali-activated natural pozzolan system which are obtained with alkaline solution containing very low silica modulus (molar ratio $SiO_2/Na_2O < 1.4$) or by using only highly concentrated NaOH and KOH solution. The new crystalline phases formed include zeolite minerals type (hydroxysodalite, sodalite, sodium hydrogen silicate hydrate, potassium aluminium silicate hydrate, sodium aluminosilicate hydrate, sodium calcium aluminium silicate hydrate) and carbonate mineral like natrite (Na_2CO_3) [36,46,48,49,53,57,63].The new minerals were reported to be formed due to the reaction between the glassy phase and the alkali from the alkaline solution [46]. Moreover, in the system with additional calcium source calcium based hydrated minerals such as calcium silicate hydrate ($CaSiO_4H_2O$) can also be formed [46].

4.2. Fourier transform infrared (FTIR) spectroscopy

Table 4 summarizes the infrared bands assigned to various wavenumbers for natural pozzolan based geopolymers. During alkali activation, every bridging oxygen atom (BO) on the surface of the original aluminosilicate is replaced by two negatively charged non-bridging oxygen atoms (NBO), which are charge compensated by alkalis. As a result, the infrared (IR) band attributable to the T-O-Si asymmetric stretching vibration of the TO_4 tetrahedral of an aluminosilicate in glass has been found to shift to lower energy with increasing alkali content [36,51,76].

4.3. Mössbauer spectroscopy

The chemical composition of natural pozzolan showed it is constituted of up to 16 wt-% of iron oxide, and it was reported that iron takes part to the reaction [42,79]. In order to understand the behaviour of iron during alkaline activation of natural pozzolan [57]Fe Mössbauer spectroscopy of natural pozzolan has been studied by Lemougna et al. [43] the findings of that work involved the followings:

- The reactivity of iron depends on the form in which it is available in the material.
- Iron exists in its two-ionic form $Fe^{2+}$and Fe^{3+} it is contained in ferroan forsterite and augite mineral in both octahedral and tetrahedral geometry.
- After geopolymerization there is the conversion of some octahedral Fe^{2+} into tetrahedral Fe^{3+} suggesting their participation in the reaction.
- Finally, iron plays role of network forming and is beneficial for the development of strength.

4.4. ^{27}Al and ^{29}Si nuclear magnetic resonance (NMR)

This test has been used to address the structural changes that happen during geopolymerization of volcanic ash with varying silica modulus and curing temperature. The test results showed that

Table 4
Infrared (IR) bands attributed to natural pozzolan based geopolymers [35,37,45,47,54,56–57,62,64,76–78].

Assignments	Wave number (cm^{-1})		Comments
	Natural pozzolan	Natural pozzolan based geopolymer	
O–H Stretching	2917–2856, 3420	2360, 3410–3455	Strong band of surface adsorbed and chemical bound water
O–H Bending	1540, 1645–1667	1540, 1645–1667	Strong band of surface adsorbed and chemically bound water
O–C–O stretching	Absent	1407–1484	Strong band due to carbonation of free Na + into Na$_2$CO$_3$
Si–O–Si, Si–O–Al asymmetric stretching	1093–1000	968–1035 879–1027	Strong band. Bridging oxygen atom (BO) of the original aluminosilicate framework. After reaction the band shift to lower value indicating non-bridging oxygen atoms have replaced bridging oxygen atoms on the surface of aluminosilicate and is charge compensated by alkalis
Symmetric stretching Si–O–Si	798	798	Medium band
stretching Si–OH	Absent	882	Strong band appears in lesser polymerized product
Si–OH Bending	Absent	840–842	Strong band appears in lesser polymerized product
Stretching Al 6-coordinated geometry (Al$_{(VI)}$–OH & Al$_{(VI)}$–O)	736–916	Absent	Should disappear after polymerization
Si–O symmetric stretching	Absent	620–715	Should appear as shoulder only in polymerized product
Si–O–Si, Al–O–Si symmetric stretching	Absent	480–600	Should appear only in polymerized product

in ^{27}Al NMR spectra the characteristic peak (16 ppm) describing the Al in 6-fold coordination disappears after geopolymerization, indicating transformation to 4-fold coordination of Al atoms [35]. The main peak centred at 62 ppm in volcanic ash characteristic of Al in 4-fold coordination shifts to higher frequency after reaction indicating Al substituting Si atom in tetrahedral sites with 3 bridging oxygen [35,80]. For higher curing temperatures partial crystallization of amorphous phases is indicated by the increase of the peak widths [35].

^{29}Si have been found to provide better insight of the structural variation in the geopolymer matrix by change of silica modulus and curing temperature. The characteristic peak of Si in tetrahedral environment lies between −60 and −120 ppm frequency. The broad peaks indicate the Si(IV) in different environments [35,81]. The variation of silica modulus in geopolymer products shifts the main peak of Q^4 from −89 to −86 ppm after reaction, which occurs because of de-shielding due to decrease of mean electronic cloud around SiO$_4$ tetrahedra, increase of the mean Si-O bond length and decrease of mean Si–O–T (T = Si or Al) bond angle [35,82].

4.5. Thermogravimetric analysis (TGA)

Mass loss during thermogravimetric analysis can be used to measure the extent of geopolymerization. Higher overall mass loss relates to higher extent of geopolymerization [51]. The TGA curve can be divided into three stages as shown in Fig. 4. The first stage corresponds to evaporation of physically adsorbed water in the geopolymer matrix and appears before 100–150 °C [35]. The second stage starting from 150 °C till 600 °C corresponds to chemically bound water, which comes from dissolution of aluminosilicate raw materials to form aluminate and silicate species. So, this stage gives useful information about the extent of geopolymerization reaction [35,61,83]. However, TGA is not representative of chemical and nano-structural evolution taking place during reaction as it considers only the final reaction product [35,84]. This is the case of a recent study where authors observed and increase of the extent of reaction by isothermal calorimetry with decreasing silica modulus, but the TGA result showed different behaviour as the recorded mass losses between 150 and 600 °C were 2.14, 2.91 and 2.67% respectively for silica modulus of 1.66, 1.50 and 1.40 [35]. Therefore, it should be used carefully and preferably in combination with other analytical tests (FTIR, Calorimetry etc.) to give final conclusion. The total mass losses and temperature range of stage I and II depend on the synthesis conditions and to the reactivity of the initial ash. The values

recorded so far vary between 3.5 and 14 wt-% [35,46,56,57]. The third stage represents the mass loss due to decomposition of carbonates, whose effect decreases with yield of the reaction [46,51,61,83]. The latter stage is generally observed in the alkali activated system with high amount of calcium and sodium oxide (Na$_2$O) content. It should be noted that in the alkali activated system the temperature range of the stage I and II overlaps due to the incorporation of calcium in the binder composition [85]. The latter being the mixture of N-A-S-H, K-A-S-H, C-A-S-H, N-(C)-A-S-H and/ or C-S-H whose decomposition take place at very low temperature (below 250 °C) [42,46,57,86,87].

4.6. Scanning electron microscopy & energy dispersive X-ray spectroscopy (SEM/EDX)

The morphology and the composition of the resulting geopolymer matrix depends on the chemical composition of natural pozzolan, curing temperature and type of alkali activating solution and its SiO$_2$/Na$_2$O molar ratio. The different features generally observed in the micro-structure includes unreacted particles and reacted phases. The latter may be constituted of geopolymer phase, hydrated gel and new crystalline phases. The geopolymer phase is based on mixture of poly (ferro-sialate-siloxo), poly (ferro-sialate-disiloxo) and poly (ferro-sialate-multisiloxo) binder types with Ca^{2+}, Mg^{2+}, and Na$^+$ as charge-balancing cations [32,35]. The
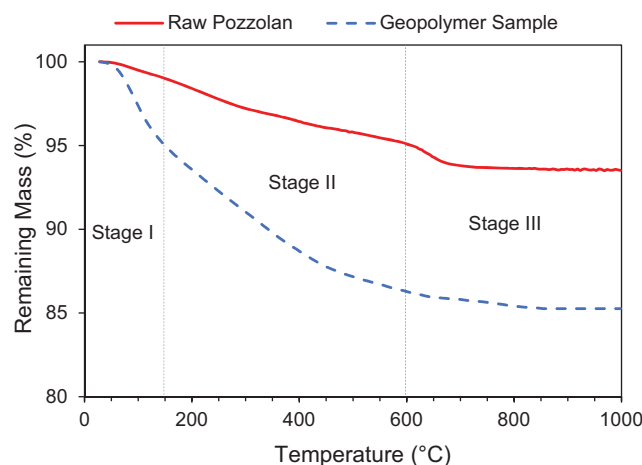
Fig. 4. Thermogravimetric curve representing 3 stages of mass loss [35,51].
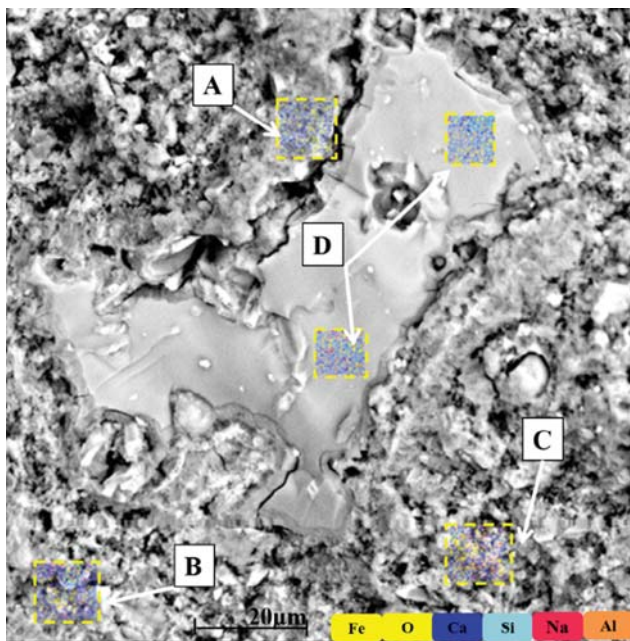
Fig. 5. High magnification combined SEM-EDS map of alkali-activated oyster shell-volcanic ash showing various phases: A) C–S–H gel; B) and C) various type of (N, C)–A–S–H gel; D) unreacted volcanic ash . adapted from [46]

hydrated phase is constituted of sodium or potassium aluminosilicate gel (N-A-S-H, K-A-S-H). Because of the presence of CaO in natural pozzolan and sometime when additional calcium source is added various types of hydrated phases sodium calcium aluminosilicate hydrate (N, C-A-S-H), calcium aluminosilicate hydrate (C-A-S-H) and calcium silicate hydrate (C-S-H) are formed. Higher curing temperatures result in micro-crystalline gel structure due to formation of zeolites while lower curing temperature results in more homogeneous gel [40]. Scanning electron microscope (SEM) images coupled with EDX results show distinguishable reacted phases and unreacted particles, as depicted in Fig. 5 [33,46]. With the increase in concentration of NaOH solution the gel structure becomes more dense with lesser amount of unreacted particles [46]. The undissolved particles in geopolymer matrix can cause formation of cracks, however, addition of optimum amount of Al_2O_3 helps to reduce the micro crack in geopolymer matrix [54]. Nevertheless, amount of Al_2O_3 beyond optimum exhibited much non-homogenous microstructure with cracks, this could be because of formation of octahedral Al at very high Al content which cannot incorporate into gel network [54].

5. Durability characteristics

Considering geopolymer binders as an alternative to OPC concrete, the durability characteristics of natural pozzolan based geopolymers should be studied in order to achieve dense, crack free micro-structure, low capillary porosity and fine pore structure [88]. As geopolymers are considered as environmental friendly binding materials, therefore, the durability characteristics of natural pozzolan based geopolymers are important to be studied.

5.1. Sulphate resistance

Bondar et al. studied the sulphate resistance of alkali activate natural pozzolan in 2.5% Na_2SO_4 and 2.5% $MgSO_4$ solution. Maximum loss of compressive strength recorded was 19.5% after 2 years of immersion in sulphate in solution. Maximum expansion

of 0.074% was recorded after 6 months of immersion. X-ray diffraction analysis of the samples immersed in sulphate solution was conducted by extruding the sample from surface and middle of the sample. Results indicate that mainly sodium aluminium sulphate ($Na_3Al(SO_4)_3$), langbeinite ($K_2Mg_2(SO_4)_3$), palyigorskite (($MgAl)_5(SiAl)_8O_{20}(OH)_2 \cdot 8H_2O$), leonite ($K_2Mg(SO_4)_2 \cdot 4H_2O$) and picomerite ($K_2Mg(SO_4)_2 \cdot 6H_2O$) minerals were formed because of the reaction with sulphate present in solution [58].

5.2. Acid resistance

Acid resistance of geopolymers have found to be closely related to the porosity of specimens, pore size diameter, connectivity of pores and presence of Na-rich gel in geopolymer gel structure [44]. It must note that the literature about this subject is very few. Till now there is only two published papers dealing with acid resistance of volcanic ash based geopolymers. This show the lack of information and the necessity for scientists to focus on this topic. The effects of adding calcium rich material (calcined oyster shell) and Al-rich material (bauxite) on 3% sulphuric acid resistance of volcanic ash based geopolymers were studied [47]. The authors reported a decrease from −2.32 to −1.91% of mass loss with the bauxite content up to 30 wt-%, and from −2.32 to −1.72 with only with 10 wt-% of calcined oyster shell added. This trend was due to the beneficial effect brought by these minerals additive on the extent of geopolymerization. Djobo et al. studied the influence of curing temperature on acid resistance of volcanic ash based geopolymers for 180 days in 5 wt-% H_2SO_4 solution [44]. For first 90 days, for samples cured at 27 °C and 80 °C the monthly mean rate of strength loss was recorded as 0 and 3.5% respectively, thereafter, the monthly mean rate of strength loss increased appreciably to 8 and 6% respectively. Maximum loss of strength for samples cured at 27 °C and 80 °C after 180 days of immersion in acidic solution was found to be 24% and 60% respectively, while ordinary Portland cement completely destroys under these conditions [44,89,90]. This result demonstrated that heat curing has detrimental effect on acid resistance of volcanic ash based geopolymer. Visually there was no surface degradation in samples till 180 days of immersion in acid, but the samples became only lighter in colour. The SEM combined with EDX analysis of samples immersed into sulfuric acid helped to identify gypsum as reaction product between sulphate from acid and calcium from volcanic ash. The formation of gypsum which was much prominent for heat cured samples was indicated as responsible of the higher strength losses compared to the sample cured at room temperature [44].

5.3. Corrosion of steel reinforcement

More alkalis present in geopolymers based on natural pozzolan makes the pH at the steel-concrete interface higher than normal OPC concrete. The pH value is normally higher then 10, which helps to improve the corrosion resistance [75,88]. However, further research is necessary to understand this parameter.

5.4. Permeability

The long term durability of concrete depends mainly on the pore network and their connectivity inside the concrete block. Thus the determination of the permeability has been found to be suitable test to assess the sustainability of concrete against aggressive agents (carbon dioxide, chloride etc.). It should be noticed that regarding geopolymer concrete from natural pozzolan there are only two research papers dealing with its transport properties capacity. The data available involve oxygen permeability and chloride penetration test.

Oxygen permeability of two Iranian natural pozzolan based geopolymers was determined by using 'cembureau permeameter' [88,91]. The results showed that oxygen permeability of natural pozzolan based geopolymers concrete varies with synthesis conditions and it ranges from 1.5×10^{-17} m^2 to 5×10^{-17} m^2 at 90 days. The authors concluded that natural pozzolan based geopolymers concrete exhibited 10–35% lower oxygen permeability compared to OPC concrete at 90 days. In the studied system, the oxygen permeability decreased with the curing temperature and extent of geopolymerization and decreased with the amount of water in the system. For the samples with lower water to binder ratio the rate of reduction of permeability was faster for 7 and 28 days of age and later was slowed down with age of sample. With increasing age of the sample permeability decreased at a higher rate of reduction at early ages. The lower water to binder ratio forms fewer capillary pores thus lower permeability. Permeability of the specimens also decreased with higher curing temperature, as higher curing temperature promotes the geopolymerization with higher dissolution and polymerization rate and water removal resulting in pore space blockage, hence a stronger structure with lower shrinkage is generated [88].

Pore structure and pore solution composition effects the rapid chloride permeability. Increase in temperature with high applied voltage, measurement before reaching steady state migration of current and passage of current by all ions in the pore solution makes the experimental implementation of rapid chloride permeability test (RCPT) difficult for the lower quality concretes as with higher passage of current at assigned voltage more heat is produced [75,88,92]. Therefore, Bondar et al. measured the rapid chloride permeability of natural pozzolan based geopolymer concrete samples according to ASTM C1202, [93], however, to reach the similar conditions as OPC mixtures the applied voltage was reduced to 20 V DC (up to 500 mA and 90 °C) instead of 60 V DC for OPC specimens for 6 h. While, Ghafoori et al. measured the RCPT of natural pozzolan based geopolymer mortar by reducing the voltage to 10 V. It was reported that with reduction of water to binder ratio the chloride permeability decreased for natural pozzolan based geopolymers by approximately 11% to 14% for 0.04% reduction in solution to binder ratio [75,88]. With increasing age of the samples, chloride permeability reduced with a higher rate of reduction at early ages [88]. Samples cured in sealed conditions showed 20% lower chloride permeability in comparison to samples cured in moist conditions [88]. With increasing concentration of alkaline activator the rapid chloride permeability has been found to decrease from 6308 C to 1054 C [75].

Long term chloride penetrability of natural pozzolan based geopolymer concrete was determined in accordance with ASTM C1556 [94], for saturated samples sealed from three sides. The only exposed surface was introduced to 2.8 M (16.25 wt-%) NaCl solution for 90 days. It should be noted that the average salinity of sea water is 3.5 wt-% [88]. The ground concrete samples were collected at every 5 mm depth by using lathe machine equipped with diamond-tipped bit. The total chloride content of the powdered samples was determined according to AASHTO T260 [88,95]. Results indicated that the total integral chloride ion penetrability of geopolymer concrete at 41 mm depth after 90 days is 0.63 to 1.13, which is in range of AASHTO T259 moderate to high (0.8–1.3) chloride ion penetrability [88,96]. The chloride penetrability was found to be lower in samples with lower water to binder ratio and is found to be 20% lower in samples cured at 40 °C with 20% lower water to binder ratio [88].

5.5. Shrinkage properties

Natural pozzolan based geopolymers have significantly lower drying shrinkage in comparison to the OPC concrete with same water to binder and cement to aggregate ratio [59,97,98]. The drying shrinkage of natural pozzolan based geopolymers depends on curing temperature, humidity and water to binder ratio. In sealed curing conditions, the higher water to binder ratio reduces the drying shrinkage [59]. For natural pozzolan based geopolymer concrete samples sealed cured at ambient temperature, with increase of water to binder ratio from 0.45 to 0.55 the drying shrinkage reduced from 1185×10^{-6} to 514×10^{-6} at 180 days [59]. Higher curing temperature also reduces the drying shrinkage which could be because of removal of water at higher temperature and further cross-linking of hydration product. The lowest amount of drying shrinkage reported was 239×10^{-6} and 161×10^{-6} for natural pozzolan based geopolymer with water to binder ratio of 0.45 and 0.55 respectively, seal cured at 60 °C [59]. Fog cured samples show higher amount of drying shrinkage because of retention of water in geopolymer matrix giving rise to more porous microstructure [59].

Kani and Allahverdi studied the effect of SiO$_2$/Na$_2$O molar ratio of natural pozzolan based geopolymer on the total shrinkage and found out that at constant Na$_2$O/Al$_2$O$_3$ molar ratio the total shrinkage at 90 days ranges between 0.29% and 0.83 % for SiO$_2$/Na$_2$O molar ratio less than 0.6 and with further increase of SiO$_2$/Na$_2$O molar ratio to 0.6 and beyond total shrinkage increases significantly from 1.52% to 4.81%. The acceptable value of total shrinkage for industrial application is less than 1% [62]. The total shrinkage also increased with increase of H$_2$O/Al$_2$O$_3$ molar ratio, and the changes occurred were more prominent compared to those happened because of varying Na$_2$O/Al$_2$O$_3$ molar ratio [62]. For Na$_2$O/Al$_2$O$_3$ molar ratio between 3.44 and 7.69 the linear shrinkage has been found to decrease, while with further increase of Na$_2$O/Al$_2$O$_3$ molar ratio the linear shrinkage increased which is associated with the gel characteristics of the geopolymer binder as linear shrinkage originates from the capillary tension with the gel framework [48,53]. Shrinkage control measurement was studied by curing the 1 and 7 days pre-cured samples hydrothermally at 85 °C for 20 h, and it was found that for all hydrothermally cured samples total shrinkage increased till 7 days and thereafter, became constant with age of sample. The most suitable results were obtained for hydrothermally cured samples after 1 day procuring, and the total shrinkage ranged between 0.26 and 0.46 % [62].

Thermal shrinkage of volcanic ash based geopolymers have been found to be approximately 2% after two cycles of heating up to 1000 °C and cooling, which is approximately 4 times lesser then metakaolin based geopolymers, indicating the suitability of these binders [42,57]. During first heating cycle, significant shrinkage has been observed for heating temperature up to 110 °C because of evaporation of less tightly bound water, after this for further heating of up to 600 °C, the sample behaves more or less stable [42,57]. During first cooling cycle, the already heated samples shrinks almost linearly at coefficient of thermal expansion of 8×10^{-6} K^{-1} to 16×10^{-6} K^{-1}. In second heating and cooling cycle, the thermal expansion coefficient has been recorded to be same as that in first cycle [42,57].

5.6. Wetting and drying cycles

Lemougna et al. investigated the compressive strength of alkali activated natural pozzolan in wet and dry condition [42,56,57]. The work showed that after 24 h immersion of samples into water (wet condition) there is a decrease of the compressive strength of up to 89%. But the compressive strength was partially or totally recovered when samples were dried overnight at 90 °C. This was attributed to the partial dissolution of Si-O-Na bond and hydrolysis of some silica bond –Si–O–Si– from hydrated minerals (zeolitic minerals) or silicate gel which are generally soluble into water. These were due to the presence of excess of alkali (Na$^+$) during the

synthesis. These observations were later confirmed by the work of Djobo et al. where alkali-activated volcanic ash with a calcium source (oyster shell) was tested [46]. The latter investigation reported a decrease of up to 50% of the compressive strength in wet condition for samples aged of 180 days. All these previous works reported only the 24 h immersion into water on strength evolution. Recently a more comprehensive studied on the performance of 28 days aged volcanic ash based geopolymer mortars specimens in 25 wetting and drying cycles was reported. Considering one cycle of drying and wetting as drying specimens at 65 °C for 24 h followed by soaking in water at room temperature for 24 h. Results indicate that samples cured at 27 °C had 24% reduction in compressive strength after 25 cycles while samples cured at 80 °C had 14% reduction in compressive strength, with no visual deterioration up to 25 cycles of wetting and drying [44]. These works showed that volcanic ash based geopolymers mortars performed well in dry and wet condition and are suitable for severe hot and dry climate.

6. Applications

Geopolymer mortar samples lie within the ASTM recommendation of building materials. While heating up to 900 °C geopolymer samples lost 40% of their initial compressive strength and shrank slowly, which indicates the suitability of these materials for low grade refractories and potential building material [35,42]. Geopolymers formed by mixture of volcanic tuff and NaOH (14 M) had an Zn^{2+} uptake efficiency of 97.78% against 78.51% volcanic tuff and uptake capacity of 8.15 and 6.54 mg/g respectively, at pH of 7 dosage of 0.7 g and therefore, have been found feasible for removal of heavy metals [99]. In a more recent study on the natural zeolite based foamed geopolymer concrete, it is recommended that zeolite based geopolymers are suitable for household masonry wall construction according to NTE 638 and NTE 643 Ecuadorian construction technical standards [78].

7. Conclusions

Natural pozzolans can be used as potential raw material for geopolymer synthesis because of their huge availability in nature, lower cost associated with extraction and comparatively lower environmental footprint. The extend of geopolymerization increases with the increase of curing temperature giving higher compressive strength at early ages with no significant impact on later age strength, however, addition of other cementitious materials helps to improve the mechanical and durability properties of these geopolymers. The work presented here describes the suitability of natural pozzolan based geopolymer as alternative binder, however, for practical application of these binder additional research studies should be conducted such as rheological characteristics, freeze thaw resistance, carbonation, alkali silica reaction, light weight geopolymer concrete, fibre reinforced geopolymer concrete and geopolymer concrete for special applications. Greater number of efforts are needed to establish standard testing procedures for geopolymer cement and concrete. Life cycle analysis (LCA) of natural pozzolan based geopolymers should be carried out to investigate the sustainability and role in reduction of greenhouse gases.

Conflit of interest

The authors declare that they have no conflict of interest.

References

[1] C. Shi, P.V. Krivenko, D. Roy, Alkali-Activated Cements and Concretes, Taylor & Francis Group, Abingdon, 2006.
[2] P.C. Hewlett (Ed.), Lea's Chemistry of Cement and Concrete, fourth ed., Elsevier Ltd., 1988.
[3] J. Newman, B.S. Choo (Eds.), Advanced Concrete Technology, Constituent Materials, Elsevier Science Ltd., Oxford, UK, 2003.
[4] R. Siddique, Effect of volcanic ash on the properties of cement paste and mortar, Resour. Conserv. Recycl. 56 (2011) 66–70.
[5] G. Cai, T. Noguchi, H. Degée, J. Zhao, R. Kitagaki, Volcano-related materials in concretes: a comprehensive review, Environ. Sci. Pollut. Res. Int. 23 (2016) 7220–7243.
[6] J.N.Y. Djobo, A. Elimbi, H.K. Tchakouté, S. Kumar, Volcanic ash-based geopolymer cements/concretes: the current state of the art and perspectives, Environ. Sci. Pollut. Res. Int. 24 (2017) 4433–4446.
[7] J.L. Provis, J.S.J. van Deventer, Alkali Activated Materials, State-of-the-Art Report, RILEM TC 224-AAM, Springer, Dordrecht Heidelberg New York London, 2014.
[8] J. Davidovits, Geopolymer Chemistry and Applications, Institut Géopolymère, 16 rue Galilée F-02100 Saint-Quentin, France, 2008.
[9] J. Davidovits, in: Properties of Geopolymer Cements, First International Conference on Alkaline Cements and Concretes, Scientific Research Institute on Binders and Materials, State Technical University, Kiev, 1994, pp. 131–149.
[10] J. Tailby, K.J.D. MacKenzie, Structure and mechanical properties of aluminosilicate geopolymer composites with Portland cement and its constituent minerals, Cem. Concr. Res. 40 (2010) 787–794.
[11] C. Villa, E.T. Pecina, R. Torres, L. Gómez, Geopolymer synthesis using alkaline activation of natural zeolite, Constr. Build. Mater. 24 (2010) 2084–2090.
[12] M. Izquierdo, X. Querol, J. Davidovits, D. Antenucci, H. Nugteren, C. Fernández-Pereira, Coal fly ash-slag-based geopolymers: Microstructure and metal leaching, J. Hazard. Mater. 166 (2009) 561–566.
[13] F. Pacheco-Torgal, J.A. Labrincha, C. Leonelli, A. Palomo, P. Chindaprasirt (Eds.), Handbook of Alkali-activated Cements, Mortars and Concretes, Woodhead Publishing, Cambridge, Philadelphia, PA, 2012.
[14] H. Kühl, Slag cement and process of making the same, US Patent 900,939 (1908).
[15] L. Chassevent, Hydraulicity of slags, Compt. Rend. 205 (1937) 670–672.
[16] A.O. Purdon, The action of alkalis on blast-furnace slag, J. Soc. Chem. Ind. (1940) 191–202.
[17] A. Buchwald, M. Vanooteghem, E. Gruyaert, H. Hilbig, N. de Belie, Purdocement: application of alkali-activated slag cement in Belgium in the 1950s, Mater. Struct. 48 (2015) 501–511.
[18] V.D. Glukhovsky, Soil Silicates (Gruntosilikaty), USSR Budivelnik Publisher, Kiev, 1959.
[19] V.D. Glukhovsky, Soil Silicates, their Properties, Technology of Manufacturing and Field of Application Doct. Tech. Sc. Degree Thesis, Kiev Civil Engineering Institute, Kiev, USSR, 1965.
[20] P. Duxson, A. Fernández-Jiménez, J.L. Provis, G.C. Lukey, A. Palomo, J.S.J. van Deventer, Geopolymer technology: The current state of the art, J. Mater. Sci. 42 (2007) 2917–2933.
[21] J.L. Provis, J.S.J. van Deventer (Eds.), Geopolymers – Structure, Processing, Properties and Industrial Applications, Woodhead Publishing Limited, 2009.
[22] A. Palomo, M.W. Grutzeck, M.T. Blanco, Alkali-activated fly ashes A cement for the future, Cem. Concr. Res. 29 (1999) 1323–1329.
[23] V. Glukhovsky, Ancient, modern and future concretes, First International Conference Alkaline Cements and Concretes, Kiev, 1994 pp. 1–8.
[24] A. Mehta, R. Siddique, An overview of geopolymers derived from industrial by-products, Constr. Build. Mater. 127 (2016) 183–198.
[25] N. Ukrainczyk, O. Vogt, E.A.B. Koenders, Geopolymer rom mixture of Trass and (Meta-) Kaolin, 2nd International Conference on the Chemistry of Construction Materials, GDCh division of Construction chemistry, Munich, Germany, 2016.
[26] ASTM C 618 – 01, Standard Specification for Coal Fly Ash and Raw or Calcined Natural Pozzolan for Use as a Mineral Admixture in Concrete, American Society for Testing and Materials, 100 Barr Harbor Drive, West Conshohocken, PA 19428-2959, United States, 2001.
[27] M.B. Sharif, R. Firdous, M.A. Tahir, Development of local bagasse ash as pozzolanic material for use in concrete, Pak. J. Eng. Appl. Sci. 17 (2015) 39–45.
[28] R. Firdous, M.B. Sharif, Performance of thermally activated sugarcane bagasse ash as supplementary cementitious material, NED Univ. J. Res. XII (2) (2016) 23–30.
[29] W.I. Rose, A.J. Durant, Fine ash content of explosive eruptions, J. Volcanol. Geotherm. Res. 186 (2009) 32–39.
[30] M. Nakagawa, T. Ohba, Minerals in volcanic ash 1: primary minerals and volcanic glass, Global Environ. Res. 6 (2002) 41–51.

[31] E. Barrie, V. Cappuyns, E. Vassilieva, R. Adriaens, S. Hollanders, D. Garcés, C. Paredes, Y. Pontikes, J. Elsen, L. Machiels, Potential of inorganic polymers (geopolymers) made of halloysite and volcanic glass for the immobilisation of tailings from gold extraction in Ecuador, Appl. Clay Sci. 109–110 (2015) 95–106.

[32] J.N.Y. Djobo, A. Elimbi, H.K. Tchakouté, S. Kumar, Mechanical activation of volcanic ash for geopolymer synthesis: effect on reaction kinetics, gel characteristics, physical and mechanical properties, R. Soc. Chem. (RSC Adv.) 6 (2016) 39106–39117.

[33] B.I. Djon Li Ndjock, A. Elimbi, M. Cyr, Rational utilization of volcanic ashes based on factors affecting their alkaline activation, J. Non-Crystall. Solids. 463 (2017) 31–39.

[34] P.N. Lemougna, K.-T. Wang, Q. Tang, U.C. Melo, X.-M. Cui, Recent developments on inorganic polymers synthesis and applications, Ceram. Int. 42 (2016) 15142–15159.

[35] J.N.Y. Djobo, A. Elimbi, H.K. Tchakouté, S. Kumar, Reactivity of volcanic ash in alkaline medium, microstructural and strength characteristics of resulting geopolymers under different synthesis conditions, J. Mater. Sci. 51 (2016) 10301–10317.

[36] D. Bondar, C.J. Lynsdale, N.B. Milestone, N. Hassani, A.A. Ramezanianpour, Effect of type, form, and dosage of activators on strength of alkali-activated natural pozzolan, Cem. Concr. Compos. 33 (2011) 251–260.

[37] H.K. Tchakoute, A. Elimbi, E. Yanne, C.N. Djangang, Utilization of volcanic ashes for the production of geopolymers cured at ambient temperature, Cem. Concr. Compos. 38 (2013) 75–81.

[38] H. Takeda, S. Hashimoto, H. Kanie, S. Honda, Y. Iwamoto, Fabrication and characterization of hardened bodies from Japanese volcanic ash using geopolymerization, Ceram. Int. 40 (2014) 4071–4076.

[39] D. Bondar, C.J. Lynsdale, N.B. Milestone, N. Hassani, A.A. Ramezanianpour, Geopolymer cement from alkali-activated natural pozzolans: effect of addition of minerals, in: Second International Conference on Sustainable Construction Materials and Technologies, Ancona, Italy, 2010.

[40] D. Bondar, C.J. Lynsdale, N.B. Milestone, N. Hassani, A.A. Ramezanianpour, Effect of adding mineral additives to alkali-activated natural pozzolan paste, Constr. Build. Mater. 25 (2011) 2906–2910.

[41] D. Bondar, C.J. Lynsdale, N.B. Milestone, N. Hassani, A.A. Ramezanianpour, Effect of heat treatment on reactivity-strength of alkali-activated natural pozzolans, Constr. Build. Mater. 25 (2011) 4065–4071.

[42] P.N. Lemougna, K.J.D. MacKenzie, U.C. Melo, Synthesis and thermal properties of inorganic polymers (geopolymers) for structural and refractory applications from volcanic ash, Ceram. Int. 37 (2011) 3011–3018.

[43] P.N. Lemougna, K.J.D. MacKenzie, G.N.L. Jameson, H. Rahier, U.F. Chinje Melo, The role of iron in the formation of inorganic polymers (geopolymers) from volcanic ash: a ^{57}Fe Mössbauer spectroscopy study, J. Mater. Sci. 48 (2013) 5280–5286.

[44] J.N.Y. Djobo, A. Elimbi, H. Kouamo Tchakouté, S. Kumar, Mechanical properties and durability of volcanic ash based geopolymer mortars, Constr. Build. Mater. 124 (2016) 606–614.

[45] J.N.Y. Djobo, L.N. Tchadjié, H.K. Tchakoute, B.B.D. Kenne, A. Elimbi, D. Njopwouo, Synthesis of geopolymer composites from a mixture of volcanic scoria and metakaolin, J. Asian Ceram. Soc. 2 (2014) 387–398.

[46] J.N.Y. Djobo, H.K. Tchakouté, N. Ranjbar, A. Elimbi, L.N. Tchadji, D. Njopwouo, Gel composition and strength properties of alkali-activated oyster shell-volcanic ash: effect of synthesis conditions, J. Am. Ceram. Soc. 99 (2016) 3159–3166.

[47] Y.J.N. Djobo, A. Elimbi, J. Dika Manga, I.B. Djon, Li. Ndjock, Partial replacement of volcanic ash by bauxite and calcined oyster shell in the synthesis of volcanic ash-based geopolymers, Constr. Build. Mater. 113 (2016) 673–681.

[48] H.K. Tchakoute, A. Elimbi, B.B. Diffo Kenne, J.A. Mbey, D. Njopwouo, Synthesis of geopolymers from volcanic ash via the alkaline fusion method: effect of Al$_2$O$_3$/Na$_2$O molar ratio of soda–volcanic ash, Ceram. Int. 39 (2013) 269–276.

[49] R.H. Haddad, O. Alshbuol, Production of geopolymer concrete using natural pozzolan: a parametric study, Constr. Build. Mater. 114 (2016) 699–707.

[50] I. Tekin, Properties of NaOH activated geopolymer with marble, travertine and volcanic tuff wastes, Constr. Build. Mater. 127 (2016) 607–617.

[51] O. Vogt, N. Ukrainczyk, F. Röser, E. Steindlberger, E.A.B. Koenders, Geopolymerisation Activity of Eifel Tuff, in: II International Conference on Concrete Sustainability (ICCS16), Madrid, Spain, pp. 653–662, 2016.

[52] M.H. Cornejo, J. Elsen, C. Paredes, H. Baykara, Thermomechanical treatment of two Ecuadorian zeolite-rich tuffs and their potential usage as supplementary cementitious materials, J. Therm. Anal. Calorim. 115 (2014) 309–321.

[53] H.K. Tchakoute, J.A. Mbey, A. Elimbi, B.B. Kenne Diffo, D. Njopwouo, Synthesis of volcanic ash-based geopolymer mortars by fusion method: effects of adding metakaolin to fused volcanic ash, Ceram. Int. 39 (2013) 1613–1621.

[54] H.K. Tchakoute, A. Elimbi, J.A. Mbey, C.J.N. Sabouang, D. Njopwouo, The effect of adding alumina-oxide to metakaolin and volcanic ash on geopolymer products: a comparative study, Constr. Build. Mater. 35 (2012) 960–969.

[55] H.K. Tchakouté, S. Kong, J.N.Y. Djobo, L.N. Tchadjié, D. Njopwouo, A comparative study of two methods to produce geopolymer composites from volcanic scoria and the role of structural water contained in the volcanic scoria on its reactivity, Ceram. Int. 41 (2015) 12568–12577.

[56] P.N. Lemougna, U.F. Chinje Melo, M.-P. Delplancke, H. Rahier, Influence of the chemical and mineralogical composition on the reactivity of volcanic ashes during alkali activation, Ceram. Int. 40 (2014) 811–820.

[57] P.N. Lemougna, U.F. Chinje Melo, M.-P. Delplancke, H. Rahier, Influence of the activating solution composition on the stability and thermo-mechanical properties of inorganic polymers (geopolymers) from volcanic ash, Constr. Build. Mater. 48 (2013) 278–286.

[58] D. Bondar, C.J. Lynsdale, N.B. Milestone, N. Hassani, Sulfate resistance of alkali activated pozzolans, Int. J. Concr. Struct. Mater. 9 (2015) 145–158.

[59] D. Bondar, C.J. Lynsdale, N.B. Milestone, N. Hassani, A.A. Ramezanianpour, Engineering properties of alkali-activated natural pozzolan concrete, ACI Mater. J. 0108-M08 (2011) 1–9.

[60] N.U. Auqui, H. Baykara, A. Rigail, M.H. Cornejo, J.L. Villalba, An investigation of the effect of migratory type corrosion inhibitor on mechanical properties of zeolite-based novel geopolymers, J. Mol. Struct. 1146 (2017) 814–820.

[61] H. Baykara, M.H. Cornejo, R. Murillo, A. Gavilanes, C. Paredes, J. Elsen, Preparation, characterization and reaction kinetics of green cement: ecuadorian natural mordenite-based geopolymers, Mater. Struct. 50 (2017) 17.

[62] E.N. Kani, A. Allahverdi, Investigating shrinkage changes of natural pozzolan based geopolymer cement paste, Iran. J. Mater. Sci. Eng. 8 (2011) 50–60.

[63] J. Moon, S. Bae, K. Celik, S. Yoon, K.-H. Kim, K.S. Kim, P.J.M. Monteiro, Characterization of natural pozzolan-based geopolymeric binders, Cem. Concr. Compos. 53 (2014) 97–104.

[64] D.M. González-García, L. Téllez-Jurado, F.J. Jiménez-Álvarez, H. Balmori-Ramírez, Structural study of geopolymers obtained from alkali-activated natural pozzolan feldspars, Ceram. Int. 43 (2017) 2606–2613.

[65] E.N. Kani, A. Allahverdi, J.L. Provis, Calorimetric study of geopolymer binders based on natural pozzolan, J. Therm. Anal. Calorim. 127 (2017) 2181–2190.

[66] E.N. Kani, A. Allahverdi, Effect of chemical composition on basic engineering properties of inorganic polymeric binder based on natural pozzolan, Ceramics – Silikáty 53 (2009) 195–204.

[67] A. Allahverdi, K. Mehrpour, E. Najafi Kani, Taftan Pozzolan-Based Geopolymer Cement, IUST Int. J. Eng. Sci. Chem. Civ. Eng. 19 (3) (2008) 1–5.

[68] P. Chindaprasirt, U. Rattanasak, Utilization of blended fluidized bed combustion (FBC) ash and pulverized coal combustion (PCC) fly ash in geopolymer, Waste Manage. (Oxford) 30 (2010) 667–672.

[69] B. Singh, G. Ishwarya, M. Gupta, S.K. Bhattacharyya, Geopolymer concrete: a review of some recent developments, Constr. Build. Mater. 85 (2015) 78–90.

[70] R.A. Robayo, R. Mejía de Gutiérrez, M. Gordillo, Natural pozzolan-and granulated blast furnace slag-based binary geopolymers, Mater. Constr. 66 (2016) e077.

[71] A. Allahverdi, K. Mehrpour, E.N. Kani, Investigating the possibility of utilizing pumice-type natural pozzonal in production of geopolymer cement, Ceramics – Silikáty 52 (2008) 16–23.

[72] E.N. Kani, A. Allahverdi, Effects of curing time and temperature on strength development of inorganic polymeric binder based on natural pozzolan, J. Mater. Sci. 44 (2009) 3088–3097.

[73] R.A. Robayo-Salazar, R. Mejía de Gutiérrrez, F. Puertas, Effect of metakaolin on natural volcanic pozzolan-based geopolymer cement, Appl. Clay Sci. 132–133 (2016) 491–497.

[74] E.N. Kani, A. Allahverdi, J.L. Provis, Efflorescence control in geopolymer binders based on natural pozzolan, Cem. Concr. Compos. 34 (2012) 25–33.

[75] N. Ghafoori, M. Najimi, B. Radke, Natural pozzolan-based geopolymers for sustainable construction, Environ. Earth Sci. 75 (2016) 55.

[76] W.K.W. Lee, J.S.J. van Deventer, Use of infrared spectroscopy to study geopolymerization of heterogeneous amorphous aluminosilicates, Langmuir 19 (2003) 8726–8734.

[77] L.N. Tchadji, J.N.Y. Djobo, N. Ranjbar, H.K. Tchakout, B.B.D. Kenne, A. Elimbi, D. Njopwouo, Potential of using granite waste as raw material for geopolymer synthesis, Ceram. Int. 42 (2016) 3046–3055.

[78] J.L.V. Lynch, H. Baykara, M. Cornejo, G. Soriano, N.A. Ulloa, Preparation, characterization, and determination of mechanical and thermal stability of natural zeolite-based foamed geopolymers, Constr. Build. Mater. 172 (2018) 448–456.

[79] E. Kamseu, C. Leonelli, D.S. Perera, U.C. Melo, P.N. Lemougna, Investigation of volcanic ash based geopolymers as potential building materials, INTERCERAM 58 (2009) 136–140.

[80] H. Rahier, J. Wastiels, M. Biesemans, R. Willlem, G. van Assche, B. van Mele, Reaction mechanism, kinetics and high temperature transformations of geopolymers, J. Mater. Sci. 42 (2007) 2982–2996.

[81] K.J.D. MacKenzie, M.E. Smith, A. Wong, A multinuclear MAS NMR study of calcium-containing aluminosilicate inorganic polymers, J. Mater. Chem. 17 (2007) 5090.

[82] K.J.D. MacKenzie, M.E. Smith, Multinuclear Solid-State NMR of Inorganic Materials, Elsevier Science Ltd., Oxford, UK, 2002.

[83] A. Nikolov, I. Rostovsky, H. Nugteren, Geopolymer materials based on natural zeolite, Case Stud. Constr. Mater. 6 (2017) 198–205.

[84] Z. Zhang, J.L. Provis, H. Wang, F. Bullen, A. Reid, Quantitative kinetic and structural analysis of geopolymers. part 2. thermodynamics of sodium silicate activation of metakaolin, Thermochim. Acta 565 (2013) 163–171.

[85] S.A. Bernal, E.D. Rodríguez, R. Mejía de Gutiérrez, M. Gordillo, J.L. Provis, Mechanical and thermal characterisation of geopolymers based on silicate-activated metakaolin/slag blends, J. Mater. Sci. 46 (2011) 5477–5486.

[86] L. Alarcon-Ruiz, G. Platret, E. Massieu, A. Ehrlacher, The use of thermal analysis in assessing the effect of temperature on a cement paste, Cem. Concr. Res. 35 (2005) 609–613.

[87] J.L. Provis, Geopolymers and other alkali activated materials: why, how, and what?, Mater Struct. 47 (2014) 11–25.

[88] D. Bondar, C.J. Lynsdale, N.B. Milestone, N. Hassani, Oxygen and chloride permeability of alkali-activated natural pozzolan concrete, ACI Mater. J. 109-M06 (2012) 1–10.

[89] T. Bakharev, Resistance of geopolymer materials to acid attack, Cem. Concr. Res. 35 (2005) 658–670.

[90] M. Alexander, A. Bertron, N. de Belie (Eds.), RILEM State-of-the-Art Report "Performance of Cement-Based Materials in Aggressive Aqueous Environments", RILEM TC 211-PAE, 2013.

[91] M. Carcassès, A. Abbas, J.-P. Ollivier, J. Verdier, An optimised preconditioning procedure for gas permeability measurement, Mater. Struct. 35 (2002) 22–27.

[92] R.I.A. Malek, D.M. Roy, in: The Permeability of Chloride Ions in Fly Ash-Cement Pastes Mortars and Concrete, Material Research Society Proceedings Pittsburgh, PA 113, 1996, pp. 291–300.

[93] ASTM C 1202 –97, Standard Test Method for Electrical Indication of Concrete's Ability to Resist Chloride Ion Penetration, American Society for Testing and Materials, 100 Barr Harbor Drive, West Conshohocken, PA 19428-2959, United States, 1997.

[94] ASTM C 1556 – 03, Standard Test Method for Determining the Apparent Chloride Diffusion Coefficient of Cementitious Mixtures by Bulk Diffusion, American Society for Testing and Materials, 100 Barr Harbor Drive, West Conshohocken, PA 19428-2959, United States, 2003.

[95] AASHTO T260 – 94, Standard Method for Sampling and Testing for Chloride Ion in Concrete and Concrete Raw Materials, American Association of State Highway and Transportation Officials, Washington DC, 1994.

[96] AASHTO T259 – 80, Standard Method of Test for Resistance of Concrete to Chloride Ion Penetration, American Association of State Highway and Transportation Officials, Washington DC, 1980.

[97] M.S. Shetty, Concrete Technology Theory and Practice, S. CHAND & COMPANY LTD., Ram Nagar, New Delhi, 2005.

[98] J. Newman, B.S. Choo (Eds.), Advanced Concrete Technology, Concrete Properties, Elsevier Science Ltd., Oxford, UK, 2003.

[99] K.K. Al-Zboon, B.M. Al-smadi, S. Al-Khawaldh, Natural volcanic tuff-based geopolymer for Zn removal: adsorption isotherm kinetic, and thermodynamic study, Water Air Soil Pollut. 227 (2016) 3580.

35

2.2. Effect of silica modulus on the geopolymerization activity of natural pozzolans
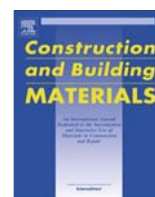
Effect of silica modulus on the geopolymerization activity of natural pozzolans

Rafia Firdous, Dietmar Stephan *

Technische Universität Berlin, Department of Civil Engineering, Building Materials and Construction Chemistry, Gustav-Meyer-Allee 25, 13355 Berlin, Germany

HIGHLIGHTS

- Synthesis of geopolymers from natural pozzolans.
- Silica modulus effects the reaction kinetics and rate of reaction.
- Much lower and higher silica moduli have an adverse effect on geopolymer product.
- Amorphous and crystalline phases partially dissolve in the alkaline medium.
- Optimum silica moduli depend on the composition of natural pozzolan.

ARTICLE INFO

ABSTRACT

The present study evaluates the effect of silica modulus on the reaction kinetics, degree of reaction and phase composition of natural pozzolan-based geopolymers. Six natural pozzolan samples have been subjected to geopolymer synthesis in the alkaline medium using sodium hydroxide and sodium silicate solutions at ambient conditions. Reaction kinetics studied by isothermal conduction calorimetry show that the early age dissolution of aluminate and silicate species depends on the SiO_2 and Na_2O molar content of the alkaline solution. The degree of reaction increases with the reduction of silica modulus. However, the reduction of silica modulus beyond certain limit has a negative influence on the mechanical properties of resultant geopolymers. The optimum silica modulus requirement depends on the mineralogical composition of the raw sample used. The rate of partial dissolution of semi-crystalline and crystalline mineral phases present in natural pozzolan depends on the silica modulus of the alkaline solution used.

© 2019 Elsevier Ltd. All rights reserved.

1. Introduction

Geopolymers are a class of inorganic binders which are characterized as semi-crystalline aluminosilicate materials and can be synthesised by reaction of aluminosilicate precursor with a concentrated alkali metal silicate or hydroxide solution [1–3]. The structure of geopolymer consists of aluminosilicate chains where aluminium and silicon atoms are tetrahedrally bound by shared oxygen atoms [1,3–5]. Owing to their good mechanical and durability properties, geopolymers have gained much attention in the last decades. Geopolymers have comparatively lower greenhouse gas emissions compared to conventional OPC-based binders which make them a foreseeable material for future [6–9]. Natural pozzolans are a tremendous source of silica and alumina. In addition, low cost associated with mining and transportation of natural pozzolans make them suitable precursor for geopolymer synthesis [10]. This material is widely available in countries with past or present volcanic activities. Several works have successfully reported the utilization of natural pozzolans of volcanic origin as geopolymer precursor. However, elucidating the criterion prevailing the reactivity of natural pozzolans in alkaline medium is still not completely understood. The microstructure, chemical, mechanical, physical and thermal properties of geopolymers depend upon the type of raw material used [1].

Several studies on the use of various volcanic ashes as geopolymer precursor have been conducted and reported that their reactivity varies considerably depending on the specific surface area, SiO_2/Al_2O_3 ratio of the amorphous phase and amount of amorphous phase [11–13]. Type of alkaline activator used has also been reported to affect the properties of resultant geopolymers. Use of KOH solution led to thermally more stable geopolymer product while the use of NaOH solution imparts higher reaction rate and therefore, higher compressive strength [14]. Use of sodium silicate

* Corresponding author.
E-mail address: stephan@tu-berlin.de (D. Stephan).

in alkaline solution enhances the mechanical properties and workability of geopolymer samples [15,16]. However, Lemougna et al. [14] reported that the variation of the composition of an alkaline solution has no substantial effect on compressive strength, which is in contradiction to other literature [10,16]. Effect of water to binder ratio for constant silica modulus has also been discussed in the literature. For higher Na_2O content the increasing water to binder ratio resulted in a drop of compressive strength and reduction in flowability, while this effect is not pronounced for lower Na_2O content [17,18]. However, the samples enriched in Na content exhibited efflorescence [13].

Geopolymerization of natural pozzolans is an exothermic process, and the reaction is characterized by a single exothermic peak [19,20]. Further, the reactivity of volcanic ashes has been reported to be lower than fly ash and metakaolin, but a higher concentration of the alkaline solution and increased curing temperature slightly helps in increasing the reactivity of volcanic ash [20–22]. Other ways to improve the mechanical properties include calcination of the raw sample, and partial replacement by secondary cementitious material as the deficiencies in silica, alumina and lime content of natural pozzolans can be compensated by the addition of mineral additives [23–26].

In the aforementioned studies, natural pozzolans originating from various countries including Cameroon, Colombia, Iran, Japan, Jordan, Kuwait, Saudi Arabia, Turkey and the USA have been utilized for synthesizing geopolymer materials. However, natural pozzolans from European countries have not been extensively studied yet for geopolymer synthesis. It is known that the final properties of geopolymers depend on the reactivity of natural pozzolan (which is closely related to the source) and the composition of the alkaline solution. Therefore, it is needed to find general synthesis conditions for natural pozzolan-based geopolymers. For the purpose, investigation of materials from other countries is necessary. Moreover, most of the works dealt with the effect of varying alkali type, concentration and curing condition on the geopolymeric potential of natural pozzolan, composition and final properties of resulting products with limited information available on the reaction kinetics and degree of reaction with varying the composition of the alkaline solution.

The present work aims at using six different natural pozzolans with comparable specific surface area, cured at ambient condition with several silica moduli of alkaline solutions and studying their effect on the mechanical properties, reaction kinetics, degree of reaction and reactivity of mineral phases. For this purpose, 16 different silica moduli in the range of 0.4–1.7 have been used to study the mechanical properties, and 12 different silica moduli have been chosen to study the degree of reaction and reaction kinetics. The emphasis is towards understanding how silica modulus effects the dissolution of aluminosilicate and the development of compressive strength. The degree of reaction is studied by thermogravimetric analysis and selective dissolution using HCl and salicylic acid. To the best of our knowledge, this is the first publication dealing with application of selective dissolution on natural pozzolan-based geopolymer systems. Reaction kinetics have been studied using isothermal calorimetry by applying pseudo-first-order kinetics. Phase composition and reactivity of various mineral phases were determined using X-ray diffraction analysis.

2. Materials and experimental methods

2.1. Materials and characterization

In this research study, six natural pozzolan samples were used, named as Rhenish trass (RT), Bavarian trass (BT1 and BT2), Pozzolan Laziale Red (PLR), Pozzolan Laziale Black (PLB) and Pozzolan

Flegrea (PF). Rhenish trass (RT) was obtained from Tubag quick-mix Gruppe GmbH & Co. KG, Germany in powder form. Bavarian trass was provided by Märker Zement GmbH, Germany in two forms, as stone (BT1) and powder (BT2). Pozzolan Laziale Red (PLR), Pozzolan Laziale Black (PLB) and Pozzolan Flegrea (PF) were supplied by Buzzi Unicem SpA, Italy all in stone form. In this research study, all the samples were ground to a comparable Blaine fineness. The natural pozzolan samples received in form of stone were ground in the labortary. Firstly, all the samples were dried at 105 ± 2 °C to constant weight followed by crushing of big stones using laboratory jaw crusher (BB100, Retsch GmbH, Germany) to size <1 mm. After that, samples were homogenized using laboratory sample divider (PT1000, Retsch GmbH, Germany) according to EN 932–2 in order to obtain equal representative portions of 125 g [27]. These portions were ground in a planetary ball mill (PULVERISETTE 5 classic line, Fritsch GmbH, Germany). Blaine fineness was determined according to EN 196-6 [28]. The particle size distribution was measured using Mastersizer 2000 of Malvern Instruments. All samples reached a Blaine fineness of $6700 ± 160$ cm^2/g and d_{50} ranging 5–23 μm. The exact Blaine fineness, density, d_{50} and d_{90} of all samples are given supplementary material. The chemical composition of all the natural pozzolans was determined using X-ray fluorescence analysis using PW 2400, PHILIPS and the results are as given in Table 1.

The mineralogical composition of all natural pozzolan samples was determined using Empyrean PANalytical diffractometer (see Section 2.3.4.). X-ray diffractograms and minerals found in all natural pozzolans are shown in Figs. 1a and 1b. Besides the crystalline components, samples also contained poorly crystalline or X-ray amorphous phases. The major crystalline mineral groups which have been found include feldspars, foids, zeolites, micas, pyroxenes, soro-silicates, neso-silicates, carbonates and oxides. The mineralogical phase composition was determined in accordance with the literature [29–36].

2.2. Preparation of alkaline solutions

In this research study, combinations of sodium hydroxide and sodium silicate solutions were used as alkaline activators. NaOH pellets of 99 wt-% purity were obtained from VWR International GmbH. NaOH solutions were prepared by dissolving NaOH pellets in deionized water and were stored at ambient temperature for at least 24 h before use. The sodium silicate solution was obtained from Woellner GmbH under the brand name of Betol 52 T with silica modulus of 2.12 (SiO_2 = 30.2 wt-%, Na_2O = 14.7 wt-%) and approx. 45 wt-% dry content. Silica moduli (Ms) used in this study are 0.707, 0.797, 0.946, 1.061, 1.158, 1.242, 1.272, 1.308, 1.365, 1.499, 1.566 and 1.716. Additionally, for compressive strength investigation silica moduli of 0.424, 0.491, 0.609 and 0.879 were also used. The molar ratios of H_2O/SiO_2, H_2O/Na_2O and Na_2O mol-% for each silica modulus are presented in Table 2. To achieve these various silica moduli, sodium hydroxide solution of 3.6, 6.6, 9.2 and 11.5 mol/L concentration was used in combination with sodium silicate. Mass ratio of sodium silicate to sodium hydroxide was kept equal to 0.5, 1, 2 and 3. The solution combinations and concentrations were chosen after detailed literature study [10,37] to cover many influencing factors for properties of geopolymer with reduced number of samples.

2.3. Experimental methods

Geopolymer paste samples were prepared using a laboratory hand mixer. Each sample was mixed for 90 s, following 30 s break in which sample was collected in the middle of the mixing bowl and afterwards was mixed for another 90 s. Therefore, total running mixing time was 3 min. The paste was poured in 20 mm cubic

Table 1
Chemical composition of all natural pozzolans.

Sample ID	BT1	BT2	RT	PLB	PLR	PF
Total	98.45	100.25	99.74	98.66	98.94	99.83
LOI	2.85	11.24	6.50	5.46	2.69	3.82
SiO_2	64.26	52.35	50.20	44.83	45.09	58.29
Al_2O_3	15.01	12.25	17.48	16.00	15.78	17.93
Fe_2O_3	5.31	4.15	5.10	10.62	10.02	3.93
MnO	0.13	0.09	0.22	0.30	0.19	0.13
MgO	0.79	0.91	1.51	4.25	4.63	0.87
CaO	3.29	13.85	8.76	9.22	10.36	2.54
Na_2O	2.74	1.67	4.03	0.59	1.44	3.53
K_2O	2.77	2.44	4.79	5.15	6.54	7.91
TiO_2	0.81	0.61	0.67	0.87	0.87	0.45
P_2O_5	0.28	0.22	0.20	0.81	0.79	0.15
SO_3	< 0.05	0.27	0.47	0.08	0.06	0.11

molds, then compacted for 2 min on compaction table. The samples were seal cured at 22 ± 2 °C and 100% relative humidity till test age. Alkaline solution to solid ratio was determined to achieve good workability for all silica moduli and was kept equal to 0.50, 0.75, 0.50, 0.43, 0.45 and 0.52 for BT1-, BT2-, RT-, PLB-, PLR- and PF-based geopolymers, respectively. Compressive strength of geopolymer cube samples was determined at 7 and 28 d. Crushed samples from hardened geopolymer paste samples were taken at 28 d age. Samples were freeze-dried by solvent exchange method using isopropanol followed by drying samples in a freeze-drying device for 7 d. Later, samples were ground by hand in a mortar and pestle and were subjected to selective dissolution analysis, thermogravimetric analysis and X-ray diffraction analysis. If needed, samples were stored in a desiccator together with soda lime to reduce the effect of carbonation. The methodology of other experiments is as discussed below.

2.3.1. Calorimetric analysis

The effect of alkaline solution concentration on reaction kinetics of natural pozzolan-based geopolymers was studied by isothermal heat flow calorimetry using device MC-CAL 100P, C3 Prozess- und Analysentechnik GmbH, Germany. Samples were mixed outside the device for 45 s each. Therefore, zero in the calorimetric curves is the point when samples were placed inside the device. From the results obtained, the reaction kinetics were determined using pseudo-first kinetic process. The pseudo-first-order kinetic equation was introduced by Langergren [38,39] as stated in Eq. (1).

$$dq/dt = -k[Q_{max} - Q_t] \qquad (1)$$

where Q_{max} and Q_t are defined as the total heat (J/g) at equilibrium and at time t, respectively. k is the rate constant of pseudo-first-order reaction and is an important parameter for understanding reaction kinetics. Upon integration of Eq. (1) it can be written as follows,

$$Q_t = Q_{max}(1 - e^{-kt}) \qquad (2)$$

Upon linearization Eq. (2) can be written as stated in Eq. (3).

$$\ln(Q_{max} - Q_t) = \ln Q_{max} - kt \qquad (3)$$

The equilibrium state is reached when the reaction is ceased which means $t = \infty$, in this case, it is considered as 2 d and 7 d. The rate constant is obtained as the slope of the best linear fit of the plot $\ln(Q_{max} - Q_t)$ vs t.

2.3.2. Selective dissolution analysis

The method of selective dissolution for determining the degree of reaction explained by RILEM TC 238-SCM based on European Technical report CEN/TR 196-4 has been implemented on natural pozzolan-based geopolymer prepared with various silica moduli

at 28 d age [40]. The detail of experimental method is provided in supplementary material. Eq. (4) was applied to calculate the degree of reaction (α).

$$\alpha = [(100fp - R_b)/100fp] \times 100\% \qquad (4)$$

where f is the mass fraction of natural pozzolan in the initial dry binder, p is the mass fraction of natural pozzolan undissolved by the acid solution and R_b is the mass of residue from natural pozzolan geopolymer paste in g/100 g of the unreacted binder.

2.3.3. Thermogravimetric analysis (TGA)

The effect of silica modulus of the alkaline solution on extent of geopolymerization reaction was determined using thermogravimetric analysis. Thermogravimetric analysis was performed using TG 209, Tarsus F3, Netzsch instrument under a nitrogen atmosphere at a flow rate of 250 mL/min. For each test 10 ± 1 mg of sample was used. The sample was first held at 25 °C for 20 min, and then heated from 25 °C to 850 °C at a heating rate of 10 °C/min.

2.3.4. X-ray diffraction (XRD) analysis

The X-ray diffraction (XRD) analysis was performed using an Empyrean PANalytical diffractometer with CuKα radiation (k = 1.540598 Å) and Ni filter, operating at 40 kV and 40 mA in continuous mode with a resolution of 0.0131° and speed of 0.0176°/s for the range of 5° to 65° for 1 h. The mineralogical phases of natural pozzolan and the resulting geopolymers were identified using HighScore Plus software with ICDD and ICSD database.

3. Results and discussion

3.1. Effect of silica modulus of the alkaline solution on compressive strength

Initially, trial samples for all silica moduli were prepared and cured till 7 d. After 7 d, RT and BT2 samples showed reactivity for all silica moduli used. PLB sample prepared with silica modulus of 0.797 showed 7 d compressive strength equal to 2.2 MPa. However, all other samples of PLB and the other natural pozzolan samples in all their combinations were not hard enough to be demoulded till 7 d. Therefore, further examinations were conducted only for RT and BT2 samples. The crystalline and amorphous phases present in the natural pozzolans determine their reactivity as seen later in Section 3.4. However, the mineralogical and chemical composition of PLB, PLR, PF and BT1 samples is the cause of their lower reactivity in the used alkaline medium as other influencing factors such as particle size, curing condition and the concentration of alkaline solution have been kept constant. It is worth noticing here that the versatile composition of natural pozzolans effects their potential for use as geopolymer
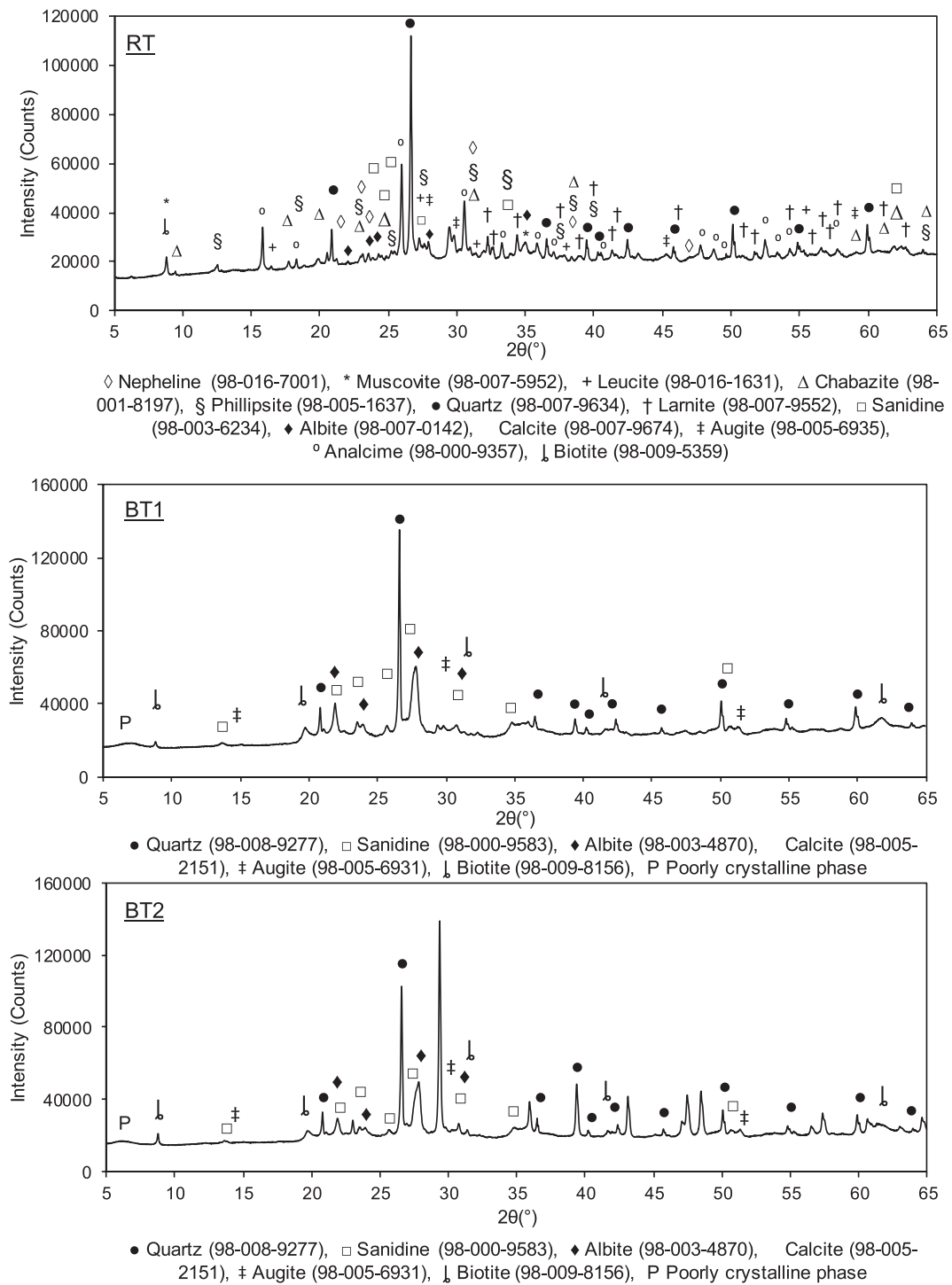
◇ Nepheline (98-016-7001), * Muscovite (98-007-5952), + Leucite (98-016-1631), △ Chabazite (98-001-8197), § Phillipsite (98-005-1637), ● Quartz (98-007-9634), † Larnite (98-007-9552), □ Sanidine (98-003-6234), ♦ Albite (98-007-0142), Calcite (98-007-9674), ‡ Augite (98-005-6935), º Analcime (98-000-9357), ⌡ Biotite (98-009-5359)

● Quartz (98-008-9277), □ Sanidine (98-000-9583), ♦ Albite (98-003-4870), Calcite (98-005-2151), ‡ Augite (98-005-6931), ⌡ Biotite (98-009-8156), P Poorly crystalline phase

● Quartz (98-008-9277), □ Sanidine (98-000-9583), ♦ Albite (98-003-4870), Calcite (98-005-2151), ‡ Augite (98-005-6931), ⌡ Biotite (98-009-8156), P Poorly crystalline phase

Fig. 1a. X-ray diffractograms of RT, BT1 and BT2 natural pozzolans.

precursor [13]. Therefore, to generalize the use of natural pozzolan as geopolymer precursor several natural pozzolans should be tested.

Results of 7 and 28 d compressive strength studied for RT and BT2 geopolymer pastes with various silica moduli are presented in Fig. 2. The results indicate the dependency of achieved compressive strength on silica modulus of the alkaline solution. Much higher or lower silica modulus are found to be not suitable for achieving higher compressive strength. The compressive strength increases with the increase of silica modulus till optimum values

of silica modulus and thereafter, the reduction of compressive has been observed. With the age of the sample, compressive strength is increasing for both natural pozzolan-based geopolymers. For RT-based geopolymers, the 7 d compressive strength increases with the increase of silica modulus till 0.946 and with further increase of silica modulus the compressive strength slightly decreases. At 28 d, RT-based geopolymers show an optimum range of silica modulus to achieve highest compressive strength; recorded as 0.946–1.272. While on either side of optimum the compressive strength is decreasing with the change of silica
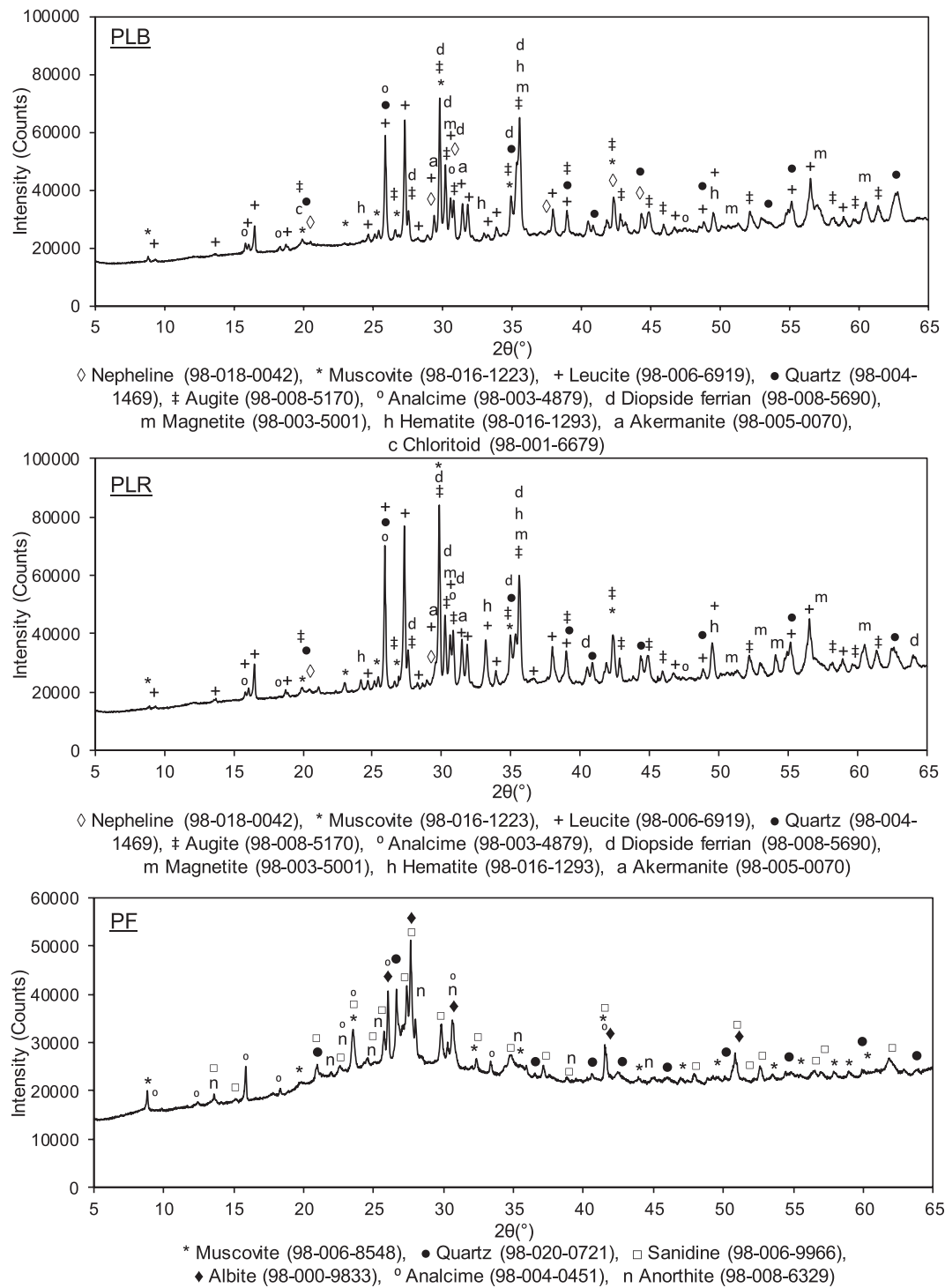
Fig. 1b. X-ray diffractograms of PLB, PLR and PF natural pozzolans.

modulus. For lower silica modulus (higher alkali concentration) the reduction rate is higher, while for higher silica modulus the reduction rate is lower. For BT2-based geopolymers, highest compressive strength has been achieved using silica modulus in a range of 0.707–0.797 at both 7 and 28 d. With additional decrease or increase of silica modulus, the compressive strength reduced on a higher rate. Reduction in compressive strength for lower silica modulus of the alkaline solution is because of an excess of alkalis present in the mixture. As previously reported, an excess of alkalis produces detrimental effects such as efflorescence and brittleness

thus reducing the compressive strength [16]. While, with the increase of silica modulus the silica content of alkaline solution increases, and compressive strength decreases due to the reduction of pH, increase of viscosity and increase in polymerization degree of silicate species of alkaline solution [1,41]. Gharzouni et al. reported that the type of siliceous species present in a silicate solution depends on the silica modulus of the solution [41]. For higher silica modulus of alkaline solution, the higher degree of polymerisation of silicate species reduces the reactivity of alkaline solution [41]. Therefore, increasing the strength by increasing the silica

Table 2
Composition of alkaline solutions used.

SiO$_2$/Na$_2$O	H$_2$O/SiO$_2$	H$_2$O/Na$_2$O	Na$_2$O (mol-%)
0.424	21.4	9.1	9.5
0.491	22.6	11.1	8.0
0.609	24.0	14.6	6.2
0.707	13.7	9.7	4.1
0.797	14.3	11.4	8.7
0.879	25.8	22.7	7.6
0.946	15.0	14.2	6.2
1.061	9.9	10.5	4.5
1.158	10.2	11.8	8.0
1.242	15.9	19.8	7.2
1.272	8.6	11.0	6.2
1.308	10.6	13.8	5.1
1.365	8.8	12.0	7.5
1.499	9.1	13.6	6.9
1.566	11.0	17.2	6.2
1.716	9.4	16.1	5.3

modulus is not recommended from properties and economic perspective.

For both natural pozzolans, the geopolymers with silica moduli 0.879 and 1.242 do not follow the trend given by all other samples. These samples are characterized by lower relative Na$_2$O than all other samples and a comparatively higher water content in alkaline solution. The H$_2$O/Na$_2$O of these mixtures is 22.7 and 19.8, respectively, while the other samples have H$_2$O/Na$_2$O in range of 9.1–17.2, where the development of compressive strength is governed by the silica modulus of the alkaline solution. However, higher H$_2$O/Na$_2$O beyond this range causes sudden reduction of compressive strength because of the lower relative content of Na$_2$O and diluting effect of water on the aptitude of free OH$^-$ to efficiently dissolve the aluminosilicate particles. Thus, generating polymerized product with lower binding properties. Therefore, attention must be given to the H$_2$O/Na$_2$O in the alkaline solution.

Comparing both natural pozzolans, it can be concluded that for different natural pozzolans the optimum range of silica modulus required depends upon the composition of the natural pozzolan as the specific surface area, curing condition and type of alkaline solution used have been kept same for both natural pozzolans.

3.2. Influence of silica modulus of the alkaline solution on reaction kinetics

The effect of various silica moduli on the kinetics of geopolymerization was studied by isothermal conduction calorimetry.

Figs. 3 and 4 present the calorimetric heat evolution for RT- and BT2-based geopolymers, respectively. The calorimetric study was performed for all silica moduli, however, for better understanding only selected samples are presented in Figs. 3 and 4. For RT- and BT2-based geopolymers, the calorimetric curves are characterized by a single peak associated with first wetting and dissolution of the reactive phases which occurs in the first few minutes of mixing the sample. This is followed by deceleration, which is assigned to the polycondensation of geopolymer product with lowering of heat release and the decrease of dissolution rate [10,19,37,42]. The time span of the deceleration phase is ranging from approx. few hours to days (approx. 3–72 h) depending on the silica modulus of alkaline solution used. Thereafter, the geopolymer reaction continues at a steady rate associated with continuous dissolution and polymerization lead to a low steady heat release [10,19,37,42,43]. This steady state reaction continues over a long time beyond the span which is shown in Figs. 3 and 4. The continuity of geopolymer reaction is indicated by an increase of compressive strength from 7 to 28 d (Fig. 2). For BT2 sample prepared with the alkaline solution with silica modulus of 0.707, 0.797 and 1.061 a second exothermic peak was observed around approx. 9, 11 and 28 h, respectively, as shown in Fig. 4. To investigate the reaction occurring at this peak, XRD analysis was conducted on samples before and after the occurrence of this peak, however, no significant change in crystalline phases was observed. Therefore, it is concluded that the 2nd exothermic peak observed in BT2 geopolymer samples is reaction happening between amorphous phases. However, the potential reason could be the diffusion control reaction or delayed dissolution of some phase. Diffusion control reaction or delayed dissolution has been also observed for alkali activated slag and fly ash geopolymers [2,44].

Fig. 5 shows the dependence of rate constant on silica modulus; with the increase of silica modulus, the rate constant has been found to decrease for both natural pozzolan systems. However, some outliers have been observed. For RT-based geopolymers, sample with silica modulus of 1.061 exhibited the highest rate constant at 2 d, which is because of higher concentration of Na$_2$O and SiO$_2$ in this sample, thereafter, the reaction continues at a relatively slower rate till 7 d (Fig. 5). Similarly, for RT-based geopolymers activated with silica modulus of 1.242 at 2 d of age, rate constant is lower. This is because of the lower concentration of Na$_2$O and SiO$_2$ in the matrix. Thus, it can be concluded that a higher concentration of Na$_2$O and SiO$_2$ in the matrix enhances the initial reaction kinetics. For lower silica moduli of alkaline solutions 0.707 and 0.797, the reaction rate is slow in the beginning compared to other samples, but at 7 d these samples have the highest
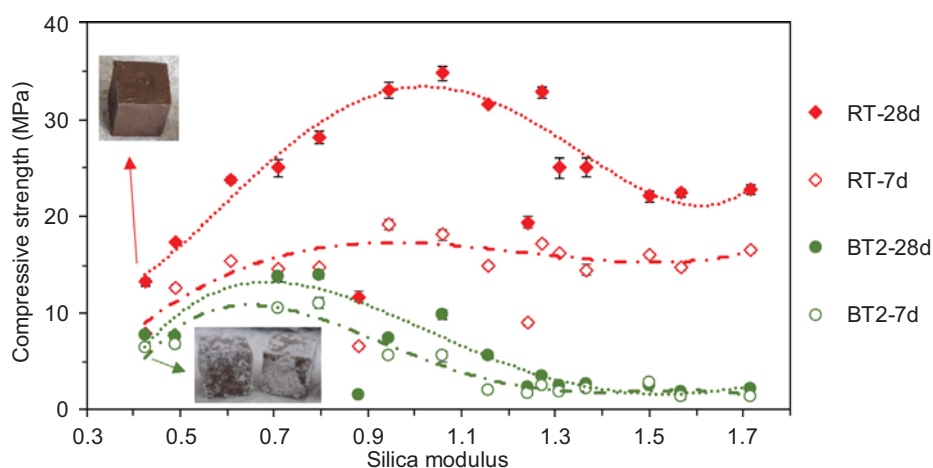

Fig. 2. 7 and 28 d compressive strength of RT- and BT2-based geopolymers.
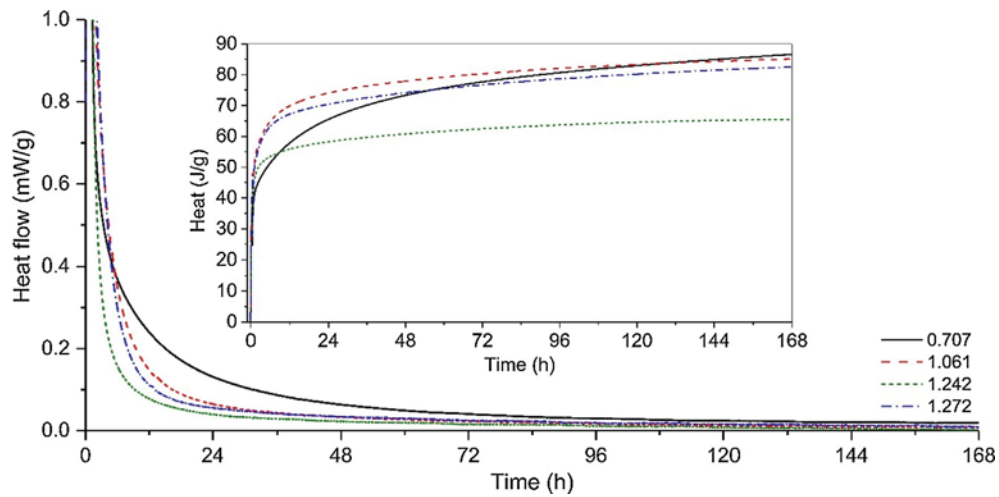
Fig. 3. Calorimetric heat evolution curves of RT-based geopolymers.
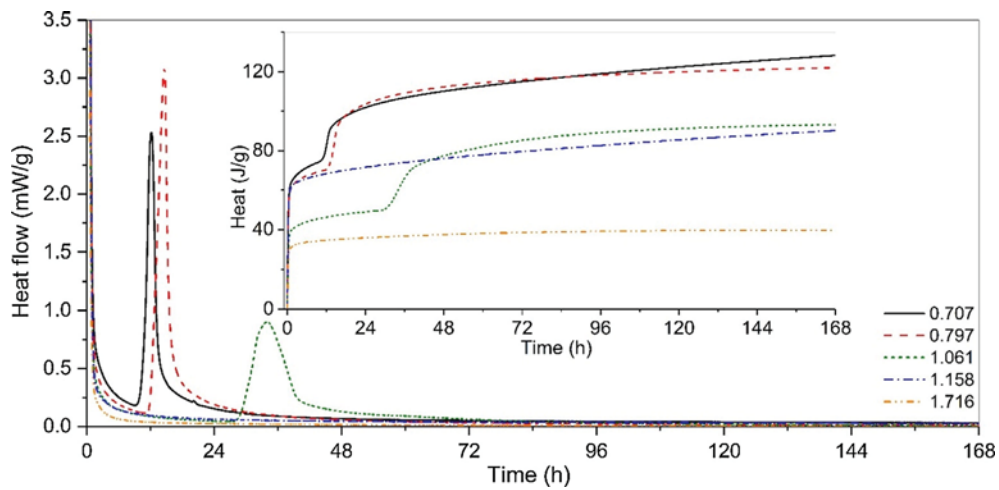
Fig. 4. Calorimetric heat evolution curves of BT2-based geopolymers.
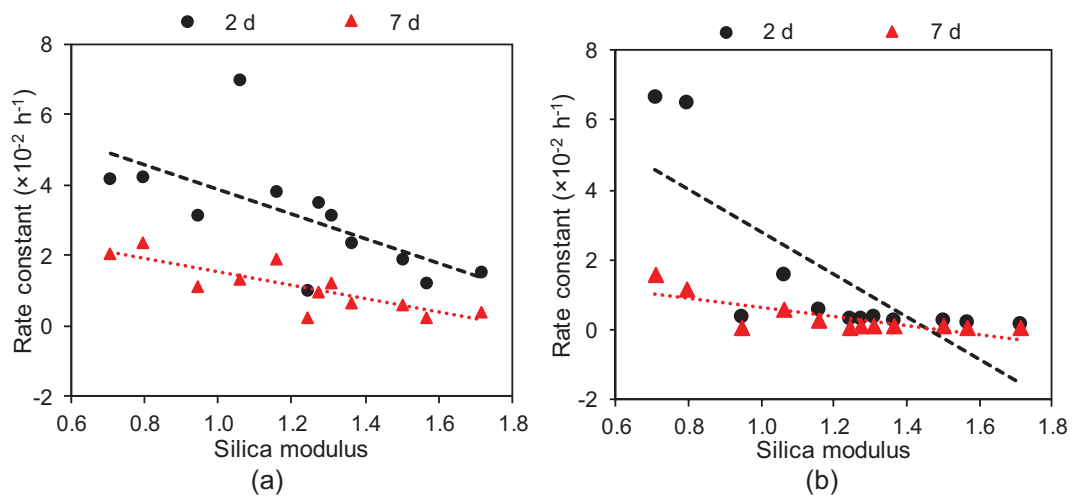
Fig. 5. Rate constant with respect to silica modulus of alkaline solution (a) for RT-based geopolymers (b) for BT2-based geopolymers.

heat and rate constant. For 0.946 silica modulus of alkaline solution, the reaction begins at a higher rate (till 2 d) and thereafter, till 7 d reaction slows down in comparison to samples activated with 0.707, 0.797 and 1.061 silica modulus. Similar characteristics have been observed for samples with silica modulus of 1.158, 1.272 and 1.308. For all other samples, the rate constant has been observed to

be low. Thus, it can be concluded that higher Na_2O and SiO_2 molar concentration in the alkaline solution, helps to accelerate the reaction in the beginning, however, care must be taken while choosing the lower silica modulus as it can also retard the reaction in early age.

For BT2-based geopolymers, the reaction is fastest for samples prepared with silica modulus of 0.707, 0.797, 1.061 and 1.158. Slower reaction with lower heat evolution has been observed for all other samples, which correlates well with the 7 d compressive strength of these geopolymers. Comparing 2 and 7 d rate constants, it can be seen that the reaction is faster in the beginning and continues at a slower rate till 7 d. Like RT geopolymers, for these geopolymer samples the rate constant increased with increasing Na_2O and SiO_2 molar concentration in the alkaline solution. For silica modulus of 0.707, the rate constant has been found to be highest in this series of samples and reaction continues at higher rate till 7 d. For silica modulus of 0.797, similar reaction kinetics have been observed. For silica modulus of 1.061, the rate constant is lower than the samples with silica moduli of 0.707 and 0.797 which means that the reaction occurs at relatively lower rate than these samples, which is because of higher SiO_2 molar content beyond optimum, therefore, the system needs longer time to reach equilibrium. For the sample with silica modulus of 1.158, no second peak has been observed, however, reaction kinetics are comparable to sample with silica modulus of 1.061. Relatively lower Na_2O and SiO_2 molar concentrations can be the reason that the 2nd exothermic peak was not observed till 7 d. The lower reactivity of all other mixtures could be the reason that for all other samples of BT2, no second peak has been observed as reaction occurs at negligible rate after few hours of mixing as indicated by lower rate constant and lower compressive strength of these samples (Figs. 2, 4 and 5).

3.3. Influence of silica modulus of the alkaline solution on extent of geopolymerization reaction

Selective dissolution and thermogravimetric analysis were used to study the effect of silica modulus of the alkaline solution on the extent of geopolymerization. Results of both methods and discussion are presented as follows.

3.3.1. Selective dissolution analysis

Selective dissolution method for determination of the degree of reaction was applied on RT- and BT2-based geopolymers of 28 d age prepared using various silica moduli of the alkaline solution. The degree of reaction vs silica modulus for both natural pozzolan geopolymers is presented in Fig. 6. Results show that the degree of reaction decreases with the increase of silica modulus of alkaline solution for both natural pozzolan-based geopolymers. RT geopolymers have a higher degree of reaction in comparison to BT2 geopolymers which is in accordance with the results of compressive strength. The higher degree of reaction at low silica modulus indicates that larger amount of geopolymer gel is formed for both natural pozzzolan-based geopolymers. Which in turn should lead to a sample that exhibits higher compressive strength. This statement suits good to BT2 geopolymers. However, for RT geopolymers the strength does not clearly increase linearly. This could be because of the reason that for RT geopolymers the higher reactivity of RT in highly concentrated solutions increases the number of ions to the extent that the ion pairing can cause steric hindrance of precipitate growth [1]. As a result, the formed geopolymer gel lacks in long-range ordering and thus has lower compressive strength [1]. Such a behaviour has not been observed in BT2 geopolymers because of lower reactivity of BT2. Further, as explained earlier the excess of alkalis has a determinantal physical effect such as
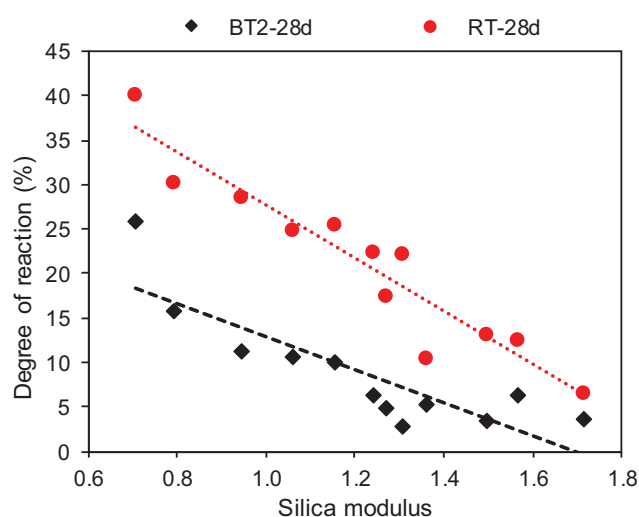

Fig. 6. Degree of reaction calculated from selective dissolution results for RT- and BT2-based geopolymers at 28 d of age.

efflorescence which may cause a reduction in compressive strength [16].

3.3.2. Thermogravimetric analysis (TGA)

The effect of silica modulus of the alkaline solution on extent of geopolymerization for natural pozzolan-based geopolymer can also be determined by measuring weight loss using thermogravimetric analysis. Fig. 7 presents TG and DTG results of RT and BT2 raw samples and RT- and BT2-based geopolymer samples made with silica modulus of 0.707 at 28 d age (labelled as RT-0.707 and BT2-0.707, respectively). Like in calorimetry, all samples were tested with TGA but selected TG and DTG curves are presented in Fig. 7 for ease of understanding. Results indicate that thermogravimetric weight loss curves are designated by three stages. The first stage has been considered from 50 to 150 °C. Typically, the first DTG peak was observed between 86 and 93 °C for RT geopolymers and between 76 and 83 °C for BT2 geopolymers. This stage is mainly characteristic of physically bound water in pores of geopolymer gel structure. This water is released during condensation and does not take part in the dissolution of aluminosilicate species [10,20,45–47]. As the second stage, weight loss from 150 to 600 °C is characterised as chemically bound water molecules and OH groups in geopolymer matrix [10,20,45,46]. Last weight loss stage has been observed from 600 to 850 °C, associated with decomposition of carbonates [10]. The DTG peak of this stage has been observed between 601 and 640 °C for RT-based geopolymers and between 646 and 684 °C for BT2 geopolymers. After geopolymerization, the overall weight loss and weight loss due to chemically bound water molecules and OH group increased for all samples and the effect of carbonate decomposition decreased for all samples.

Davidovits characterised the water present in geopolymer structure in three types; physically bound water, chemically bound water molecules (zeolitic water) and OH groups [4]. It is important to recall here that in the raw mix the chemically bound water comes from different crystalline and amorphous phases and in the geopolymer sample the chemically bound water molecules come from the dissolution of aluminosilicate species to form aluminate and silicate species and remain after condensation. While the OH groups are present at the surface and edges of each geopolymeric chains [4,47]. Therefore, to investigate the extent of geopolymerization, chemically bound water molecules and OH groups were quantified for both natural pozzolan-based geopoly-
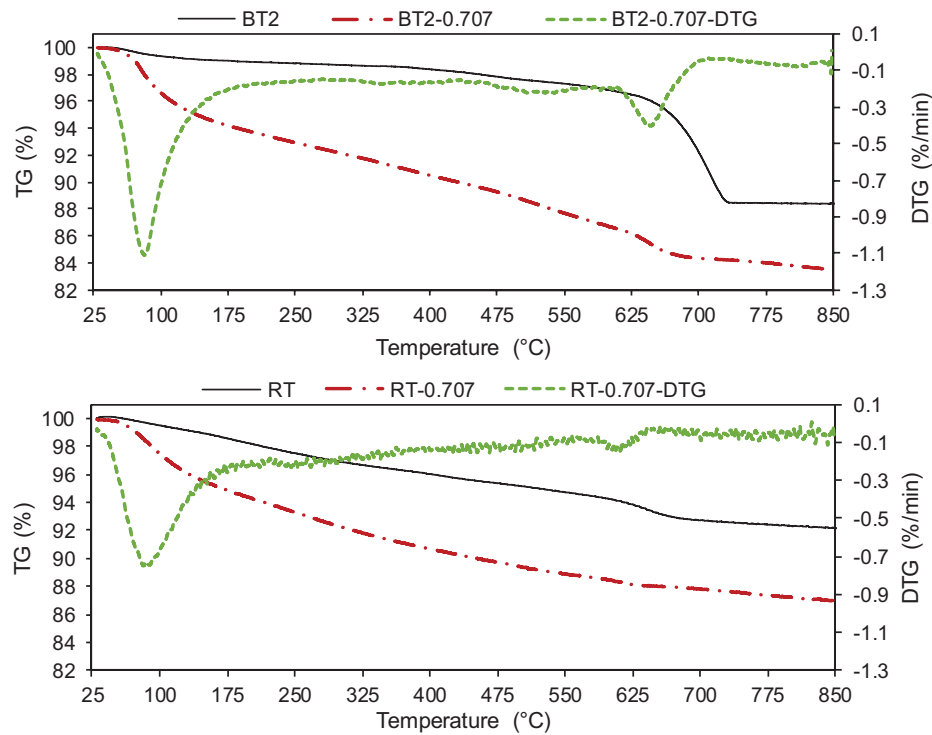
Fig. 7. TG and DTG curves of RT and BT2 samples and RT- and BT2-based geopolymer activated with alkaline solution silica modulus of 0.707 at 28 d age.

mers activated with various silica moduli of the alkaline solutions. For this purpose, weight loss for a temperature range of 150–300 °C corresponding to the liberation of chemically bound water molecules and weight loss for the temperature range of 300–600 °C corresponding to decomposition of OH groups were calcu-lated for each geopolymer sample [4,47]. Fig. 8 presents the mass loss in the mentioned temperature range for chemically bound water molecules and OH groups vs silica modulus for RT- and BT2-based geopolymers measured at 28 d age. Results show that with the increase in the silica modulus of alkaline solution the amount of chemically bound water molecules decreases for BT2 geopolymers. For RT geopolymers, the mass loss of chemically bound water molecules firstly increases with the increase of silica modulus and afterwards, it decreases with further increase in silica

modulus. The chemically bound water molecules for both natural pozzolans-based geopolymers follow the trends as shown by com-pressive strength. Hence, a higher amount of chemically bound water molecules shows the formation of more condense geopoly-meric gel thus generating higher compressive strength.

The mass loss of OH groups in Fig. 8 decreases with the increase of silica modulus for both natural pozzolan geopolymers. This could be in the way that the extent of dissolution decreases with increasing silica modulus. These results are in good agreement with the results of selective dissolution and reaction kinetics. How-ever, the absolute values of OH weight loss for BT2 are higher than for RT. To explain this, it must be considered that thermogravimet-ric analysis cannot provide the exact degree of polymerization in geopolymeric gel phases and is not specific to the amount of
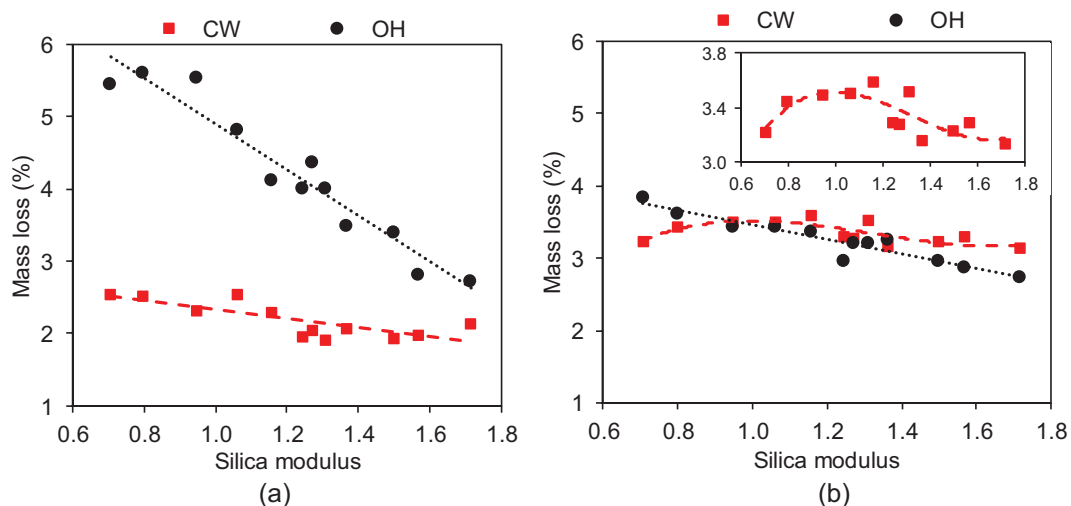

Fig. 8. Mass loss of chemically bound water molecules (CW) and OH groups (OH) for (a) BT2- and (b) RT-based geopolymers at 28 d age.

reacted silica and alumina (like selective dissolution). Selective dissolution is considered to give consistent results if the same amount of reacted silica and alumina is in the sample, and therefore can be applied on different natural pozzolans. On the other hand, OH group weight loss depends not only on dissolved silica and alumina but also on the polymerization degree of the precipitated gel. Therefore, the OH group weight loss alone is not enough to explain the extent of dissolution in geopolymer gel and must be combined with the other methods for accurate investigation. The higher OH group weight loss in BT2 geopolymer may indicate a lower degree of polymerization. Further, for RT geopolymers, selective dissolution indicates the presence of higher amount of reaction product formed for all silica moduli and thermogravimetric analysis shows that the product formed is more condensed compared to BT2 geopolymers, thus RT geopolymers produces higher compressive strength. However, for BT2 geopolymers lower amount of reaction product is formed and thermogravimetric analysis shows that the product formed is less condensed and has a lower degree of polymerization thus exhibiting lower compressive strength.

3.4. Influence of silica modulus of the alkaline solution on phase composition and reactivity of various minerals

The XRD patterns of natural pozzolan-based geopolymers were compared with respective raw natural pozzolan. XRD analysis was made for all the silica moduli used in this study, but for easy understanding selected samples are shown here. Some of the crystalline mineral phases present in the unreacted natural pozzolan are also present in geopolymer product. However, several minerals have been found to partially dissolve during geopolymerization reaction. Fig. 9 shows the X-ray diffractogram of raw RT and RT geopolymers at the age of 28 d made with various silica moduli. Comparing the unreacted RT with resulting geopolymer samples, changes in amorphous and crystalline phases can be observed. After geopolymer reaction, the centre of the amorphous hump has shifted from approx. 27° to approx. 31° which is attributed to the formation of geopolymeric gel. Similar formation has also been reported in the literature [43,48]. In addition, the increase in the amorphous hump compared to unreacted RT samples has been observed for all RT geopolymer samples, indicating that the amount of semi-crystalline phase has increased, as shown in Fig. 9. The increase in semi-crystalline phase is attributed to the formation of geopolymeric gel which depends on the concentration

of the alkaline solution used. The diffractograms indicate that the amount of geopolymeric gel formed slightly increases with the increase of silica modulus till 1.061 and thereafter, it slightly decreases, which is in accordance with the compressive strength of these samples and chemical bound water molecules evaluated by TGA. However, the partial dissolution of crystalline phases is more for lower silica modulus and decreases with the increase of silica modulus. The partially dissolved crystalline phases include phillipsite, chabazite, larnite and calcite, as shown in Fig. 9. Several studies have reported the pozzolanic reactivity of zeolite minerals and partial dissolution of calcite in cementitious systems [24,49,50]. Thus, indicating the potential reactivity of these minerals in geopolymer system. Some crystalline phases which overlap in their reflexes with the aforementioned phases including sanidine, leucite, biotite, muscovite and nepheline, may also be participating in geopolymer reaction. The partial dissolution of muscovite in alkaline medium was also described by [12]. At 29.8° reflex intensity increases which is assigned to the formation of semi-crystalline geopolymer gel phase displaying similarity to zeolite Y structure (98–020-0636). It can form due to partial dissolution and geopolymerization of an amorphous phase and some crystalline phases like larnite, phillipsite and chabazite in the presence of alkaline solution. Further, broadening of reflexes around 35.0° and 37.8° has been observed, which arises due to formation of aluminosilicate gel structure, as reported in literature [51].

Fig. 10(a) and (b) show the XRD of BT2 and BT2-based geopolymers at the age of 28 d made with various silica moduli. The partially crystalline hump present at 5.5°–8.5° attributes to the presence of zeolite or clay minerals (Fig. 10(a)). The shape of the partially crystalline hump from 5.5°–8.5° with centre at approx. 8° changes after geopolymerization and the centre of the hump moves to approx. 7.2° which is the indication of the formation of aluminosilicate gel (Fig. 10(a)). Such formation has been also reported in literature [51]. The main amorphous hump is ranging 24°–34° and moves its centre from approx. 27° to 31° because of the formation of geopolymeric gel [43,48]. Looking at Fig. 10(b), the samples made with silica modulus of 0.707 and 0.797 have highest dissolution rate of crystalline phases and highest amount of amorphous phase formed which is in accordance with compressive strength and calorimetric analysis. The excess efflorescence formation is also reflected by XRD as new reflexes attributed to natrite (98-009-5549, γ-Na_2CO_3) can be seen in Fig. 10(b). However, in RT geopolymers formation of natrite was not observed

◊ Nepheline, * Muscovite, + Leucite, △ Chabazite, § Phillipsite, ● Quartz, † Larnite,
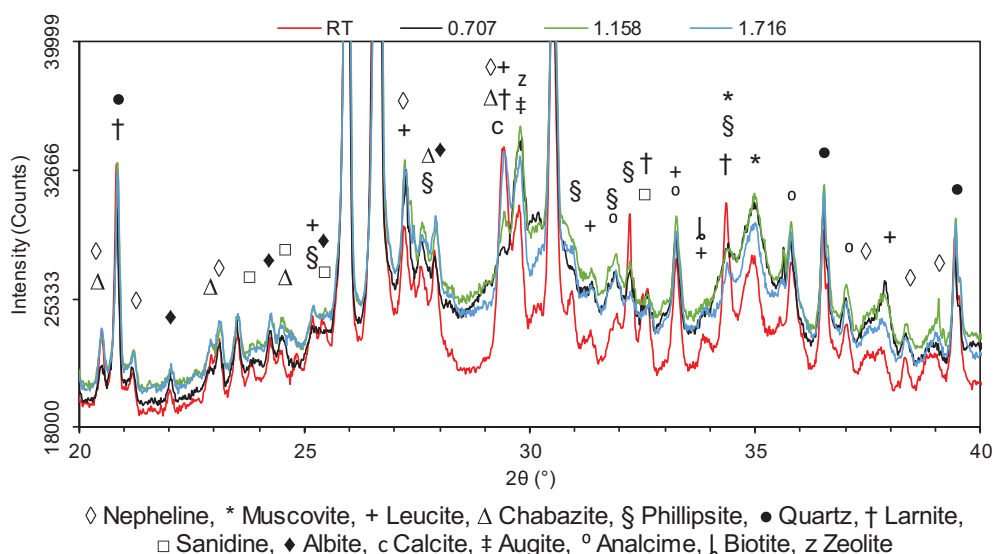□ Sanidine, ◆ Albite, c Calcite, ‡ Augite, ° Analcime, ↓ Biotite, z Zeolite

Fig. 9. Comparison of RT and RT-based geopolymers made with silica modulus of 0.707, 1.158 and 1.716 at 28 d of age.

P Poorly crystalline phase , ⌡ Biotite

(a)

● Quartz, □ Sanidine, ♦ Albite, c Calcite, ‡ Augite, n Natrite
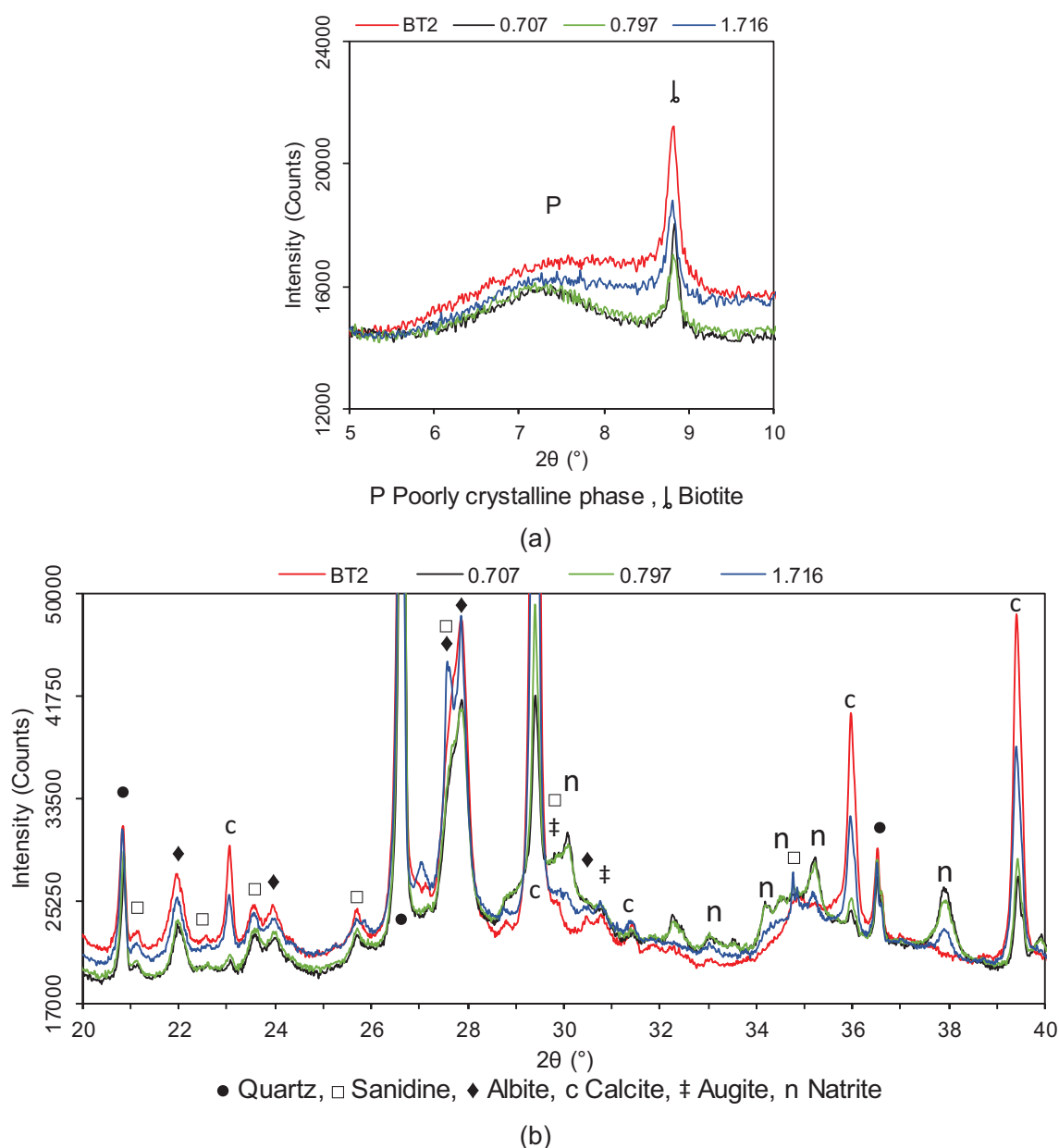
(b)

Fig. 10. Comparison of BT2 and BT2-based geopolymers made with silica modulus of 0.707, 0.797 and 1.716 at 28 d of age (a) in 2θ range 5–10° (b) in 2θ range 20–40°.

indicating that RT geopolymers exhibit negligibly small efflorescence. For BT2 geopolymers, the amount and rate of formation of efflorescence for each sample depend on the concentration of the alkaline solution used. Crystalline phases present in BT2 including calcite, biotite and sanidine participate in geopolymerization as indicated by their partial dissolution (Fig. 10(a) and (b)). Some new crystalline phases were also formed e.g. for silica modulus of 0.707 and 0.797 a new phase formed at 32.5° and for silica modulus of 1.716 new reflex was observed at approx. 27.0° and 34.8°. The reflex at 32.5° can be because of semi-crystalline aluminosilicate gel [1]. However, the sample prepared with silica modulus of 1.716 has the highest amount of soluble silica; therefore, the new reflexes observed in this sample can be silica-rich phase(s). Though, these reflexes were not clearly identified with the database used.

These results also give insight about the low reactivity of BT1, PLB, PLR and PF. As the reactive crystalline mineral phases found in RT and BT2 are absent in the above mentioned natural poz-

zolans. This might be a reason for the low reactivity of BT1, PLB, PLR and PF. Comparing BT1 and BT2, the lower content of calcite in BT1 can be the reason for its lower reactivity. Furthermore, the composition and reactivity of the glass phase present in all pozzolans may differ. However, the high number and in some cases the variable composition of the mineral phases present in natural pozzolans disable an accurate determination of the chemical composition of the glass phases. Nevertheless, the results show that the glass phase of natural pozzolans participate in geopolymer reaction, which is in agreement with the literature [12].

4. Conclusions

The chemical and mineralogical composition of natural pozzolans effect their reactivity in alkaline medium. The dissolution of aluminate and silicate species increases with the reduction of silica modulus, and at higher silica modulus the dissolution of the raw sample decreases. However, the mechanical properties of

the resultant gel formed depend on the degree of polymerization of gel structure. Low silica modulus of alkaline solution leads to efflorescence and a lower degree of polymerization, thus reducing compressive strength. While at higher silica modulus, the compressive strength reduces again. Therefore, increasing the silica modulus to achieve higher compressive strength is not recommended from economical and properties perspective. The reaction kinetics depend on silica modulus, a faster reaction can be obtained by increasing the alkalinity of the solution, but care should be taken for adverse effects. Results show the suitability of selective dissolution method to determine quantitatively the amount of geopolymer product formed for natural pozzolan-based geopolymers. RT showed higher reactivity in the used alkaline medium in comparison to BT2 as indicated by a higher amount of geopolymer gel formed. Determination of the amount of chemically bound water molecules from TGA gives insight about the influence of silica modulus on compressive strength. A higher amount of chemically bound water molecules indicates the formation of a more condensed geopolymer product, thus exhibiting higher compressive strength. The natural pozzolan samples which have lower reactivity in the alkaline medium are more prone to exhibit efflorescence at lower silica modulus. Various solid phases of the raw material, including both crystalline and amorphous phases, participate in geopolymer reaction. However, the extent of participation of each mineral phase depends on the silica modulus of alkaline solution used. The crystalline phases participating in geopolymerization by their partial dissolution include phillipsite, chabazite, larnite, calcite, biotite and sanidine. The geopolymer gel formed is amorphous or semi-crystalline. The more crystalline parts of resultant geopolymer gel correspond to zeolite structure.

Declaration of Competing Interest

The authors declare that they have no conflict of interest.

Acknowledgements

References

[1] P. Duxson, A. Fernández-Jiménez, J.L. Provis, G.C. Lukey, A. Palomo, J.S.J. van Deventer, Geopolymer technology: the current state of the art, J. Mater. Sci. 42 (9) (2007) 2917–2933.

[2] F. Pacheco-Torgal, J.A. Labrincha, C. Leonelli, A. Palomo, P. Chindaprasirt (Eds.), Handbook of Alkali-activated Cements, Mortars and Concretes, Woodhead Publishing, Cambridge, Philadelphia, PA, 2012.

[3] J.L. Provis, J.S.J. van Deventer, Alkali Activated Materials, State-of-the-Art Report, RILEM TC 224-AAM, Springer, Dordrecht, Heidelberg, New York, London, 2014.

[4] J. Davidovits, Geopolymer Chemistry and Applications, Institut Géopolymère, Saint-Quentin, France, 2008.

[5] J. Davidovits, Properties of geopolymer cements, in: First International Conference on Alkaline Cements and Concretes, Scientific Research Institute on Binders and Materials Kiev State Technical University, 1994, pp. 131–149.

[6] J. Tailby, K.J.D. MacKenzie, Structure and mechanical properties of aluminosilicate geopolymer composites with Portland cement and its constituent minerals, Cem. Concr. Res. 40 (5) (2010) 787–794.

[7] C. Villa, E.T. Pecina, R. Torres, L. Gómez, Geopolymer synthesis using alkaline activation of natural zeolite, Constr. Build. Mater. 24 (11) (2010) 2084–2090.

[8] M. Izquierdo, X. Querol, J. Davidovits, D. Antenucci, H. Nugteren, C. Fernández-Pereira, Coal fly ash-slag-based geopolymers: microstructure and metal leaching, J. Hazard. Mater. 166 (1) (2009) 561–566.

[9] R. Robayo-Salazar, J. Mejía-Arcila, R. Mejía de Gutiérrez, E. Martínez, Life cycle assessment (LCA) of an alkali-activated binary concrete based on natural volcanic pozzolan: a comparative analysis to OPC concrete, Constr. Build. Mater. 176 (2018) 103–111.

[10] R. Firdous, D. Stephan, J.N.Y. Djobo, Natural pozzolan based geopolymers: a review on mechanical, microstructural and durability characteristics, Constr. Build. Mater. 190 (2018) 1251–1263.

[11] H.K. Tchakoute, A. Elimbi, E. Yanne, C.N. Djangang, Utilization of volcanic ashes for the production of geopolymers cured at ambient temperature, Cem. Concr. Compos. 38 (2013) 75–81.

[12] B.I. Djon Li Ndjock, A. Elimbi, M. Cyr, Rational utilization of volcanic ashes based on factors affecting their alkaline activation, J. Non-Cryst. Solids 463 (2017) 31–39.

[13] P.N. Lemougna, U.F. Chinje Melo, M.-P. Delplancke, H. Rahier, Influence of the chemical and mineralogical composition on the reactivity of volcanic ashes during alkali activation, Ceram. Int. 40 (1) (2014) 811–820.

[14] P.N. Lemougna, U.F. Chinje Melo, M.-P. Delplancke, H. Rahier, Influence of the activating solution composition on the stability and thermo-mechanical properties of inorganic polymers (geopolymers) from volcanic ash, Constr. Build. Mater. 48 (2013) 278–286.

[15] M.J. Nadoushan, A.A. Ramezanianpour, The effect of type and concentration of activators on flowability and compressive strength of natural pozzolan and slag-based geopolymers, Constr. Build. Mater. 111 (2016) 337–347.

[16] D. Bondar, C.J. Lynsdale, N.B. Milestone, N. Hassani, A.A. Ramezanianpour, Effect of type, form, and dosage of activators on strength of alkali-activated natural pozzolans, Cem. Concr. Compos. 33 (2) (2011) 251–260.

[17] M.M. Yadollahi, A. Benli, R. Demirboğa, The effects of silica modulus and aging on compressive strength of pumice-based geopolymer composites, Constr. Build. Mater. 94 (2015) 767–774.

[18] N. Ghafoori, M. Najimi, B. Radke, Natural pozzolan-based geopolymers for sustainable construction, Environ. Earth Sci. (2016) 1–16. 75:1110(14).

[19] E.N. Kani, A. Allahverdi, J.L. Provis, Calorimetric study of geopolymer binders based on natural pozzolan, J. Therm. Anal. Calorim. 127 (3) (2017) 2181–2190.

[20] J.N.Y. Djobo, A. Elimbi, H.K. Tchakouté, S. Kumar, Reactivity of volcanic ash in alkaline medium, microstructural and strength characteristics of resulting geopolymers under different synthesis conditions, J. Mater. Sci. 51 (22) (2016) 10301–10317.

[21] I. Tekin, Properties of NaOH activated geopolymer with marble, travertine and volcanic tuff wastes, Constr. Build. Mater. 127 (2016) 607–617.

[22] E.N. Kani, A. Allahverdi, Effects of curing time and temperature on strength development of inorganic polymeric binder based on natural pozzolan, J. Mater. Sci. 44 (12) (2009) 3088–3097.

[23] D. Bondar, C.J. Lynsdale, N.B. Milestone, N. Hassani, A.A. Ramezanianpour, Effect of adding mineral additives to alkali-activated natural pozzolan paste, Constr. Build. Mater. 25 (6) (2011) 2906–2910.

[24] J.N.Y. Djobo, H.K. Tchakouté, N. Ranjbar, A. Elimbi, L.N. Tchadji, D. Njopwouo, Gel composition and strength properties of alkali-activated oyster shell-volcanic ash: effect of synthesis conditions, J. Am. Ceram. Soc. 99 (9) (2016) 3159–3166.

[25] Y.J.N. Djobo, A. Elimbi, J. Dika Manga, I.B. Djon Li Ndjock, Partial replacement of volcanic ash by bauxite and calcined oyster shell in the synthesis of volcanic ash-based geopolymers, Constr. Build. Mater. 113 (2016) 673–681.

[26] H.K. Tchakoute, A. Elimbi, J.A. Mbey, C.J.N. Sabouang, D. Njopwouo, The effect of adding alumina-oxide to metakaolin and volcanic ash on geopolymer products: a comparative study, Constr. Build. Mater. 35 (2012) 960–969.

[27] EN 932-2. Test for general properties of aggregates - Part 2: Method for reducing laboratory samples; 1999.

[28] EN 196-6. Methods of testing cement – Part 6: Determination of fineness; 2010.

[29] R. Funiciello, G. Giordano. La nuova carta geologica di Roma: litostratigrafia e organizzazione stratigrafica: The Geological Map of Rome: lithostratigraphy and stratigraphic organisation. (Periodici tecnici) Memorie descrittive della Carta Geologica d'Italia 2008; 80.

[30] H.-E. Schwiete, U. Ludwig, K.-H. Wigger, Die Konstitution einiger rheinischer und bayrischer Trasse, Westdeutscher Verlag, Köln Opladen, 1961.

[31] K. Jasmund, G. Hentschel, Seltene Mineralparagenesen in den Kalksteineinschlüssen der Lava des Ettringer Bellerberges bei Mayen (Eifel). Beiträge Mineral, Petrogr. (Beiträge zur Mineralogie und Petrographie) 10 (3) (1964) 296–314.

[32] E. Liebig, E. Althaus, Pozzolanic activity of volcanic tuff and suevite: effects of calcination, Cem. Concr. Res. 28 (4) (1998) 567–575.

[33] U. Ludwig, H.E. Schwiete, Untersuchungen an Deutschen Trassen, Silicates Ind. (1963) 439–447.

[34] M. Fleischer, New mineral names, Am. Miner. 50 (1965) 2096–2111.

[35] R. Villa. Determinazione del peso di volume su campioni di terreno prelevati presso la cava di pozzolana di Ponte Lucano - Tivoli (RM). Nota Technica, Buzzi Unicem S.p.a 2014.

[36] O. Vogt, N. Ukrainczyk, F. Röser, E. Steindlberger, E.A.B. Koenders, Geopolymerisation activity of eifel tuff, in: II International Conference on Concrete Sustainability (ICCS16), 2016, pp. 653–662.

[37] J.N.Y. Djobo, A. Elimbi, H.K. Tchakouté, S. Kumar, Volcanic ash-based geopolymer cements/concretes: the current state of the art and perspectives, Environ. Sci. Pollut. Res. 24 (5) (2017) 4433–4446.

[38] H. Yuh-Shan, Citation review of Lagergren kinetic rate equation on adsorption reactions, Scientometrics 59 (1) (2004) 171–177.

[39] J.-P. Simonin, On the comparison of pseudo-first order and pseudo-second order rate laws in the modeling of adsorption kinetics, Chem. Eng. J. 300 (2016) 254–263.

[40] Y.A. Villagrán-Zaccardi, A. Vollpracht, E. Gruyaert, N. de Belie, Recommendation of RILEM TC 238-SCM: determination of the degree of

reaction of siliceous fly ash and slag in hydrated cement paste by the selective dissolution method, Mater. Struct. 51 (1) (2018) 835.

[41] A. Gharzouni, E. Joussein, B. Samet, S. Baklouti, S. Pronier, I. Sobrados, et al., The effect of an activation solution with siliceous species on the chemical reactivity and mechanical properties of geopolymers, J. Sol-Gel Sci. Technol. 73 (1) (2015) 250–259.

[42] J.N.Y. Djobo, A. Elimbi, H.K. Tchakouté, S. Kumar, Mechanical activation of volcanic ash for geopolymer synthesis: effect on reaction kinetics, gel characteristics, physical and mechanical properties, R. Soc. Chem. (RSC Adv.) 6 (45) (2016) 39106–39117.

[43] Z. Zhang, J.L. Provis, H. Wang, F. Bullen, A. Reid, Quantitative kinetic and structural analysis of geopolymers. Part 2. Thermodynamics of sodium silicate activation of metakaolin, Thermochim. Acta 565 (2013) 163–171.

[44] B.S. Gebregziabiher, R.J. Thomas, S. Peethamparan, Temperature and activator effect on early-age reaction kinetics of alkali-activated slag binders, Constr. Build. Mater. 113 (2016) 783–793.

[45] L. Weng, K. Sagoe-Crentsil, Dissolution processes, hydrolysis and condensation reactions during geopolymer synthesis: part I—Low Si/Al ratio systems, J. Mater. Sci. 42 (9) (2007) 2997–3006.

[46] R. Firdous, D. Stephan, Y. Jin, Investigation of rhenish and bavarian trass as geopolymer precursor Weimar, Germany 2018(Book 2), in: 20th International Conference of Building Materials - Ibausil 2018, 2018, pp. 617–624.

[47] H.K. Tchakouté, C.H. Rüscher, S. Kong, E. Kamseu, C. Leonelli, Comparison of metakaolin-based geopolymer cements from commercial sodium waterglass and sodium waterglass from rice husk ash, J. Sol-Gel Sci. Technol. 78 (3) (2016) 492–506.

[48] Z. Sun, A. Vollpracht, Isothermal calorimetry and in-situ XRD study of the NaOH activated fly ash, metakaolin and slag, Cem. Concr. Res. 103 (2018) 110–122.

[49] G. Mertens, R. Snellings, K. van Balen, B. Bicer-Simsir, P. Verlooy, J. Elsen, Pozzolanic reactions of common natural zeolites with lime and parameters affecting their reactivity, Cem. Concr. Res. 39 (3) (2009) 233–240.

[50] T. Matschei, B. Lothenbach, F.P. Glasser, The role of calcium carbonate in cement hydration, Cem. Concr. Res. 37 (4) (2007) 551–558.

[51] T. Bakharev, Geopolymeric materials prepared using Class F fly ash and elevated temperature curing, Cem. Concr. Res. 35 (6) (2005) 1224–1232.

Effect of silica modulus on the geopolymerization activity of natural pozzolans

Rafia Firdous[1], Dietmar Stephan[1]*

[1]Technische Universität Berlin, Department of Civil Engineering, Building Materials and

Construction Chemistry, Gustav-Meyer-Allee 25, 13355 Berlin, Germany

*Corresponding author E-mail: stephan@tu-berlin.de

Table 1
Physical properties of all samples used in this study

Sample ID	Density (g/cm³)	Blaine fineness (cm²/g)	d_{90} (µm)	d_{50} (µm)
BT1	2.6309	6641	38.551	12.567
BT2	2.6391	6746	22.867	5.393
RT	2.5955	6623	19.031	6.892
PLB	2.7922	6539	75.530	22.918
PLR	2.8437	6829	64.455	14.987
PF	2.5193	6576	51.125	13.238

- **Experimental method for selective dissolution analysis**

Several methods for determination of the degree of reaction of SCM's are available [1–3]. In the present research, the method of selective dissolution for determining the degree of reaction has been applied to natural pozzolan-based geopolymer prepared with various silica moduli. Selective dissolution method is an economical method and easy to perform. For this purpose, the method explained by RILEM TC 238-SCM-based on European Technical report CEN/TR 196-4 has been implemented [3]. The hardened geopolymer samples were immersed in isopropanol for 24 h followed by freeze-drying for 7 d. To reduce the effect of carbonation outer layer of the sample was not included. Immediately before application of selective dissolution experiment, samples were ground by hand with mortar and pestle to < 125 µm. If necessary, the samples were stored (after freeze drying or grinding) in a desiccator under

vacuum with soda lime to reduce the effect of carbonation. Prior to dissolving the sample in acid solution, the ground samples and filter paper of pore diameter 2 – 3 μm were oven dried at 105 °C for 1 h and were stored in a desiccator. The filter paper was weighted to a precision of 0.0001 g after drying. The acid solution consisted of 41 mL concentrated HCl (37 wt.-%) and 50 g salicylic acid, made up to 1 L with methanol. 2.000 ± 0.001 g of ground geopolymer samples was mixed with 200 mL of prepared acid solution on a magnetic stirrer for 30 min, followed by filtering the samples through pre-moisten filter paper under vacuum to obtain the insoluble residue. The glass beaker was washed thoroughly with methanol to obtain all residue on filter paper. During the filtration process, the filter paper was observed to get violet colour which is because of the precipitation of salicylic acid due to evaporation of methanol. Therefore, the filter paper was washed with methanol until it became white. Afterwards, the residue with filter paper was dried in an oven at 105 °C for 2 h and was weighted to a precision of 0.0001 g. Subtracting the weight of clean filter paper from the weight of residue and filter paper provided the weight of residue. Eq. 1 was applied to calculate the degree of reaction (α).

$$\alpha = [(100\text{fp} - R_b)/100\text{fp}] \times 100\,\%$$ (1)

Where f is the mass fraction of natural pozzolan in the initial dry binder, p is the mass fraction of natural pozzolan undissolved by the acid solution and R_b is the mass of residue from natural pozzolan geopolymer paste in g/100 g of the unreacted binder. Because of the lower sulphate content present in the natural pozzolans, sulphate correction was not applied.

References

[1] Durdziński PT, Ben Haha M, Bernal SA, Belie N de, Gruyaert E, Lothenbach B et al. Outcomes of the RILEM round robin on degree of reaction of slag and fly ash in blended cements. Materials and Structures 2017;50(2):835.

[2] Han F, Liu J, Yan P. Comparative study of reaction degree of mineral admixture by selective dissolution and image analysis. Construction and Building Materials 2016;114:946–55.

[3] Villagrán-Zaccardi YA, Vollpracht A, Gruyaert E, Belie N de. Recommendation of RILEM TC 238-SCM: Determination of the degree of reaction of siliceous fly ash and slag in hydrated cement paste by the selective dissolution method. Materials and Structures 2018;51(1):835.

2.3. Impact of the mineralogical composition of natural pozzolan on properties of resultant geopolymers

Preprint Version

Submitted in the journal "Journal of Sustainable Cement-Based Materials"

Manuscript number: TSCM-2020-0075

Submission date: 01 June 2020

Authors: Rafia Firdous, Dietmar Stephan

Impact of the mineralogical composition of natural pozzolan on properties of resultant geopolymers

Rafia Firdous[a] and Dietmar Stephan[a]*

[a]*Institute of Civil Engineering, Building Materials and Construction Chemistry, Technische Universität Berlin, Gustav-Meyer-Allee 25, 13355 Berlin, Germany*

*Corresponding author E-mail: stephan@tu-berlin.de

Biographical information

Rafia Firdous

Since 2016 PhD candidate at Technische Universität Berlin in research group of Prof. Stephan. Completed master's studies in Civil Engineering in 2014 from University of Engineering and Technology, Lahore, Pakistan.

Dietmar Stephan

PhD studies (1996-1999) at Universität Siegen. Senior scientist for cement chemistry at Heidelberg Cement (1999-2001). Habilitation candidate (2001-2006) at Technische Universität München. Akademischer Oberrat (2006-2011) at Universität Kassel and habilitation in 2010. Since 2011 professor for Building Materials and Construction Chemistry at Technische Universität Berlin.

Impact of the mineralogical composition of natural pozzolan on properties of resultant geopolymers

This paper presents a comparison between the impact of different mineralogical compositions of natural pozzolans for geopolymer synthesis. Beyond an optimum silica modulus, the compressive strength either increases on low rate or decreases with age. The presence of zeolite minerals enhances the reactivity of natural pozzolans. In contrast, the presence of calcite can lead to the incorporation of calcium into the reaction products. At the same time, the carbonate can enhance the formation of sodium carbonate, which can deplete the alkalis and water from binder gel, thereby reducing the rate of compressive strength development. In severe cases, the crystallization pressure of sodium carbonate can cause a complete disintegration of the structure. These effects are pronounced for samples outside the optimum silica modulus range and for low reactive pozzolans.

Keywords: natural pozzolan; compressive strength; degree of reaction; crystalline mineral; calcite; sodium carbonate

1.   Introduction

Use of natural pozzolans for alkali-activated materials / geopolymers is another way to reduce the carbon dioxide (CO_2) footprint of construction industry [1,2]. Several studies have shown the potential of natural pozzolans as geopolymer precursor [3]. Being a rich source of silica- and alumina-bearing phases, natural pozzolans are potential raw materials for geopolymers [3,4]. The effect of the ionic concentrations of an alkaline solution on the properties of resultant geopolymers synthesized from several natural pozzolans showed varying compressive strength and microstructural characteristics [5–7], indicating that the reactivity of different natural pozzolans is affected mainly by their chemical and mineralogical composition [8,9]. Furthermore, not only X-ray amorphous but also crystalline phases can participate in geopolymer reaction [8,10]. Though, the

2

impact of the mineralogical composition of a pozzolan on its reactivity is only partially understood. For example, the composition of natural pozzolans like volcanic ashes depends on the composition of lava and the external conditions at the time of formation until the current age [11]. These compositional variations limit the formulation of general rules for the use of natural pozzolans as geopolymer precursor. In order to extrapolate the use of natural pozzolans, it is necessary to carry out comparative studies between different natural pozzolans, taking into account the effect of mineralogy on the properties of the resultant geopolymer and to understand the reasons behind the different reactivity of these natural pozzolans.

A further impact on the performance of natural pozzolan-based geopolymers is the formation of alkali salts [5,12,13]. Carbonation, in general, is the formation of carbonates within the binder which reduces the pH of the system and can degrade the binding gel, whereas efflorescence is the precipitation of the salts on the surface because of the reaction of free alkalis with environmental CO_2 [14,15]. Efflorescence under the surface of the sample is known as subflorescence [14], which can cause crystallization pressure in the voids, thus generating inner tensile stresses, causing weakening of the structure and reducing the compressive strength [14,16]. Moreover, the formation of efflorescence can cause depletion of alkalis, thus hindering the further progress of reaction [5,14,16] and therefore, the rate of strength gain can decrease. However, the impact of the mineralogical composition of natural pozzolan on the carbonation and efflorescence is not studied.

Therefore, this study aims at a comparison of two natural pozzolans with different mineralogical composition as precursors for geopolymers at short and long curing times. These differences will enable to compare the underlying differences in the geopolymeric potential of these precursors. These pozzolans include a zeolite-

3

containing pozzolan and a calcite-containing pozzolan. The impact of crystalline phases and the reasons for the performance of each pozzolan are discussed. Furthermore, the impact of the crystalline phases on compressive strength, degree of reaction and microstructure are discussed. At the outset, several silica moduli were used to examine the development of the compressive strength of the resultant geopolymers until an age of 90 d. Based on these results, the three silica moduli which exhibited the highest compressive strength for each natural pozzolan were used to study the impact of mineralogy via X-ray diffraction (XRD) analysis and degree of reaction by thermogravimetric analysis (TGA) and selective dissolution at 7, 28 and 90 d.

2. Materials and methods

2.1. Materials

Two natural pozzolans from Germany, named as Rhenish trass (RT) and Bavarian trass (BT), were used in this study. Their chemical compositions, provided in Table 1, were determined by X-ray fluorescence (XRF), using a PHILIPS PW 2400. Specific surface area is a factor determining the reactivity of natural pozzolans, therefore, the Blaine fineness (measured in accordance with [17]) of RT and BT was kept equal to 6600 and 6700 cm^2/g, respectively. To achieve this Blaine fineness, RT was further milled in a planetary ball mill (PULVERISETTE 5 classic line, Fritsch GmbH), while the BT powder was used as received. XRD analysis was performed using a PANalytical Empyrean with CuKα radiation ($\lambda = 1.54$ Å) and Ni filter operating at 40 kV and 40 mA in continuous mode, with a resolution of 0.0131° and a speed of 0.0176 °/s, in a range from 5° to 65° 2θ. The phase evaluation was performed using HighScore Plus software with inorganic crystal structure database (ICSD). Figure 1 presents the X-ray diffractograms of both natural pozzolans with their mineralogical phases. Besides the

4

crystalline phases indicated, at least one glass phase was present in both samples. The determined mineralogical phases were in accordance with the literature [18–21]. The mineralogical analysis of both pozzolans showed that RT contained albite, augite, biotite, calcite, larnite, leucite, muscovite, nepheline, quartz, sanidine, and several zeolite minerals such as chabazite, phillipsite and analcime. In contrast, BT contained albite, augite, biotite, quartz, sanidine, and a prominent amount of calcite. Quantification of the phases was not done as the high number of phases (with in most cases flexible chemical and crystallographic characteristics) would lead to a limited accuracy of the quantification.

For the desired study, geopolymer samples were prepared with alkaline solutions of several silica moduli ($Ms = SiO_2/Na_2O$, mol/mol) and were tested at various ages. The silica moduli used and the detailed molar ratios of H_2O/SiO_2 and H_2O/Na_2O are presented in Table 2. To achieve the various silica moduli, sodium hydroxide (NaOH) solutions were combined with a sodium silicate solution (Betol 52T from Woellner GmbH, $Ms = 2.12$, $SiO_2 = 30.2$ wt.-%, $Na_2O = 14.7$ wt.-%). NaOH solutions were prepared by dissolving NaOH pellets (99 wt.-%, VWR International GmbH) in deionized water at least 24 h before use, to allow full dissolution and equilibration.

2.2. *Experimental methodology*

The pastes were prepared by mixing natural pozzolan with the alkaline solution for 3 min, with an in-between break of 30 s, using a laboratory hand mixer. The samples were then molded into cubes ($2 \cdot 2 \cdot 2$ cm³) and compacted on a vibration table for 2 min. The samples were seal cured at 22 ± 2 °C and 100% relative humidity till the test age. The alkaline solution to solid ratio was determined, in order to attain pastes of standard consistency in accordance with [22] and was kept at 0.50 for RT and 0.75 for BT geopolymers.

5

The compressive strengths of the hardened geopolymer samples were measured at 7, 28 and 90 d age, using a Toni Technik Model 2060, Zwick Roell. The samples were prepared using silica moduli, as given in Table 2. Based on the results of compressive strength tests, geopolymer samples prepared with silica moduli of 0.946, 1.061 and 1.272 for RT and 0.707, 0.797 and 1.061 for BT were further investigated by X-ray diffraction (XRD) analysis, thermogravimetric analysis (TGA) and selective dissolution analysis at 7, 28 and 90 d age. These tests were performed to study the impact of the different mineralogical composition of these natural pozzolans on the phase composition and degree of reaction by indirect and direct methods. For these investigations, crushed samples from the hardened geopolymer pastes were taken at the ages mentioned above and the reaction was stopped with solvent exchange using isopropanol and freeze-drying. In case of storage, the samples were placed in a desiccator with silica gel and sodium hydroxide (on support, Merck, KGaA) to reduce the effect of environmental carbonation.

XRD on powdered (by mortar and pestle) geopolymer samples was performed using the method explained in section 2.1. TGA was performed using a TG 209 Tarsus F3, Netzsch Instruments, under a nitrogen atmosphere at a flow rate of 40 mL/min. For each test, 10 ± 1 mg of ground sample was used. Each sample was first held at 25 °C for 20 min and then heated from 25 to 850 °C at a heating rate of 10 °C/min. Selective dissolution was performed to directly quantify the degree of reaction, using a method explained by RILEM TC 238-SCM, based on European technical report CEN/TR 196-4 [23]. The degree of reaction (α) was calculated using Eq. (1):

$$\alpha = \{1 - [Rb/(100 \cdot f \cdot p)]\} \cdot 100 \ \% \hspace{2cm} (1)$$

Where f is the mass fraction of natural pozzolan in the initial dry binder, p is the mass fraction of natural pozzolan undissolved by the acid solution, and Rb is the mass

6

of residue from natural pozzolan geopolymer paste in g/100 g of the unreacted binder. Because of the low sulphate content present in the natural pozzolans, sulphate correction was not applied. The detailed experimental method has been explained in [8].

To allow further conclusions form the results obtained from the pozzolan samples, a natural calcite sample (6700 cm^2/g) was reacted with sodium silicate solution (Ms = 1.061) for 8, 28 and 90 d age and tested with XRD and TGA, by following the same methodology as explained above.

3.   Results

3.1.   Compressive strength

Figure 2 and 3 present the dependence of the compressive strength on curing time and the silica modulus of alkaline activator for RT- and BT-based geopolymers, respectively. Throughout the text, the samples are labelled with their respective natural pozzolan, silica modulus and/or age. The compressive strength changed non-linearly with the age of the sample, and the rate of strength gain with age depended on the silica modulus of the alkaline activator and the type of natural pozzolan used. For RT-based geopolymers (Figure 2a, 2b, 2c) the rate of strength gain was faster from 7 to 28 d as compared to the interval from 28 to 90 d, which in turns reveals that the rate of geopolymer reaction is faster at early ages but continues over a longer time. The sample with the lowest Ms (RT-0.707, Figure 2a) exhibited an increase in strength from 7 to 28 d and a drop in strength at 90 d. Similar behavior was also observed for samples made with the highest silica moduli (1.305, 1.499, 1.716). The samples made with silica moduli of 0.946, 1.061, 1.158 and 1.272 exhibited the highest rate of strength gain with age. The sample RT-1.272 achieved 29% and 55% of 90 d compressive strength at 7 and 28 d, respectively. Its highest rate of strength gain was observed between 28 and 90

7

d. The outstanding behavior of this sample is further investigated by selective dissolution in section 3.3.2.

To see the effect of the silica modulus, the compressive strength was plotted against silica moduli for various ages (Figure 2d). It clearly shows the presence of a so-called optimum range of silica modulus, where the highest compressive strength is achieved. At 7 d, the strength increased with rising silica modulus until 0.946, after which it decreased slightly with a further increase in the silica modulus. At 28 and 90 d, the samples prepared with the silica moduli 0.946, 1.061, 1.158 and 1.272 exhibited the highest compressive strength. For these optimum range samples, the strength was found to increase over the whole time of observation. However, several samples outside this range exhibited either a very low rate of increase of strength or even a decrease of strength with the age of the sample, as described above.

For BT-based geopolymers (Figure 3), the highest compressive strength was obtained for samples prepared with silica moduli of 0.707, 0.797, 0.946 and 1.061, which can be considered as the optimum range for BT. The rate of strength gain was highest for silica modulus of 0.707. Like in RT geopolymers, the strength and rate of strength gain both decreased outside the optimum silica modulus range. For BT, samples with activator solution high in SiO_2 exhibited much lower strength than samples with a higher Na_2O content (Figure 3c). However, for several samples, the formation of sodium carbonate (confirmed by XRD) remained a problem (Figure 3a, 3b, 3d). The samples made with silica moduli of 1.158 and 1.272 (Figure 3b) lost their structure entirely at 90 d due to sodium carbonate and were therefore untestable (compressive strength equal to zero).

For both geopolymers, higher silica modulus of alkaline solution reduced the compressive strength likely due to a decreasing rate of reaction. As the reduction in pH

8

61

of alkaline solution, higher viscosity of the alkaline solution and a higher degree of silicate polymerization in alkaline solution slows down the geopolymer reaction [24,25]. The reduction of compressive strength with age in RT can be attributed to a possible collapse of geopolymer gel due to alkali depletion or unstable geopolymer gel formation [26].

For each natural pozzolan, three samples exhibiting the highest compressive strength were chosen for the analyses presented in sections 3.2 and 3.3. For RT geopolymers, these samples included silica moduli of 0.946, 1.061 and 1.272; while for BT geopolymers, samples with silica moduli of 0.707, 0.797 and 1.061; each at 7, 28 and 90 d.

3.2. *Impact of mineralogical composition*

To explore the reasons for the different performance of the two pozzolans, the impact of mineralogical composition was studied by comparing the raw pozzolans with respective geopolymer samples by XRD. Figure 4a and 4b present the diffractograms of RT and BT and their corresponding geopolymer samples at 90 d, respectively. The diffractograms of other silica moduli and ages depicted similar trends and are therefore presented in the supplementary material (Figure S1 to S3). Comparing the raw pozzolans with their geopolymers, changes in the crystalline and amorphous phases can be discerned. Again, a quantification of the phases was not done as due to the complex nature of the samples, considerably low accuracy of the quantification is to expect. Nevertheless, a relative comparison of the peak intensities is possible. Several crystalline minerals present in RT and BT reduced substantially in their reflex heights after the reaction, which indicates that these minerals have partially participated in geopolymer reaction. For RT, the participating crystalline phases include phillipsite (reflexes at 25.2°, 32.5° and 34.4° 2θ), chabazite (24.8°, 27.5° and 29.4° 2θ), larnite

9

(32.2° and 34.4° 2θ) and calcite (only main peak at 29.4° 2θ visible) (Figure 4a). The diffractogram of raw pozzolan BT (Figure 1, Figure 4) shows compared to RT a much stronger main reflex of calcite (29.4° 2θ) and also several other reflexes of calcite (23.1°, 35.9° and 39.5° 2θ) indicating a higher calcite content in BT. All these reflexes were found to reduce strongly in BT geopolymer sample, while the reflex intensities of biotite, albite and sanidine may also have slightly reduced.

In both RT and BT geopolymers, the formation of a new semi-crystalline phase was observed by the shift of the amorphous hump center from approx. 27° to 31° 2θ for all samples. Furthermore, a significant increase in the height of the amorphous hump between the raw and reacted sample was observed for RT, while for BT a slight increase in the height of the amorphous hump was observed. Such a shift and increase of amorphous hump is attributed to the formation of geopolymeric gel [27,28]. Moreover, in BT geopolymers, the shape of the amorphous hump ranging from 5.5° – 8.5° 2θ changed and its center moved to higher 2θ values, which may correspond to the participation of this partially crystalline phase in geopolymer reaction [29]. In RT geopolymers, the successive increase in the intensity of the reflex at 29.8° 2θ corresponds likely to the formation of zeolite-like geopolymeric gel [29], while broadening of reflexes around 35° and 37.8° 2θ at all ages reflects the formation of an aluminosilicate gel structure.

The formation of sodium carbonate in BT geopolymers (as also seen in Figure 3) was reflected by XRD as the new phase natrite (γ-Na_2CO_3, ICSD No. 95549), at all ages. It should be mentioned here that the actually formed carbonate phase is thermonatrite ($Na_2CO_3 \cdot H_2O$, ICSD No. 6293) which converted to natrite by the applied freeze-drying. This was confirmed by collecting the material from the sample surface and directly testing by XRD. Such conversion was useful for accurate measurement of

10

bound water in geopolymer gel which is presented in section 3.3.1, while for all other methods the hydration state of sodium carbonate is not relevant. The formation of this phase and aragonite has been attributed to carbonation or efflorescence [14,30].

3.3. Degree of reaction

The degree of reaction can be determined indirectly by water contained in the geopolymer gel or directly by selective dissolution. In this part, both methods are used to firstly determine the degree of reaction and secondly to see the impact of the formed sodium carbonate on geopolymer reaction.

3.3.1. Thermogravimetric analysis (TGA)

Figure 5 shows the results of RT- and BT-based geopolymers prepared with silica modulus of 1.061, while the other results are presented in the supplementary material (Figure S4). The thermogravimetric curves (TG) are characterized by two mass loss steps (Figure 5a and 5b), with the first step mainly representing the liberation of loosely bound water, followed by a more or less continuous liberation of more tightly bound water molecules and OH groups till 600 °C [26,31]. The second mass loss step starting at 600 °C, represents calcite ($CaCO_3$) decomposition [32,33]. The intensity of this second mass loss step decreased with geopolymerization, indicating once again the participation of calcite in geopolymer reaction. For all the reacted samples, the overall mass loss increased in comparison to the raw samples, however, the rate of increase was different for both natural pozzolan-based geopolymers, and it depended on the silica modulus of alkaline solution and age of the sample.

Winnefeld et al. [34,35] described that the mass loss for total bound water from 30 – 600 °C could be used as a relative measure of the degree of reaction. Therefore, similar investigations are made on RT and BT geopolymers and results are presented in

11

Figure 6. For RT geopolymers (Figure 6a), a continuous geopolymer reaction till 90 d can be seen by the increase of bound water content. The samples RT-0.946 and RT-1.061 had a higher amount of bound water at 7 d, in comparison to RT-1.272. However, all samples had nearly the same bound water content at 28 d. The compressive strength of these samples at 7 and 28 d followed a similar trend. At 90 d, all samples showed nearly the same amount of bound water, while compressive strength being highest for sample RT-1.272. The higher compressive strength could be due to the higher amount of soluble silica in this sample in comparison to the other samples (Table 2).

For the BT geopolymers (Figure 6b), the bound water content increased from 7 to 28 d, indicating an increase in the extent of the geopolymer reaction. Sample BT-1.061 had the lowest amount of bound water at all ages and also the lowest compressive strength. Similarly, BT-0.707 and BT-0.797 had comparable compressive strength and bound water content at 7 d. However, at 28 d the compressive strength of BT-0.707 was higher than that of the other samples, as was the bound water content. At 90 d, the bound water content decreased slightly for all samples, which is expected to be a result of sodium carbonate formation. As it has been reported by Zhang et al., Na^+ and OH^- in a geopolymer can react with environmental CO_2, thus taking water out of the geopolymer matrix and forming alkali carbonate [16]. These findings support the slow rate of strength gain observed at later ages, as the depletion of mobile Na^+ and OH^- resulting from sodium carbonate formation hindered geopolymer reaction and thus effected the strength development. As no sodium carbonate was observed in RT geopolymers, therefore, this impact is only observed in BT geopolymers. However, the impact of mineralogical composition on sodium carbonate formation will be discussed in section 4.

12

3.3.2. Selective dissolution analysis

The results of the degree of reaction, calculated from the selective dissolution for RT- and BT-based geopolymers, are presented in Figure 7a and 7b, respectively. For RT geopolymers (Figure 7a), the degree of reaction increased with sample age for all silica moduli of the alkaline activator. For each sample age, the degree of reaction was higher for lower silica modulus, which is in accordance with the compressive strength and thermogravimetric analysis. However, at 7 d, the compressive strengths of the three samples of RT-based geopolymers were in a close range, while bound water content by thermogravimetric analysis showed a lower value for RT-1.272 and the degree of reaction by selective dissolution showed a value almost 18% lower. This sample had the highest amount of soluble silica. For the sake of comparison, selective dissolution analysis was also applied on both liquid and dried sodium silicate solution with the results showing no dissolution of sodium silicate in the acidic system used. It can therefore be said that the increase in compressive strength for sample RT-1.272 was a result of the presence of the hardened activator, with a lower amount of geopolymer gel formed, as shown by selective dissolution. This also confirms that higher SiO_2 content in a system leads to a lower dissolution of aluminosilicate phases.

For each age of the BT geopolymers (Figure 7b), a higher silica modulus of alkaline solution led to a lower degree of reaction, which is in accordance with the compressive strength and thermogravimetric analysis. However, the degree of reaction, by selective dissolution, was found to decrease significantly till 28 d and stayed afterwards apparently constant. The accurate determination of degree of reaction by selective dissolution for these samples is hindered by sodium carbonate. As the sodium carbonate collected from the surface of geopolymer samples dissolved entirely in the used acidic solutions, hence giving false indication of the degree of reaction.

13

4. Discussion

Based on the available literature, the low performance of BT-based geopolymers can be attributed to efflorescence or subflorescence. As the subflorescence can cause inner tensile pressure which can weaken the structure, reduce the rate of strength gain by alkali depletion or in extreme cases, destruction of the sample (Figure 3b). Considering the impact of mineralogical composition, BT contains an appreciable amount of calcite which participated in the geopolymeric reaction (Figure 4 and 5). Consequently, the reaction of calcite could be a potential source of carbonate for sodium carbonate formation next to the efflorescence caused by atmospheric CO_2. To confirm this possibility, natural calcite was subjected to reaction with the sodium silicate solution, and the paste samples were tested with XRD and TGA. Such study is made only to mimic this reaction, as the tested natural calcite and calcite present in the natural pozzolan can differ in particle size and degree of crystallinity. Nevertheless, using a natural calcite sample clarifies its general behavior in the discussed system.

The reaction of calcite with sodium silicate solution resulted in an increase of background in XRD and natrite was observed (Figure 8a), which was also detected in the geopolymers of BT. The increase in the background indicates the formation of a semi-crystalline reaction product. TGA (Figure 8b) gave three distinct thermal decomposition events in the reacted calcite sample at various ages. The first decomposition is likely because of the liberation of loosely bound water. The second decomposition is associated with the decarbonization of calcite, and a third mass loss begins at approx. 800 °C. The strong decrease in the mass loss of calcite in reacted samples indicates significant but incomplete participation of calcite in reaction. Natrite does not decompose in the examined temperature rage [36]. Therefore, the mass losses around 100 and 800 °C are likely because of the semi-crystalline phase observed by

14

XRD. Based on the chemistry of the system (calcium carbonate + sodium silicate solution), calcium-containing binder gel is likely to form. Upon reaction of limestone with sodium silicate solution, the formation of C-S-H, N-C-S-H and N-S-H have been reported by [37]. Combing these results, the first mass loss in TGA (around 100 °C) is due to the water liberation from a semi-crystalline phase, while a mass loss around 800 °C can be attributed to the dehydroxylation of C-S-H gel [33,38].

It can thus be stated that calcite has both positive and negative roles in geopolymer reaction, as on the one hand, it can participate in gel formation, while on the other hand, it leads to the formation of alkali carbonates. The inclusion of Ca^{2+} from calcite can replace alkalis in the gel structure, thus leaving free alkalis in the system which can react with CO_3^{2-} from calcite and form alkali carbonate. These reactions increase the rate of alkali depletion and water as indicated by TGA (Figure 6b), thus weakening the structure and causing lack of strength development.

As the source of carbonate for sodium carbonate formation can also be calcite and not only atmospheric CO_2, the definition of efflorescence and subflorescence might be extended, or a new term like self-florescence or auto-florescence can be introduced. The alkali carbonate formation in BT is responsible for its reduced performance as the calcite supplies carbonate from the beginning of the reaction. Consequently, alkali carbonates can form in large quantity inside the sample (and may damage the structure by introducing tensile forces) whereas the CO_2 penetration depth for alkali-activated slags has been reported to be 1 mm/year [39]. Therefore, the damage because of calcite is likely more severe than the formation of carbonates with CO_2 from the air in the experimental duration.

Furthermore, compressive strength showed dependency on silica modulus (Figure 2 and 3). For BT, several samples showed sodium carbonate formation while

15

samples rich in alkalis showed high compressive strength. Several samples outside the optimum range showed a complete collapse because of sodium carbonate. This can be understood in the way that for the samples achieving high compressive strength, their tensile strength is also high enough to bear the crystallization pressure caused by the growth of sodium carbonate. While for a low reactive sample, the crystallization pressure is too high and damage to the structure (in some cases till the total disintegration) occurred.

Considering the differences in the mineralogy of both natural pozzolans and resultant reaction products, the higher reactivity of RT is may be due to the presence of zeolites actively participating in the reaction. Previous studies have shown the pozzolanic reactivity of zeolite minerals (chabazite, phillipsite, analcime) [40,41]. For a tuff majorly composed of zeolite (mordenite) upon its reaction with sodium silicate solution, the formation of N-A-S-H gel has been observed [42]. The formation of zeolite-like geopolymer gel in RT geopolymers and participation of zeolite minerals is in good agreement with the literature. Additionally, RT also contained calcite which had also participated in the reaction (Figure 4a), but the formation of sodium carbonate was not observed. This can be because of two reasons, (1) low content of calcite in RT, (2) the higher reaction degree of RT suppresses the negative effect of calcite. As a result, RT exhibited higher compressive in comparison to BT. For BT, a lower silica modulus of the alkaline solution was required to achieve useful strength. Moreover, the formation of sodium carbonate hindered the determination of the degree of reaction by selective dissolution indicating that selective dissolution cannot be accurately applied to low reactive natural pozzolan samples, which are prone to carbonate formation.

5.   Conclusions

In this work, two natural pozzolans were subjected to geopolymer synthesis. For a low

16

reactive pozzolan, a lower silica modulus of the alkaline solution is required to achieve higher compressive strength. A pozzolan rich in zeolite minerals is a more suitable precursor than a pozzolan containing calcite. The presence of calcite in natural pozzolan can enhance the availability of calcium for binder gel. In contrast, the carbonate can enhance the precipitation of efflorescence-like phases, which can cause depletion of alkalis and water, thus weakening the geopolymer structure and reducing the compressive strength. The adverse effects of carbonate are more evident for samples outside the optimum range because of their low reactivity. Selective dissolution by acidic solutions is not suitable for low reactive natural pozzolans containing calcite prone to sodium carbonate formation. As this carbonate also dissolves in the used acidic solutions, thereby giving a false indication of the degree of reaction. Use of alcohol-based solutions for an accurate determination of the degree of reaction for such systems could prevent this error. The formed geopolymer gel is majorly X-ray amorphous, and for a zeolite-containing pozzolan, the more crystalline parts of geopolymer gel have a zeolite-like structure.

Geolocation information

Berlin, Germany.

Acknowledgements

17

Conflict of Interest

None

Appendix A

Supplementary material

References

[1] Robayo-Salazar R, Mejía-Arcila J, Mejía de Gutiérrez R, et al. Life cycle assessment (LCA) of an alkali-activated binary concrete based on natural volcanic pozzolan: A comparative analysis to OPC concrete. Constr. Build. Mater. 2018;176:103–111.

[2] van Deventer JSJ, San Nicolas R, Ismail I, et al. Microstructure and durability of alkali-activated materials as key parameters for standardization. J. Sustain. Cem. Mater. 2015;4:116–128.

[3] Firdous R, Stephan D, Djobo JNY. Natural pozzolan based geopolymers: A review on mechanical, microstructural and durability characteristics. Constr. Build. Mater. 2018;190:1251–1263.

[4] Hewlett PC, Lea FM, editors. Lea's chemistry of cement and concrete. 4th edn. Oxford: Elsevier Butterworth-Heinemann; 2004.

[5] Bondar D, Lynsdale CJ, Milestone NB, et al. Effect of type, form, and dosage of activators on strength of alkali-activated natural pozzolans. Cem. Concr. Compos. 2011;33:251–260.

[6] Firdous R, Stephan D, Jin Y. Investigation of Rhenish and Bavarian Trass as Geopolymer Precursor. 20th International Conference of Building Materials - Ibausil 2018, 12 – 14 September 2018, Weimar, Germany. 2018;Book 2:617–624.

[7] Khalifeh M, Saasen A, Vrålstad T, et al. Experimental study on the synthesis and characterization of aplite rock-based geopolymers. J. Sustain. Cem. Mater. 2016;5:233–246.

[8] Firdous R, Stephan D. Effect of silica modulus on the geopolymerization activity of natural pozzolans. Constr. Build. Mater. 2019;219:31–43.

[9] Lemougna PN, Chinje Melo UF, Delplancke M-P, et al. Influence of the chemical and mineralogical composition on the reactivity of volcanic ashes during alkali activation. Ceram. Int. 2014;40:811–820.

18

[10] Djon Li Ndjock BI, Elimbi A, Cyr M. Rational utilization of volcanic ashes based on factors affecting their alkaline activation. J. Non-Cryst. Solids. 2017;463:31–39.

[11] Snellings R, Mertens G, Elsen J. Supplementary Cementitious Materials. Rev. Mineral. Geochem. 2012;74:211–278.

[12] Firdous R, Stephan D. Influence of heat treatment and mechanical activation on reactivity of natural pozzolan for geopolymer synthesis. In V. Caprai, & H. J. H. Brouwers (Eds.), Proceedings of 2nd International Conference of Sustainable Building Materials (ICSBM 2019), Eindhoven, The Netherlands, 12 – 15 August 2019. 2019;Vol. 2, ID 057:138–155, ISBN (print):978-90-386-4911-5, In press.

[13] Kani EN, Allahverdi A, Provis JL. Efflorescence control in geopolymer binders based on natural pozzolan. Cem. Concr. Compos. 2012;34:25–33.

[14] Zhang Z, Provis JL, Ma X, et al. Efflorescence and subflorescence induced microstructural and mechanical evolution in fly ash-based geopolymers. Cem. Concr. Compos. 2018;92:165–177.

[15] Shi C, Krivenko PV, Roy D. Alkali-Activated Cements and Concretes. Abingdon: Taylor & Francis Group; 2006.

[16] Zhang Z, Provis JL, Reid A, et al. Fly ash-based geopolymers: The relationship between composition, pore structure and efflorescence. Cem. Concr. Res. 2014;64:30–41.

[17] EN 196-6. Methods of testing cement – Part 6: Determination of fineness. 2010. Brussels: CEN.

[18] Jasmund K, Hentschel G. Seltene Mineralparagenesen in den Kalksteineinschlüssen der Lava des Ettringer Bellerberges bei Mayen (Eifel). Beiträge Mineral. Petrogr. 1964;10:296–314.

[19] Schwiete H-E, Ludwig U, Wigger K-H. Die Konstitution einiger rheinischer und bayrischer Trasse. Köln Opladen: Westdeutscher Verlag; 1961.

[20] Liebig E, Althaus E. Pozzolanic activity of volcanic tuff and suevite: effects of calcination. Cem. Concr. Res. 1998;28 (4):567–575.

[21] Ludwig U, Schwiete HE. Untersuchungen an Deutschen Trassen. Silicates Ind. 1963:439–447.

[22] EN 196-3. Method of testing cement - Part 3: Determination of setting times and soundness. 2016. Brussels: CEN.

[23] Villagrán-Zaccardi YA, Vollpracht A, Gruyaert E, et al. Recommendation of RILEM TC 238-SCM: Determination of the degree of reaction of siliceous fly ash and slag in hydrated cement paste by the selective dissolution method. Mater. Struct. 2018;51:835.

19

[24] Duxson P, Fernández-Jiménez A, Provis JL, et al. Geopolymer technology: The current state of the art. J. Mater. Sci. 2007;42:2917–2933.

[25] Gharzouni A, Joussein E, Samet B, et al. The effect of an activation solution with siliceous species on the chemical reactivity and mechanical properties of geopolymers. J. Sol-Gel Sci. Technol. 2015;73:250–259.

[26] Provis JL, van Deventer JSJ, editors. Geopolymers: Structure, processing, properties and industrial applications. Boca Raton, Fla.: CRC; Oxford : Woodhead; 2009.

[27] Zhang Z, Provis JL, Wang H, et al. Quantitative kinetic and structural analysis of geopolymers. Part 2. Thermodynamics of sodium silicate activation of metakaolin. Thermochim. Acta. 2013;565:163–171.

[28] Sun Z, Vollpracht A. Isothermal calorimetry and in-situ XRD study of the NaOH activated fly ash, metakaolin and slag. Cem. Concr. Res. 2018;103:110–122.

[29] Bakharev T. Geopolymeric materials prepared using Class F fly ash and elevated temperature curing. Cem. Concr. Res. 2005;35:1224–1232.

[30] Bernal SA, Provis JL, Brice DG, et al. Accelerated carbonation testing of alkali-activated binders significantly underestimates service life: The role of pore solution chemistry. Cem. Concr. Res. 2012;42:1317–1326.

[31] Davidovits J. Geopolymer Chemistry and Applications. Saint-Quentin, France: Institut Géopolymère; 2008.

[32] Bernal SA, Juenger MCG, Ke X, et al. Characterization of supplementary cementitious materials by thermal analysis. Mater. Struct. 2017;50:570.

[33] Scrivener K, Snellings R, Lothenbach B, editors. A Practical Guide to Microstructural Analysis of Cementitious Materials. Boca Raton: CRC Press; 2016.

[34] Ben Haha M, Le Saout G, Winnefeld F, et al. Influence of activator type on hydration kinetics, hydrate assemblage and microstructural development of alkali activated blast-furnace slags. Cem. Concr. Res. 2011;41:301–310.

[35] Winnefeld F, Ben Haha M, Le Saout G, et al. Influence of slag composition on the hydration of alkali-activated slags. J. Sustain. Cem. Mater. 2015;4:85–100.

[36] Kim J-W, Lee H-G. Thermal and carbothermic decomposition of Na_2CO_3 and Li_2CO_3. Metall. Mater. Trans. 2001;32B:17–24.

[37] Ortega-Zavala DE, Santana-Carrillo JL, Burciaga-Díaz O, et al. An initial study on alkali activated limestone binders. Cem. Concr. Res. 2019;120:267–278.

20

[38] Tajuelo Rodriguez E, Garbev K, Merz D, et al. Thermal stability of C-S-H phases and applicability of Richardson and Groves' and Richardson C-(A)-S-H(I) models to synthetic C-S-H. Cem. Concr. Res. 2017;93:45–56.

[39] Bernal SA, Provis JL, Green DJ. Durability of Alkali-Activated Materials: Progress and Perspectives. J. Am. Ceram. Soc. 2014;97:997–1008.

[40] Mertens G, Snellings R, van Balen K, et al. Pozzolanic reactions of common natural zeolites with lime and parameters affecting their reactivity. Cem. Concr. Res. 2009;39:233–240.

[41] Xu H, van Deventer JSJ. The geopolymerisation of alumino-silicate minerals. Int. J. Miner. Process. 2000;59:247–266.

[42] Baykara H, Cornejo MH, Murillo R, et al. Preparation, characterization and reaction kinetics of green cement: Ecuadorian natural mordenite-based geopolymers. Mater. Struct. 2017;50:188.
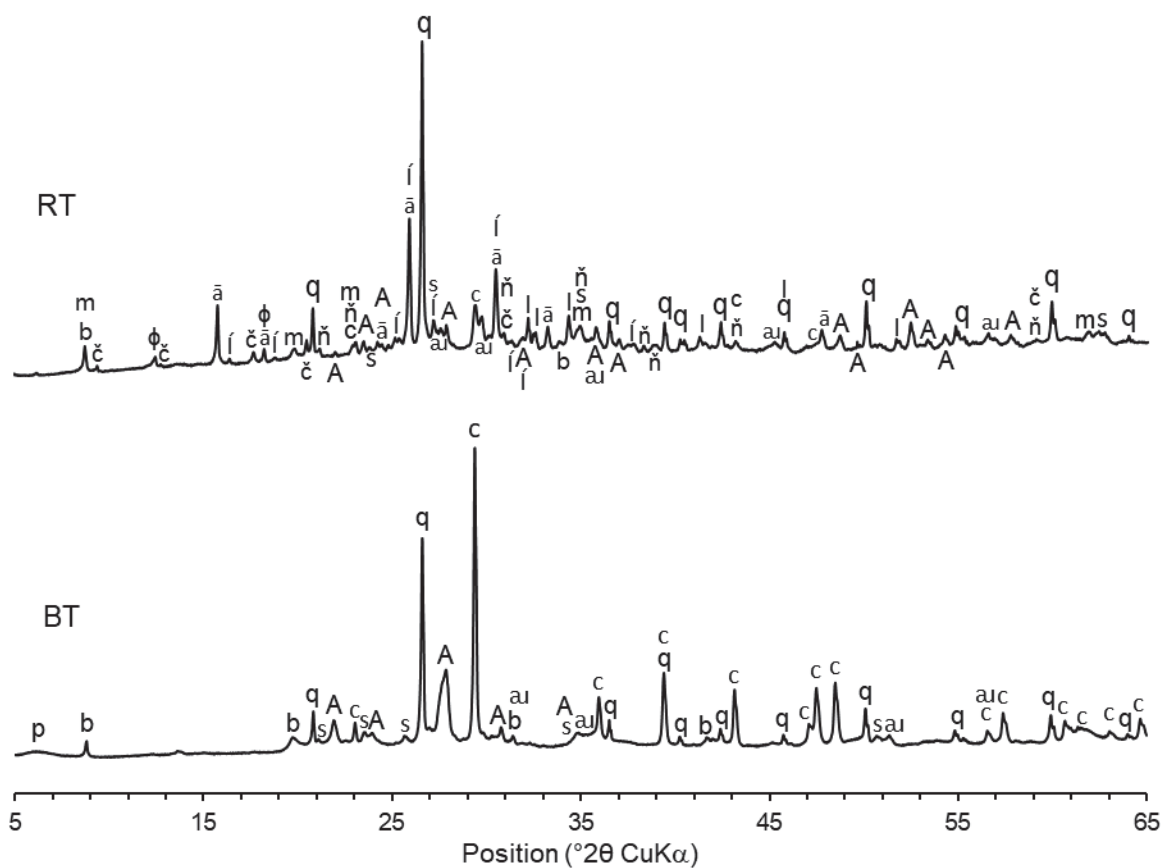
21

Table 1. Chemical compositions of RT and BT natural pozzolans in wt.-%.

Sample	LOI	SiO_2	Al_2O_3	Fe_2O_3	MnO	MgO	CaO	Na_2O	K_2O	SO_3
RT	6.50	50.20	17.48	5.10	0.22	1.51	8.76	4.03	4.79	0.47
BT	11.24	52.35	12.25	4.15	0.09	0.91	13.85	1.67	2.44	0.27

LOI is the loss on ignition at 1000 °C

Table 2. Molar ratios of all alkaline solutions used in this study.

SiO_2/Na_2O	0.707	0.797	0.946	1.061	1.158	1.272	1.308	1.365	1.499	1.716
H_2O/SiO_2	13.7	14.3	15.0	9.9	10.2	8.6	10.6	8.8	9.1	9.4
H_2O/Na_2O	9.7	11.4	14.2	10.5	11.8	11.0	13.8	12.0	13.6	16.1

Figure 1. Diffractograms of RT and BT with mineral phases and their ICSD numbers.

A Albite (70142), ā Analcime (9357), aɹ Augite (56935), b Biotite (95359), c Calcite (79674), č Chabazite (34173), l Larnite (79552), Í Leucite (161631), m Muscovite (75952), ň Nepheline (167001) , p Poorly crystalline phase, φ Phillipsite (51637), q Quartz (79634), s Sanidine (36234)
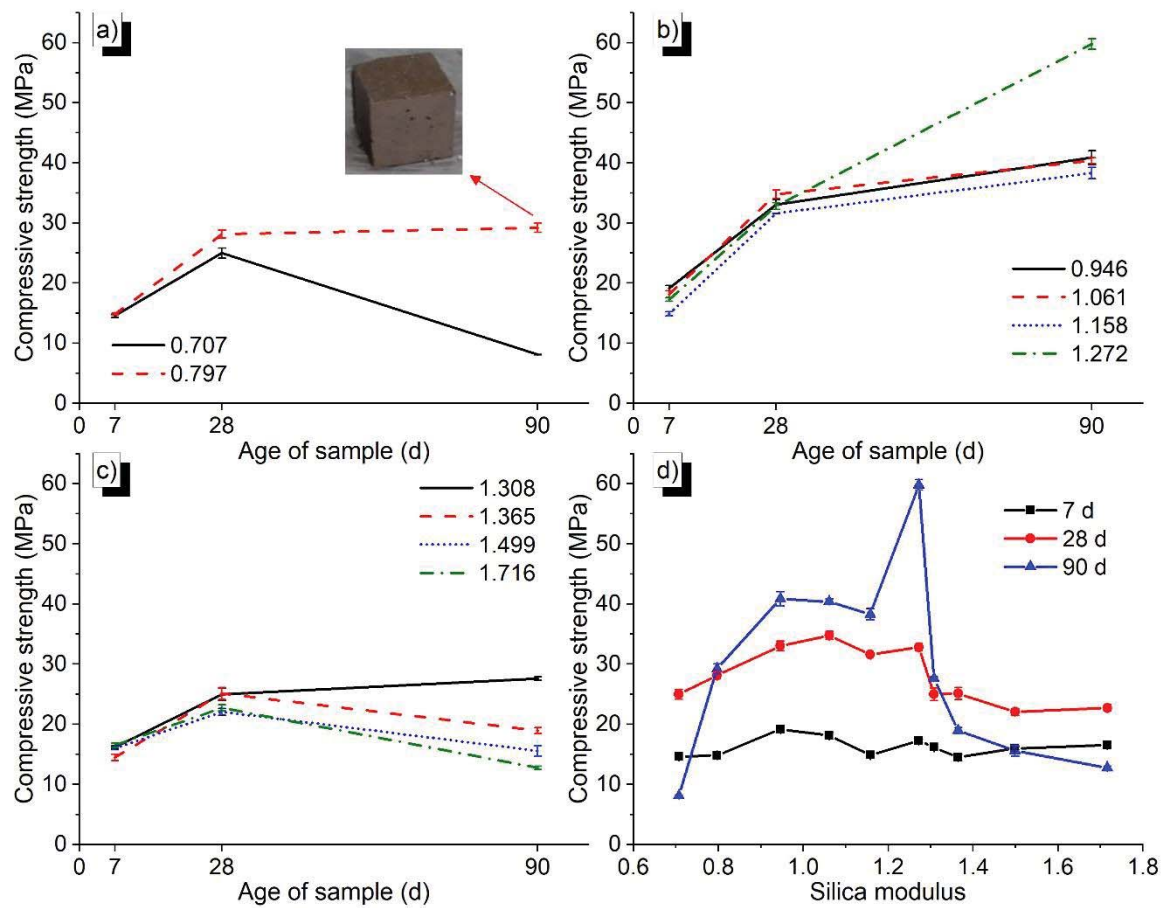
Figure 2. Compressive strength of RT-based geopolymers for different ages and silica moduli.
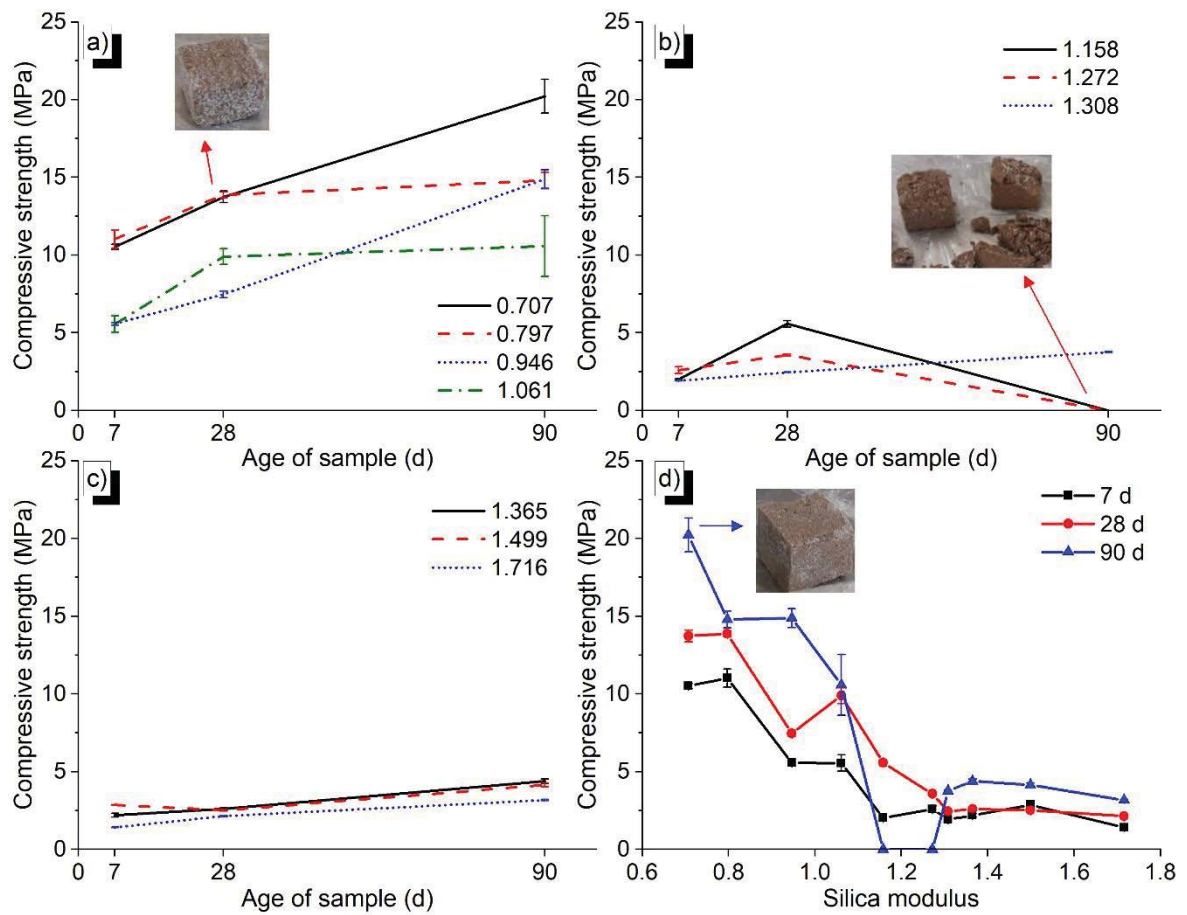
Figure 3. Compressive strength of BT-based geopolymers for different ages and silica moduli

ň Nepheline, m Muscovite, Í Leucite, č Chabazite, ɸ Phillipsite, l Larnite,
s Sanidine, A Albite, c Calcite, aʋ Augite, ā Analcime, b Biotite, z Zeolite
q Quartz, n Natrite, a Aragonite, p Partially crystalline phase

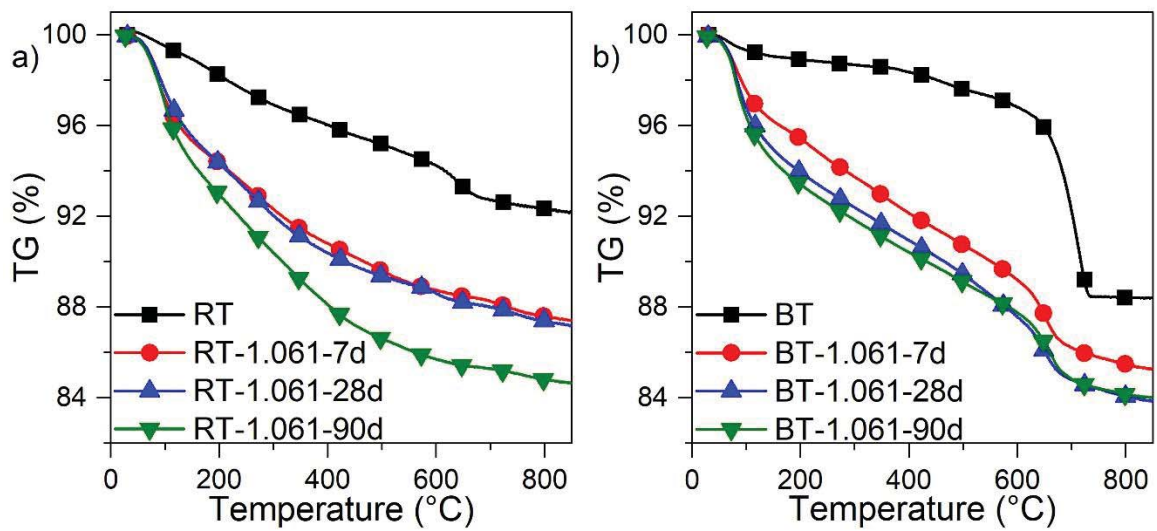Figure 4. XRD of (a) RT and (b) BT with respective geopolymer samples at 90 d.
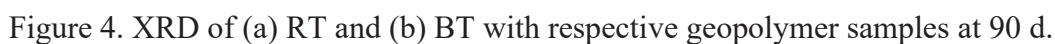
Figure 5. TG curves of (a) RT, (b) BT and their respective geopolymers (Ms = 1.061) at 7, 28 and 90 d age.
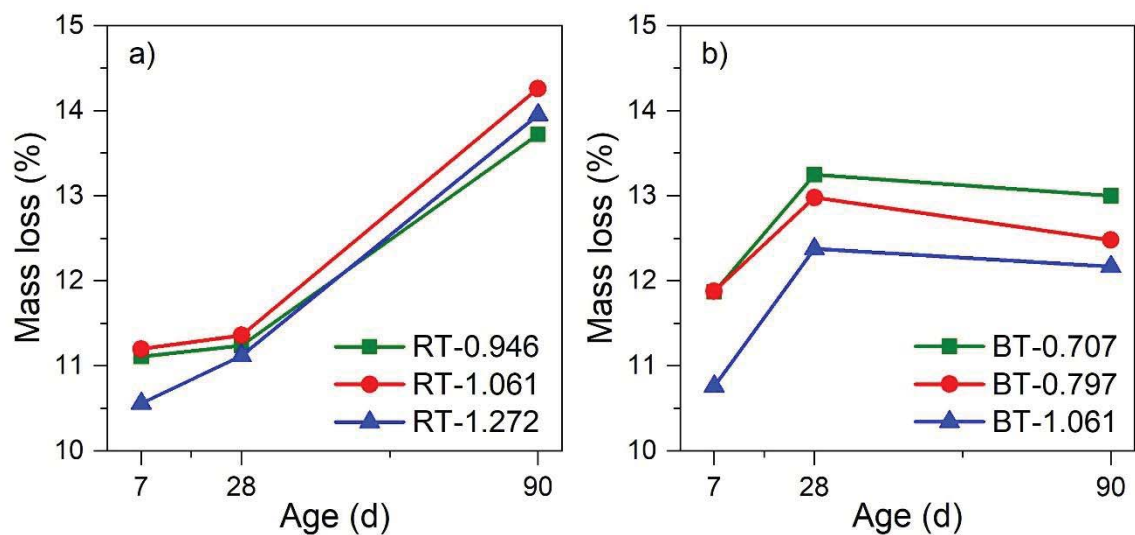

Figure 6. Weight loss from TGA (30 – 600 °C) of (a) RT- and (b) BT-based geopolymers at different ages in wt.-%.
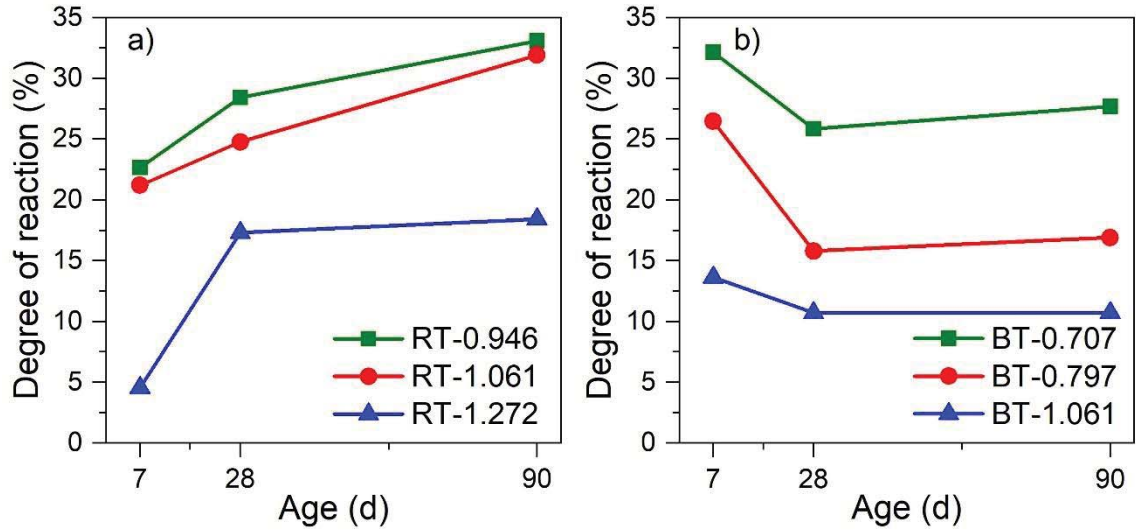
Figure 7. Degree of reaction based on selective dissolution plotted against age for (a) RT and (b) BT geopolymers.
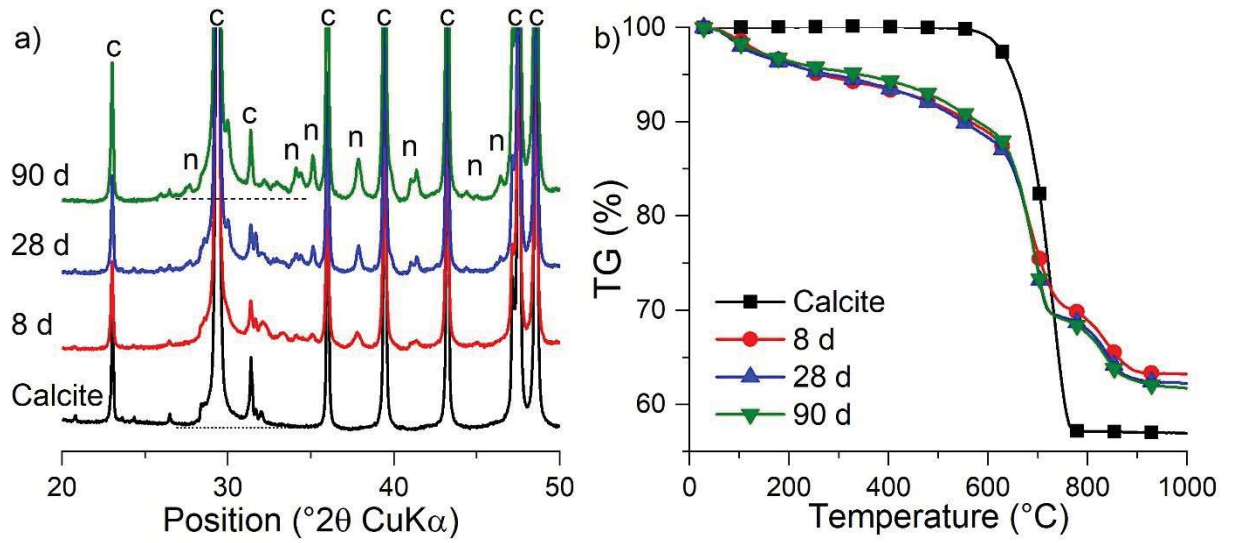
Figure 8. (a) XRD and (b) TGA of calcite sample reacted with sodium silicate solution at various ages

Impact of the mineralogical composition of natural pozzolan on properties of resultant geopolymers

Rafia Firdous[a] and Dietmar Stephan[a]*

[a]Institute of Civil Engineering, Building Materials and Construction Chemistry, Technische Universität Berlin, Gustav-Meyer-Allee 25, 13355 Berlin, Germany

*Corresponding author E-mail: stephan@tu-berlin.de

1
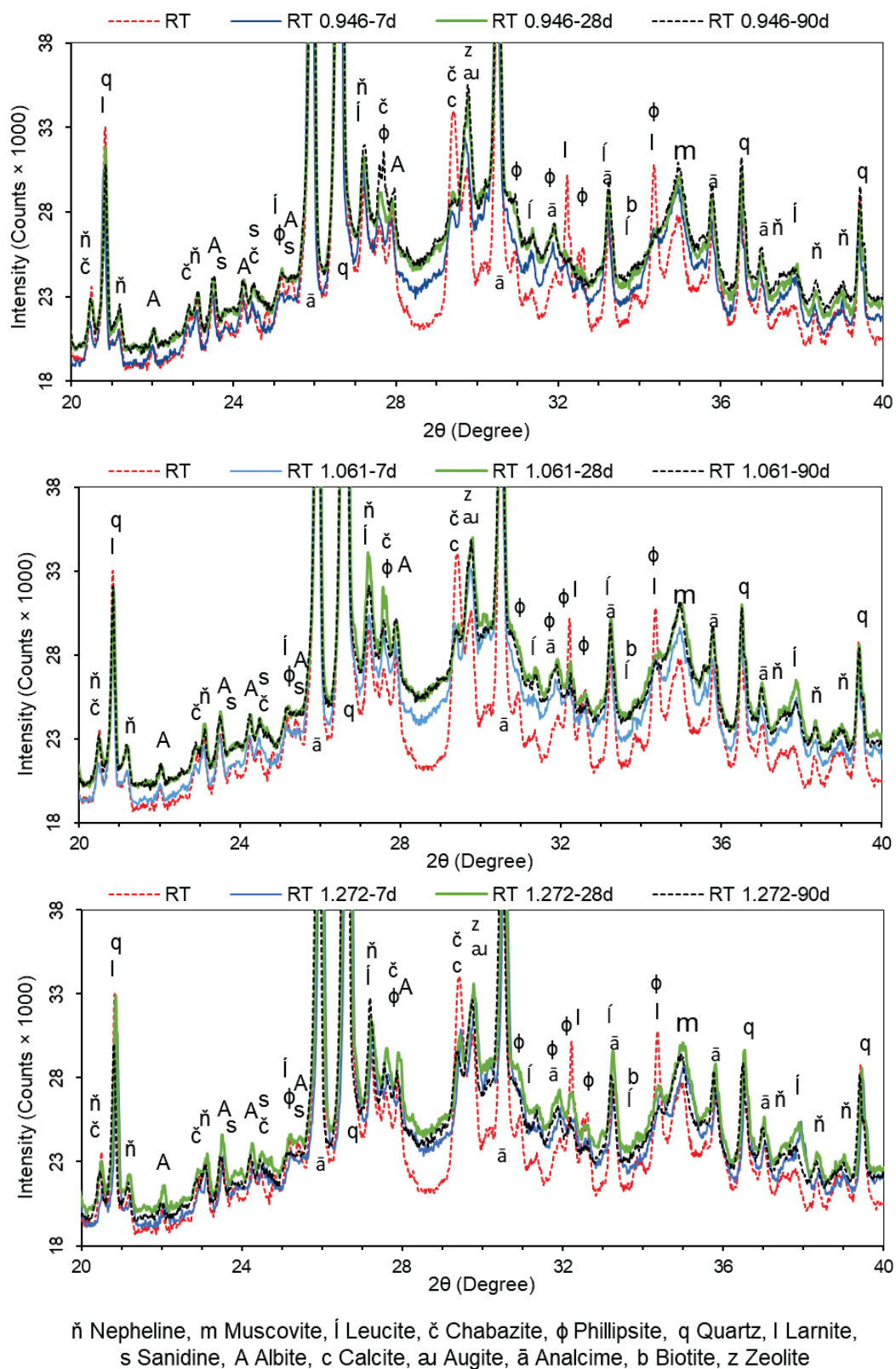
Figure S1. XRD of RT and its geopolymers with various silica moduli at the ages of 7, 28 and 90 d

Figure S2. XRD of BT and its geopolymers with various silica moduli at the ages of 7, 28 and 90 d (in range of 5° – 10° 2θ)

Figure S3. XRD of BT and its geopolymers with various silica moduli at the ages of 7, 28 and 90 d (in range of 20° – 40° 2θ)

4

Figure S4. TG curves of RT and BT with their geopolymers at 7, 28 and 90 d age

2.4. Influence of heat treatment and mechanical activation on reactivity of natural pozzolan for geopolymer synthesis

Authors: Rafia Firdous, Dietmar Stephan

Influence of heat treatment and mechanical activation on reactivity of natural pozzolan for geopolymer synthesis

Rafia Firdous[1], Dietmar Stephan[1*]

[1]Technische Universität Berlin, Department of Civil Engineering, Building Materials and Construction Chemistry, Gustav-Meyer-Allee 25, 13355 Berlin, Germany
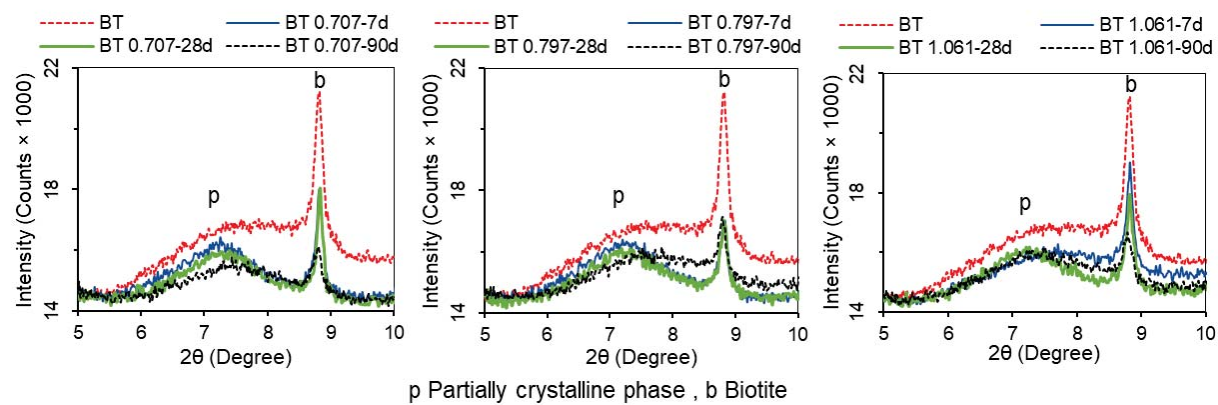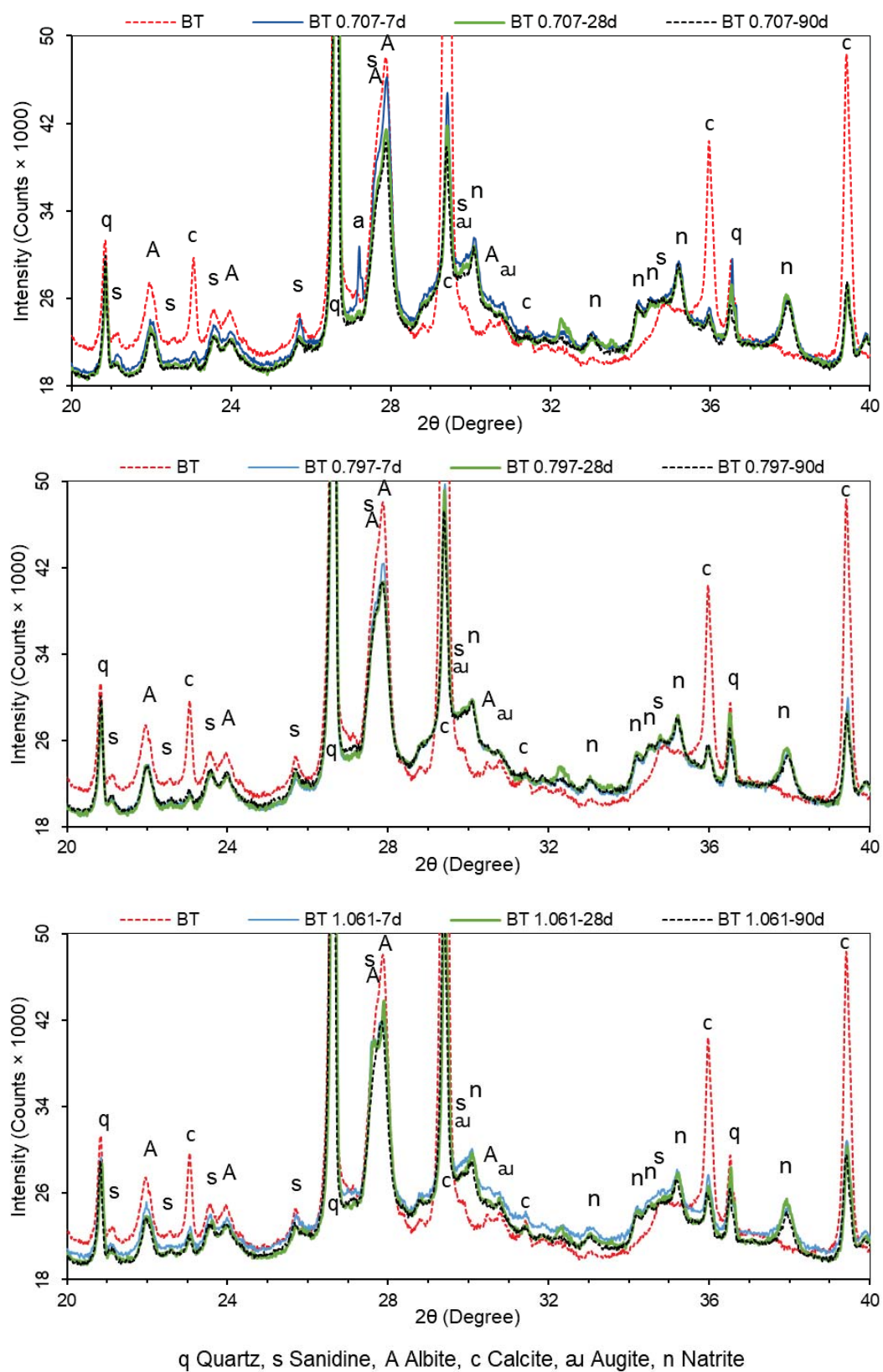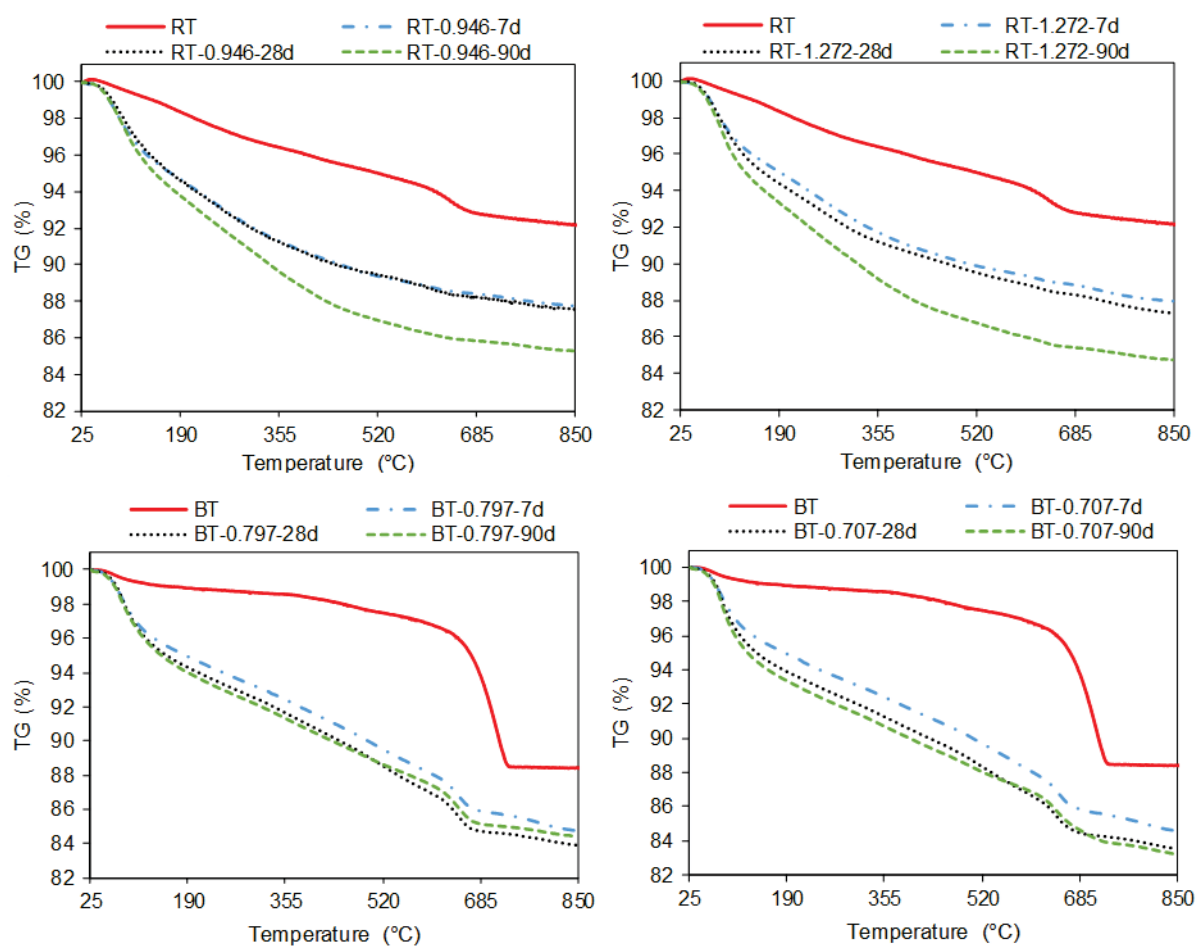*Corresponding author E-mail: stephan@tu-berlin.de

Abstract - Natural pozzolans are suitable raw material for geopolymer synthesis as they are a tremendous source of silica and alumina with ease of mining and transportation accompanying lesser cost and lower environmental footprint than for artificial precursors. In this research study, a natural pozzolan formed as a result of meteorite impact has been used for the production of geopolymers. A comparative study has been made between heat treatment and mechanical activation as reactivity alteration methods. The geopolymer samples have been synthesised using raw and altered pozzolans. Several silica moduli of the alkaline solution and curing at ambient conditions were used. Results show that the heat treatment is more suitable as a reactivity alteration method compared to the mechanical activation as indicated by higher compressive strength and accelerated geopolymer reaction. Based on these results, microstructural characteristics have been studied for the geopolymer samples made with raw natural pozzolan and heat-treated pozzolan. Findings indicate that the heat-treated pozzolan has higher reactivity because of partial conversion of calcite to lime. A shift of optimum silica modulus to higher value in order to achieve maximum compressive strength has also been observed. Results of ATR-FTIR show the shift of various bands with the time due to uptake of Al into the structure. On the one hand, broadening of the band corresponding to Al/Si-O-Si indicates disorder introduced by initial geopolymerization. On the other hand, sharpening of this band denotes an increase in order with the age of geopolymer. TGA gives insight about the changes occurred during geopolymerization and shows the formation of C-S-H gel in geopolymer of heat-treated natural pozzolan. Results of XRD and SEM reveal that geopolymer gel is nevertheless mainly a mixture of N-A-S-H and (C)-N-A-S-H phase with the incorporation of Mg, Fe and K as charge-balancing cations.

Keywords: Geopolymer, natural pozzolan, compressive strength, alkaline solution, heat treatment.

1 Introduction

Global warming is the increase in the average atmospheric temperature over long-time, and it is one of the major issues which the world is facing currently. Scientists around the globe are thriving to find ways to reduce the green-house gas emissions. Building industry is one of the major contributors to global warming because of high production and consumption of cement [1]. Hence, there is a need to develop building materials with comparatively low CO_2 emissions for specific applications in order to cut short the use of cement. In this context, geopolymers have gained a lot of interest in recent decades. Comparatively low green-house gas emission, good mechanical and durability properties make them a foreseeable material for specific applications [1–3]. Geopolymers are a class of inorganic binders which possess a polymeric Si-O-Al framework structure and can be synthesised by reaction of aluminosilicate source material with a concentrated alkaline solution [2, 4, 5]. Several aluminosilicate sources including natural and artificial pozzolans can be used as geopolymer precursor. Studies conducted till to date show that the natural pozzolans of volcanic origin can be used for geopolymer synthesis [6–13]. However, there is limited published data on the usability of other natural pozzolans for geopolymer synthesis which include diatomaceous earths, opaline cherts, shales, pumicites and materials formed by meteorite impact. This research study focusses on the use of natural pozzolan formed as a result of meteorite impact for

1

geopolymer synthesis. The material named as breccia Suevite or Bavarian trass was formed approx. 14.5 million years ago when a meteorite hit the earth in a region later called the Nördlinger Ries, Germany [14].

Studies show that natural pozzolans have lower reactivity in alkaline medium in comparison to artificial pozzolans such as fly ash and metakaolin [8, 15]. Several methods have been applied to improve their reactivity including mechanical activation, heat treatment, partial replacement by secondary cementitious materials and alkali fusion [8, 16–19]. Bondar et al. applied heat treatment by calcinating four different natural pozzolans at different temperatures. Results showed that the calcination can have positive and negative effects on the reactivity of natural pozzolan depending on the mineralogy of the raw sample [18]. Djobo et al. investigated the effect of mechanical activation on Cameroonian volcanic ash and found that mechanical activation helps in improving the reactivity, however, excess milling beyond a certain limit can have adverse effect on the reactivity of volcanic ash [16]. Alkali fusion includes calcination in the presence of alkali hydroxides. Tchakoute et al. applied the alkali fusion technique on Cameroonian volcanic ash using NaOH pellets and burning at 550 °C for 1 h. Geopolymer samples synthesised using this fused volcanic ash and metakaolin showed good mechanical properties, short setting time and low shrinkage [19]. Several materials such as kaolinite, metakaolin, bauxite, calcined oyster shell and slag have been used as partial replacement of natural pozzolan for geopolymer synthesis [17, 20–22]. Results pointed out that the addition of kaolinite give similar compressive strength has no appreciable effect on the improvement of compressive strength [17]. Whereas, replacement by slag and metakaolin improves the properties of resultant geopolymer [21, 22]. The inclusion of bauxite has been found a promising way to reduce efflorescence while the addition of calcined oyster shell helps in reduction of setting time [20].

However, there are limited published studies available on the comparison of different reactivity enhancement methods and their effect on the properties of the geopolymer product. This research study aims to compare two reactivity alteration methods, i.e. heat treatment and mechanical activation and to study their effect on final geopolymer product. Geopolymer samples have been obtained by mixing raw natural pozzolan, heat-treated or mechanical activated natural pozzolan with an alkaline solution. For the purpose, three different silica moduli of alkaline solution have been used. Based on the results of compressive strength and reaction kinetics, one reactivity enhancement method has been chosen to study its effect on the microstructural properties of final geopolymer made with several silica moduli at various ages. TGA, XRD, ATR-FTIR and SEM have been used to study the microstructural characteristics.

2 Materials and methods

2.1 Materials and characterization

− Pozzolans

Natural pozzolan from Germany named as Bavarian trass (BT) has been used in this study. Bavarian trass was supplied by Märker Zement GmbH, Germany. Chemical composition was determined by XRF analysis using PW 2400, PHILIPS and is given in Table 1.

Table 1: Chemical composition of all natural pozzolans.

Sample / wt.%	Total	LOI	SiO$_2$	Al$_2$O$_3$	Fe$_2$O$_3$	MnO	MgO	CaO	Na$_2$O	K$_2$O	TiO$_2$	P$_2$O$_5$	SO$_3$
BT	100.25	11.24	52.35	12.25	4.15	0.09	0.91	13.85	1.67	2.44	0.61	0.22	0.47

Bavarian trass (BT) was subjected to heat treatment and mechanical activation. Heat treatment was conducted by calcining the sample at 700 °C for 3 h, followed by cooling to room temperature in a desiccator with silica gel. While, the mechanical activation was performed by milling in a planetary ball mill (PULVERISETTE 5 classic line, Fritsch GmbH, Germany) at a speed of 200 rpm for 5 min or 10 min with media to material ratio of 1:0.16. The grinding bowl made of hardened steel consisting of 125 ml capacity was filled with 80 g of pozzolan sample. 15 grinding balls made of hardened steel of 20 mm diameter were used for milling. The calcined Bavarian trass has been named as BTC and milled Bavarian trass for 5 and 10 min has been named as BT5 and BT10, respectively. It should be noted here that applying reactivity alteration methods add additional cost to the production of the building material. Therefore, from

2

economical and industrial perspective more practical methodology was adopted. Specific surface area as measured by Blaine fineness according to EN 196-6 [23] was recorded as 6746 cm²/g for BT sample. For BTC as a result of heat treatment specific surface area increased to 7141 cm²/g. While for BT5 and BT10 the specific surface area was recorded as 7018 cm²/g and 11721 cm²/g. Figure 1a presents the particle size distributions of BT, BTC, BT5 and BT10 samples measured using Mastersizer 2000 of Malvern Instruments and Figure 1b shows the d_{50} particle size for BT, BT5 and BT10 samples. With the applied mechanical activation method, a reduction of 23% and 43% in d_{50} has occurred for BT5 and BT10, respectively. X-ray diffraction analysis was performed on BT, BTC, BT5 and BT10 using the method as described in section 2.2. Figure 2 presents the X-ray diffractograms of all pozzolans with the mineralogical phases. The mineralogical phases were determined in accordance with the literature [24–29]. In addition to mentioned crystalline phases, BT sample also contain a glass phase. Due to heat treatment, some amount of calcite has been found to decompose (calcite peaks reduced in height) and formation of lime has been observed in XRD in BTC sample (as shown in Figure 2). Partially crystalline phases present in BT which may correspond to the presence of clay and zeolite minerals also decomposed as a result of heat treatment. XRD detects entirely no differences between BT, BT5 and BT10.

(a)   (b)
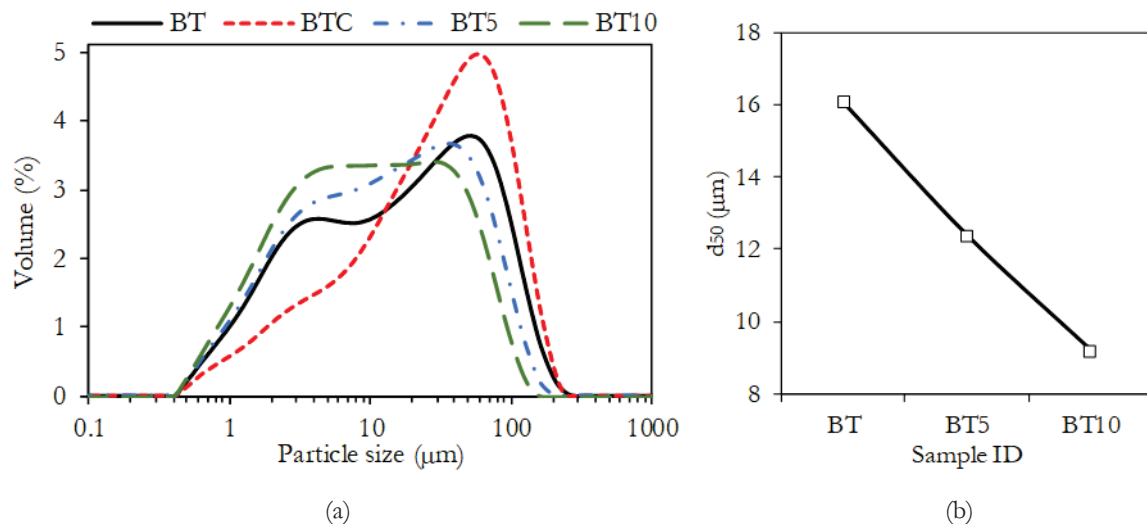
Figure 1: (a) Particle size distribution for BT, BTC, BT5 and BT10 samples, (b) d_{50} for BT, BT5 and BT10 samples.

−   Alkaline activator

Alkaline activator consisting of combinations of sodium hydroxide (NaOH) and sodium silicate solutions (Na₂SiO₃) were used. NaOH of 99 wt.% purity was obtained from VWR International GmbH in pellets. NaOH solutions were prepared by dissolving NaOH pellets in deionized water at least 24 h before use. Sodium silicate solution (Betol 52T) was obtained from Woellner GmbH with silica modulus of 2.12. The NaOH solution and Na₂SiO₃ solution were mixed in different fractions to obtain the alkaline solutions of desired silica modulus. Three silica moduli of alkaline solution of 0.707 (H₂O/Na₂O molar ratio = 9.7), 0.797 (H₂O/Na₂O molar ratio = 11.4) and 1.061 (H₂O/Na₂O molar ratio = 10.5) were used for BT and BTC geopolymers, while silica modulus of 0.707 was used for BT5 and BT10 geopolymer samples.

2.2   Experimental methodology

The geopolymer paste samples were prepared using a laboratory hand mixer with a mixing time of 3 min. In-between break of 30 s was taken after mixing the sample for 90 s to collect all the sample in the centre of the bowl for homogeneous mixing. After complete mixing, the paste was poured in 20 mm cubic molds and was compacted using vibration table for 2 min. Samples were sealed using plastic foil from all sides and were cured at 21 ± 1 °C and 100% relative humidity till test age. Alkaline solution to solid ratio was kept equal to 0.75 for all geopolymer samples to achieve good workability.

The compressive strength of cubic samples was determined at 7, 28, 90 and 180 d age. Pieces of broken samples were collected at 7, 28 and 90 d age and geopolymer reaction was stopped for examination by TGA, XRD, ATR-FTIR and SEM-EDX. The reaction was stopped by solvent exchange using isopropanol. Samples were submerged in isopropanol for 24 h followed freeze-drying for 7 d. Afterwards, samples were ground by hand in mortar and pestle to a size <125 μm. In the case of storing, the samples were stored in a desiccator with sodium hydroxide (on support) obtained from Merck, KGaA, Germany to avoid environmental carbonation.

q Quartz (98-008-9277), □ Sanidine (98-000-9583), ♦ Albite (98-003-4870), c Calcite (98-005-2151), ‡ Augite (98-005-6931), ♭ Biotite (98-009-8156), P Poorly crystalline phase, L Lime (98-006-0199)
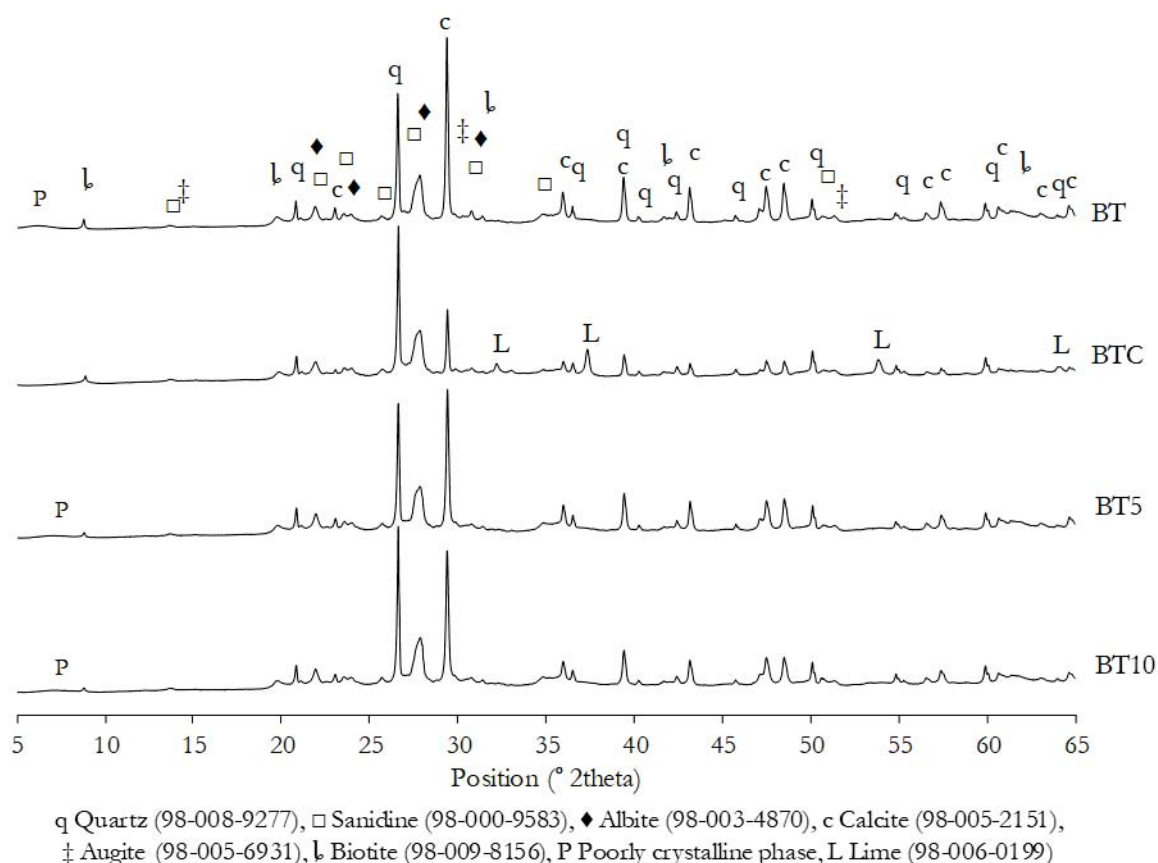
Figure 2: X-ray diffractograms of BT, BTC, BT5 and BT10 samples.

Isothermal conduction calorimetry was performed to understand the reaction kinetics and to study the effect of heat treatment and grinding on the reactivity of natural pozzolan. For the calorimetric study, device MC-CAL 100P, C3 Prozess- und Analysentechnik GmbH, Germany was used. Samples were mixed outside the device for 45 s each with vortexer. Therefore, zero in the calorimetric curves is the point when samples were placed inside the device.

Thermogravimetric analysis (TGA) was performed using TG 209, Tarsus F3, Netzsch Instruments under a nitrogen atmosphere at a flow rate of 250 mL/min. For each test, 10 ± 1 mg of sample was used. The sample was first held at 25 °C for 20 min, and then heated from 25 °C to 850 °C at a heating rate of 10 °C/min.

Fourier transform infrared spectroscopy (FTIR) was performed on raw natural pozzolan and respective geopolymer samples using Spectrum Two of PerkinElmer fitted with diamond crystal via the attenuated total reflection (ATR) method. IR spectra were obtained between 4000 to 400 cm-1 with a resolution of 1 cm-1.

4

X-ray diffraction analysis (XRD) was performed using an Empyrean PANalytical diffractometer with Ni filter and CuKα radiation (k = 1.540598 Å), operating at 40 kV and 40 mA in continuous mode with a resolution of 0.0131° and speed of 0.0176 °/s for a range of 5° to 65° for 1 h. The phase evaluation was performed using HighScore Plus software with ICDD and ICSD.

Polished freeze-dried samples were impregnated in epoxy resin to study the microstructure and elemental distribution. For the purpose, scanning electron microscopy fitted with energy-dispersive X-ray spectrometer (SEM-EDX) was performed using device GeminiSEM500, ZEISS operated at 15 kV.

Throughout the manuscript, the geopolymer samples made with BT, BTC, BT5 and BT10 are labelled with the respective raw sample, silica modulus used to prepare each geopolymer and the age of the sample.

3   Results and discussion

3.1   Effect of heat treatment on compressive strength

Figure 3 presents the compressive strength development of BT and BTC geopolymer samples. Results indicate that heat treatment of BT improved the reactivity as found by an increase of compressive strength in BTC geopolymer samples. An increase of 32% and 45% in compressive strength has been observed at 90 d age for samples BTC-0.797 and BTC-1.061, in comparison to corresponding BT samples. While for sample BTC-0.707, 7- and 28-d compressive strength was improved and thereafter, no significant improvement in compressive strength has been observed. Considering the BT geopolymer, the optimum silica modulus to achieve highest compressive strength was recorded as 0.707, while for BTC geopolymers it is found as 0.797. Thus, the optimum silica modulus shifted to higher silica modulus for BTC geopolymers in comparison to BT geopolymers. This confirms the improvement in reactivity of this natural pozzolan and a reduction in the alkali concentration of the solution used, which is beneficial from both economic and environmental perspective.
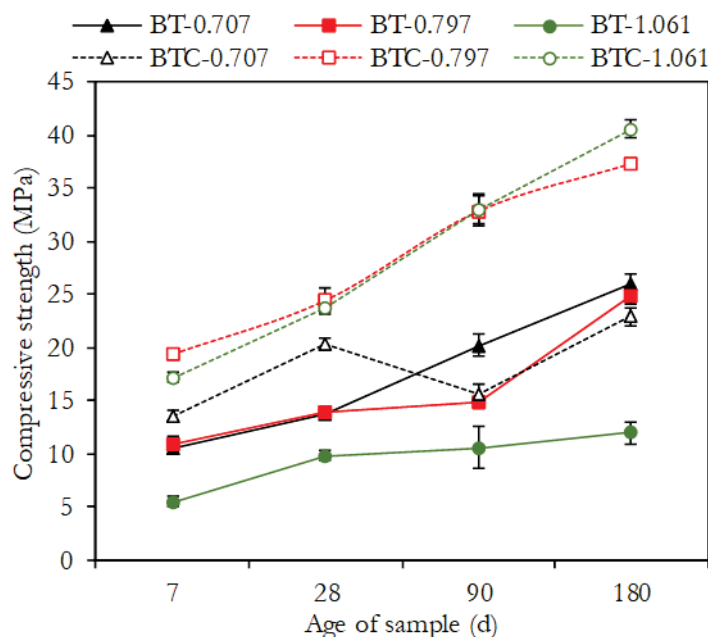
Figure 3: Compressive strength of BT and BTC geopolymers at different ages.

Table 2 presents the visual observation of BT and BTC samples prepared with various silica moduli at 90 d. The pictures presented in Table 2 show that for sample BTC-0.707, efflorescence formation increased in comparison to sample BT-0.707. While for sample BTC-0.797 and BTC-1.061, the formation of efflorescence decreased in comparison to samples BT-0.797 and BT-1.061. The formation of efflorescence is because of an excess of free alkalis in geopolymer matrix which react with carbon dioxide from the

5

environment and produce sodium carbonate which precipitates at the surface or in pores of geopolymer matrix.

Table 2: Visual observation of BT and BTC sample at 90 d age.

Silica modulus	0.707	0.797	1.061
BT			
BTC			

3.2 Effect of mechanical activation on compressive strength

The effect of mechanical activation as the reactivity alteration process has also been studied by compressive strength and the results are presented in Figure 4. A slight improvement in strength with grinding has been found. However, no significant improvement in strength has been observed at all ages of the sample, and the values are mostly within the range of standard deviation.
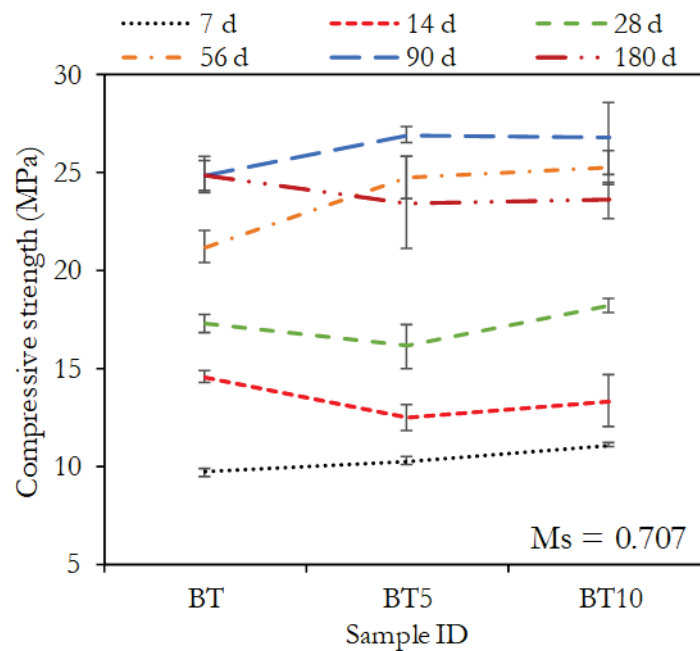
Figure 4: Effect of mechanical activation on the compressive strength of BT sample.

3.3 Effect of heat treatment on reaction kinetics

Figure 5 presents the calorimetric curves for BTC compared to BT samples. Results show that geopolymer reaction for BT geopolymer samples is characterised by two exothermic peaks. The initial peak occurs when natural pozzolan and alkaline solution come in contact and is therefore attributed to wetting and dissolution of reactive phases. This peak is followed by deacceleration which is associated with polycondensation thus the amount of heat released decreases. Thereafter, a second exothermic peak has been observed which is assigned to a delayed dissolution of some phases. Delayed dissolution of calcium-rich phases leading to a second exothermic peak was observed by Gebregziabiher et al. [30]. The formation of early product in

6

----

alkali-activated system depletes the alkalis and the relative silica concentration increases, which in turn retards the dissolution of calcium phases [30]. For samples BT-0.707, BT-0.797 and BT-1.061, second exothermic peak was observed at 11 h, 12.6 h and 28.3 h with a maximum at approx.12.5 h, 14.5 h and 34.7 h, respectively.

Comparing BT and BTC geopolymer samples, the rate of reaction increased for all calcinated samples in comparison to BT samples indicated by higher heat evolved over 168 h, higher heat flow in first hours and shift of second exothermic peak to an earlier time or complete disappearance. For sample BTC-0.797 and BTC-1.061 this peak was not observed at all. For BTC-0.707 sample, this peak moved to approx. 8 h and appears only as a slight hump (Figure 5). These findings are in accordance with the results of compressive strength, as for sample BTC-0.707 compressive strength is also lower than for sample BTC-0.797 and BTC-1.061 which can be described by the delayed dissolution and therefore, lack in a gain of compressive strength. Comparing BTC-0.707, BTC-0.797 and BTC-1.061 to each other, the rate of dissolution increases with the decrease of silica modulus.
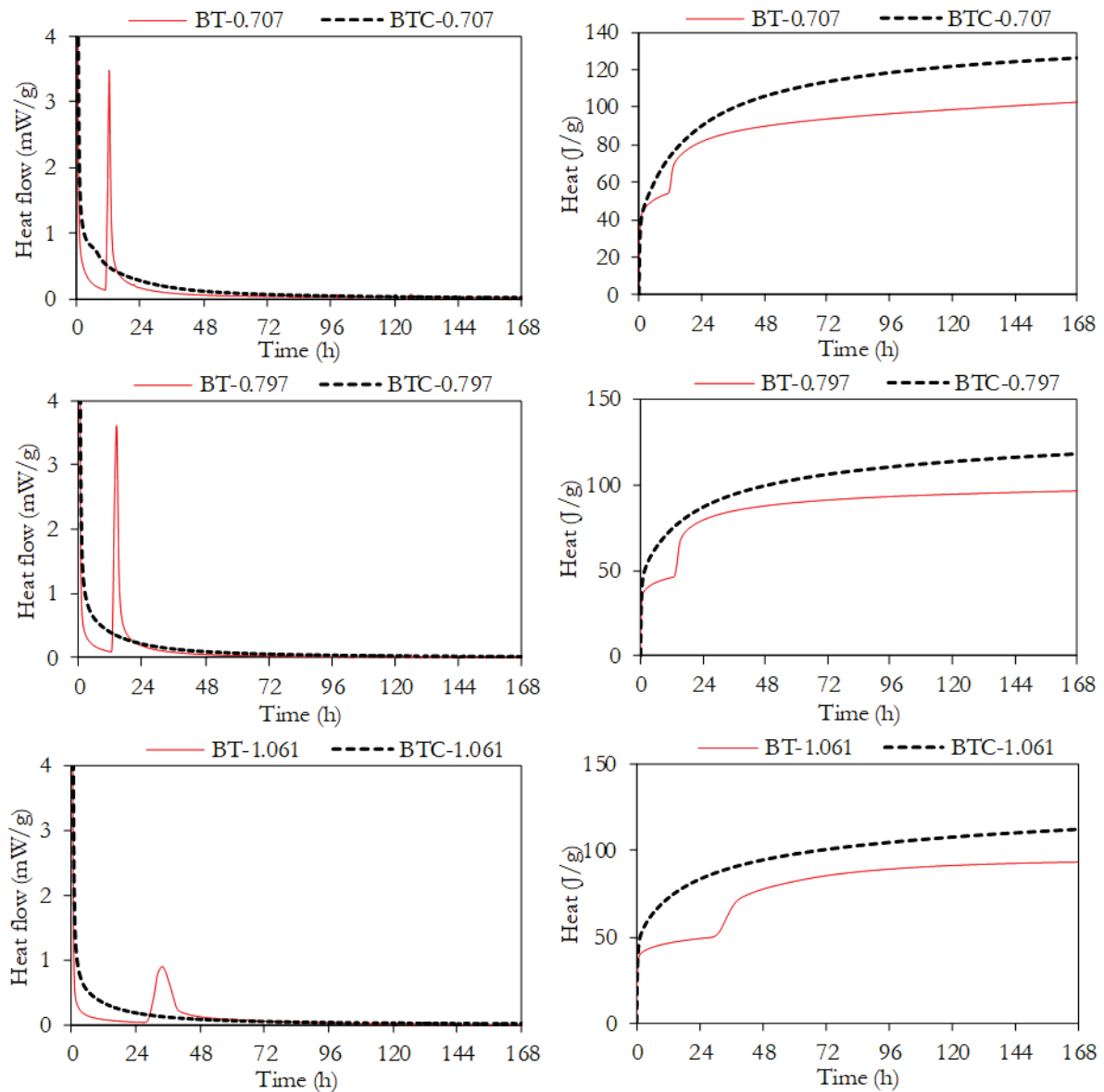
Figure 5: Heat evolution curves for BT and BTC geopolymers.

7

The improvement of pozzolanic reactivity as a result of calcination for this natural pozzolan has also been reported by [25], however the authors found that a possible reason of such improvement was presence of smectite minerals. In the current research, this mineral group has not been identified. Therefore, the reason for such improvement in reactivity as a result of the heat treatment is most likely the conversion of calcite to lime which imparts higher reactivity [31]. This is because the reaction of lime with water leads to a rise in the pH of the system which enhances the dissolution of aluminosilicate species [32]. Thus, the rate of reaction increases and 2nd exothermic peak shifts to earlier times. Henceforth, the increase in dissolution rate results in a higher amount of precipitated geopolymer gel associated with an increase of compressive strength in most cases (Figure 3) and heat evolved over 168 h (Figure 5) of calcinated samples in comparison to BT samples. This finding also enables to explain the alteration of efflorescence development depicted in Table 2. The samples with silica moduli 0.797 and 1.061 precipitate enough geopolymer gel to incorporate most of the alkalis of activator solution. Therefore, lower efflorescence product is formed. On the other hand, the alkaline concentration in sample BTC-0.707 is too high and most of it has not been incorporated in geopolymer gel and thus it leads to formation of higher amount of efflorescence (as seen in Table 2).

3.4   Effect of mechanical activation on reaction kinetics

To study the influence of mechanical activation on reaction kinetics, isothermal conduction calorimetry was conducted. Firstly, BT, BT5 and BT10 raw samples were separated in two fractions by a 40 μm sieve, afterwards, calorimetry was conducted on these separated fractions. The fractions of material were separated to understand the effectiveness of mechanical activation on the fine and coarse fractions of the sample, such that the first hump of bimodal particle size distribution was separated (Figure 1). Geopolymer samples were prepared with silica modulus of 0.707 for each fineness and are labelled as BT-0.707, BT5-0.707 and BT10-0.707. The results of the calorimetric study are presented in Figure 6 for both fractions of samples.

Results indicate that the fraction <40 μm exhibits higher reactivity than fraction >40 μm. Mechanical activation in the ball mill is more effective in reducing the size of larger particles. The calorimetry curves of BT samples show that the part of sample <40 μm develops approx. twice as much hydration heat after 168 h as that >40 μm. Total heat slightly increases with increasing fineness of sample (from BT over BT5 to BT10) for fraction <40 μm. While for the fraction >40 μm, total heat released stays nearly unchanged from BT to BT5 but increases significantly for BT10-0.707.

It is important to note here that the second exothermic peak occurs only for fraction <40 μm for sample BT-0.707 and BT5-0.707. While for sample BT10-0.707, it occurs for both fractions. By increasing the overall fineness of sample (from BT over BT5 to BT10), this reaction triggers to earlier time and heat flow value decreases but time span over which reaction occurs is increased. These observations indicate that with the increase in fineness the reaction degree is increasing at a lower rate; therefore, only a slight improvement in compressive strength has been observed. However, to see a significant impact of mechanical activation, sample may be milled for a longer time, but care must be taken while choosing a reactivity alteration method and its economic advantages.

XRD analysis was performed on the separated fractions of BT, BT5 and BT10 as shown in Figure 7 to understand calorimetric analysis. The results show that the fractions <40 μm have excess amount of calcite while the fractions >40 μm are enriched in minerals such as quartz, sanidine and albite which have higher Mohs scale hardness. Further the fraction BT <40 μm has highest amount of calcite while as a result of milling the calcite content is slightly decreasing in BT5 <40 μm and BT10 <40 μm. Therefore, as a result in calorimetric analysis the height of 2nd exothermic peak is decreasing with increasing milling time.

With increasing milling time, the calcite content in fraction >40 μm is consequently increasing. This is because of possible agglomeration of soft and small calcite particles during milling. In BT10 geopolymer samples both fractions exhibit the 2nd exothermic peak. This can be because of sufficiently high content of calcite in both fractions. The agglomeration leads also in coarse fraction to a sufficient amount of calcite content to develop the 2nd peak. While the hard minerals are not much effected by grinding and therefore, doesn't exhibit any appreciable differences in their reactivity.

8
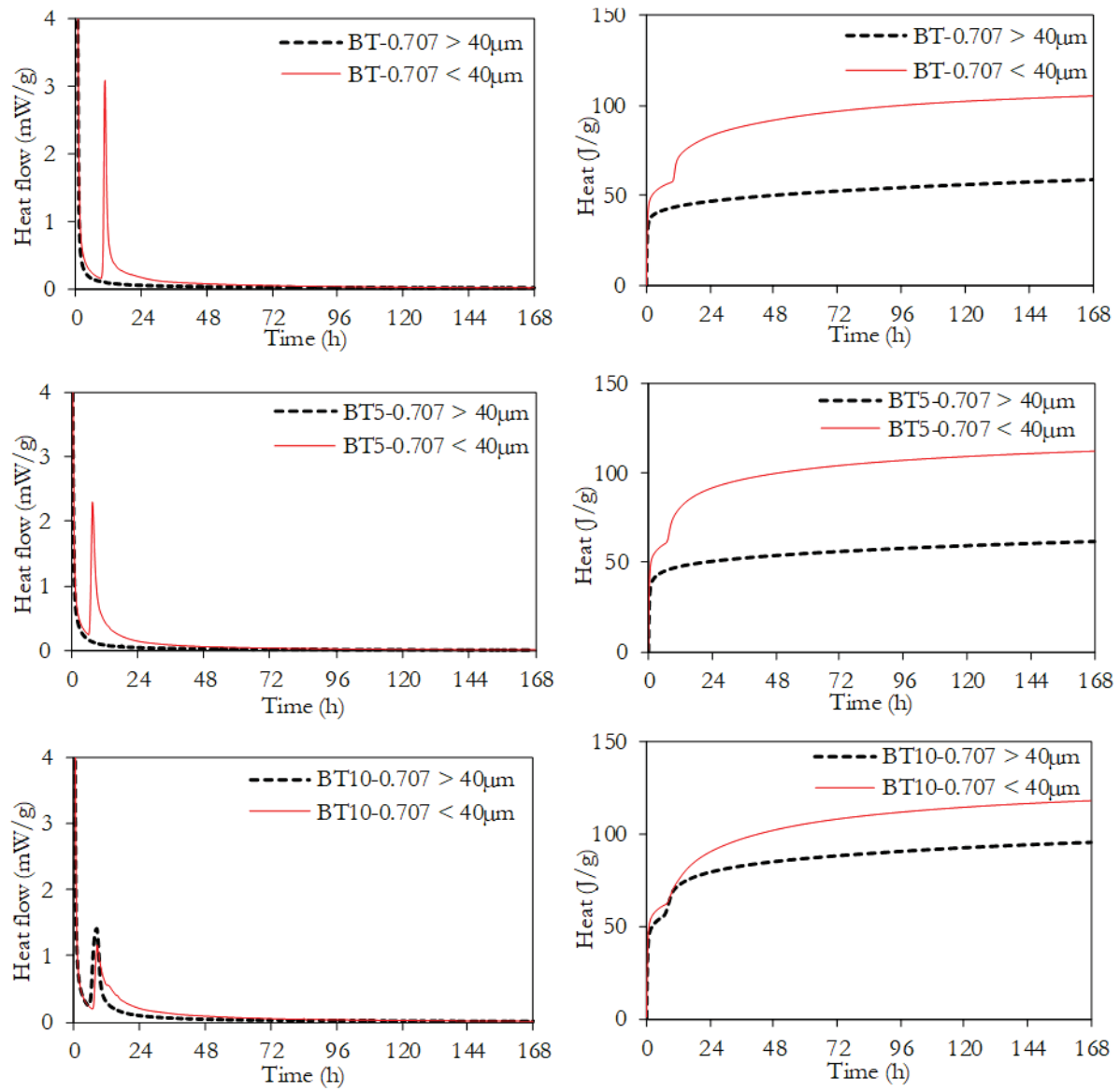
Figure 6: Heat evolution curves for BT, BT5 and BT10 geopolymers.

(a)   (b)   (c)
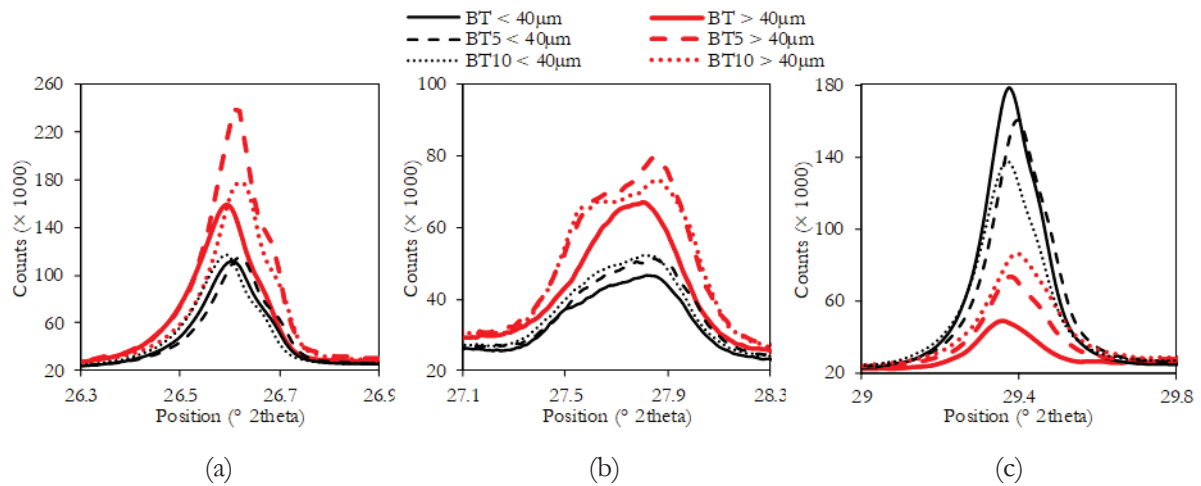
Figure 7: Diffractograms of BT, BT5 and BT10 fractions below and above 40 μm showing reflexes for (a) quartz (b) sanidine and albite (c) calcite.

9

Comparing both reactivity alteration methods, the effect of heat treatment is more prominent than reduced particle size. Looking at Figure 1, BTC sample has a higher fraction of coarser particles in comparison to BT5 and BT10 samples. But the inclusion of more reactive phases such as lime imparts higher reactivity than reduced size of particles. Based on these results, heat treatment has a higher influence on the reactivity of BT. Therefore, further detailed microstructural analysis has been made only on BT- and BTC-based geopolymers in following sections.

4   Microstructural characteristics

4.1   Thermogravimetric analysis (TGA)

Thermogravimetric analysis was performed on BT and BTC geopolymer samples at the age of 7, 28 and 90 d. Results for the sample prepared with silica modulus of 0.797 for both pozzolans are presented in Figure 8. The overall mass loss for BT and BTC geopolymers prepared with silica modulus of 0.797 is higher at all ages than in raw pozzolans. Similar behaviour has been also observed for BT and BTC geopolymer samples prepared with silica modulus of 0.707 and 1.061 which are not shown here. The overall mass loss seems to increase with the age of sample slightly. This increase in the mass loss is attributed to geopolymerization reaction.
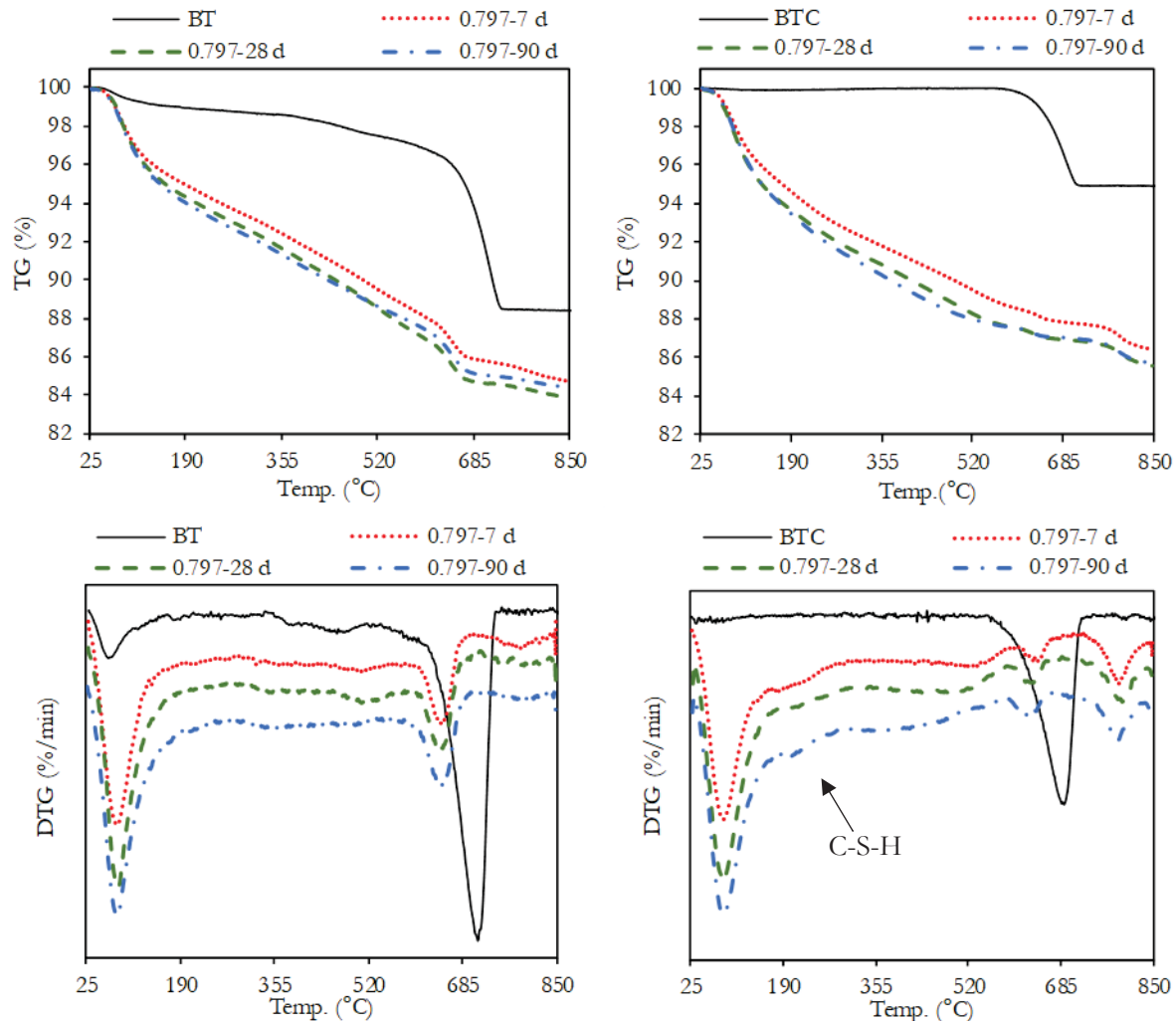
Figure 8: TG and DTG curves of BT and BTC samples at 7, 28 and 90 d age.

Mass loss till approx. 150 °C is considered as the liberation of loosely bound water. Mass loss from 150 – 600 °C is attributed to liberation of stronger chemically bound water. As a result of geopolymerization,

10

bound water is introduced in the system as a part of geopolymer gel which is formed due to dissolution and subsequent precipitation of aluminate and silicate species. This mass loss in the range of 30 – 600 °C can be correlated to the amount of reaction product formed [33]. Results presented in Table 3 show that dehydration in the temperature range of 30 – 600 °C is affected by the change of silica modulus of alkaline solution used and the age of the sample. For samples BTC-0.797 and BTC-1.061, the mass loss in mentioned temperature range increases with age while for all others it initially increases from 7 to 28 d and then decreases till 90 d. Such a reduction in water content with the age can be caused by efflorescence formation in these samples with age [34]. The last stage in TG refers to decarbonization (600 – 850 °C) and shows that the carbonate content of samples is reduced as a result of geopolymerization [35, 36].

The effects mentioned above are observed in both BT and BTC geopolymers. Additionally, for BTC geopolymers, two other peaks in DTG have also been found, i.e. a diffuse peak in the temperature range of 160 – 300 °C with its centre at approx. 200 °C and a sharp peak above 790 °C with a maximum at approx. 795 °C. The first peak is attributed to dehydration of C-S-H gel which has been observed to form in case of availability of reactive calcium [35, 36]. This peak has been observed in all BTC geopolymer samples but in none of the BT geopolymer samples. This shows that as a result of calcination, calcite converts to lime which imparts more reactive calcium. After that, the second peak observed only in BTC geopolymer samples is attributed to the decomposition of C-S-H to wollastonite; such decomposition has been also observed in the literature and was also confirmed here by conducting XRD on the decomposed residue [36, 37].

Table 3: Mass losses in the temperature range of 30 – 600 °C for BT and BTC geopolymer samples at various ages.

Age of sample	Mass loss (wt.%)					
	BT-0.707	**BT-0.797**	**BT-1.061**	**BTC-0.707**	**BTC-0.797**	**BTC-1.061**
7 d	11.87	11.88	10.76	11.44	11.40	10.38
28 d	13.25	12.98	12.38	11.74	12.40	10.98
90 d	13.00	12.48	12.17	11.43	12.77	11.40

4.2   X-ray diffraction analysis (XRD)

Figures 9 and 10 show the XRD diffractograms of BT and BTC geopolymers at the age of 7, 28 and 90 d prepared with silica modulus of 0.797, respectively. XRD analysis was made on all samples, but for easy understanding selected samples have been shown here.

In raw BT and BT geopolymer samples, two amorphous humps were recorded ranging approx. 5° – 8° and 24° – 34°. While in raw BTC and BTC geopolymer samples only the second hump mentioned above has been recorded. The first hump in raw BT and BT-based geopolymers was not identifiable, but it may correspond to the presence of clay or zeolite minerals. As a result of geopolymerization the shape of this amorphous hump changed indicated by the shift of the centre of the hump. This may be due to the formation of aluminosilicate gel phase.

In both raw pozzolans, the centre of the second amorphous hump was recorded at 27°. While in both pozzolan-based geopolymer samples the centre of the second amorphous hump shifted to higher 2 theta values i.e. 31°. Such a shift has been described to occur due to the formation of geopolymeric gel [38–40]. Further, in BT geopolymer sample made with silica modulus of 0.707 at 7 d and in BTC geopolymer samples made with silica modulus of 1.061 at 28 d a new reflex has been observed to form at approx. 27°. This reflex has not been observed in all other samples. It is attributed to the formation of aragonite (98-028-0991) which is a polymorph of calcium carbonate and may form under high alkaline conditions [41, 42]. However, the lower stability of this phase is the reason that it has been not observed in other samples.

As seen earlier, efflorescence formation was observed for BT and BTC geopolymer samples. XRD results reveal that efflorescence is caused by precipitation of natrite (γ-Na_2CO_3 ,98-009-5549). This is formed because of the reaction of excess free alkalis in the geopolymer system with environmental carbon dioxide. Looking at Figures 9 and 10, the participation of calcite and lime in geopolymer reaction can be clearly observed as indicated by the reduction of reflex height of calcite while reflexes of lime are completely absent

----

in geopolymer samples. This confirms the previous finding that lime imparts higher reactivity than calcite as indicated by its complete participation in geopolymer reaction. Other crystalline phases may be participating in geopolymer reaction include biotite and sanidine, as indicated by slight changes in the reflexes for these minerals.

q Quartz (98-008-9277), □ Sanidine (98-000-9583), ♦ Albite (98-003-4870), c Calcite (98-005-2151), ‡ Augite (98-005-6931), ♮ Biotite (98-009-8156), P Poorly crystalline phase, n Natrite (98-009-5549)

Figure 9: Comparison of raw BT and BT geopolymer sample at the age of 7, 28 and 90 d for geopolymer sample prepared with silica modulus of 0.797.

q Quartz (98-008-9277), □ Sanidine (98-000-9583), ♦ Albite (98-003-4870), c Calcite (98-005-2151), ‡ Augite (98-005-6931), ♮ Biotite (98-009-8156), L Lime (98-006-0199), n Natrite (98-009-5549)
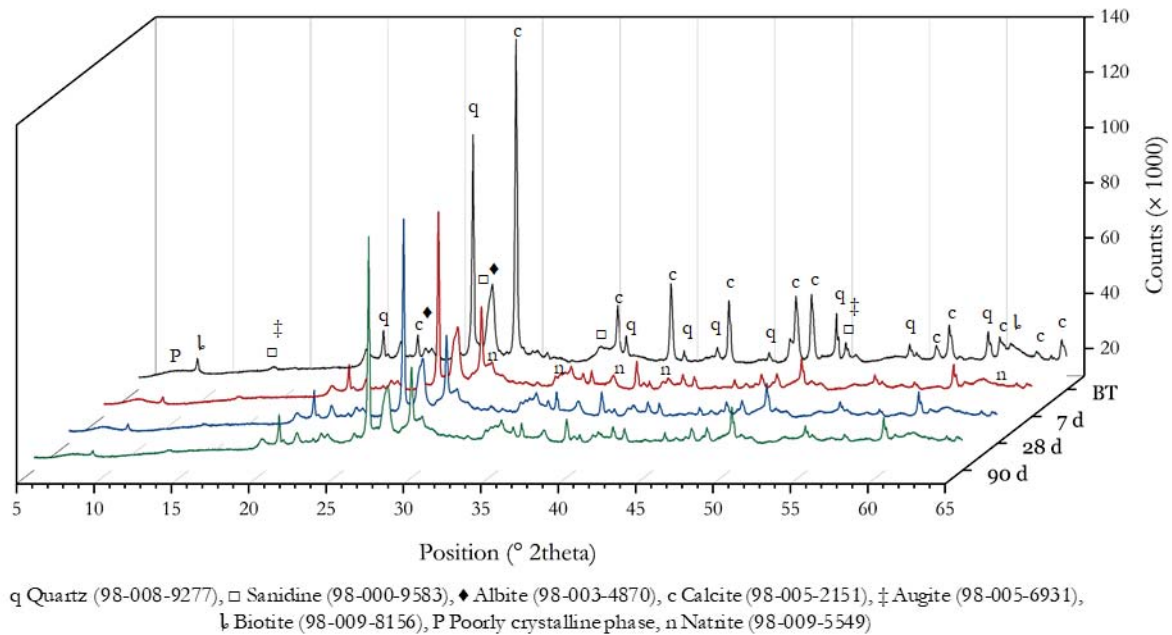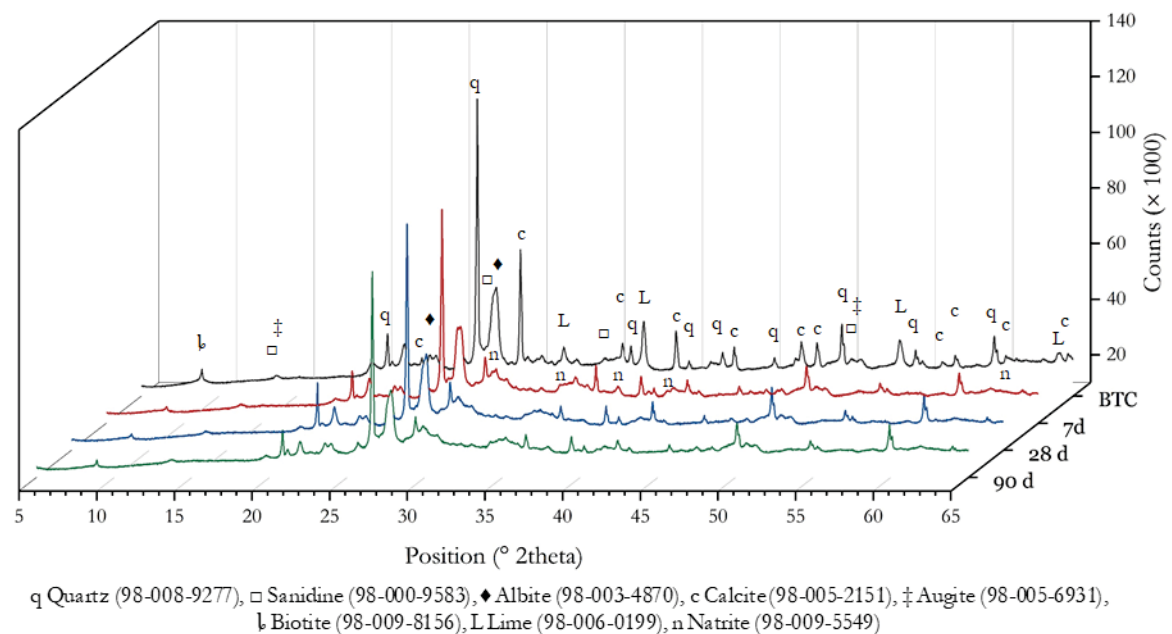
Figure 10: Comparison of raw BTC and BTC geopolymer sample at the age of 7, 28 and 90 d for geopolymer sample prepared with silica modulus of 0.797.

12

4.3 Fourier transform infrared spectroscopy (FTIR)

ATR-FTIR spectra were collected for the BT and BTC raw samples and their respective geopolymer samples at 7, 28 and 90 d ages. Results have been presented in Figure 11. FTIR analysis was made on all geopolymer samples and they showed comparable characteristics; therefore, for the easy understanding sample prepared with silica modulus of 0.707 has been shown here. The major characteristic peaks have been observed in region 1600 to 400 cm^{-1}. In region 4000 to 1600 cm^{-1} only one broad hump around 3100 cm^{-1} has been observed which indicates the OH stretching vibration.
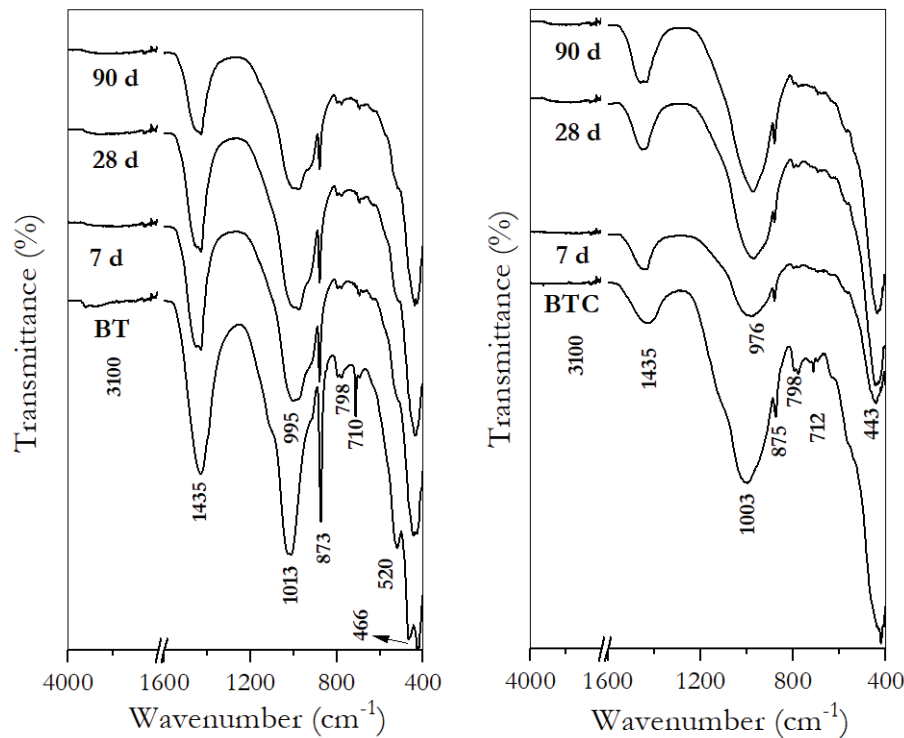
Figure 11: ATR-FTIR spectra of raw BT and BTC samples and BT and BTC geopolymer samples prepared with silica modulus of 0.707 at 7, 28 and 90 d age.

An intense band in raw BT and raw BTC samples at 1013 and 1003 cm^{-1}, respectively, attributed to asymmetric stretching of Al/Si-O-Si has been found to move to lower wavenumber i.e. 995 and 976 cm^{-1} in respective geopolymer samples. This is significant of changes that occurred as a result of the dissolution of the raw sample to form Al-rich geopolymer gel. As the SiO_4 tetrahedra of silica-rich network of the raw sample are broken and precipitates take AlO_4 tetrahedra up [9, 43]. Further, broadening of bands observed at 995 and 976 cm^{-1} in comparison to respective raw sample has been observed. This broadening is significant of structural disorder with the addition of water in structure [44]. Moreover, in BTC geopolymers the band present at 976 cm^{-1} is sharpening with age, which indicates the increasing order in the phase [43].

Another significant change observed between raw BT and BTC samples is the reduction of the carbonate group as a result of heat treatment. As the stretching bands of O-C-O observed at 1435, 873 and 710 cm^{-1} in raw BT sample and at 1435, 875 and 712 cm^{-1} in raw BTC sample reduced in intensity while comparing BT and BTC samples to each other. Moreover, comparing the BT and BTC geopolymer samples, a clear reduction in this band has been observed as a result of geopolymerization. This indicates the participation of carbonates in geopolymer reaction. Further, a characteristic band corresponding to symmetrical stretching of Si-O-Si has been observed in both geopolymer samples at 798 and 520 cm^{-1}. Bending vibration band of Si-O-Si has been observed at 466 cm^{-1} in BT geopolymers and at 420 cm^{-1} in BTC geopolymers. This shift from higher to lower wavenumber is significant of incorporation of Al in gel structure [43].

13

4.4   Scanning electron microscopic (SEM) analysis coupled with energy dispersive X-ray spectroscopy (EDX)

Figures 12 and 13 show the scanning electron microscope micrographs and elemental maps of same region of the selected samples obtained for BT and BTC geopolymers, respectively. The microstructure illustrates a heterogeneous morphology, while elemental maps show a nonhomogeneous distribution of several elements. Looking at the micrographs of BT geopolymers, three different zones in microstructure labelled as 1, 2 and 3 and microcracks are visible (Figure 12). The microcracks may appear as a result of the sample preparation method. Zone 1 in the micrograph shows a sponge-like structure which corresponds to Na-rich aluminosilicate geopolymer gel as indicated by the presence of Na, Al, Si and O in this zone from elemental maps. In addition to Na, the presence of Mg and Fe has also been recorded in this zone. While the elemental maps of K and Ca show that there is a small amount of K present while no Ca has been observed. Comparison of Si and Al elemental maps in this zone shows that the reaction product is richer in Al. Thus, it signifies that zone 1 potentially consists of N-A-S-H geopolymer gel incorporating Mg and Fe cations.

Zone 2 shows a natural pozzolan particle under alkali attack and dissolution of the particle. The particle has broken to small fragments under alkaline solution attack. Meanwhile, the reaction product is precipitated in cavities as indicated by the elemental map. Further, the elemental maps show that K and Ca are non-uniformly distributed in gel structure in contrast to zone 1. Zone 3 shows an unreacted particle of natural pozzolan which is rich in Si and O, and can be a quartz particle.
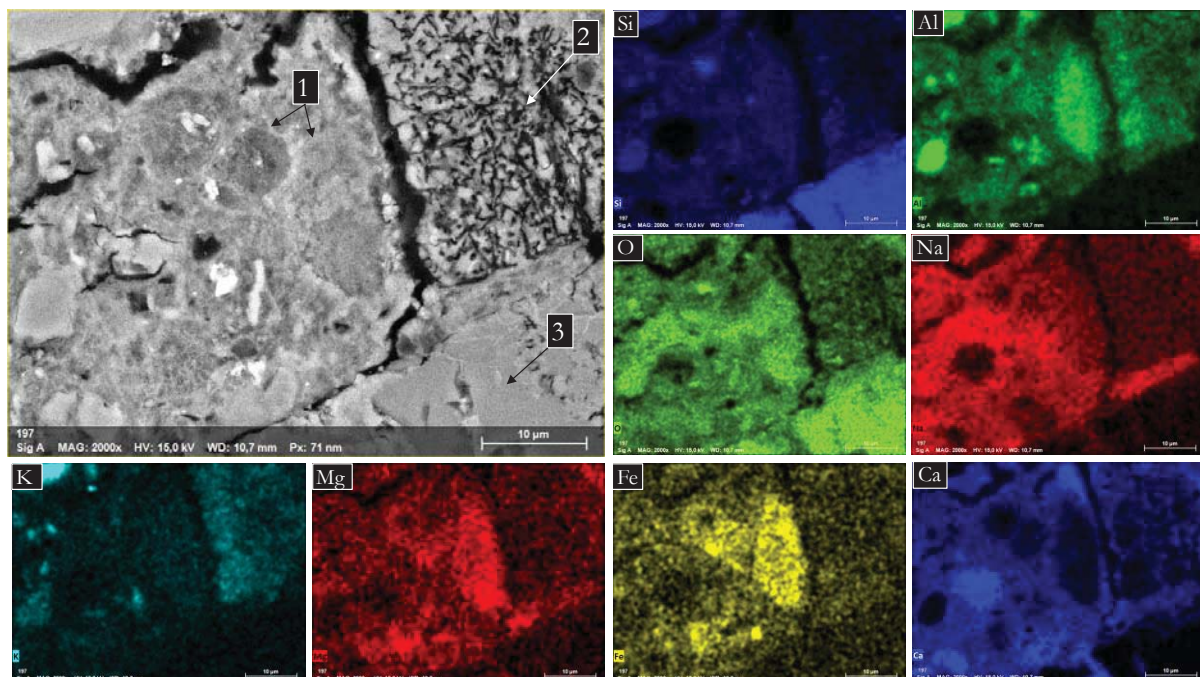
Figure 12: SEM image and elemental maps of BT geopolymer made with silica modulus of 0.707 at 7 d age.

Figure 13 presents a micrograph and elemental maps for BTC geopolymer sample. At least two types of gel phases can be seen marked as 1 and 2. The micrograph of the BTC geopolymer sample depicts a more homogeneous and compact microstructure with a more uniform distribution of several elements than the BT geopolymer. Like BT geopolymers, zone 1 shows Na-rich aluminosilicate gel, with an absence of Ca and the presence of Mg and Fe cations. As seen in BT geopolymers, this gel also has sponge-like structure. Zone 2 is characterized by a heterogeneous morphology with a compact gel structure where Na- and Ca-rich regions are overlapping each other. Further, in BTC micrograph a clear reduction in the size of unreacted particles of natural pozzolan can be seen in comparison to BT geopolymer sample. The geopolymer binder strongly binds the unreacted particles present. Comparing the elemental maps of Si and

14

Al, the geopolymer gel in BTC geopolymers is rich in Si. This justifies the higher reactivity of BTC and higher compressive strength as Si-O bonds are stronger than corresponding Al-O bonds [2]. Combining the results of BT and BTC geopolymers, it is obvious that the geopolymer binder is heterogeneous in nature and consists majorly of N-A-S-H, within cooperation of Mg, K, Fe and Ca.
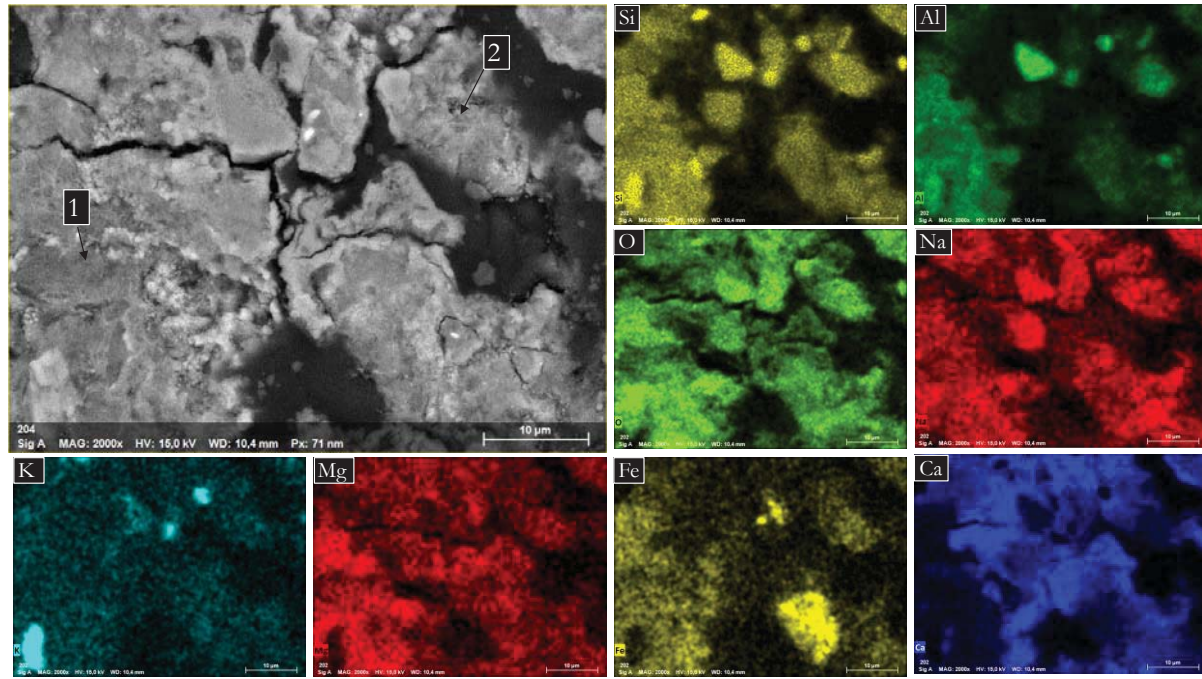

Figure 13: SEM image and elemental maps of BTC geopolymers made with silica modulus of 0.707 at 7 d age.

5   Conclusions

In this work, the natural pozzolan Bavarian trass obtained from Germany has been subjected to heat treatment and mechanical activation as reactivity enhancement methods. Results show that pozzolans in their natural state and after implementation of reactivity enhancement methods can be used as a precursor for geopolymer synthesis. The chemical composition, particle size and mineralogical phase composition of natural pozzolan effects the properties of resultant geopolymer product. The calcite-rich natural pozzolans can be used as geopolymer precursor by heat treatment, as the conversion of calcite to lime imparts higher reactivity and thus, an increase in compressive strength. An economical mechanical activation method was applied as reactivity enhancement method. However, no significant improvement in compressive strength has been observed as a result of mechanical activation. The calorimetric study showed that the fine fraction of natural pozzolan largely contributes to the reactivity. While mechanical activation helps majorly in reducing the size of coarser fraction thus only a slight improvement in reactivity has been observed. Comparing both reactivity enhancements methods, it is seen that the effect of calcination is more prominent than the reduced particle size.

For geopolymer samples prepared with calcined Bavarian trass (BTC), less amount of efflorescence was observed in comparison to BT samples for high silica modulus samples. As a result of heat treatment, an increase in the optimum silica modulus required to achieve higher compressive strength has also been observed. Therefore, the choice of reactivity enhancement method should be made depending on the properties, economic and environmental advantages. The second exothermic peak observed in the calorimetric study of BT geopolymers is assigned to the delayed dissolution of some phase(s) likely calcium rich phases. This delayed dissolution shifted to an earlier time for BTC geopolymers because of higher reactivity of BTC. The chemically bound water in the geopolymer structure gives insight about the dependence of the rate of reaction on silica modulus and age of the sample. Crystalline mineral phases such as calcite, lime, biotite and sanidine participate in geopolymer reaction by either complete or partial

15

----

dissolution in alkaline medium. Phase composition of geopolymer gel shows that it consists of N-A-S-H and (C)-N-A-S-H with the incorporation of Mg, Fe and K in the structure for both BT and BTC geopolymers.

6 Acknowledgements

References

1. Robayo-Salazar R, Mejía-Arcila J, Mejía de Gutiérrez R et al. (2018) Life cycle assessment (LCA) of an alkali-activated binary concrete based on natural volcanic pozzolan: A comparative analysis to OPC concrete. Constr. Build. Mater. 176: 103–111. doi: 10.1016/j.conbuildmat.2018.05.017

2. Pacheco-Torgal F, Labrincha JA, Leonelli C et al. (eds) (2012) Handbook of Alkali-activated Cements, Mortars and Concretes. Woodhead Publishing in materials. Woodhead Publishing, Cambridge, Philadelphia, PA

3. Duxson P, Fernández-Jiménez A, Provis JL et al. (2007) Geopolymer technology: The current state of the art. J. Mater. Sci. 42(9): 2917–2933. doi: 10.1007/s10853-006-0637-z

4. Provis JL, van Deventer JSJ (eds) (2009) Geopolymers - Structure, processing, properties and industrial applications. Woodhead Publishing Limited

5. Provis JL, van Deventer JSJ (2014) Alkali Activated Materials, State-of-the-Art Report, RILEM TC 224-AAM. Springer, Dordrecht, Heidelberg, New York, London

6. Firdous R, Stephan D, Jin Y (2018) Investigation of Rhenish and Bavarian Trass as Geopolymer Precursor. 20th International Conference of Building Materials - Ibausil 2018, 12 – 14 September 2018, Weimar, Germany (Book 2): 617–624.

7. Firdous R, Stephan D (2019) Effect of silica modulus on the geopolymerization activity of natural pozzolans. Constr. Build. Mater. 219: 31–43. doi: 10.1016/j.conbuildmat.2019.05.161

8. Firdous R, Stephan D, Djobo JNY (2018) Natural pozzolan based geopolymers: A review on mechanical, microstructural and durability characteristics. Constr. Build. Mater. 190: 1251–1263. doi: 10.1016/j.conbuildmat.2018.09.191

9. Djobo JNY, Elimbi A, Tchakouté HK et al. (2016) Reactivity of volcanic ash in alkaline medium, microstructural and strength characteristics of resulting geopolymers under different synthesis conditions. J. Mater. Sci. 51(22): 10301–10317. doi: 10.1007/s10853-016-0257-1

10. Allahverdi A, Mehrpour K, Kani EN (2008) Investigating the possibility of utilizing pumice-type natural pozzonal in production of geopolymer cement. Ceram. – Silik. 52(1): 16–23

11. Bondar D, Lynsdale CJ, Milestone NB et al. (2011) Effect of type, form, and dosage of activators on strength of alkali-activated natural pozzolans. Cem. Concr. Compos. 33(2): 251–260. doi: 10.1016/j.cemconcomp.2010.10.021

12. Ghafoori N, Najimi M, Radke B (2016) Natural pozzolan-based geopolymers for sustainable construction. Environ. Earth Sci. 75:1110(14): 1–16. doi: 10.1007/s12665-016-5898-5

13. Haddad RH, Alshbuol O (2016) Production of geopolymer concrete using natural pozzolan: A parametric study. Constr. Build. Mater. 114: 699–707. doi: 10.1016/j.conbuildmat.2016.04.011

14. Hewlett PC (ed) (1988) Lea's Chemistry of Cement and Concrete, 4th edn. Elsevier Ltd.

15. Djobo JNY, Elimbi A, Tchakouté HK et al. (2017) Volcanic ash-based geopolymer cements/concretes: The current state of the art and perspectives. Environ. Sci. Pollut. Res. 24(5): 4433–4446. doi: 10.1007/s11356-016-8230-8

16

----

16. Djobo JNY, Elimbi A, Tchakouté HK et al. (2016) Mechanical activation of volcanic ash for geopolymer synthesis: Effect on reaction kinetics, gel characteristics, physical and mechanical properties. R. Soc. Chem. (RSC Adv.) 6(45): 39106–39117. doi: 10.1039/C6RA03667H

17. Bondar D, Lynsdale CJ, Milestone NB et al. (2011) Effect of adding mineral additives to alkali-activated natural pozzolan paste. Constr. Build. Mater. 25(6): 2906–2910. doi: 10.1016/j.conbuildmat.2010.12.031

18. Bondar D, Lynsdale CJ, Milestone NB et al. (2011) Effect of heat treatment on reactivity-strength of alkali-activated natural pozzolans. Constr. Build. Mater. 25(10): 4065–4071. doi: 10.1016/j.conbuildmat.2011.04.044

19. Tchakoute HK, Mbey JA, Elimbi A et al. (2013) Synthesis of volcanic ash-based geopolymer mortars by fusion method: Effects of adding metakaolin to fused volcanic ash. Ceram. Int. 39(2): 1613–1621. doi: 10.1016/j.ceramint.2012.08.003

20. Djobo YJN, Elimbi A, Dika Manga J et al. (2016) Partial replacement of volcanic ash by bauxite and calcined oyster shell in the synthesis of volcanic ash-based geopolymers. Constr. Build. Mater. 113: 673–681. doi: 10.1016/j.conbuildmat.2016.03.104

21. Robayo RA, Mejía de Gutiérrez R, Gordillo M (2016) Natural pozzolan-and granulated blast furnace slag-based binary geopolymers. Mater. Constr. 66(321): e077. doi: 10.3989/mc.2016.03615

22. Djobo JNY, Tchadjié LN, Tchakoute HK et al. (2014) Synthesis of geopolymer composites from a mixture of volcanic scoria and metakaolin. J. Asian Ceram. Soc. 2(4): 387–398. doi: 10.1016/j.jascer.2014.08.003

23. EN 196-6 (2010) Methods of testing cement – Part 6: Determination of fineness

24. Schwiete H-E, Ludwig U, Wigger K-H (1961) Die Konstitution einiger rheinischer und bayrischer Trasse. Westdeutscher Verlag, Köln Opladen

25. Liebig E, Althaus E (1998) Pozzolanic activity of volcanic tuff and suevite: effects of calcination. Cem. Concr. Res. 28 (4): 567–575

26. Chukanov NV, Chervonnyi AD (2016) Infrared spectroscopy of minerals and related compounds. Springer Berlin Heidelberg

27. Ludwig U, Schwiete HE (1963) Untersuchungen an Deutschen Trassen. Silicates Ind.: 439–447

28. Fleischer M (1965) New mineral names. Am. Miner. 50: 2096–2111

29. Stark J, Wicht B (2000) Zement und Kalk: Der Baustoff als Werkstoff. Springer Berlin Heidelberg

30. Gebregziabiher BS, Thomas RJ, Peethamparan S (2016) Temperature and activator effect on early-age reaction kinetics of alkali-activated slag binders. Constr. Build. Mater. 113: 783–793. doi: 10.1016/j.conbuildmat.2016.03.098

31. Triantafyllou G, Christidis G, Markopoulos T (2003) Influence of porosity and grain size of carbonate rocks in the reactivity of lime. Mineral Exploration and Sustainable Development, Eliopoulos et al., eds. Millpress, Rotterdam: 931–934

32. Černý R, Rovnaníková P (2002) Transport processes in concrete. Spon Press, Taylor & Francis Group, London

33. Ben Haha M, Le Saout G, Winnefeld F et al. (2011) Influence of activator type on hydration kinetics, hydrate assemblage and microstructural development of alkali activated blast-furnace slags. Cem. Concr. Res. 41(3): 301–310. doi: 10.1016/j.cemconres.2010.11.016

34. Zhang Z, Provis JL, Reid A et al. (2014) Fly ash-based geopolymers: The relationship between composition, pore structure and efflorescence. Cem. Concr. Res. 64: 30–41. doi: 10.1016/j.cemconres.2014.06.004

35. Djobo JNY, Tchakouté HK, Ranjbar N et al. (2016) Gel Composition and Strength Properties of Alkali-Activated Oyster Shell-Volcanic Ash: Effect of Synthesis Conditions. J. Am. Ceram. Soc. 99(9): 3159–3166. doi: 10.1111/jace.14332

36. Scrivener K, Snellings R, Lothenbach B (eds) (2016) A Practical Guide to Microstructural Analysis of Cementitious Materials. Taylor & Francis Group

----

37. Tajuelo Rodriguez E, Garbev K, Merz D et al. (2017) Thermal stability of C-S-H phases and applicability of Richardson and Groves' and Richardson C-(A)-S-H(I) models to synthetic C-S-H. Cem. Concr. Res. 93: 45–56. doi: 10.1016/j.cemconres.2016.12.005

38. Zhang Z, Provis JL, Wang H et al. (2013) Quantitative kinetic and structural analysis of geopolymers. Part 2. Thermodynamics of sodium silicate activation of metakaolin. Thermochim. Acta 565: 163–171. doi: 10.1016/j.tca.2013.01.040

39. Sun Z, Vollpracht A (2018) Isothermal calorimetry and in-situ XRD study of the NaOH activated fly ash, metakaolin and slag. Cem. Concr. Res. 103: 110–122. doi: 10.1016/j.cemconres.2017.10.004

40. Lecomte I, Henrist C, Liégeois M et al. (2006) (Micro)-structural comparison between geopolymers, alkali-activated slag cement and Portland cement. J. Eur. Ceram. Soc. 26(16): 3789–3797. doi: 10.1016/j.jeurceramsoc.2005.12.021

41. van Deventer JSJ, San Nicolas R, Ismail I et al. (2015) Microstructure and durability of alkali-activated materials as key parameters for standardization. J. Sustain. Cem. Mater. 4(2): 116–128. doi: 10.1080/21650373.2014.979265

42. Komnitsas K, Zaharaki D, Perdikatsis V (2007) Geopolymerisation of low calcium ferronickel slags. J. Mater. Sci. 42(9): 3073–3082. doi: 10.1007/s10853-006-0529-2

43. Walkley B, San Nicolas R, Sani M-A et al. (2016) Phase evolution of C-(N)-A-S-H/N-A-S-H gel blends investigated via alkali-activation of synthetic calcium aluminosilicate precursors. Cem. Concr. Res. 89: 120–135. doi: 10.1016/j.cemconres.2016.08.010

44. Baykara H, Cornejo MH, Murillo R et al. (2017) Preparation, characterization and reaction kinetics of green cement: Ecuadorian natural mordenite-based geopolymers. Mater. Struct. 50: 188. doi: 10.1617/s11527-017-1057-z

18

2.5. Factors effecting the properties of alkali activated natural pozzolan based geopolymers

Authors: Rafia Firdous, Dietmar Stephan

Factors Effecting the Properties of Alkali Activated Natural Pozzolan Based Geopolymers

R. Firdous, Berlin/D, D. Stephan, Berlin/D

Technische Universität Berlin, Institut für Bauingenieurwesen, Fachgebiet Baustoffe und Bauchemie, Gustav-Meyer-Allee 25, 13355 Berlin, Germany

1. Introduction

Geopolymer science has gained a lot of interest in recent decades because of superior mechanical and durability characteristics and potentially lower environmental foot-prints /1/. Geopolymers are a class of inorganic binders which are synthesised using aluminosilicate precursor with a concentrated alkaline solution /2, 3/. Natural pozzolans are one of the suitable precursors for geopolymer synthesis /2, 4/. The properties of geopolymers are widely affected by several influencing factors, including the type of source material, particle size distribution, fineness, alkali concentration, amount of water, curing conditions and age of specimen /5/. Owing to lower reactivity of natural pozzolan compared to fly ash and metakaolin, several reactivity enhancement methods are possible to apply such as addition of mineral admixture, mechanical activation and heat treatment /6–8/. This manuscript explains briefly the effect of the alkali type in alkaline solution, concentration of alkaline solution, ambient or heat curing on reaction kinetics and properties of resultant geopolymer product using two different natural pozzolans.

2. Materials and methods

In this research study, natural pozzolans originating from Italy has been used for geopolymer synthesis. Pozzolans Laziale black (PB) and pozzolan Flegrea (PF) was supplied by Buzzi Unicem SpA, Italy. The chemical and mineralogical composition of both natural pozzolans is as given in Table 1 and Table 2.

Table 1. Chemical composition of PB and PF

Sample / wt.%	LOI	SiO_2	Al_2O_3	Fe_2O_3	MnO	MgO	CaO	Na_2O	K_2O
PB	5.5	44.8	16.0	10.6	0.3	4.3	9.2	0.6	5.2
PF	3.8	58.3	17.9	3.9	0.1	0.9	2.5	3.5	7.9

Table 2. Mineralogical composition of PB and PF

Sample	Minerals found
PB	Nepheline, Leucite, Analcime, Muscovite, Augite, Diopside ferrian, Akermanite, Chloritoid, Quartz, Magnetite, Hematite
PF	Sanidine, Albite, Anorthite, Analcime, Muscovite, Quartz

The geopolymer samples were prepared by mixing these natural pozzolans with sodium hydroxide, potassium hydroxide and sodium silicate solution. Sodium hydroxide and potassium hydroxide solutions labelled as NH and KH (obtained from VWR International GmbH), respectively, were prepared by dissolving pellets of 99 wt.% purity in deionized water to give a concentration of 12 and 16 mol/kg. Sodium silicate solutions (NS) of silica modulus equal to 0.7 and 0.8 were prepared by mixing sodium hydroxide solutions and a sodium silicate solution with silica modulus equal to 2.12 (obtained from Woellner GmbH). For comparison of PB- and PF-based geopolymers both natural pozzolans were ground to comparable Blaine fineness in range of 6560 $\pm$ 20 cm^2/g. Geopolymer paste samples were prepared by mixing natural pozzolan and alkaline solution using laboratory hand mixer for 3 min followed by compaction for 2 min. For compressive strength determination 20 mm cubic samples were prepared. Samples were cured using two methods as: ambient curing at 22 $\pm$ 2 °C, 100% RH and heat curing at 40 °C, 100% RH for first 28 days, followed by ambient curing till 90 days. Reaction kinetics were determined using isothermal conduction calorimetry at 20 °C. Samples were mixed outside the device for 45 s each.

3. Results and discussion

In a previous study by the authors, the effect of silica modulus of alkaline solution was studied in detail /2/. Therefore, based on these findings firstly the trial samples were prepared for a wide range of concentrations for all three alkaline solutions. Based on these trial samples, concentration used in this study were selected for studying the effect of alkali metal type, concentration and curing method on two different natural pozzolans.

Results of 7-, 28- and 90-days compressive strength of PF and PB geopolymers cured at ambient curing conditions are presented in Fig. 1. Results show that PB have better reactivity compared to PF for all type and concentrations of alkaline solutions used at ambient concentration. PF based-geopolymers showed poor reactivity with NH and NS solution, while showed comparatively better reactivity with KH

solution. PB showed an increase in compressive strength with the age of sample, indicating that geopolymer reaction spans over long time. At ambient curing conditions, the higher reactivity of PB in comparison to PF is because of the differences in chemical composition of both natural pozzolans. Looking at Table 1, PB has higher wt.% of MgO and CaO compared to PF, which can be a possible reason for its higher reactivity.
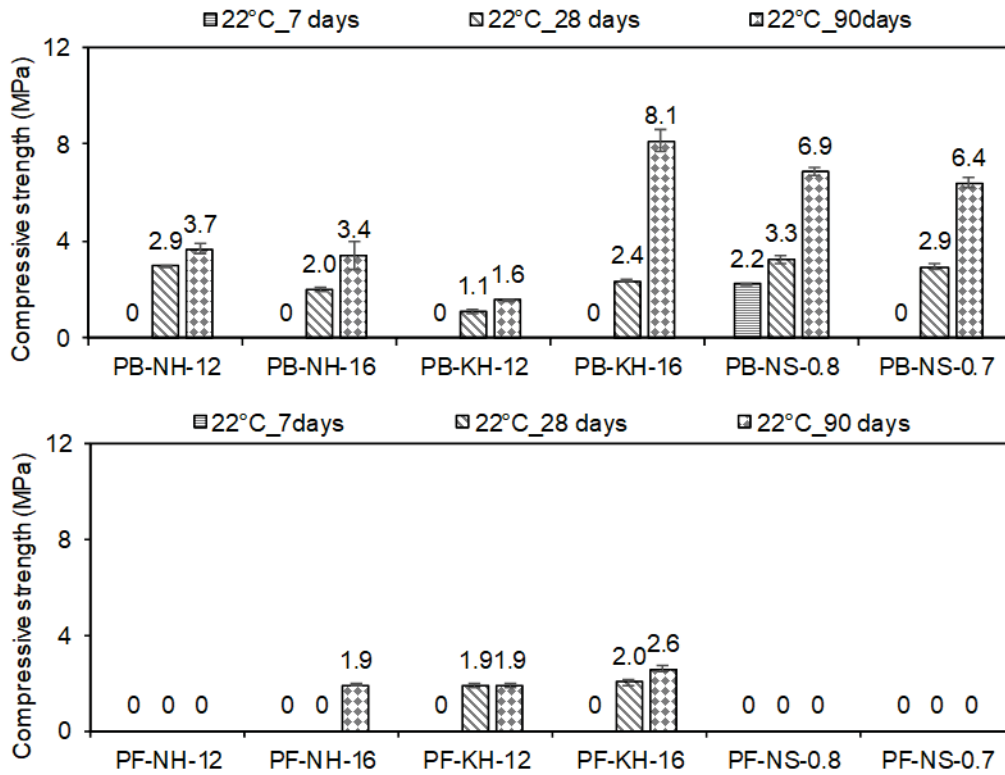
Fig. 1. Compressive strength of PB and PF geopolymers cured at 22 °C and 100% RH at various ages

Fig. 2 presents the calorimetric heat evolution curves for PB and PF geopolymers. The first exothermic peak recorded occurs within first few minutes of mixing of the specimen. This peak is attributed to the first wetting. The first exothermic peak is followed by the deacceleration which is in literature ascribed to polycondensation of geopolymer product /2, 9/. The rate of deacceleration has been observed to vary with the change of alkaline solution type and concentration (Fig. 2). PB samples prepared with KH solutions exhibit highest heat evolution in deacceleration region. However, compressive strength value recorded for these samples shows that condensed geopolymer gel amount is too less till 7 days to carry any load. Thereafter, geopolymer reaction continues at steady rate as indicated by increase in compressive

strength. PB samples prepared with NH-12 exhibited a wide peak starting on 6th day and ending on 7th day. The reaction occurring at this peak has been thought to be delayed dissolution of some phases as also seen in /2/. PB samples prepared with NS solution shows faster deacceleration and thereafter, continuous heat evolution till 7th day. The lower reaction kinetic of these samples is very likely because of lower pH of these solution as compared to NH and KH solutions.
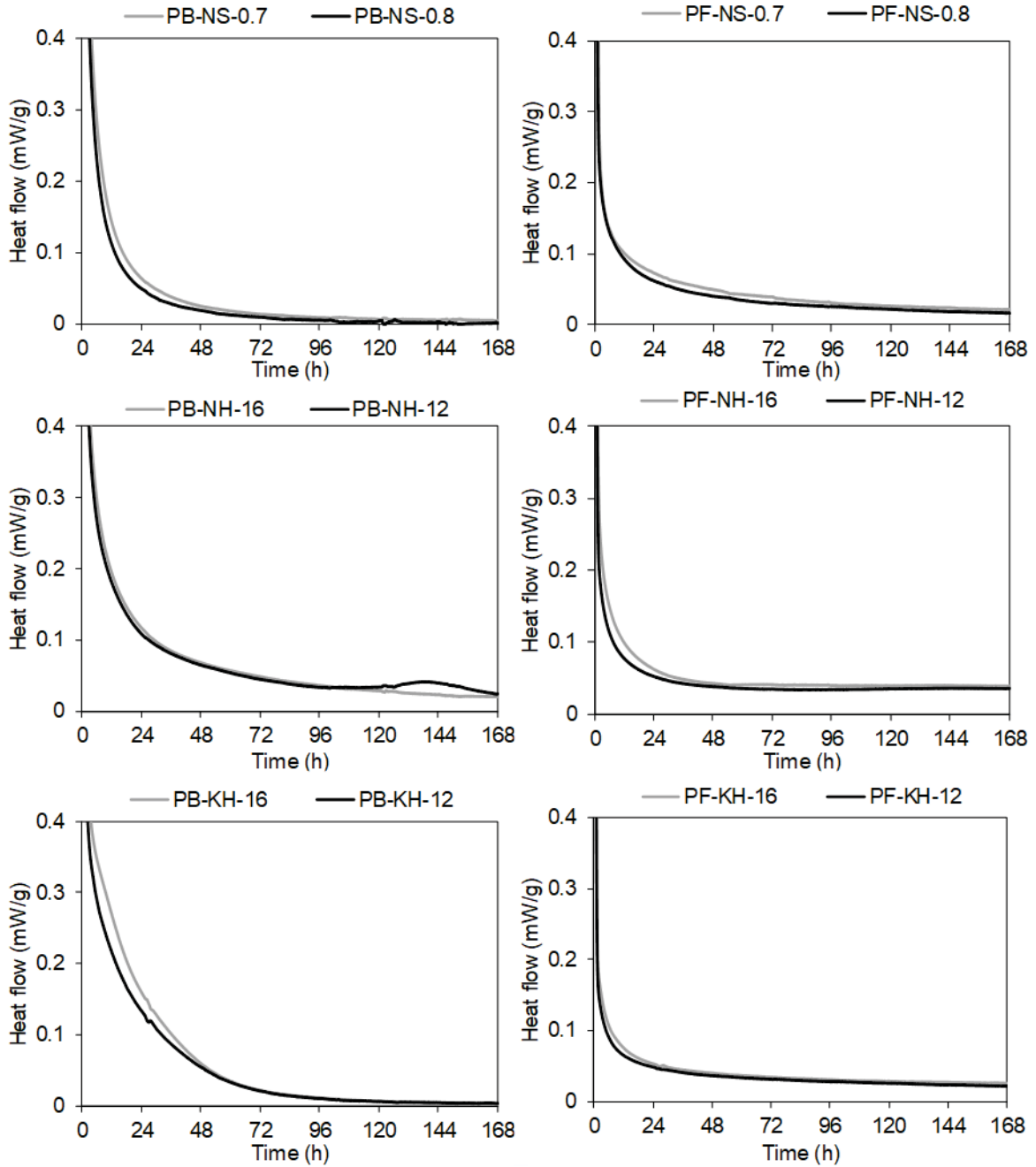
Fig. 2. Heat evolution curves for PB and PF geopolymers recorded for 7 days

Looking at PF samples in Fig. 2, it can be seen that all samples have lower reactivity as compared to PB samples. This is also indicated by compressive strength of these samples. However, these samples show continuous heat evolution at a steady rate. This indicates that in these samples geopolymer reaction is occurring at very slow rate and therefore, the system needs much longer time to reach polymerization stage.

Owing to lower reactivity of used natural pozzolans, a heat curing regime was applied on these geopolymers in order to study its effect on the properties of the resultant geopolymer. Compressive strength results of PB and PF geopolymers cured at heat curing regime are presented in Fig. 3. Results show that PB samples prepared with NS solution exhibited improvement in reactivity as indicated by enhancement of compressive strength. While, PB samples prepared with NH and KH solution also exhibited improvement in compressive strength at 28 days. However, for nearly all PB samples loss of strength after 28 days of curing has been observed. The reason for such a loss in compressive strength is not clear.
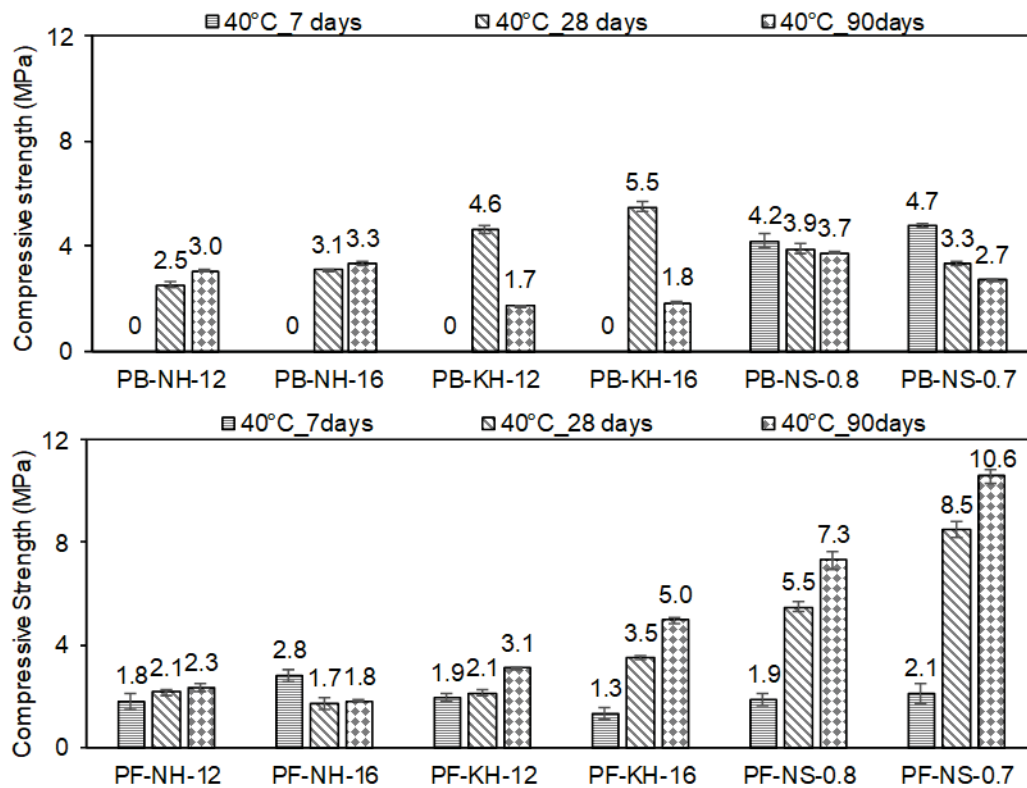
Fig. 3. Compressive strength of PB and PF geopolymers cured at heat curing regime

PF performed higher reactivity for all combinations of alkaline solution used at heat curing regime. PF geopolymer samples prepared with NS-0.7 exhibited highest compressive strength at all ages in comparison to other samples. The higher alkalinity of this sample compared to NS-0.8 indicates that synthesis of PF for geopolymer production require both higher concentration of alkalis and silicates in reactive form.

4. Conclusions

The geopolymerization of various natural pozzolans is affected by the composition of natural pozzolans, type of alkaline solution, concentration of alkaline solution and curing conditions. These results also show that geopolymer reaction can be accelerated using higher curing temperature. Nevertheless, heat curing regime can also effect reactivity of some natural pozzolan negatively. Therefore, a careful regime should be chosen after considering all possible factors. Use of silicate based alkaline solution imparts higher compressive strength because of availability of reactive silica.

Acknowledgements

References

/1/ R.A. Robayo-Salazar, R. Mejía de Gutiérrrez, F. Puertas:
"Effect of metakaolin on natural volcanic pozzolan-based geopolymer cement"
Appl. Clay Sci. (2016) 132-133, 491-497

/2/ R. Firdous, D. Stephan:
"Effect of silica modulus on the geopolymerization activity of natural pozzolans"
Constr. Build. Mater. (2019) 219, 31-43

/3/ J.L. Provis, J.S.J. van Deventer (Eds.): "Geopolymers - Structure, processing, properties and industrial applications"
Woodhead Publishing Limited (2009)

/4/ R. Firdous, D. Stephan, Y. Jin:
"Investigation of Rhenish and Bavarian Trass as Geopolymer Precursor"
20th International Conference of Building Materials - Ibausil 2018, 12 – 14 September 2018, Weimar, Germany (2018), Book 2, 617–624.

/5/ R. Firdous, D. Stephan, J.N.Y. Djobo:
"Natural pozzolan based geopolymers: A review on mechanical, microstructural and durability characteristics"

Constr. Build. Mater. (2018) <u>190</u>, 1251–1263.

/6/ D. Bondar, C.J. Lynsdale, N.B. Milestone, N. Hassani, A.A. Ramezanianpour:
   "Effect of heat treatment on reactivity-strength of alkali-activated natural pozzolans"
Constr. Build. Mater. (2011) <u>25</u>, 4065–4071.

/7/ J.N.Y. Djobo, A. Elimbi, H.K. Tchakouté, S. Kumar:
   "Mechanical activation of volcanic ash for geopolymer synthesis: Effect on reaction
    kinetics, gel characteristics, physical and mechanical properties"
    R. Soc. Chem. (RSC Adv.) (2016) <u>6</u>, 39106–39117.

/8/ D. Bondar, C.J. Lynsdale, N.B. Milestone, N. Hassani, A.A. Ramezanianpour:
   "Effect of adding mineral additives to alkali-activated natural pozzolan paste"
    Constr. Build. Mater. (2011) <u>25</u>, 2906–2910.

/9/ J.N.Y. Djobo, A. Elimbi, H.K. Tchakouté, S. Kumar:
   "Reactivity of volcanic ash in alkaline medium, microstructural and strength
    characteristics of resulting geopolymers under different synthesis conditions"
    J. Mater. Sci. (2016) <u>51</u>, 10301–10317.

2.6. Reaction of calcium carbonate minerals in sodium silicate solution and its role in alkali-activated systems

Authors: Rafia Firdous, Tamino Hirsch, Detlef Klimm,

Barbara Lothenbach, Dietmar Stephan

Reaction of calcium carbonate minerals in sodium silicate solution and its role in alkali-activated systems

Rafia Firdous [a], Tamino Hirsch [a], Detlef Klimm [b], Barbara Lothenbach [c], Dietmar Stephan [a,*]

[a] Technische Universität Berlin, Department of Civil Engineering, Building Materials and Construction Chemistry, Gustav-Meyer-Allee 25, 13355 Berlin, Germany

[b] Leibniz-Institut für Kristallzüchtung, Max-Born-Str. 2, 12489 Berlin, Germany

[c] Empa, Laboratory for Concrete & Construction Chemistry, 8600 Dübendorf, Switzerland

* Corresponding author e-mail: stephan@tu-berlin.de

Graphical abstract

a) Initial stage   b) Partial dissolution of CaCO3   c) Growth of precipitates

Na+   SiO4^4-   H2O   Ca2+   CO3^2-   C-N-S-H   Na2CO3·H2O
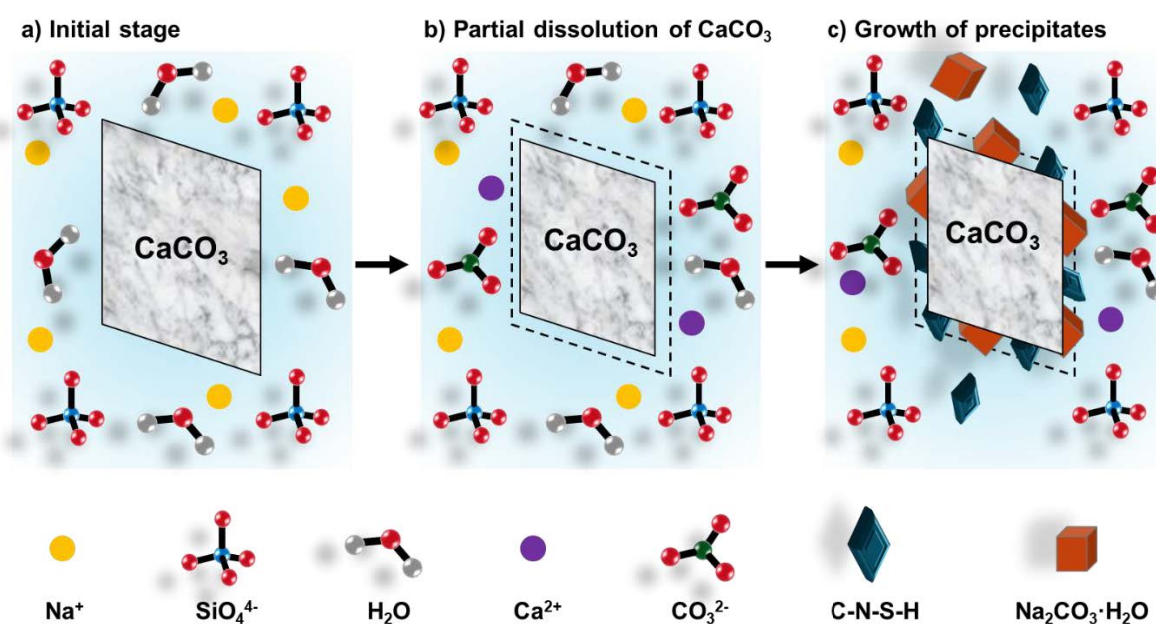
Abstract

This article investigates the role of calcium carbonate minerals in an alkali-activated system through their reaction with sodium silicate solution. The early reaction kinetics and reaction products are investigated using isothermal conduction calorimetry, in-situ XRD and in-situ FTIR. Later reaction products are identified with thermodynamic modelling and analysis of the paste samples after 8 and 90 d using XRD, TGA, DSC and mass spectrometry. After a few hours of reaction, natron precipitates as the first crystalline carbonate phase, while changes in the connectivity of silicates are observed due to the precipitation of C-S-H, which may contain Na. After 8 and 90 d, C-S-H is observed together with thermonatrite instead of natron. It is shown that calcium carbonate is not just a filler in an alkali-activated system but can provide Ca to form C-S-H and can also enhance the availability of carbonate for the formation of alkali carbonates.

Keywords

1. Introduction

In the development of environmentally friendly construction materials, alkali-activated binders / geopolymers have gained much interest in recent years (Komnitsas and Zaharaki, 2007). Reasonable mechanical and durability characteristics of these binders make them popular in the field of construction materials (Duxson et al., 2007). Natural or artificial pozzolans containing a substantial amount of reactive silica and alumina can be the sole precursor for these binders in the presence of an alkali hydroxide or alkali silicate solution (Xu and van Deventer, 2002; Pacheco-Torgal et al., 2012; Provis and van Deventer, 2014). The properties of the resultant reaction product largely depend on the curing conditions, the composition of the alkaline solution, the chemical composition and mineralogy of the precursor (Duxson et al., 2007; Rattanasak and Chindaprasirt, 2009). The alkali-activated binders and geopolymers are differentiated based on the calcium content of the precursor and the phases present in the resultant binder (Herrmann et al., 2017). A low-calcium system tends to produce binders such as geopolymers, which may contain phases such as N-A-S-H gel, while a high-calcium system produces an alkali-activated binder containing phases such as C-S-H or C-A-S-H gel (Pacheco-Torgal et al., 2012; Herrmann et al., 2017; Niu et al., 2020a). Low-calcium pozzolans such as volcanic ash, fly ash (FA) and metakaolin (MK) are the most commonly used precursors for geopolymers, while ground granulated blast furnace slag (GGBFS) is a prominent precursor for high-calcium systems (Pacheco-Torgal et al., 2012; Herrmann et al., 2017; Lu et al., 2020). The use of natural resources is becoming more prominent as the availability of FA and GGBFS resources is limited in several countries and the use of MK is not practical due to the environmental footprint associated with its production (Snellings et al., 2012; Sharif et al., 2015; Firdous and Sharif, 2016; Snellings, 2016). Several research studies have been published in recent years on the use of natural pozzolans (NPs) for geopolymerization (Bondar et al., 2011a; Firdous et al., 2018b; Firdous et al., 2018a; Firdous and Stephan, 2019a). The mineralogical compositions of natural pozzolans vary considerably, thus making it challenging to define generally valid

61   rules for their use in geopolymer production (Bondar et al., 2011b; Djon Li Ndjock et al.,

62   2017; Firdous and Stephan, 2019a).

63

64   Previous studies have shown that the incorporation of reactive calcium sources (such as

65   GGBFS) in NP-, FA- and MK-based geopolymers enhances the mechanical and durability

66   properties of these binders (Yip et al., 2005; Gao et al., 2015a, 2015b; Robayo et al., 2016;

67   Najimi et al., 2018). This is because of the precipitation of C-S-H gel in addition to

68   geopolymer gel, which fills the pores and acts as a microaggregate, thus increasing the

69   compressive strength of these binders (Yip et al., 2005). Furthermore, the addition of

70   GGBFS improves the silica-to-amorphous alumina ratio, thus increasing the dissolution of

71   precursors and the formation of geopolymer gel (Robayo et al., 2016). Another possible

72   source of calcium could be calcium carbonates ($CaCO_3$), such as calcite. In nature,

73   tremendous amounts of calcium carbonate are available in the form of calcite and this

74   mineral phase is often found in natural as well as in artificial pozzolans (Firdous and

75   Stephan, 2019a; Moukannaa et al., 2019; Firdous and Stephan, 2020; Niu et al., 2020b; Niu

76   et al., 2020a). By use of non-calcined calcium carbonate in alkali-activated systems, the

77   environmental burden of its calcination, as in cement production, can be reduced (Juenger,

78   2018). However, the reactivity of calcium carbonates in the alkali-activated / geopolymer

79   system has been seldomly investigated. A study reported that the addition of oyster shell

80   (tempered to remove organic substances) helped to reduce the setting time and resulted in a

81   minor improvement in compressive strength. The comparatively high crystallinity of oyster

82   shells was reported to be the reason that the improvement in mechanical properties was not

83   more significant (Djobo et al., 2016). By the addition of marble and travertine waste in the

84   natural pozzolan geopolymer, a compressive strength of up to 46 MPa can be achieved at

85   90 d of age using a 10 M NaOH solution (Tekin, 2016). Moreover, a recent study showed the

86   utilization of limestone as a precursor for alkali-activated binders (Ortega-Zavala et al.,

87   2019). However, the reaction mechanisms of calcium carbonate in the alkali-activated /

88   geopolymer system are not described. In recent studies, the unusual calorimetric behaviour

89   of a natural pozzolan in a geopolymer system was found to be related to its calcite content

90   (Firdous and Stephan, 2019b, 2019a); the exact reason for such behaviour was not

91   understood. As mentioned above, calcium carbonate is found nearly all over the world and is

92   therefore often present in natural as well as artificial pozzolans (Firdous and Stephan, 2020;

93   Niu et al., 2020a; Niu et al., 2020b). Based on these observations and the presence of

94   calcium carbonates in many pozzolans, it is investigated how the various polymorphs of

95   calcium carbonate react in alkali-activated systems and how they affect the reaction product

96   and resulting binder composition.

97

98   The current study aims to investigate the reactivity of calcium carbonate and especially

99   calcite in sodium silicate solution. The emphasis is on understanding which phases develop

100   and what role calcium carbonate could play in the formation of alkali-activated binders under

101   alkaline conditions. For this purpose, eight calcium carbonate samples were used and

102   subjected to react with the sodium silicate solution. Isothermal conduction calorimetry (ICC),

103   in-situ and ex-situ X-ray diffraction analysis (XRD), in-situ Fourier transform infrared

104   spectroscopy (FTIR), thermogravimetric analysis (TGA), differential scanning calorimetry

105   (DSC) and mass spectrometry (MS) were used to evaluate the reaction kinetics and phase

106   development over the first days and months of the reaction. Scanning electron microscopy

107   (SEM) was performed to analyse the microstructure of the reacted samples. Thermodynamic

108   modelling was utilised to examine the expected long-term behaviour. The results of this

109   investigation can be used as an ideal system for the role of the calcium carbonate phase in

110   an alkaline medium.

111

112

113

2. Materials and methods

For this study, both natural and synthetic calcium carbonate ($CaCO_3$) samples were used to explore the factors influencing the reactivity of calcium carbonates in an alkaline medium. Additionally, two polymorphs, calcite and aragonite, were tested to investigate the impact of the crystal structure of calcium carbonate on its reactivity. The samples included one natural aragonite, one chemical-grade calcium carbonate (>98.5 wt.-% pure), four natural calcite samples and two limestone samples. The abbreviations used in this study for each sample, their origin, Blaine fineness, d_{50} and d_{90} particle sizes are given in Table 1. The particle size distribution curves are presented in Fig. S1 of the supplementary material. Blaine fineness was measured in accordance with EN 196-6 (EN 196-6, 2010). Samples were milled in a laboratory ball mill to the desired fineness. Particle size distribution curves, including d_{50} and d_{90}, were determined using laser granulometry (Mastersizer 2000 from Malvern Instruments). The mineral phases present in each sample were investigated using XRD. All calcite samples (C-CMX, C-NMX, C-PK, C-GR), limestone samples (L-RUD, L-KAR) and $CaCO_3$ chemical (C-CHEM) contained only the calcite polymorph of $CaCO_3$, while the aragonite sample (A-SIC) contained mostly aragonite and a minor amount of calcite. Only three samples contained other minor impurities detectable by XRD. All minor phases are listed in Table 1, and the diffractograms of raw samples are presented in Fig. S2 of the supplementary material. The symbols used in XRD figures, the ICSD (inorganic crystal structure database) card numbers and the chemical formulas of all mineral phases mentioned in the manuscript are summarized in Table S1 of the supplementary material.

Table 1. Characteristics of all calcium carbonates used and the minor mineral phases in each sample as identified by XRD. The abbreviations are A for aragonite, C for natural or chemical calcites and L for limestones, as well as an abbreviation of the sample's place of origin.

Sample	Origin	Abbreviation	Blaine fineness (cm^2/g)	d_{50} (μm)	d_{90} (μm)	Minor phases *
Aragonite	Sicily, Italy	A-SIC	6230	3.3	24.0	Calcite
$CaCO_3$ chemical	AppliChem GmbH	C-CHEM	7050	4.6	12.7	-
Calcite	Chihuahua, Mexico	C-CMX	6690	6.2	42.2	-
Calcite	Naica, Mexico	C-NMX	7520	4.2	31.1	-
Calcite	Balochistan, Pakistan	C-PK	7200	5.2	28.7	-
Calcite	Schönbrunn, Germany	C-GER	7000	5.2	27.1	Dolomite
Limestone	Rüdersdorf, Germany	L-RUD	7990	4.4	13.1	Quartz
Limestone	Karsdorf, Germany	L-KAR	7770	4.8	13.9	Dolomite, quartz

* Dolomite ($CaMg(CO_3)_2$), quartz (SiO_2)

The pastes were prepared from 5 g of a solid precursor which reacted with a sodium silicate solution (water glass) at a solution-to-precursor ratio of 0.88. This equals to 53.3 wt.-% solid precursor and 46.7 wt.-% sodium silicate solution in the paste sample. The composition of the used sodium silicate solution was 20.2 wt.-% SiO_2, 19.8 wt.-% Na_2O and 60.0 wt.-% H_2O (molar SiO_2/Na_2O ratio of 1.1). This equals a $H_2O/(CaCO_3+SiO_2+Na_2O)$ ratio of 0.39 (g/g) and a $CaCO_3/SiO_2$ ratio of 3.39 (mol/mol). Samples were prepared by pouring the powder into a calorimetric vessel with the sodium silicate solution already inside. A vortex mixer was used to mix each sample for 60 s. If samples had to be cured, they were seal cured at 20 ± 1 °C until test age. The early reaction and phase development were observed with calorimetry, the pH value of the solution from leached samples, in-situ XRD and in-situ FTIR.

153   Isothermal conduction calorimetry was performed using the device MC-CAL 100P, C3

154   Prozess- und Analysentechnik GmbH for the first 6 d. A vortex mixer was used for mixing

155   each sample outside the calorimeter. The time zero in the calorimetric curves is the time

156   when the solution and powder came in contact. Measured heat flows were normalized to the

157   weight of the calcium carbonate sample.

158

159   To follow the relative changes of the pH value during reaction, the prepared samples were

160   cured for different time intervals and subsequently leached (1 g of paste sample was

161   leached in 10 mL of water) for 30 min each, and after that the pH value of the solution was

162   measured. A SG78 pH meter from Mettler Toledo was used for pH measurements. Standard

163   buffers for pH electrode calibration were pH 4, 7 and 9. Direct extraction of the pore solution

164   from the binder was also tried but was not successful.

165

166   The early phase development in the paste samples during the first 59 h at 20 °C

167   (conditioned sample stage) was measured in-situ using the Empyrean XRD device from

168   PANalytical. After mixing, pastes were poured into the XRD sample holder, which was

169   subsequently placed in the device and covered with Kapton foil to reduce carbonation and

170   evaporation of water. The first scan was started 3.5 min after the contact of solution and

171   powder, and each scan took 23.6 min (step size of 0.0131°, range from 12° to 56.8° 2θ in

172   continuous mode). An X-ray tube operating at 40 kV and 40 mA generated CuKα radiation (λ

173   = 1.54 Å), and the radiation was subsequently passed through a Ni filter. Diffractograms

174   collected over time were analysed using HighScore plus software. First, the Kα_2 peaks were

175   removed, then a peak search and background approximation were performed. The peaks

176   corresponding to various phases were assigned by the ICDD (International Centre for

177   Diffraction Data) and the ICSD (Inorganic Crystal Structure Database). After this, the fitting

178   of the peak position, peak area, full width at half maximum, and shape was conducted.

179   Finally, the development of peak areas for selected peaks was chosen for analysis.

180

181   In-situ FTIR analysis was performed on paste samples using Spectrum Two from

182   PerkinElmer fitted with a diamond crystal using the attenuated total reflection (ATR) method.

183   IR spectra were obtained between 4000 and 400 cm^{-1}, with a resolution of 1 cm^{-1}. Paste

184   samples were poured on the diamond and sealed with a polyimide film. Spectra were

185   obtained every 20 min, with the first spectrum collected 2 min after mixing.

186

187   In order to investigate the temporal development, hardened samples cured for 8 and 90 d

188   were ground by hand with a mortar and pestle made from agate and examined using ex-situ

189   powder XRD, DSC-TGA and TGA-MS. Furthermore, scanning electron microscopy (SEM)

190   and thermodynamic modelling was performed.

191

192   Ex-situ XRD was performed on these powder samples using a PANalytical Empyrean with Ni

193   filter and CuKα radiation (λ = 1.54 Å), operating at 40 kV and 40 mA in continuous mode,

194   with a resolution of 0.0131° and a speed of 0.0176 °/s, with a range from 5° to 65° 2θ. The

195   phase evaluation was done using HighScore Plus software with ICDD and ICSD databases.

196   Furthermore, Rietveld refinements for quantification were performed on reacted samples by

197   using rutile as internal standard.

198

199   A selected sample (C-PK) with an age of 90 d was characterised by simultaneous thermal

200   analysis. This sample was freeze-dried before DSC-TGA and TGA-MS were performed (to

201   convert thermonatrite into natrite) in order to minimise the bound water; see section 3.2.2.

202   The simultaneous thermal analysis was carried out in two separate sets of experiments, 1)

203 differential scanning calorimetry and thermogravimetry (DSC-TGA) and 2) thermogravimetry

204 combined with exhaust gas mass spectrometry (TGA-MS). The MS analysis of the gases

205 emitted by the thermally treated sample could not be performed simultaneously with DSC, as

206 MS requires a comparably large sample amount which is inappropriate for the accurate

207 measurement of DSC. Therefore, two separate subsets of the same sample were measured

208 and compared via the respective TGA measurements.

209

210 The DSC-TGA was performed using a Netzsch STA 449 F3 Jupiter equipped with a DSC

211 sample holder. Both the reference and sample crucibles were made from aluminium oxide

212 with lids of the same material. The sample had a mass of 11 mg, and the temperature was

213 regulated from 24 – 1000 °C at a heating rate of 10 °C/min. The baseline signal was

214 recorded by performing the same program with the same empty crucibles.

215

216 TGA-MS was performed with a Netzsch STA 409C/CD coupled to a BALZERS QMS 403

217 mass spectrometer. The STA 409C/CD was equipped with a carbon furnace, a DTA/TG

218 sample holder and aluminium oxide crucibles. The sample weighing 53 mg was measured at

219 a heating rate of 10 °C/min from 20 – 1000 °C in an argon flow of 100 mL/min. Part of the

220 gas flowed through a skimmer of glassy carbon to the mass spectrometer. For MS

221 measurement, the liberation of H_2O and CO_2 from the sample was considered. The

222 baselines of TGA and MS were determined with the same experimental set-up.

223

224 Scanning electron microscopy (SEM) was performed using a low-vacuum scanning electron

225 microscope GeminiSEM500, ZEISS. The gas pressure in the sample chamber was 100 Pa

226 and a voltage of 15 kV was used to examine the samples, which were neither ground nor

227 coated. The signal of secondary electrons was used to obtain the micrographs of

228 microstructure.

229   In order to predict the phases to be expected in a mixture of calcium carbonate and sodium

230   silicate solution in the long term, thermodynamic modelling was performed using the Gibbs

231   energy minimisation software GEMS (Wagner et al., 2012; Kulik et al., 2013) in version 3.5

232   combined with the PSI-Nagra 12/07 thermodynamic database (T. Thoenen, W. Hummel, U.

233   Berner, E. Curti, 2014) (this database includes gaseous and aqueous species as well as the

234   thermodynamic values for calcite and aragonite). Furthermore, C-S-H (the CNASH model

235   developed by Myers et al. (Myers et al., 2014)), lime, portlandite, sodium oxide and

236   amorphous silica from the Cemdata18 database (Lothenbach et al., 2019) were included.

237   Moreover, several sodium-calcium carbonates which might form in such systems as

238   summarized in Table 2 were included. The activity coefficients of the aqueous species were

239   calculated using the Truesdell-Jones extension to the Debye-Hückel equation:

240
$$log_{10}\gamma_i = \frac{-A_\gamma z_i^2 \sqrt{I}}{1 + \dot{a}B_\gamma \sqrt{I}} + b_\gamma I + log_{10} \frac{X_{jw}}{X_w}$$

241   where γ_i equals to the activity coefficient, z_i is the charge of the ith species, A_γ and B_γ are

242   temperature- and pressure-dependent coefficients, I is the effective molal ionic strength, X_{jw}

243   the molar quantity of water and X_w the total molar amount of the aqueous phase. The

244   common ion size parameter $\dot{a}$ equals to 3.31 Å and b_γ, a short-range interaction parameter,

245   is 0.098 kg/mol, using NaOH as background electrolyte (Helgeson et al., 1981). The

246   thermodynamic calculations were performed for a temperature of 20 °C.

247

248   **Table 2.** Thermodynamic properties of the Na-Ca carbonates added to PSI-Nagra and the

249   Cemdata18 database in this study.

Phase	ΔG°f [1] (kJ mol⁻¹)	ΔH°f [2] (kJ mol⁻¹)	S° [3] (J mol⁻¹K⁻¹)	Ref
Nahcolite: $NaHCO_3$	-851.0	-951.7	92.6	(Monnin and Schott, 1984)
Natron: $Na_2CO_3 \cdot 10H_2O$	-3428.1	-4089.5	530.3	(Monnin and Schott, 1984)

	Δ_fG°[1]	Δ_fH°[2]	S°[3]	
Thermonatrite: $Na_2CO_3 \cdot H_2O$	-1285.9	-1438.8	136.5	(Monnin and Schott, 1984)
Trona: $Na_2CO_3 \cdot NaHCO_3 \cdot 2H_2O$	-2380.6	-2689.5	276.6	(Monnin and Schott, 1984)
Gaylussite: $Na_2Ca(CO_3)_2 \cdot 5H_2O$	-3372.0	-3834.0	386.7	(Königsberger et al., 1999)
Pirssonite: $Na_2Ca(CO_3)_2 \cdot 2H_2O$	-2658.1	-2955.8	239.1	(Königsberger et al., 1999)

250 [1] Gibbs free energy of formation; [2] Enthalpy of formation; [3] Entropy

251

252 ## 3. Results and discussion

253 ### 3.1. Early reaction kinetics and phase development

254 ### 3.1.1. Calorimetry, in-situ XRD and pH

255 The reaction kinetics within the first days of reaction as studied with isothermal conduction

256 calorimetry are shown in Fig. 1. The results show that the reaction is exothermic for all

257 samples. The first peak, which occurs within the first few minutes after liquid and solid come

258 into contact, is mainly attributed to the external mixing of the samples and the initial wetting

259 and dissolution of the reactive phase. This is followed by a deceleration whose rate is

260 different for each sample. Thereafter, a second exothermic peak is observed for A-SIC, C-

261 CHEM, C-NMX, C-PK, C-GER and L-RUD, indicating a sudden reaction. For the samples C-

262 CMX and L-KAR, this peak is not observed but may appear at a later time than the duration

263 of the experiment. The time at which the second exothermic peak occurs is different for each

264 sample. The sample A-SIC with aragonite shows this second calorimetric peak in a medium

265 period, which indicates that the modification of calcium carbonate has no significant effect on

266 the time of the second exothermic event.

267

268 The possible reasons for different reaction kinetics could be, for example, the specific

269 surface areas, particle size distributions or mineralogical impurities in the raw samples.

270 Based on the literature, reduction in particle size or increase in specific surface area tends to

271 increase the dissolution of the reactive phases (Tenoutasse, 1967; Minard et al., 2007;

272   Firdous et al., 2018a; Joseph et al., 2019; Moukannaa et al., 2019). Whereas the presence

273   of mineralogical impurities can impact the reactions in several ways (Kumar et al., 2010); for

274   example, the presence of aluminate can slow down the dissolution of silicates under alkaline

275   conditions (Snellings, 2013). Considering the particle size distribution of the samples (Fig.

276   S1), they can be classified into three groups according to their bimodal particle size

277   distribution curves (Fig. S1); also, the values for d_{50} and d_{90} (Table 1) as well as the Blaine

278   fineness vary between the samples. However, a closer look on these differences in particle

279   size distribution and connected parameters shows that the time of appearance of the second

280   exothermic event does not clearly correlate with particle size distribution presented in Fig.

281   S1.

282

283   The presence of minerals other than calcium carbonate in the samples could also have an

284   impact. Presence of dolomite seems not to influence the time of the second calorimetric

285   peak, as C-GER has the peak relatively early, but L-KAR does not show any peak in the

286   time of observation. Quartz could play a role, as both limestone samples, which contain

287   quartz, show the peak late or not at all. On the other hand, samples which contain only

288   calcite or aragonite (C-CHEM, C-PK, A-SIC and C-NMX) develop the second thermal event

289   early (approx. 6 h), at a medium time (approx. 56 h) or not within the time of observation (like

290   C-CMX), which seems to indicate that the impact of both quartz and dolomite is negligible.

291

292   The presence of minor amounts of $Ca(OH)_2$ or CaO could be the reason for the early peak of

293   C-CHEM, as Bertram and Klimm (Bertram and Klimm, 2004) found that commercial $CaCO_3$

294   may also contain traces of CaO, which forms $Ca(OH)_2$ in the presence of water. For the

295   natural samples, it is less likely that they initially contain CaO or $Ca(OH)_2$. Although traces of

296    $Ca(OH)_2$ can also be formed from the reaction of $CaCO_3$ with NaOH: $CaCO_3 + 2Na^+ + 2OH^-$

297    $\rightarrow Ca(OH)_2 + 2Na^+ + CO_3^{2-}$ in the alkaline environment. This reaction can take place,

298 especially if the reaction of the calcium source is faster than the formation of C-S-H (Bergold

299 et al., 2013, 2015). However, it should be noted that $Ca(OH)_2$ is not observed by XRD as

300 described below; therefore, this is also a less likely possibility.
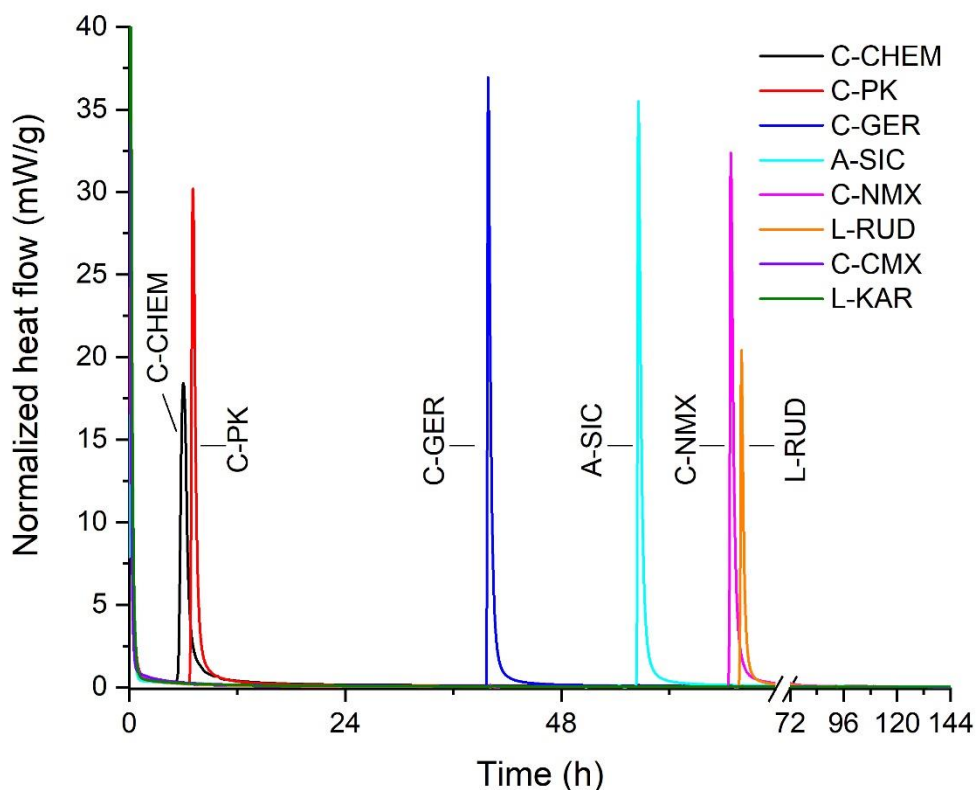
301

302

303 **Fig. 1.** Comparison of the calorimetric signals of all examined calcium carbonate samples.

304 The samples in the legend are sorted according to the time of appearance of the second

305 thermal event. The last two samples (C-CMX and L-KAR) do not show a second thermal

306 event within 144 h.

307

308 It can be said that the observed reaction kinetics are the combined results of several factors,

309 which may include the aforementioned criteria, but no strong correlation to the here

310 described factor can be proven. To understand the reaction occurring during the second

311 exothermic peak, in-situ XRD was conducted on C-CHEM and C-PK, as these sample

312 exhibit the peak at the earliest. Fig. 2 presents the correlation between in-situ XRD, heat flow

313   and pH value (of solutions from leached samples) measured over time for C-CHEM.

314   Whereas the results of C-PK are presented in Fig. S3 of supplementary material. This

315   makes it possible to draw a correlation between phase development and reaction kinetics at

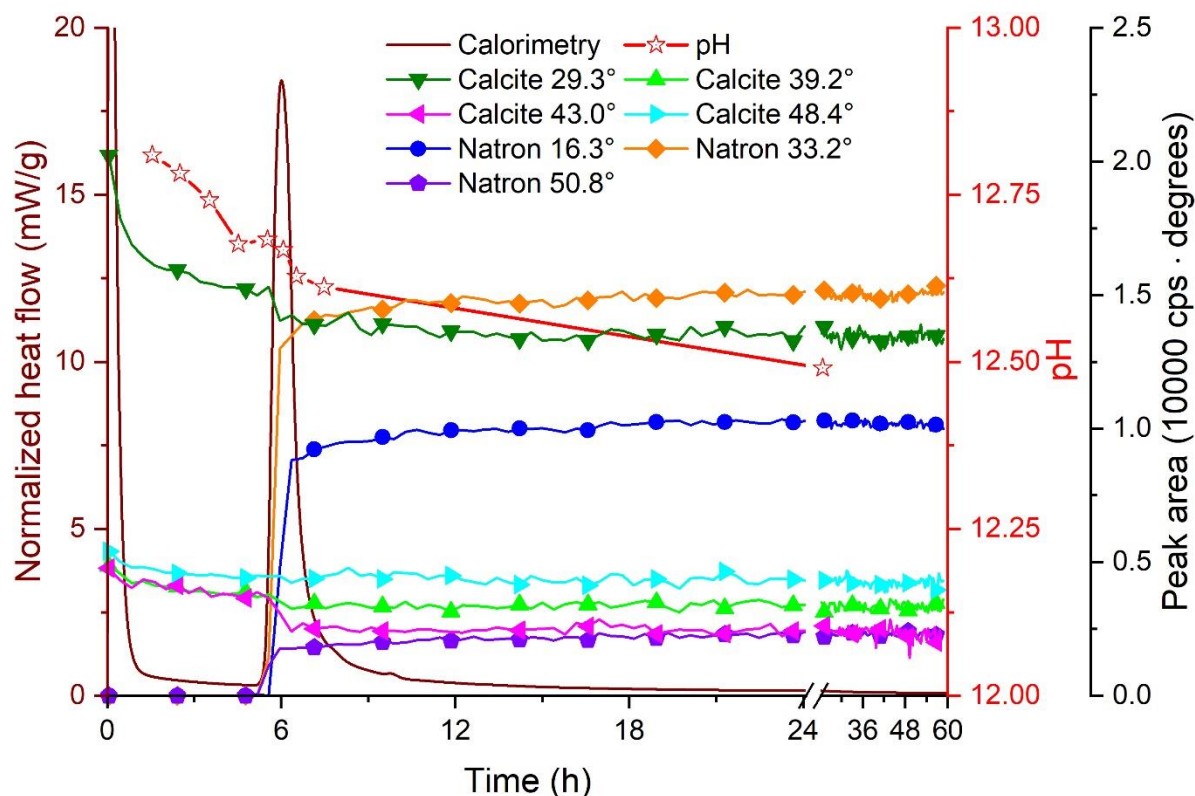316   the same time point.

317

318

319   **Fig. 2.** Comparison of the calorimetry, in-situ XRD of C-CHEM (areas of the natron-related

320   peaks at 16.3° and 33.2° are divided by 10 and 30, respectively, for better presentation) and

321   the pH value of the solution from leached samples.

322

323   The results shown in Fig. 2 and Fig. S3 indicate that during the initial calorimetric peak,

324   calcite is dissolved, as seen by the reduced peak areas of calcite at 29.3°, 39.2°, 43.0° and

325   48.4° 2θ, while no crystalline reaction products are formed within the first few hours. Until

326   approx. 5 h and 6.5 h, in sample C-CHEM and C-PK, respectively, calcite continues to

327   dissolve at a low rate, consistent with the low heat development observed in calorimetry,

328   while the pH value of the sample decreases. Note that the presented pH values refer to

329   samples suspended and leached in water so that only the trends and not the absolute pH

330   value is representative for the sample; the absolute pH value of the sample will be higher

331   than that shown in Fig 2.

332

333   At the second thermal event, where the heat release suddenly increases, the precipitation of

334   natron ($Na_2CO_3 \cdot 10H_2O$) is observed with XRD (Fig. 2 and Fig. S3), while the pH value of the

335   sample increases slightly due to the reaction $2NaOH + CaCO_3 + 10H_2O \rightarrow Na_2CO_3 \cdot 10H_2O +$

336    $Ca^{2+} + 2OH^-$. Thus, the second exothermic event is due to the formation of natron and/or the

337   formation of poorly crystalline C-S-H, which is better visible with the FTIR and the thermal

338   analysis discussed below. The formation of C-S-H and natron at the time of this sudden heat

339   release indicates that the nucleation of C-S-H could be the decisive factor for the observed

340   sudden heat release as well as for the largely different kinetics. This is similar to Portland

341   cements, where the nucleation of C-S-H has been observed to be the decisive factor for the

342   acceleration of the alite reaction after the "dormant" period (Scrivener et al., 2015; Scrivener

343   et al., 2019). Furthermore, it is to notice that both samples (C-CHEM and C-PK) exhibit

344   similar reactions in in-situ XRD, showing that both natural and chemical sources of calcium

345   carbonate behave comparable under the applied conditions.

346

347   **3.1.2. In-situ FTIR**

348   In-situ Fourier transform infrared spectroscopy (FTIR) was performed on C-PK and C-CHEM

349   during their reaction with sodium silicate solution. These samples were chosen such that the

350   natural and synthetic calcium carbonates were tested that exhibited the second calorimetric

351   peak at the earliest time. Fig. 3 presents the infrared (IR) spectra of raw materials (C-CHEM,

352   sodium silicate solution) and selected data from the in-situ FTIR of their reaction. The in-situ

353   FTIR results of C-PK, together with raw samples, are presented in Fig. S4 of the

354   supplementary material. A summary of the bands observed in the sodium silicate solution

355   and calcium carbonate is presented in Table 3. The infrared spectrum of sodium silicate

356   solution (SoSi) showed the main silicate network group signals in the range of 1200 – 400

357   cm^{-1} (Roggendorf et al., 1996). The broad band from 3700 – 2400 cm^{-1} indicates the

358   existence of more than one type of hydrogen bonding with different bonding energies and

359   different structural surroundings (Roggendorf et al., 1996).

360

361   **Table 3.** Summary of bands observed in sodium silicate solution and calcium carbonate.

Wavenumber (cm^{-1})	Assignment	Ref
Sodium silicate solution		
425, 550	Si-O-Si deformation vibrations	(Bobrowski et al., 2012)
890	Si-O stretching vibration of Q^1	(Bobrowski et al., 2012)
750, 810, 966	Si-O-Si vibrations	(Roggendorf et al., 1996)
1640	H_2O deformation vibration	(Roggendorf et al., 1996; Bobrowski et al., 2012)
2400 – 2100	Hydrogen bridge bonds between $Si(OH)_4$ tetrahedra and a silicate network	(Roggendorf et al., 1996; Bobrowski et al., 2012)
3700 – 2400	OH group stretching vibration	(Roggendorf et al., 1996)
Calcium carbonate		
713	Out-of-plane bending vibration of CO_3^{2-}	(Fernández-Carrasco et al., 2012)
873	Split-in-plane bending vibration of CO_3^{2-}	(Fernández-Carrasco et al., 2012)
1424	Asymmetric stretching vibration of CO_3^{2-}	(Fernández-Carrasco et al., 2012)

362

363   As a result of the reaction between calcium carbonate and sodium silicate solution, the OH

364   bands present in sodium silicate solution (3700 – 2400 cm^{-1}) decrease, while the band

365   corresponding to the vibration of hydrogen bridges between $Si(OH)_4$ tetrahedra and a silicate

366   network (2400 – 2100 cm^{-1}) becomes more prominent, showing that the silicate is

367   incorporated in a polymerized (possibly solid) phase. The signal of water molecules

368   observed at 1640 cm^{-1} remains unchanged. The carbonate band of the precursor at 1424

369   cm^{-1} initially moved its centre to 1396 cm^{-1}, indicating the liberation of CO_3^{2-} into the solution

370   (Griffin et al., 2014). Later on, the centre shifts to 1370 cm^{-1}, which can be an indicator of the

371   formation of natron (Kiefer et al., 2018). The time of natron formation in in-situ FTIR is earlier

372   compared to calorimetry and in-situ XRD. This is likely because calorimetry and in-situ XRD

373   were performed at 20 °C, whereas in-situ FTIR was not equipped with a temperature

374   controlling unit. Thus, the temperature during in-situ FTIR measurement was above 20 °C

375   and therefore the reactions are likely faster. The CO_3^{2-} split-in-plane bending visible at 873

376   cm^{-1} is not only characteristic for calcite but can also be due to natron. However, the 713 cm^{-1}

377   band is characteristic for calcite, thus showing that unreacted calcite is still present.
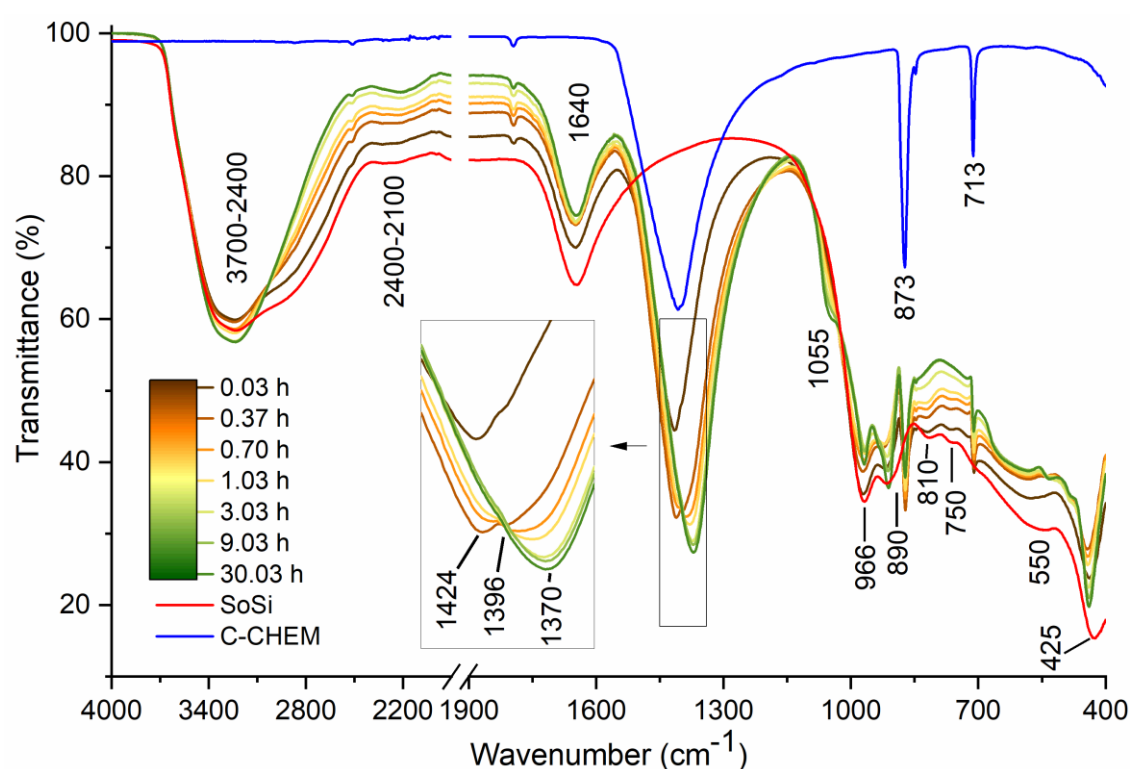
378

Fig. 3. IR spectra of C-CHEM, sodium silicate solution (SoSi) and in-situ data from their
reaction labelled with the time in h.

382

383   The changes in the main silicate network range can be observed by the formation of a new

384   band at 1055 cm^{-1}, which is interpreted by Yu et al. (Yu et al., 1999) as a Si-O stretching

385 vibration of Q^2 in C-S-H. The band present at 966 cm^{-1} is sharpening, which can be due to a

386 Si-O asymmetric stretching vibration in Q^2 (García Lodeiro et al., 2009). The peak at 890 cm$^-$

387 ^{1} is superimposed by the formation of a new peak. The small changes observed in the region

388 of 600 – 400 cm^{-1} are likely due to SiO_4 deformation vibrations (Yu et al., 1999). These

389 results tentatively indicate that the silicate from the sodium silicate solution partially reacts to

390 C-S-H. This finding is studied further in the followings sections.

391

392 **3.2. Later age reaction and reaction products**

393 **3.2.1. Powder XRD**

394 Fig. 4 presents the XRD of raw samples compared to 8 and 90 d reacted samples of C-

395 CHEM, C-NMX, C-GER and A-SIC; the samples C-PK, C-CMX, L-RUD and L-KAR are

396 presented in Fig. S5 of the supplementary material. The comparison of the raw samples with

397 the reacted samples shows changes in the crystalline and amorphous phases. In all the

398 reacted samples, calcite is partially dissolved, as indicated by the reduction of the calcite

399 peak areas (Fig. 4 A, B, C and Fig. S5 A, B, C, D), which is in agreement with the

400 observations from in-situ XRD described in section 3.1.1. The most prominent new

401 crystalline phase formed in all reacted samples after 8 and 90 d is thermonatrite

402 ($Na_2CO_3 \cdot H_2O$).

403

404 Additionally, in all calcite samples, the background is slightly increased around 29.5° 2θ at 8

405 and 90 d, indicating the formation of a poorly crystalline phase such as C-S-H, which likely

406 also contains some amount of sodium as suggested by (Firdous and Stephan, 2019b;

407 Ortega-Zavala et al., 2019) and is shown here later by thermodynamic calculations. Also, the

408 main calcite peak at 29.4° 2θ in the reacted samples is broadening at the base, which may

409 indicate structural disorder on the surface of calcite grains in the used alkaline conditions or

410 the formation of a poorly crystalline phase. The quantification by Rietveld refinement of the

411   sample C-CHEM at 8 d shows that this sample contains 44.6 wt.-% calcium carbonate, 8.9

412   wt.-% thermonatrite and 46.5 wt.-% X-ray amorphous content. In comparison, the

413   composition of sample C-CHEM at 90 d is found to be 40.0 wt.-% calcium carbonate, 9.2

414   wt.-% thermonatrite and 50.7 wt.-% X-ray amorphous content. Comparing these values with

415   the composition of the sample at the time of mixing (53.3 wt.-% calcium carbonate, 46.7 wt.-

416   % sodium silicate solution), a time-dependent reduction in the calcium carbonate content, as

417   well as increases of the shares of the X-ray amorphous phase and thermonatrite content,

418   can be seen.

419

420   The peak areas of aragonite in A-SIC are also decreasing (Fig. 4D), showing that aragonite

421   also participates in the reaction. Comparable to the calcite samples, the new crystalline

422   reaction products observed in the reacted A-SIC also include thermonatrite. Additionally, in

423   A-SIC (Fig. 4D), a broad peak at around 29.5° 2θ is visible, which could indicate the

424   formation of low Ca/Si C-S-H (Grangeon et al., 2016; L'Hôpital et al., 2016). The observation

425   of C-S-H in these samples is consistent with the observation by in-situ FTIR (Fig. 3). This

426   shows that aragonite also partially dissolves in the used alkaline system and behaves

427   comparably to calcite irrespective of its crystal structure. The XRD of C-GER (Fig. 4C)

428   shows that the minor phase dolomite also participates strongly in the reaction.
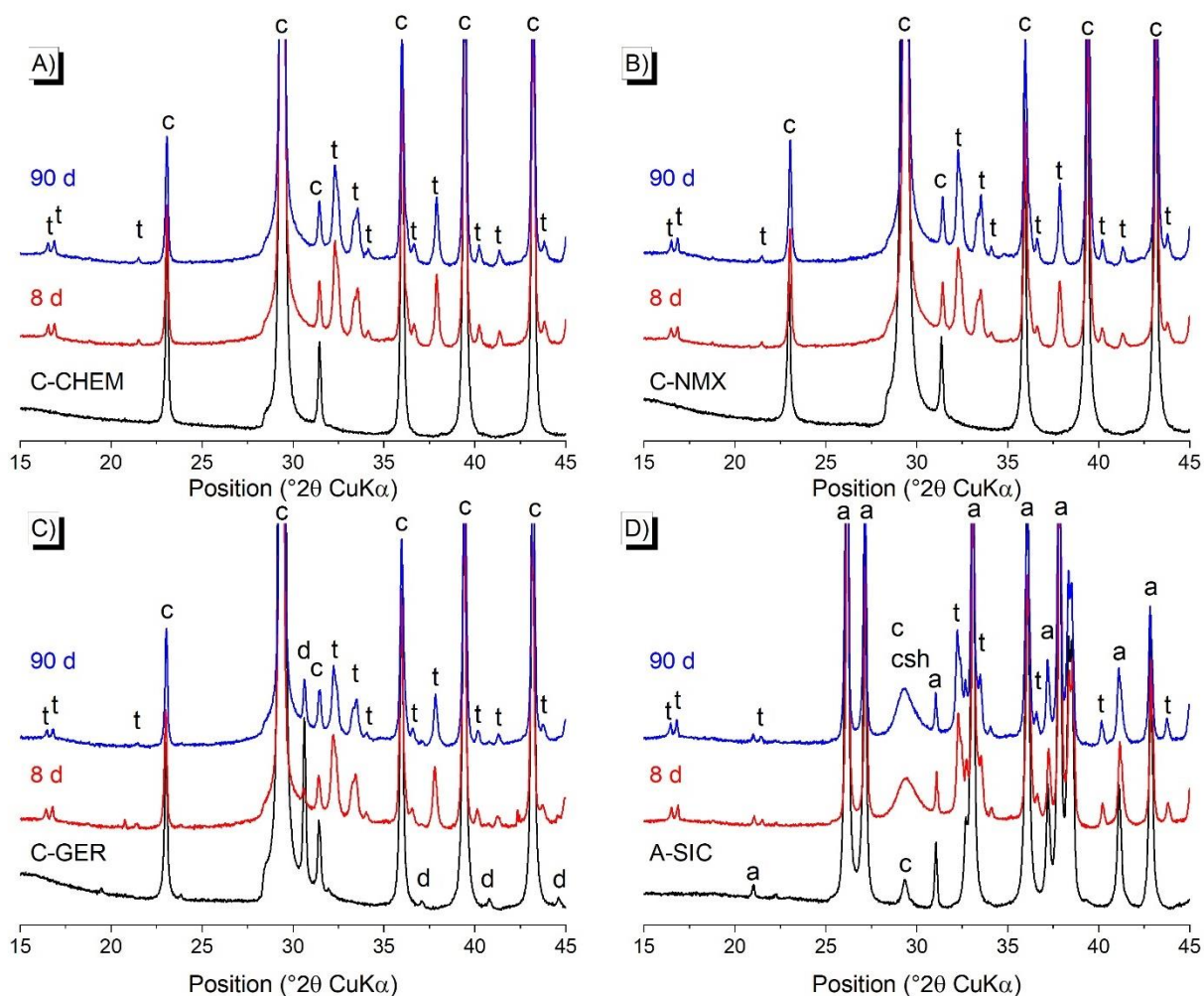
429

430

Fig. 4. Powder XRD of raw samples, 8 and 90 d reacted samples for A) C-CHEM, B) C-

NMX, C) C-GER and D) A-SIC. Symbols in the figure are c: calcite, t: thermonatrite, d:

dolomite, a: aragonite and csh: C-S-H.

434

It should be noted that at early reaction time (up to 59 h) only the formation of natron was

observed by in-situ XRD, while at later ages (8 and 90 d), thermonatrite was visible with the

powder XRD, indicating a replacement of natron ($Na_2CO_3 \cdot 10H_2O$) by thermonatrite

($Na_2CO_3 \cdot H_2O$), possibly because of kinetics reasons.

439

440

3.2.2. Thermal analysis and mass spectrometry

To obtain a deeper insight into the reaction products formed after 90 d of reaction, simultaneous thermal analyses using DSC-TGA (Fig. 5) and TGA-MS (Fig. 6) were performed. As a higher sample mass should be used in TGA-MS, the thermal events and the associated gas liberations can be slightly shifted to higher temperatures. Nevertheless, as during both MS and DSC also TGA was performed. Therefore, the signals of DSC and MS can be compared using their respective TGA signals.

Before the examination with DSC-TGA and TGA-MS, the powdered sample was freeze-dried to remove the water contained in thermonatrite, which resulted in the conversion of thermonatrite ($Na_2CO_3 \cdot H_2O$) to natrite (Na_2CO_3). This dehydration of thermonatrite eliminates the only crystalline phase in the sample, which contains water (see section 3.2.1.) and thus facilitates the identification of water contained in non-crystalline phases using TGA and MS.

In Fig. 5, the first mass loss of the TGA combined with the DSC occurs immediately at the beginning of heating and is associated with an endothermic signal. The TGA signal of TGA-MS (Fig. 5 and Fig. 6) shows this mass loss at a slightly higher temperature due to the higher sample mass used. The MS shows mainly signals of OH and H_2O for this mass loss (Fig. 6), indicating water released from non-crystalline phases, which can be expected to be C-S-H (Ben Haha et al., 2011).

The next mass losses occur between approximately 400 – 700 °C and 700 – 775 °C (Fig. 5). Likewise, DSC shows a slight bending for the first gentle mass loss (400 – 700 °C) and a sharp, intense signal for the mass loss between 700 – 775 °C. For both events, MS reveals

466   separate signals of C, O, CO and CO_2. This indicates the liberation of carbon dioxide from at

467   least two different phases in the samples. The first mass loss (400 – 700 °C) is likely due to

468   a carbonate-containing reaction product. It is unlikely that this decarbonation is from natrite,

469   as its decomposition temperature given in the literature is above 1200 °C (Kim and Lee,

470   2001). The large mass loss between approximately 700 – 775 °C combined with sharp DSC

471   and MS signals originates from the CO_2 emitted from the unreacted calcite in the sample.

472

473   In DSC at approximately 850 °C, a small but sharp endothermic signal is visible, which could

474   indicate a solid-to-solid phase transition or a melting process. A likely phase is natrite

475   (Na_2CO_3), whose melting temperature is reported to be 850 °C (Kim and Lee, 2001). This

476   DSC peak is superimposed by a broader endothermic peak which stretches from 800 – 950

477   °C and is accompanied by an equivalent mass loss in TGA (Fig. 5). Furthermore, it is

478   accompanied by the detection of H_2, CO and some other carbon and oxygen species in MS

479   (Fig. 6). The signal of CO and other carbon species does not necessarily indicate carbon

480   dioxide liberation, as at this high temperature the liberated gases react with the carbon of the

481   skimmer of the MS device. The detection of H_2 indicates water liberation from the sample,

482   which is converted to H_2 and carbon species (C, CO, CO_2) in contact with the carbon-

483   containing skimmer. The endothermic peak from 800 – 950 °C and the water liberation could

484   be from the destabilisation of C-S-H into wollastonite ($CaSiO_3$) and SiO_2, as previously

485   observed by (Myers et al., 2015; Tajuelo Rodriguez et al., 2017) in this temperature range.
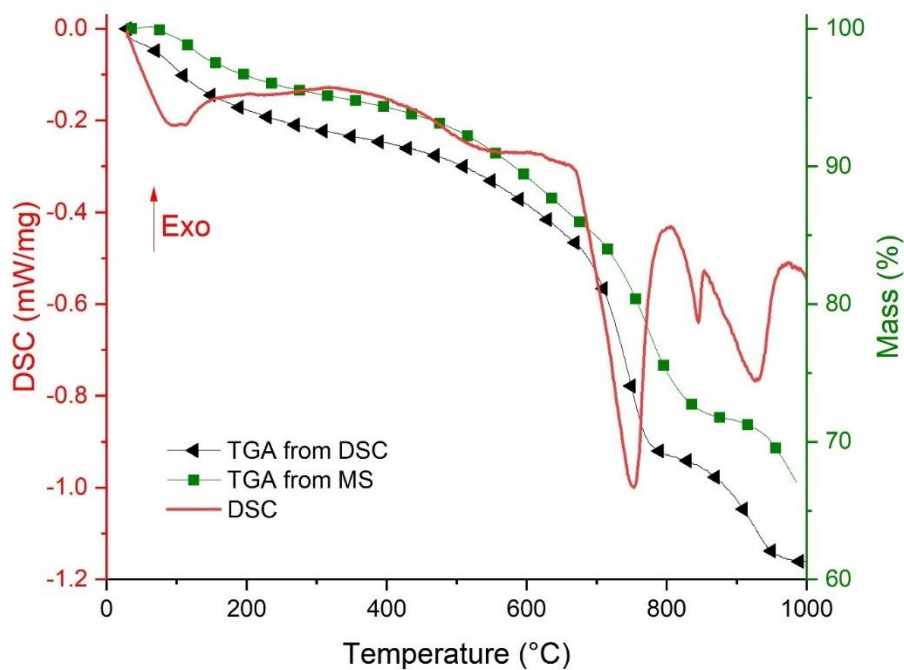
486

Fig. 5. Both signals of DSC-TGA and the TGA signal of TGA-MS. The backgrounds of all measurements were subtracted.
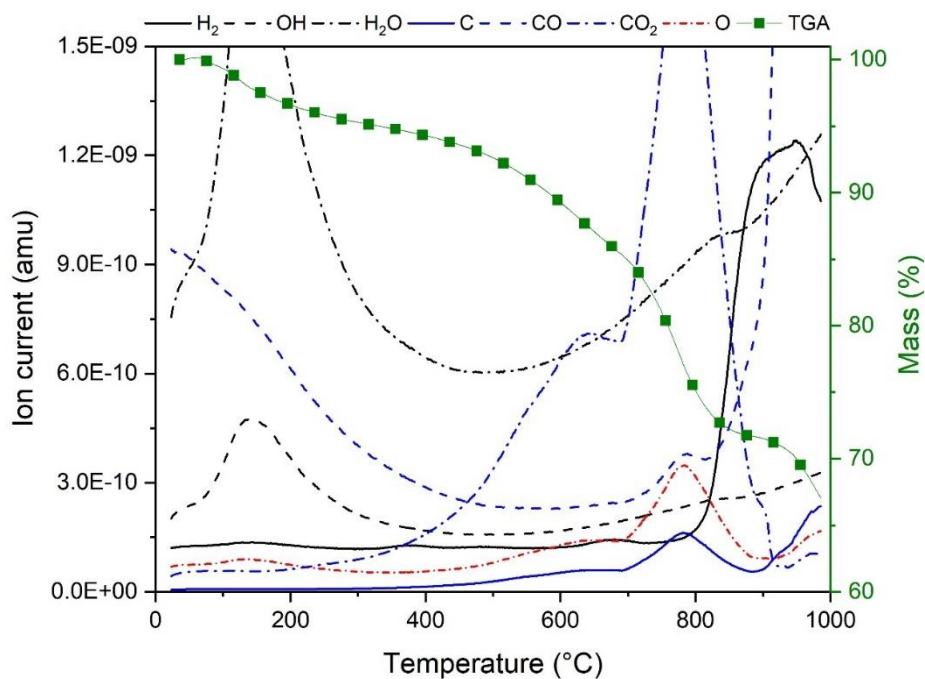

Fig. 6. Background corrected thermogravimetric signal and related mass spectrometry of gases emitted by the sample (TGA-MS). This TGA curve is also shown in Fig. 5 for better comparison.

3.2.3. Scanning electron microscopy

Scanning electron microscopy was performed on C-CHEM and C-PK samples of 8 d age

and is presented in Fig. 7. The samples are characterized by a heterogeneous morphology.

In Fig. 7A, mainly irregular small particles can be recognized (labelled as 1 in Fig. 7A),

representing one of the reaction products, possibly the C-S-H. Furthermore, bigger, mainly

smooth, and more angular particles can be observed in some places (labelled as 2 in Fig.

7A). These are likely partially reacted calcite particles. The sample of C-PK shows similar

characteristics. For Fig. 7B, a particular part of the sample was chosen, which allows to

recognize further details. Especially the right half of the micrograph shows the same

unregular (labelled as 1 in Fig. 7B) and bigger angular particles. Additionally, in the centre a

large angular particle (labelled as 3 in Fig. 7B), whose outer shape and step-like surface

structure likely arise from the very good cleavage of calcite. Furthermore, on its right side,

the particle exhibits an elongated depression (labelled as 4 in Fig. 7B), which is filled with the

irregular reaction product. Down-left from this particle, another grain with an intensely

perforated surface can be seen (labelled as 5 in Fig. 7B). In this way, the SEM results

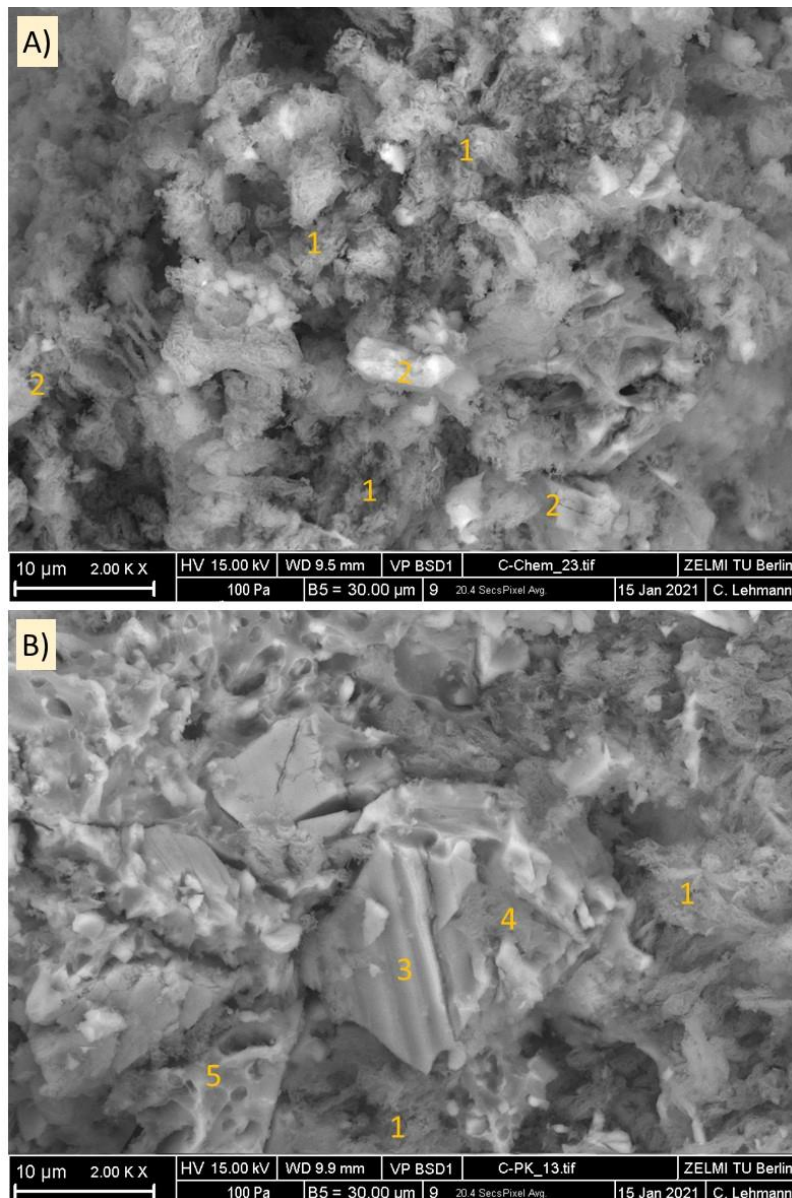confirm the participation of calcite in the reaction and formation of the reaction products.

Fig. 7. Scanning electron microscope images of 8 d old A) C-CHEM and B) C-PK samples.

3.2.4. Thermodynamic modelling

Fig. 8 presents a thermodynamic model in which calcite was reacted with a sodium silicate

solution as in the experiments. The calculation shows the effect of the amount of calcite

participating in the reaction on the hydrates to expect, which mimics the progressive calcite

reaction observed in the experiments. The calculated thermodynamic model gives an insight

into the mechanisms and possible phases that form in the equilibrium state.

522

523 The calculations indicate that Na-containing C-S-H is already expected to form at a low-

524 reacting amount of calcite, as the CNASH solid solution model of (Myers et al., 2014;

525 Lothenbach et al., 2019) predicts a high content of the theoretical end-member INFCN

526 (chemical composition $(CaO)_1(Na_2O)_{0.3125}(SiO_2)_{1.5}(H_2O)_{1.1875}$). These findings coincide with

527 the results of simultaneous thermal analysis (TGA-DSC and TGA-MS). Furthermore, in-situ

528 FTIR showed the formation of C-S-H by the appearance of the band at 1055 cm^{-1} (Fig. 3).

529 Additionally, thermonatrite is predicted to precipitate next to C-S-H. With increasing reaction

530 degree of calcite, the amount of C-S-H increases and thermonatrite ($Na_2CO_3 \cdot H_2O$) is

531 replaced by natron ($Na_2CO_3 \cdot 10H_2O$) (Fig. 8). Thermodynamic calculations indicate the

532 thermodynamically stable phases (end products) and do not necessarily reflect intermediate

533 states during the reaction, while the experimental results also show the intermediate states

534 during the reaction. The prediction of thermonatrite and natron by thermodynamics (Fig. 8)

535 supports the findings of in-situ and powder XRD (Fig. 2, Fig. 4), though the experimental

536 results show that first natron and then thermonatrite is formed. The thermodynamic

537 modelling (Fig. 8) indicates that the predicted stabilities of natron and thermonatrite are quite

538 comparable in these solutions containing high concentrations of Na and carbonate, such that

539 either a small difference in the kinetics of formation and/or errors in the used thermodynamic

540 data could affect the result. If both solids are oversaturated to a similar degree in the original

541 solution, their formation depends mainly on the nucleation kinetics.

542

543 With the further rise in calcite dissolution, the precipitation of gaylussite is predicted.

544 Gaylussite has been observed in the carbonation / efflorescence formation of geopolymers

545 (Bernal et al., 2012; Walling et al., 2018) but was not observed in the current experiments.

546 Furthermore, the model predicts that in maximum, approximately 34 wt.-% of the calcite

547 could participate in the reaction. This is in agreement with experimental XRD results, which

548 showed an only partial reaction of calcite up to 90 days. However, the XRD of samples with

549 an age of up to 90 d reveal thermonatrite as the only sodium-containing carbonate, while no

550 natron and gaylussite are observed, which could indicate a kinetic limitation of their

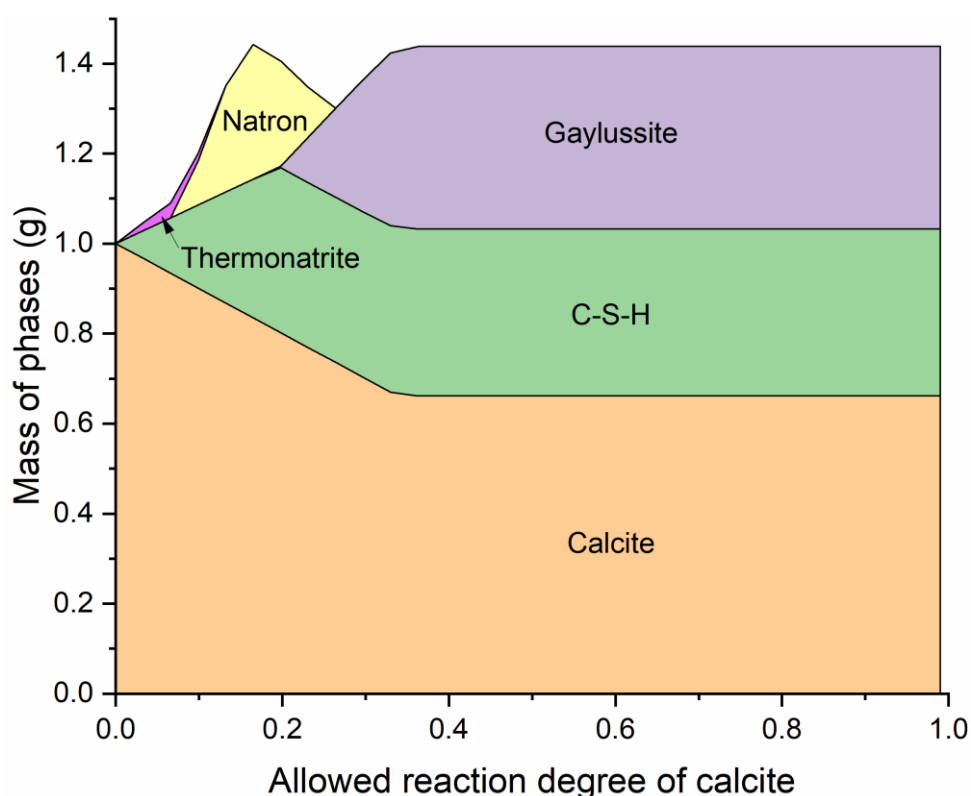551 formation or a limited reaction of calcite.

552

553

554 **Fig. 8.** Thermodynamic model of the reaction of calcite with sodium silicate solution. Results

555 shown for an increasing degree of calcite reaction plotted against the overall mass of phases

556 formed.

557

558 To account for the possible errors in the thermodynamic data used (Table 2), the sensitivity

559 of the predictions of the thermodynamic modelling on changes in the Gibbs free energy is

560 examined. The values of the thermodynamic quantities of the sodium and calcium-sodium

561 carbonate hydrates in Table 2 vary slightly between different publications (Monnin and

562 Schott, 1984; Woods and Garrels, 1987; Robie and Hemingway, 1995; Königsberger et al.,

563 1999; Krupka et al., 2010). These differences are equivalent to variations of the solubility

564   products by approximately ± 0.5 log units or a change of the Gibbs free energy (G°) by ±

565   2.85 kJ/mol.

566

567   The thermodynamic model in Fig. 8 predicted the formation of thermonatrite, natron and

568   gaylussite depending on the degree of calcite reaction. The Gibbs free energies of these

569   three phases were systematically varied (Table S2) by ± 2.85 kJ/mol and the alteration of the

570   Gibbs free energy can influence which phases form at which degree of reaction.

571

572   The formation of thermonatrite is only suppressed in the case of an increase of the Gibbs

573   free energy of thermonatrite (G° + 2.85 kJ/mol), which corresponds to a significant

574   destabilization of this phase. The increase of G° of gaylussite and especially natron can

575   substantially decrease the range of degree of reaction in which thermonatrite forms but

576   complete disappearance of thermonatrite is not predicted. When the G° of natron is

577   increased, the range of thermonatrite formation substantially increases. These results are in

578   good agreement with the XRD results for 8 and 90 d showing the formation of thermonatrite

579   only. The increase of G° of gaylussite leads to its replacement by pirssonite. The order in

580   which the phases form depending on the degree of reaction of calcite is not affected by any

581   applied changes to G°. The general order regarding the increasing degree of reaction is

582   thermonatrite → natron → gaylussite/pirssonite (but not all of these phases appear in all

583   cases).

584

585   **3.2.5. Role of calcite reaction in geopolymerization**

586   A clear second exothermic peak has been observed for natural pozzolan reacted with

587   sodium silicate solution in a calorimetric study (Firdous and Stephan, 2019a), although no

588   precise interpretation of this event could be offered. Combining those observations (Firdous

589   and Stephan, 2019a) with the findings of the present study, the second exothermic peak can

590   be assigned to the reaction of the calcite present in that natural pozzolan with the sodium

591   silicate solution.

592

593   The formation of thermonatrite in alkali-activated / geopolymer systems has been reported

594   before where the reaction of alkalis with CO_2 from air resulted in the formation of

595   efflorescence products or carbonation (Bernal et al., 2012; Firdous and Stephan, 2019a,

596   2019b). The present study shows that thermonatrite in alkali-activated samples can also

597   form due to the reaction of calcium carbonate with a sodium silicate solution. Such a reaction

598   of calcium carbonate in alkali-activated systems can supply Ca^{2+} for the formation of C-S-H

599   as observed in the present study. The Na^+ ions remaining in the solution can potentially

600   react with the CO_3^{2-} provided by the calcium carbonate and water to form thermonatrite. The

601   growth of thermonatrite within the structure of an already hardened binder can potentially

602   cause inner crystallization pressure, weakening the structure and reducing mechanical

603   strength of the samples as reported by (Zhang et al., 2014; Firdous and Stephan, 2020).

604   Therefore, a reaction of calcium carbonate with sodium silicate solution can contribute to a

605   similar effect. The schematic diagram shown in Fig. 9 presents the general reaction

606   mechanism and its impact in alkali-activated binder based on the findings of (Zhang et al.,

607   2014; Firdous and Stephan, 2020) and the current study. An increase of the inner

608   crystallization pressure beyond the tensile strength of the sample can lead to a disintegration

609   of the sample (Firdous and Stephan, 2020). The results of the current study provide a

610   potential reason for the experimentally observed lower performance of calcium carbonate-

611   containing pozzolans in alkali-activated / geopolymer systems.
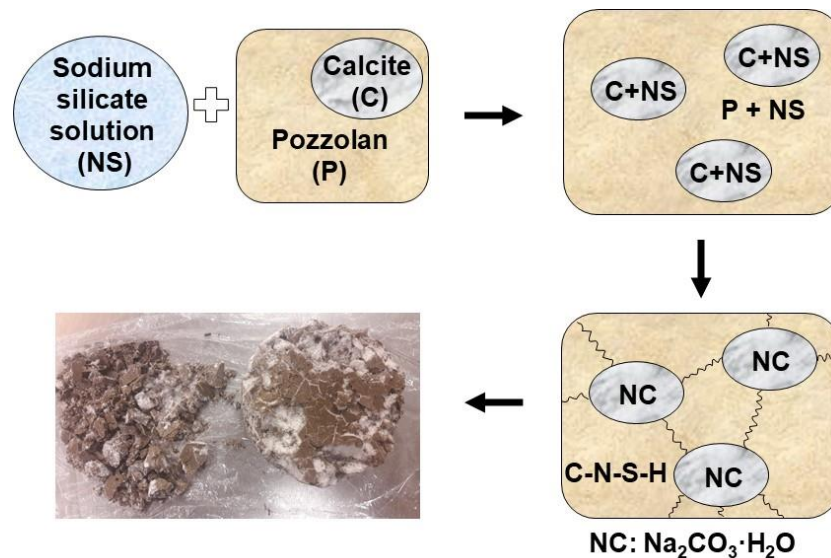
612

Fig. 9. Schematic representation of the damaging mechanism of an alkali-activated pozzolan by the formation of sodium carbonate hydrate. The photograph shows samples of an alkali-activated binder ripped in pieces by the growth of sodium carbonate hydrate (sample BT-1.272 of study (Firdous and Stephan, 2020).

4. Conclusions

The use of natural resources such as natural and other pozzolans or materials from mine tailings for the production of alternative binders such as geopolymers/alkali-activated binders is an environmentally friendly solution and leads to a sustainable development. The natural raw materials or natural pozzolans comprise of several mineralogical phases often including calcium carbonates and these mineralogical phases define their reactivity. The current study evaluates the early reaction of calcium carbonate with sodium silicate solution and the role of this reaction in geopolymer/alkali-activated binders. It can be concluded that calcium carbonate in the polymorphs calcite and aragonite is not inert under alkaline conditions. Calcium carbonate acts partially as a filler and partially as a reactive phase in alkali-activated systems. The reaction with sodium silicate solution results in the formation of C-S-H, which likely contains some sodium. The reaction starts with the dissolution of calcium carbonate

631 and a delayed formation of natron as the first crystalline precipitate. Later, thermonatrite is

632 found instead of natron, which is perhaps due to kinetic reasons. A sharp second exothermic

633 event observed in calorimetry is connected to natron precipitation as seen in XRD. The

634 formation of C-S-H was observed by FTIR and exhaust gas analysis in mass spectrometry.

635 C-S-H nucleation could be the decisive factor for the sudden heat release observed at the

636 time of natron formation. Thermodynamic calculations showed that upon the reaction of

637 calcite in sodium silicate solution, the formation of C-S-H (incorporating sodium) and in

638 dependency of the degree of reaction different sodium-containing carbonates can be

639 expected. On the one hand, the reaction of calcium carbonate with sodium silicate solution

640 resulted in the formation of sodium-containing calcium silicate hydrate and on the other hand

641 it resulted in the formation of thermonatrite. Such growth of thermonatrite within the binder

642 gel depleted the alkali-activated binder in water and cations for further progress of the

643 reaction. Its precipitation within the hardened binder can result in the generation of inner

644 crystallization pressure, which when exceeding the tensile strength of the binder can result in

645 the collapse of the sample. Therefore, the findings of this study are directly related to the

646 understanding of the use of several types of pozzolans for the alkali-activated binders.

647

648 **Acknowledgements**

653

654 **Conflict of Interest**

655 The authors declare that they have no conflicts of interest.

656

Appendix A

Supplementary material

References

Ben Haha, M., Le Saout, G., Winnefeld, F. and Lothenbach, B., Influence of activator type on hydration kinetics, hydrate assemblage and microstructural development of alkali activated blast-furnace slags. Cem. Concr. Res., 2011, 41 (3), 301–310. doi:10.1016/j.cemconres.2010.11.016.

Bergold, S.T., Goetz-Neunhoeffer, F. and Neubauer, J., Quantitative analysis of C–S–H in hydrating alite pastes by in-situ XRD. Cem. Concr. Res., 2013, 53 (5), 119–126. doi:10.1016/j.cemconres.2013.06.001.

Bergold, S.T., Goetz-Neunhoeffer, F. and Neubauer, J., Mechanically activated alite: New insights into alite hydration. Cem. Concr. Res., 2015, 76 (1), 202–211. doi:10.1016/j.cemconres.2015.06.005.

Bernal, S.A., Provis, J.L., Brice, D.G., Kilcullen, A., Duxson, P. and van Deventer, J.S.J., Accelerated carbonation testing of alkali-activated binders significantly underestimates service life: The role of pore solution chemistry. Cem. Concr. Res., 2012, 42 (10), 1317–1326. doi:10.1016/j.cemconres.2012.07.002.

Bertram, R. and Klimm, D., Assay measurements of oxide materials by thermogravimetry and ICP-OES. Thermochim. Acta, 2004, 419 (1-2), 189–193. doi:10.1016/j.tca.2004.03.003.

678 Bobrowski, A., Kmita, A., Starowicz, M., Hutera, B. and Stypuła, B., Effect of Magnesium

679 Oxide Nanoparticles on Water Glass Structure. Arch. Foundry Eng., 2012, 12 (3), 9–12.

680 doi:10.2478/v10266-012-0073-2.

681 Bondar, D., Lynsdale, C.J., Milestone, N.B., Hassani, N. and Ramezanianpour, A.A., Effect

682 of heat treatment on reactivity-strength of alkali-activated natural pozzolans. Constr.

683 Build. Mater., 2011a, 25 (10), 4065–4071. doi:10.1016/j.conbuildmat.2011.04.044.

684 Bondar, D., Lynsdale, C.J., Milestone, N.B., Hassani, N. and Ramezanianpour, A.A., Effect

685 of type, form, and dosage of activators on strength of alkali-activated natural pozzolans.

686 Cem. Concr. Compos., 2011b, 33 (2), 251–260. doi:10.1016/j.cemconcomp.2010.10.021.

687 Djobo, Y.J.N., Elimbi, A., Dika Manga, J. and Djon Li Ndjock, I.B., Partial replacement of

688 volcanic ash by bauxite and calcined oyster shell in the synthesis of volcanic ash-based

689 geopolymers. Constr. Build. Mater., 2016, 113, 673–681.

690 doi:10.1016/j.conbuildmat.2016.03.104.

691 Djon Li Ndjock, B.I., Elimbi, A. and Cyr, M., Rational utilization of volcanic ashes based on

692 factors affecting their alkaline activation. J. Non-Cryst. Solids, 2017, 463, 31–39.

693 doi:10.1016/j.jnoncrysol.2017.02.024.

694 Duxson, P., Fernández-Jiménez, A., Provis, J.L., Lukey, G.C., Palomo, A. and van Deventer,

695 J.S.J., Geopolymer technology: The current state of the art. J. Mater. Sci., 2007, 42 (9),

696 2917–2933. doi:10.1007/s10853-006-0637-z.

697 EN 196-6, *Methods of testing cement – Part 6: Determination of fineness.* CEN, Brussels,

698 2010.

699 Fernández-Carrasco, L., Torrens-Martín, D., Morales, L.M. and Martínez-Ramírez, S.,

700 Infrared spectroscopy in the analysis of building and construction materials. In *Infrared*

701 *spectroscopy – materials science, engineering and technology*, ed. T. Theophile. InTech,

702 2012, pp. 369–382.

703   Firdous, R. and Sharif, M.B., Performance of Thermally Activated Sugarcane Bagasse Ash

704   as Supplementary Cementitious Material. NED Univ. J. Res., 2016, XII (2), 23–30.

705   Firdous, R. and Stephan, D., Effect of silica modulus on the geopolymerization activity of

706   natural pozzolans. Constr. Build. Mater., 2019a, 219, 31–43.

707   doi:10.1016/j.conbuildmat.2019.05.161.

708   Firdous, R. and Stephan, D., Influence of heat treatment and mechanical activation on

709   reactivity of natural pozzolan for geopolymer synthesis. In V. Caprai, & H. J. H. Brouwers

710   (Eds.), Proceedings of 2nd International Conference of Sustainable Building Materials

711   (ICSBM 2019), Eindhoven, The Netherlands, 12 – 15 August 2019, 2019b, Vol. 2, ID

712   057, 138–155, ISBN (print):978-90-386-4911-5, Accepted/In press - 1 Nov 2019.

713   Firdous, R. and Stephan, D., Impact of the mineralogical composition of natural pozzolan on

714   properties of resultant geopolymers. J. Sustain. Cem. Mater., 2020, 176 (1), 1–16.

715   doi:10.1080/21650373.2020.1809028.

716   Firdous, R., Stephan, D. and Djobo, J.N.Y., Natural pozzolan based geopolymers: A review

717   on mechanical, microstructural and durability characteristics. Constr. Build. Mater.,

718   2018a, 190, 1251–1263. doi:10.1016/j.conbuildmat.2018.09.191.

719   Firdous, R., Stephan, D. and Jin, Y., Investigation of Rhenish and Bavarian Trass as

720   Geopolymer Precursor. 20th International Conference of Building Materials - Ibausil

721   2018, 12 – 14 September 2018, Weimar, Germany, 2018b, Book 2, 617–624.

722   Gao, X., Yu, Q.L. and Brouwers, H.J.H., Properties of alkali activated slag–fly ash blends

723   with limestone addition. Cem. Concr. Compos., 2015a, 59, 119–128.

724   doi:10.1016/j.cemconcomp.2015.01.007.

725   Gao, X., Yu, Q.L. and Brouwers, H.J.H., Reaction kinetics, gel character and strength of

726   ambient temperature cured alkali activated slag–fly ash blends. Constr. Build. Mater.,

727   2015b, 80, 105–115. doi:10.1016/j.conbuildmat.2015.01.065.

728　García Lodeiro, I., Macphee, D.E., Palomo, A. and Fernández-Jiménez, A., Effect of alkalis

729　　　on fresh C–S–H gels. FTIR analysis. Cem. Concr. Res., 2009, 39 (3), 147–153.

730　　　doi:10.1016/j.cemconres.2009.01.003.

731　Grangeon, S., Claret, F., Roosz, C., Sato, T., Gaboreau, S. and Linard, Y., Structure of

732　　　nanocrystalline calcium silicate hydrates: insights from X-ray diffraction, synchrotron X-

733　　　ray absorption and nuclear magnetic resonance. J. Appl. Cryst., 2016, 49 (3), 771–783.

734　　　doi:10.1107/S1600576716003885.

735　Griffin, D., Grover, M., Kawajiri, Y. and Rousseau, R., A methodology for monitoring

736　　　concentrations of complex waste solutions. Proceedings of the Waste Management

737　　　Conference, Phoenix, Arizona, 2-6 March 2014, 2014, 1–15.

738　Helgeson, H.C., Kirkham, D.H. and Flowers, G.C., Theoretical prediction of the

739　　　thermodynamic behavior of aqueous electrolytes by high pressures and temperatures:

740　　　IV. Calculation of activity coefficients, osmotic coefficients, and apparent molal and

741　　　standard and relative partial molal properties to 600°C and 5 kb. Am. J. Sci., 1981, 281

742　　　(10), 1249–1516. doi:10.2475/ajs.281.10.1249.

743　Herrmann, A., Koenig, A. and Dehn, F., Structural concrete based on alkali-activated

744　　　binders: Terminology, reaction mechanisms, mix designs and performance. Struct.

745　　　Concr., 2017, 130 (1-2), 213. doi:10.1002/suco.201700016.

746　Joseph, S., Skibsted, J. and Cizer, Ö., A quantitative study of the C_3A hydration. Cem.

747　　　Concr. Res., 2019, 115 (1), 145–159. doi:10.1016/j.cemconres.2018.10.017.

748　Juenger, M.C.G., Low CO_2 cement for sustainable concrete. In *Routledge Handbook of*

749　　　*Sustainable and Resilient Infrastructure*, ed. P. Gardoni. Routledge, Abingdon, Oxon,

750　　　New York, NY, 2018, pp. 377–386.

751   Kiefer, J., Stärk, A., Kiefer, A. and Glade, H., Infrared Spectroscopic Analysis of the

752   Inorganic Deposits from Water in Domestic and Technical Heat Exchangers. Energies,

753   2018, 11 (4), 798. doi:10.3390/en11040798.

754   Kim, J.-W. and Lee, H.-G., Thermal and carbothermic decomposition of Na_2CO_3 and Li_2CO_3.

755   Metall. Mater. Trans., 2001, 32B (1), 17–24. doi:10.1007/s11663-001-0003-0.

756   Komnitsas, K. and Zaharaki, D., Geopolymerisation: A review and prospects for the minerals

757   industry. Miner. Eng., 2007, 20 (14), 1261–1277. doi:10.1016/j.mineng.2007.07.011.

758   Königsberger, E., Königsberger, L.C. and Gamsjäger, H., Low-temperature thermodynamic

759   model for the system Na_2CO_3-$MgCO_3$-$CaCO_3$-H_2O. Geochim. Cosmochim. Acta, 1999,

760   63, 3105–3119.

761   Krupka, K.M., Cantrell, K.J. and McGrail, B.P., Thermodynamic data for geochemical

762   modeling of carbonate reactions associated with CO_2 sequestration – Literature Review.

763   Pacific Northwest National Laboratory Richland, Washington 99352, 2010, 135 pp.

764   Kulik, D.A., Wagner, T., Dmytrieva, S.V., Kosakowski, G., Hingerl, F.F., Chudnenko, K.V.

765   and Berner, U.R., GEM-Selektor geochemical modeling package: revised algorithm and

766   GEMS3K numerical kernel for coupled simulation codes. Comput. Geosci., 2013, 26

767   (012025), 189. doi:10.1007/s10596-012-9310-6.

768   Kumar, S., Kumar, R. and Mehrotra, S.P., Influence of granulated blast furnace slag on the

769   reaction, structure and properties of fly ash based geopolymer. J. Mater. Sci., 2010, 45

770   (3), 607–615. doi:10.1007/s10853-009-3934-5.

771   L'Hôpital, E., Lothenbach, B., Kulik, D.A. and Scrivener, K., Influence of calcium to silica

772   ratio on aluminium uptake in calcium silicate hydrate. Cem. Concr. Res., 2016, 85, 111–

773   121. doi:10.1016/j.cemconres.2016.01.014.

774   Lothenbach, B., Kulik, D.A., Matschei, T., Balonis, M., Baquerizo, L., Dilnesa, B., Miron, G.D.

775   and Myers, R.J., Cemdata18: A chemical thermodynamic database for hydrated Portland

776   cements and alkali-activated materials. Cem. Concr. Res., 2019, 115, 472–506.

777   doi:10.1016/j.cemconres.2018.04.018.

778   Lu, Z., Merkl, J.-P., Pulkin, M., Firdous, R., Wache, S. and Stephan, D., A Systematic Study

779   on Polymer-Modified Alkali-Activated Slag-Part II: From Hydration to Mechanical

780   Properties. Materials (Basel, Switzerland), 2020, 13 (15). doi:10.3390/ma13153418.

781   Minard, H., Garrault, S., Regnaud, L. and Nonat, A., Mechanisms and parameters controlling

782   the tricalcium aluminate reactivity in the presence of gypsum. Cem. Concr. Res., 2007,

783   37 (10), 1418–1426. doi:10.1016/j.cemconres.2007.06.001.

784   Monnin, C. and Schott, J., Determination of the solubility products of sodium carbonate

785   minerals and an application to trona deposition in Lake Magadi (Kenya). Geochim.

786   Cosmochim. Acta, 1984, 48, 571–581.

787   Moukannaa, S., Nazari, A., Bagheri, A., Loutou, M., Sanjayan, J.G. and Hakkou, R., Alkaline

788   fused phosphate mine tailings for geopolymer mortar synthesis: Thermal stability,

789   mechanical and microstructural properties. J. Non-Cryst. Solids, 2019, 511, 76–85.

790   doi:10.1016/j.jnoncrysol.2018.12.031.

791   Myers, R.J., Bernal, S.A. and Provis, J.L., A thermodynamic model for C-(N-)A-S-H gel:

792   CNASH_ss. Derivation and validation. Cem. Concr. Res., 2014, 66, 27–47.

793   doi:10.1016/j.cemconres.2014.07.005.

794   Myers, R.J., L'Hôpital, E., Provis, J.L. and Lothenbach, B., Composition-solubility-structure

795   relationships in calcium (alkali) aluminosilicate hydrate (C-(N,K-)A-S-H). Dalton Trans.,

796   2015, 44 (30), 13530–13544. doi:10.1039/c5dt01124h.

797   Najimi, M., Ghafoori, N. and Sharbaf, M., Alkali-activated natural pozzolan/slag mortars: A

798   parametric study. Constr. Build. Mater., 2018, 164, 625–643.

799   doi:10.1016/j.conbuildmat.2017.12.222.

800   Niu, H., Abdulkareem, M., Sreenivasan, H., Kantola, A.M., Havukainen, J., Horttanainen, M.,

801   Telkki, V.-V., Kinnunen, P. and Illikainen, M., Recycling mica and carbonate-rich mine

802   tailings in alkali-activated composites: A synergy with metakaolin. Miner. Eng., 2020a,

803   157, 106535. doi:10.1016/j.mineng.2020.106535.

804   Niu, H., Kinnunen, P., Sreenivasan, H., Adesanya, E. and Illikainen, M., Structural collapse

805   in phlogopite mica-rich mine tailings induced by mechanochemical treatment and

806   implications to alkali activation potential. Miner. Eng., 2020b, 151, 106331.

807   doi:10.1016/j.mineng.2020.106331.

808   Ortega-Zavala, D.E., Santana-Carrillo, J.L., Burciaga-Díaz, O. and Escalante-García, J.I., An

809   initial study on alkali activated limestone binders. Cem. Concr. Res., 2019, 120, 267–

810   278. doi:10.1016/j.cemconres.2019.04.002.

811   Pacheco-Torgal, F., Labrincha, J.A., Leonelli, C., Palomo, A. and Chindaprasirt, P. (eds.),

812   *Handbook of Alkali-activated Cements, Mortars and Concretes,* Woodhead Publishing in

813   materials, 2012, Woodhead Publishing, Cambridge, Philadelphia, PA.

814   Provis, J.L. and van Deventer, J.S.J., *Alkali Activated Materials, State-of-the-Art Report,*

815   *RILEM TC 224-AAM*, 2014, Springer, Dordrecht, Heidelberg, New York, London.

816   Rattanasak, U. and Chindaprasirt, P., Influence of NaOH solution on the synthesis of fly ash

817   geopolymer. Miner. Eng., 2009, 22 (12), 1073–1078. doi:10.1016/j.mineng.2009.03.022.

818   Robayo, R.A., Mejía de Gutiérrez, R. and Gordillo, M., Natural pozzolan-and granulated

819   blast furnace slag-based binary geopolymers. Mater. Constr., 2016, 66 (321), e077.

820   doi:10.3989/mc.2016.03615.

821   Robie, R.A. and Hemingway, B.S., Thermodynamic Properties of Minerals and Related

822   Substances at 298.15 K and 1 bar (105 Pascals) Pressure and at Higher Temperatures,

823   U.S. Geological Survey Bulletin 2131. U.S. Geological Survey, Washington, D.C., 1995,

824   470 pp.

825 Roggendorf, H., Grond, W. and Hurbanic, M., Structural characterization of concentrated

826 alkaline silicate solutions by 29Si-NMR spectroscopy, FT-IR spectroscopy, light

827 scattering, and electron microscopy - Molecules, colloid, and dissolution artefacts.

828 Glastech. Ber. Glass Sci. Technol., 1996, 69 (7), 216–231.

829 Scrivener, K., Ouzia, A., Juilland, P. and Kunhi Mohamed, A., Advances in understanding

830 cement hydration mechanisms. Cem. Concr. Res., 2019, 124, 105823.

831 doi:10.1016/j.cemconres.2019.105823.

832 Scrivener, K.L., Juilland, P. and Monteiro, P.J.M., Advances in understanding hydration of

833 Portland cement. Cem. Concr. Res., 2015, 78, 38–56.

834 doi:10.1016/j.cemconres.2015.05.025.

835 Sharif, M.B., Firdous, R. and Tahir, M.A., Development of Local Bagasse Ash as Pozzolanic

836 Material for Use in Concrete. Pak. J. Eng. Appl. Sci., 2015, 17, 39–45.

837 Snellings, R., Solution-Controlled Dissolution of Supplementary Cementitious Material

838 Glasses at pH 13: The Effect of Solution Composition on Glass Dissolution Rates. J. Am.

839 Ceram. Soc., 2013, 96 (8), 2467–2475. doi:10.1111/jace.12480.

840 Snellings, R., Assessing, Understanding and Unlocking Supplementary Cementitious

841 Materials. RILEM Tech. Lett., 2016, 1, 50–55. doi:10.21809/rilemtechlett.2016.12.

842 Snellings, R., Mertens, G. and Elsen, J., Supplementary Cementitious Materials. Rev.

843 Mineral. Geochem., 2012, 74 (1), 211–278. doi:10.2138/rmg.2012.74.6.

844 T. Thoenen, W. Hummel, U. Berner, E. Curti, The PSI/Nagra Chemical Thermodynamic

845 Data Base 12/07. PSI Report 14-04, Villigen PSI, Switzerland, 2014, ISSN:1019-0643.

846 Tajuelo Rodriguez, E., Garbev, K., Merz, D., Black, L. and Richardson, I.G., Thermal stability

847 of C-S-H phases and applicability of Richardson and Groves' and Richardson C-(A)-S-

848 H(I) models to synthetic C-S-H. Cem. Concr. Res., 2017, 93, 45–56.

849 doi:10.1016/j.cemconres.2016.12.005.

850 Tekin, I., Properties of NaOH activated geopolymer with marble, travertine and volcanic tuff

851   wastes. Constr. Build. Mater., 2016, 127, 607–617.

852   doi:10.1016/j.conbuildmat.2016.10.038.

853 Tenoutasse, N., Untersuchungen über die Kinetik der Hydratation des Tricalciumaluminats in

854   Gegenwart von Calciumsulfat und Calciumchlorid. Zem-Kalk-Gips, 1967, 20 (10), 459–

855   467.

856 Wagner, T., Kulik, D.A., Hingerl, F.F. and Dmytrieva, S.V., GEM-selektor geochemical

857   modeling package: TSolMod library and data interface for multicomponent phase

858   models. Can. Mineral., 2012, 50 (5), 1173–1195. doi:10.3749/canmin.50.5.1173.

859 Walling, S.A., Bernal, S.A., Gardner, L.J., Kinoshita, H. and Provis, J.L., Blast furnace slag-

860     $Mg(OH)_2$ cements activated by sodium carbonate. RSC Adv., 2018, 8 (41), 23101–

861   23118. doi:10.1039/C8RA03717E.

862 Woods, T.L. and Garrels, R.M., Thermodynamic Values at Low Temperature for Natural

863   Inorganic Materials: An Uncritical Summary. Oxford University Press, New York, New

864   York, 1987.

865 Xu, H. and van Deventer, J.S.J., Geopolymerisation of multiple minerals. Miner. Eng., 2002,

866   15 (12), 1131–1139. doi:10.1016/S0892-6875(02)00255-8.

867 Yip, C.K., Lukey, G.C. and van Deventer, J.S.J., The coexistence of geopolymeric gel and

868   calcium silicate hydrate at the early stage of alkaline activation. Cem. Concr. Res., 2005,

869   35 (9), 1688–1697. doi:10.1016/j.cemconres.2004.10.042.

870 Yu, P., Kirkpatrick, R.J., Poe, B., McMillan, P.F. and Cong, X., Structure of Calcium Silicate

871   Hydrate (C-S-H): Near-, Mid-, and Far-Infrared Spectroscopy. J. Am. Ceram. Soc., 1999,

872   82 (3), 742–748. doi:10.1111/j.1151-2916.1999.tb01826.x.

873   Zhang, Z., Provis, J.L., Reid, A. and Wang, H., Fly ash-based geopolymers: The relationship

874   between composition, pore structure and efflorescence. Cem. Concr. Res., 2014, 64, 30–

875   41. doi:10.1016/j.cemconres.2014.06.004.

876

877

Highlights

- Calcium carbonate in its various polymorphs reacts with sodium silicate solution

- This reaction results in formation of Na-containing C-S-H and sodium carbonates

- Formation of natron and C-S-H are observed at time of second calorimetric peak

- Formation of natron or thermonatrite depends upon the kinetics of reaction

- With higher reaction degree of calcite, formation of gaylussite is predicted

Appendix A: Supplementary material for:

Reaction of calcium carbonate minerals in sodium silicate solution and its role in alkali-activated systems

Rafia Firdous [a], Tamino Hirsch [a], Detlef Klimm [b], Barbara Lothenbach [c], Dietmar Stephan [a,*]

[a] Technische Universität Berlin, Department of Civil Engineering, Building Materials and Construction Chemistry, Gustav-Meyer-Allee 25, 13355 Berlin, Germany

[b] Leibniz-Institut für Kristallzüchtung, Max-Born-Str. 2, 12489 Berlin, Germany

[c] Empa, Laboratory for Concrete & Construction Chemistry, 8600 Dübendorf, Switzerland

* Corresponding author E-mail: stephan@tu-berlin.de

Fig. S1. Particle size distributions of all raw samples.
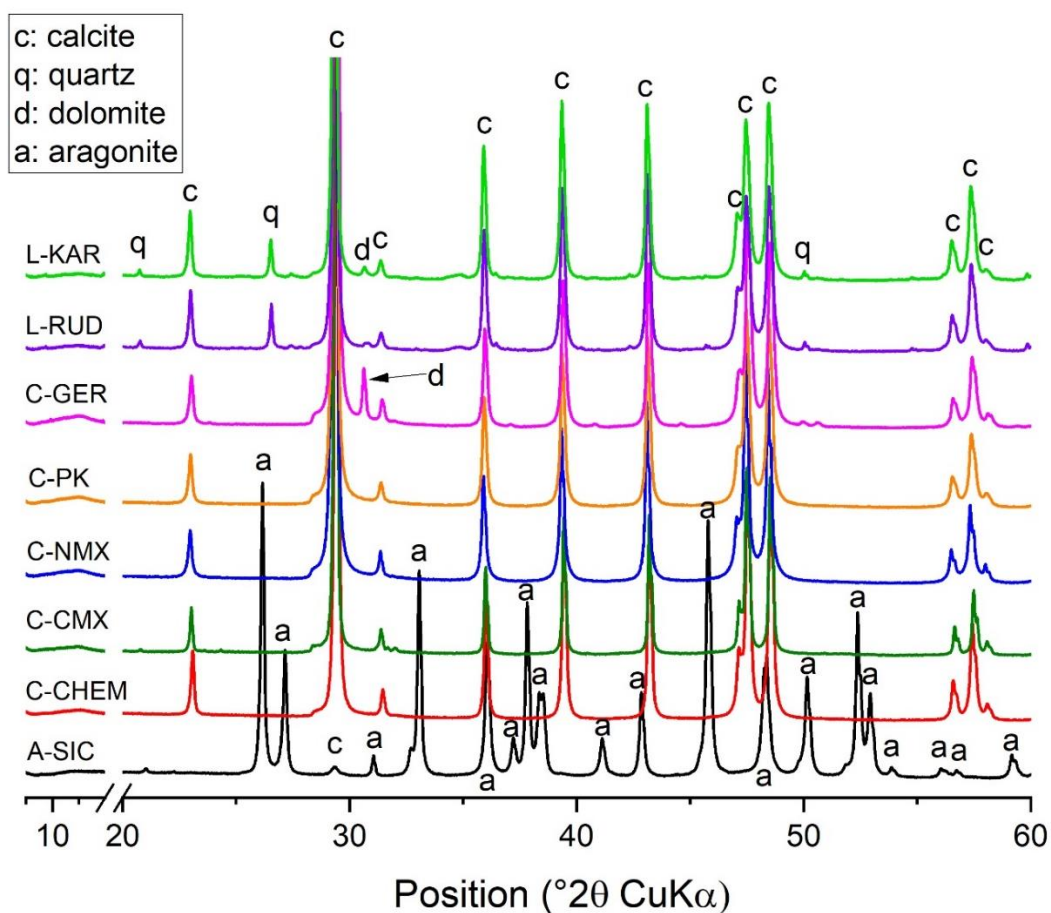
Fig. S2. X-ray diffractograms of raw samples with identified phases. The small quartz peak found in C-GER, C-PK, C-NMX, C-CMX, C-CHEM and A-SIC is due to the sample holder used.

Table S1. Symbols and ICSD card numbers for all mineral phases mentioned in the manuscript.

Symbol	Phase	Chemical formula	ICSD card number
c	Calcite	$CaCO_3$	166365
q	Quartz	SiO_2	89278
d	Dolomite	$CaMg(CO_3)_2$	171530
a	Aragonite	$CaCO_3$	169895
t	Thermonatrite	$Na_2CO_3 \cdot H_2O$	6293
n	Natron	$Na_2CO_3 \cdot 10H_2O$	16033
nt	Natrite	Na_2CO_3	281362
r	Rutile	TiO_2	51932
csh	C-S-H	C-S-H	--

161
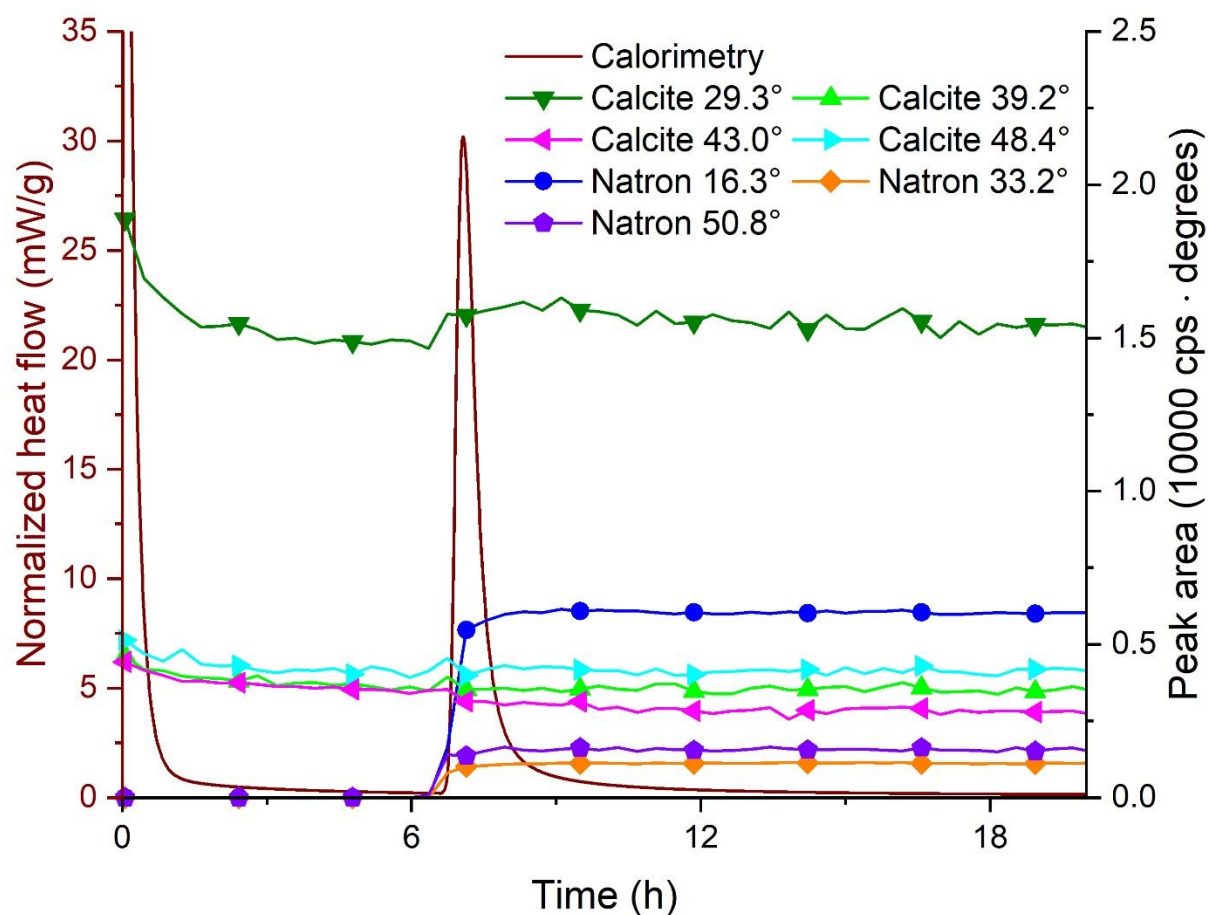
Fig. S3. Comparison of the calorimetry, in-situ XRD of C-PK (areas of the natron-related peaks at 16.3° and 33.2° are divided by 10 and 30, respectively, for better presentation).
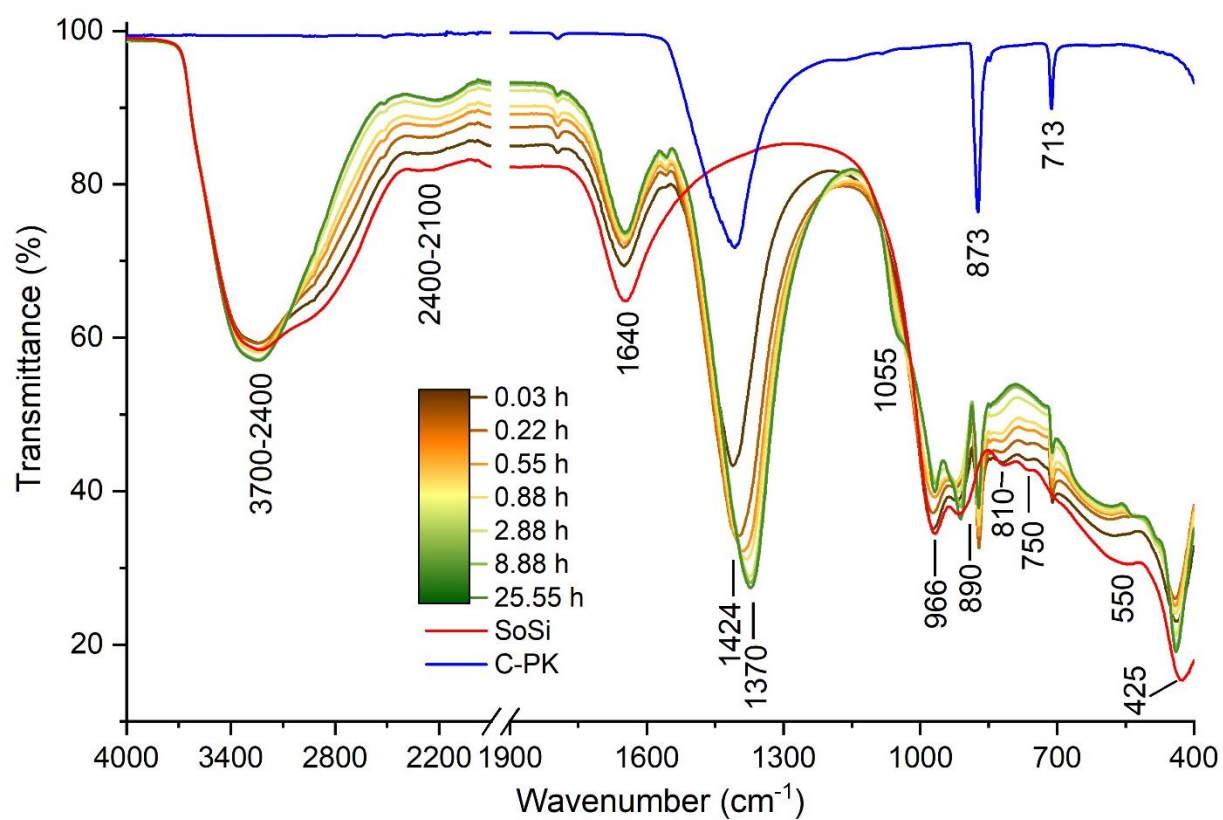
Fig. S4. IR spectra of C-PK, sodium silicate solution (SoSi) and in-situ data from reaction labelled with time in h.
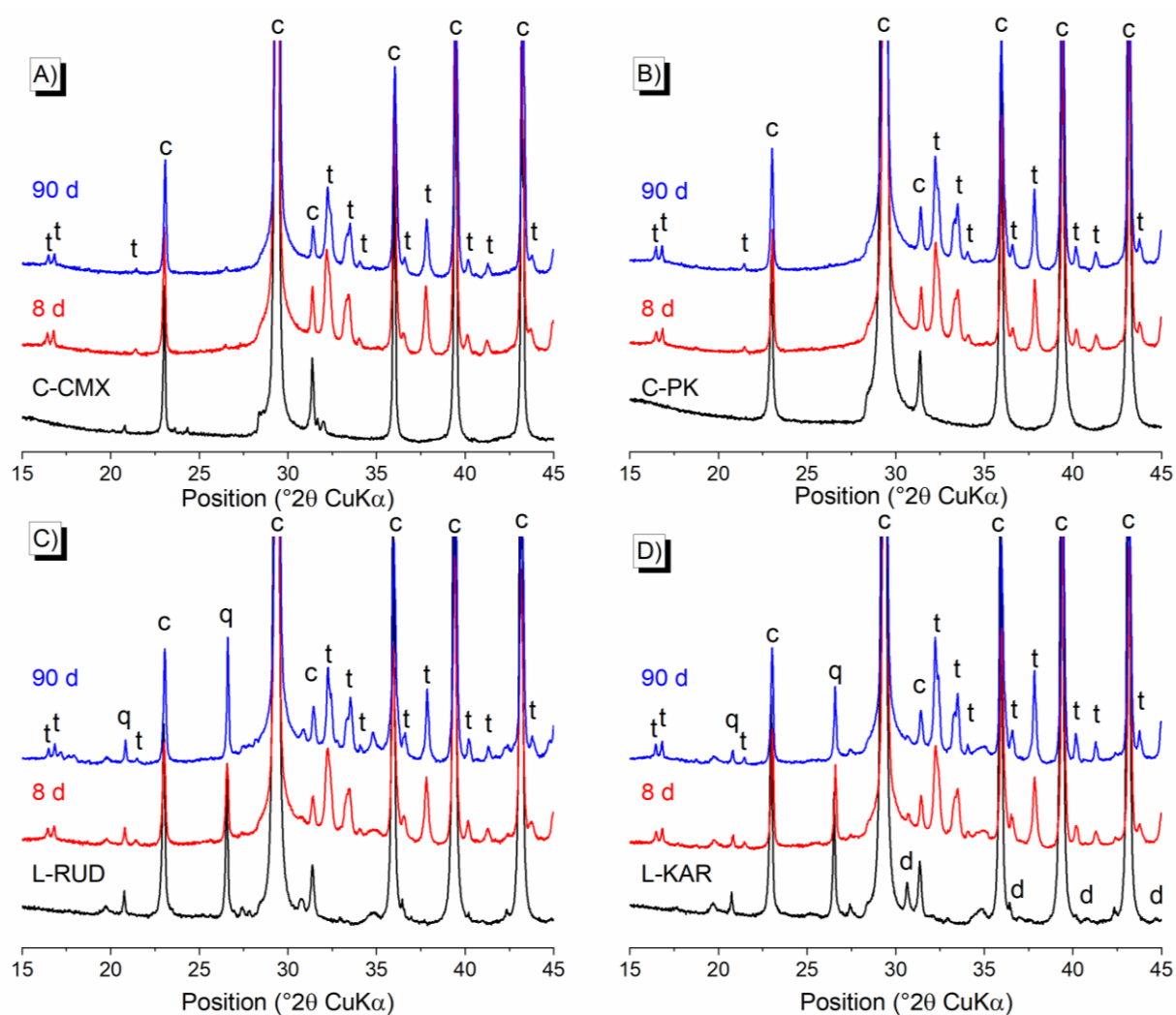
Fig. S5. Powder XRD of raw samples, 8 and 90 d reacted samples for A) C-CMX, B) C-PK, C) L-RUD and D) L-KAR. Symbols on picture indicate c: calcite, t: thermonatrite, d: dolomite q: quartz and a: aragonite.

Table S2. Thermodynamically predicted phases depending on changes in the Gibbs free energy (G°) of gaylussite, thermonatrite and natron by ± 2.85 kJ/mol each. This change in the Gibbs free energy equals approximately a variation of the solubilities of these phases by approximately a half log-unit. The predicted phases are abbreviated as T: thermonatrite, N: natron, G: gaylussite and P: pirssonite. The order of the letters abbreviating the carbonates formed indicates their appearance depending on the degree of reaction of calcite. The cell in the middle with the underlined bold content is the equivalent to Fig. 8 in the article.

G° of gaylussite →	-2.85 kJ/mol			+/- 0 kJ/mol			+ 2.85 kJ/mol		
G° of thermonatrite →	-2.85 kJ/mol	+/- 0 kJ/mol	+ 2.85 kJ/mol	-2.85 kJ/mol	+/- 0 kJ/mol	+ 2.85 kJ/mol	-2.85 kJ/mol	+/- 0 kJ/mol	+ 2.85 kJ/mol
G° of natron − 2.85 kJ/mol	T N G	T N G	N G	T N	T N	N	T N	T N	N
+/- 0 kJ/mol	T N G	T N G	N G	T N G	**<u>T N G</u>**	N G	T N P	T N P	N P
+ 2.85 kJ/mol	T G	T G	G	T G	T G	G	T P	T P	P

Chapter 3

Reactivity of minerals

The findings of the previous publication added in chapter 2 gave indications about the reactivity of crystalline minerals observed in the used natural pozzolans in geopolymer system. However, the available literature on the reactivity of crystalline minerals in highly alkaline conditions is limited. Therefore, the present study is conducted to determine the reactivity and resultant phase formation upon reaction of several crystalline minerals, one amorphous mineral and one synthetic phase with sodium hydroxide (NaOH) and sodium silicate solutions. NaOH solution is one of the common alkaline solutions used for geopolymer synthesis. Therefore, this part of work considered the reactivity of the minerals observed in Rhenish and Bavarian trass with NaOH solution and selected minerals with sodium silicate solution. For this study, the minerals were received from several origins as given in Table 3.1. Consequently, the minerals present in the natural pozzolans can differ in particle size and degree of crystallinity from the minerals used in this study. Moreover, several minerals such as zeolites can have varying composition. Because of these factors, the reactivity of minerals existing in the examined natural pozzolans and used in this study can be different. Nevertheless, such a study helps to get first indications about the behaviour of these minerals in the used alkaline conditions and in predicting the reactivity of pozzolans containing these minerals.

3.1. Materials and methods

For this study, fifteen mineral samples are used which were ground in laboratory ball mill (KM 1, MLW company) to comparable Blaine fineness. The origin of each mineral phase and Blaine fineness are given in Table 3.1. All mineral samples were characterised with X-ray diffraction analysis (XRD), and the identified mineral phases together with their ICSD card numbers or RRUFF ID are listed in Table 3.2. Moreover, the crystalline reaction products/new phases observed in this chapter are also listed in Table 3.2 with their ICSD card numbers or RRUFF ID, chemical compositions and the respective symbols used for them in this chapter.

166

Table 3.1. Origin and Blaine fineness of each mineral used in this study.

Sr. no.	Sample name	Origin	Blaine fineness (cm²/g)
1	Albite	Vånne, south east Evje, south Norway	6820
2	Augite	Hochstein mountain, Ettringen, Eifel, Rheinland-Pfalz, Germany	6910
3	Biotite	Eretveit, Iveland, near to Evje, south Norway	7050
4	Calcite	Chihuahua, Mexico	6690
5	Chabazite	Steinbruch Freisen, Baumholder, Nordpfälzer Bergland, Germany	7490
6	Clinochlore	Possibly Ilmen mountains, south Ural Mountains, Chelyabinsk Oblast, Russia	6830
7	Glass phase	Campi Flegrei, Naples, Italy	6720
8	Kaolinite	Sedlec u Karlových Var, Karlovy Vary, Bohemia, Czech Republic	> 9000
9	Larnite	*VUSTAH, Czech Republic (Synthetic)	6740
10	Leucite	Roccamonfina, Italy	6650
11	Montmorillonite	Open-pit mine in north Oberwiddersheim, Vogelsberg, Hessen, Germany	5760
12	Muscovite	*Berliner Mineralien Zentrum	6700
13	Nepheline	Central Europe	7460
14	Phillipsite	*Mineralogische Sammlungen at TU Berlin	8830
15	Sanidine	Volkesfeld, Eifel, Rheinland-Pfalz, Germany	6620

*Provided by

The reactivity of these minerals with sodium hydroxide solution of 16 mol/kg concentration and sodium silicate solution of silica modulus 1.061 was investigated by isothermal conduction calorimetry, X-ray diffraction (XRD) analysis and thermogravimetric analysis (TGA). Reaction kinetics for first few days were determined by isothermal conduction calorimetry. For each sample, 1 g of mineral sample was mixed with 0.82 g of NaOH solution or 0.88 g of sodium silicate solution using a vortex mixer for 1 min. Immediately after mixing, samples were placed inside the device (MC-CAL 100P, C3 Prozess- und Analysentechnik GmbH) which measured the heat flow at 20 °C. To investigate the reaction products forming till 8, 28 and 90 d of reaction, XRD analysis and TGA were used. The samples were prepared as described for calorimetric examination and were seal cured at 20 ± 1 °C till test age. Before implementation of XRD and TGA, pieces of samples were collected at desired ages and reaction was stopped by solvent exchange using isopropanol followed by freeze-drying. Thereafter, these freeze-dried samples were ground to fine powder by hand with an agate mortar pestle. XRD was measured with Empyrean of PANalytical with Ni filter and CuKα radiation (λ = 1.54 Å), operating at 40 kV and 40 mA in

continuous mode, with a resolution of 0.0131° and a speed of 0.0176 °/s in a range from 5° to 65° 2θ. The phase evaluation was performed using HighScore Plus software (PANalytical) using ICDD, ICSD and RRUFF databases. TGA was executed using a TG 209 Tarsus F3 from Netzsch Instruments, under a nitrogen atmosphere at a flow rate of 40 mL/min. For each test, 5 ± 1 mg of ground sample was used. Each sample was first held at 25 °C for 20 min and then heated from 25 °C to 850 °C at a heating rate of 10 °C/min.

Table 3.2. Symbol, name, ICSD card number (or RRUFF ID when marked with **) and chemical composition of all crystalline phases observed in this chapter. Chemical compositions are taken form the respective ICSD or RRUFF data.

Symbol	Name	ICSD card number	Chemical composition
a	Albite	34916	$(Na_{0.75}Ca_{0.25})Al_{1.26}Si_{2.74}O_8$
an	Analcime	2930	$Na(AlSi_2O_6)(H_2O)$
au	Augite	16905	$(Mg_{0.6}Fe_{0.2}Al_{0.2})Ca(Si_{1.5}Al_{0.5})O_6$
b	Biotite	95359	$K(Fe_{2.554}Al_{0.446})((Al_{1.55}Si_{2.45})O_{10})(OH)_2$
c	Calcite	40116	$CaCO_3$
cb	Chabazite	34654	$Ca_2Al_4Si_8O_{24}(H_2O)_{13}$
cbn	Chabazite-Na	201464	$Na_{3.16}(Al_{3.72}Si_{8.28}O_{24})(H_2O)_{9.68}$
cl	Clinochlore	156708	$(Mg_{11.148}Fe_{0.852})((Si_{4.99}Al_{3.01})O_{20}(OH)_{16})$
ct	Clinotobermorite	403090	$Ca_5(Si_6O_{16}(OH)_2)(H_2O)_4)$
g	Gaylussite	4424	$CaNa_2(CO_3)_2(H_2O)_5$
h	Hydrosodalite	413496	$Na_8(AlSiO_4)_6(H_2O)_2(OH)_2$
k	Kaolinite	68698	$NaAlSi_3O_8$
l	Larnite	79550	$Ca_2(SiO_4)$
le	Leucite	161630	$K(AlSi_2O_6)$
mt	Montmorillonite	R110053**	$(Na,Ca)_{0.3}(Al,Mg)_2Si_4O_{10}(OH)_2 \cdot nH_2O$**
m	Muscovite	202261	$KAl_{2.9}Si_{3.1}O_{10}(OH)_2$
nt	Natrite	16024	Na_2CO_3
n	Nepheline	27584	$KNa_3(Al_4Si_4O_{16})$
pl	Phillipsite	161306	$K_{0.88}(Na_{0.73}Ca_{0.312})(Al_3Si_5O_{16})(H_2O)_{5.924}$
ph	Phlogopite	181311	$K_{0.966}(Mg_{2.52}Fe_{0.48})((Si_{2.71}Al_{1.29})O_{10})(OH)_2$
pi	Pirssonite	9012	$CaNa_2(CO_3)_2(H_2O)_2$
p	Portlandite	202220	$Ca(OH)_2$
q	Quartz	89279	SiO_2
s	Sanidine	64961	$(K_{0.93}Na_{0.07})(AlSi_3O_8)$
sh	Sodium hydrogensilicate pentahydrate	21051	$Na_3(HSiO_4)(H_2O)_5$
t	Thermonatrite	15959	$Na_2(CO_3)(H_2O)$

**RRUFF ID and composition from RRUFF database

3.2. Results and discussion

3.2.1. Reactivity of minerals with sodium silicate solution

The selected minerals tested for their reactivity in sodium silicate solution included albite-rich plagioclase (later referred to as albite), augite, chabazite, clinochlore, muscovite and sanidine. The heat flow measured over time for several mineral phases is shown in Fig. 3.1. The reaction of each mineral is characterized by a single exothermic peak associated with the first interaction and wetting, which occurs within the first few minutes. This is followed by deceleration of heat evolution. The rate of deceleration is different for every mineral. After the deceleration, the reaction attains a steady state. These findings show that each crystalline mineral phase exhibits a unique heat flow upon reaction with sodium silicate solution; this may define its participation in geopolymer reaction and will be examined further by XRD and TGA at various ages of the mineral-activator mixes..
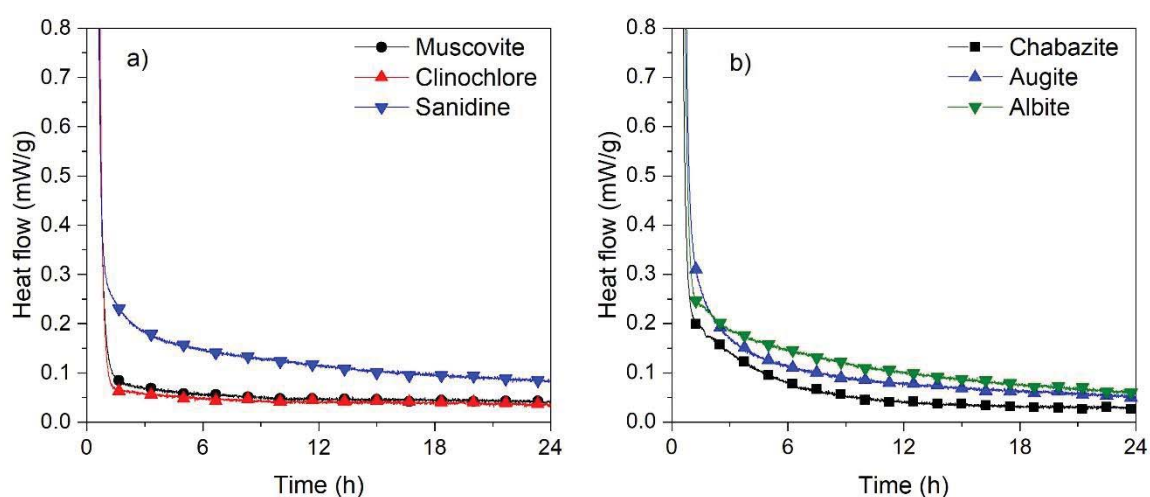

Fig. 3.1. Calorimetric heat evolution curves for crystalline mineral phases subjected to reaction with sodium silicate solution. The heat flow is normalized to weight of mineral sample.

The reaction product of chabazite with sodium silicate showed one decomposition event in TGA (Fig. 3.2B), while in XRD, a clear increase in the amorphous hump can be seen (Fig. 3.2A). Furthermore, with the age of sample, a slight shift of the main chabazite reflexes was observed, indicating the formation of Na-rich chabazite. The similarity of TGA (Fig. 3.2B) curves for chabazite and its reacted samples also confirmed the structural similarity of both the raw and reacted samples. The precipitation of amorphous product and the formation of Na-rich chabazite, confirm the reactivity of chabazite in the alkaline medium used.
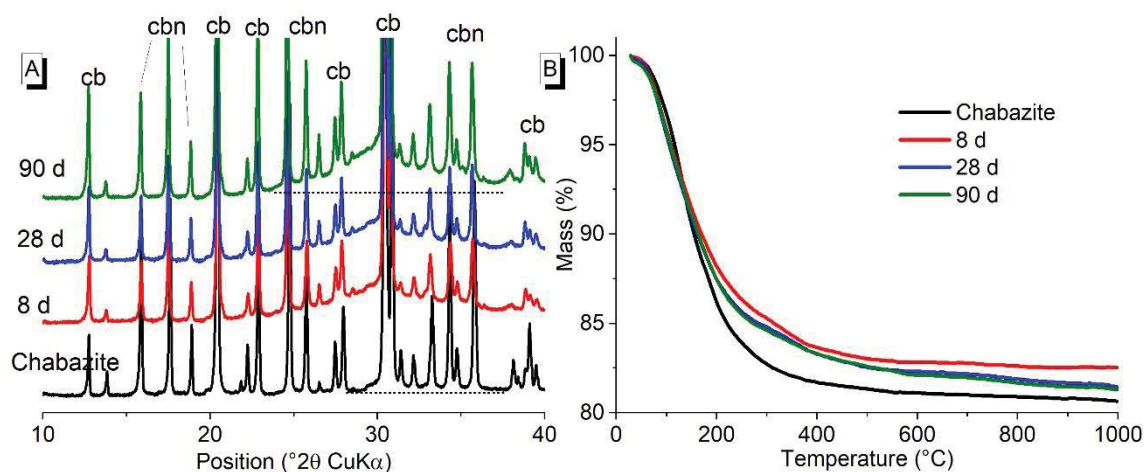
Fig. 3.2. (A) XRD, (B) TGA of the raw chabazite and its reacted samples at 8, 28 and 90 d. For the symbols used refer to Table 3.2.

The reaction of clinochlore with sodium silicate solution showed formation of amorphous hump and some new reflexes (marked with arrows in Fig. 3.3A). With the reaction time, the main clinochlore reflexes decreased in intensity while several other reflexes increased in intensity. This could be because of less preferred orientation while sample preparation either due to the formation of reaction products or dissolution of the clinochlore particles from the edges. Furthermore, TGA conducted at 8 d showed a reduction in the typical clinochlore decomposition events (Fig. 3.3B). Additionally, mass loss around 100 °C can be due to liberation of physically bound water likely from the sodium silicate solution. At 28 d, the TGA curve showed a continuous mass loss which can be because of formed semi-crystalline phase. Thus, indicating that clinochlore may have partially participated in the reaction.
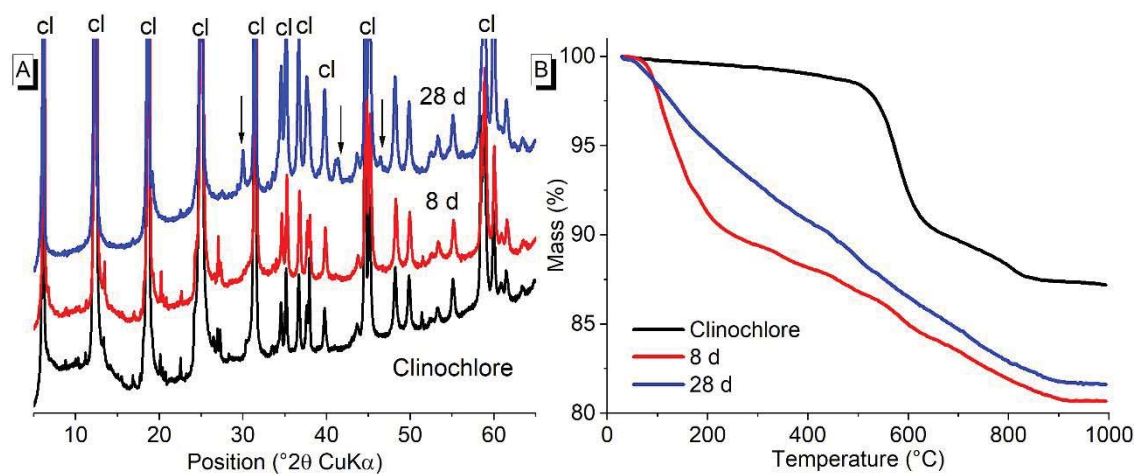

Fig. 3.3. (A) XRD, (B) TGA of the raw clinochlore and its reacted samples at 8 and 28 d. For the symbols used refer to Table 3.2.

Comparing XRD of sanidine and its reacted samples (Fig. 3.4A), no new reflexes were observed, but the reflexes of sanidine reduced in intensity. This reduction in the intensity of reflexes can be, on the one hand, due to the reaction of mineral while on the other hand it can be due to reduced content of mineral in the mineral-activator mixtures. As in the mineral-activator samples the absolute amount of mineral is already less from the beginning. At 8 d, the TGA of sanidine (Fig. 3.4B) showed the presence of unreacted sodium silicate solution. However, the TG curve exhibited a continuous mass loss at 28 d. A reduction in mass loss from 8 to 28 d may reflect the consumption of alkaline solution in the reaction. Therefore, TGA may indicate the formation of a new X-ray amorphous phase and that sanidine is partially affected by the alkaline conditions.
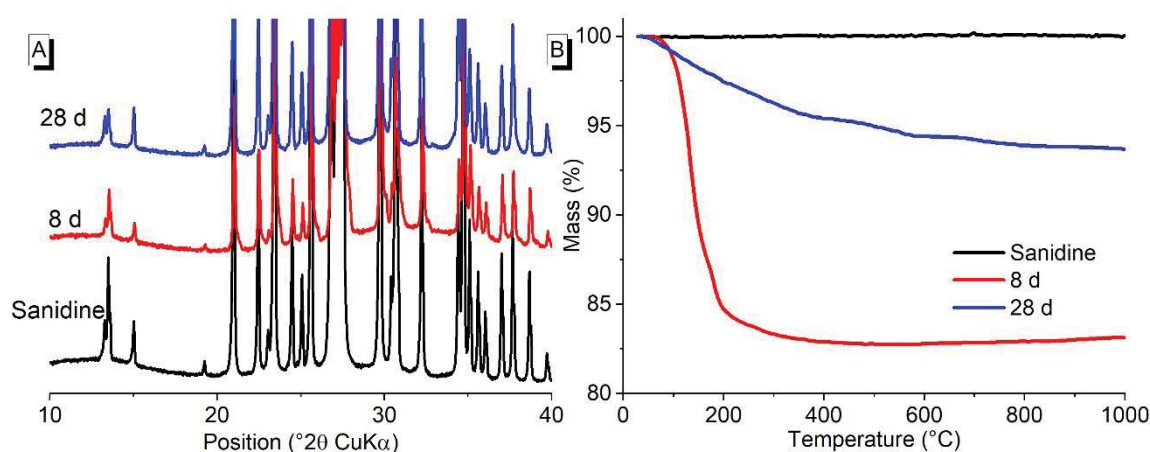

Fig. 3.4. (A) XRD, (B) TGA of the raw sanidine and its reacted samples at 8 and 28 d.

The other minerals, including albite, augite and muscovite, exhibited no new reflexes in XRD (Fig. 3.5A, 3.5C, 3.5E), but the heights of the existing reflexes were somewhat reduced. Such a reduction in intensity can be due to similar reasons as discussed in above paragraph. TGA showed only the presence of unreacted sodium silicate solution (Fig. 3.5B, 3.5D, 3.5F). Thus, it is clear that the reactivity of these minerals in a geopolymer system is low.
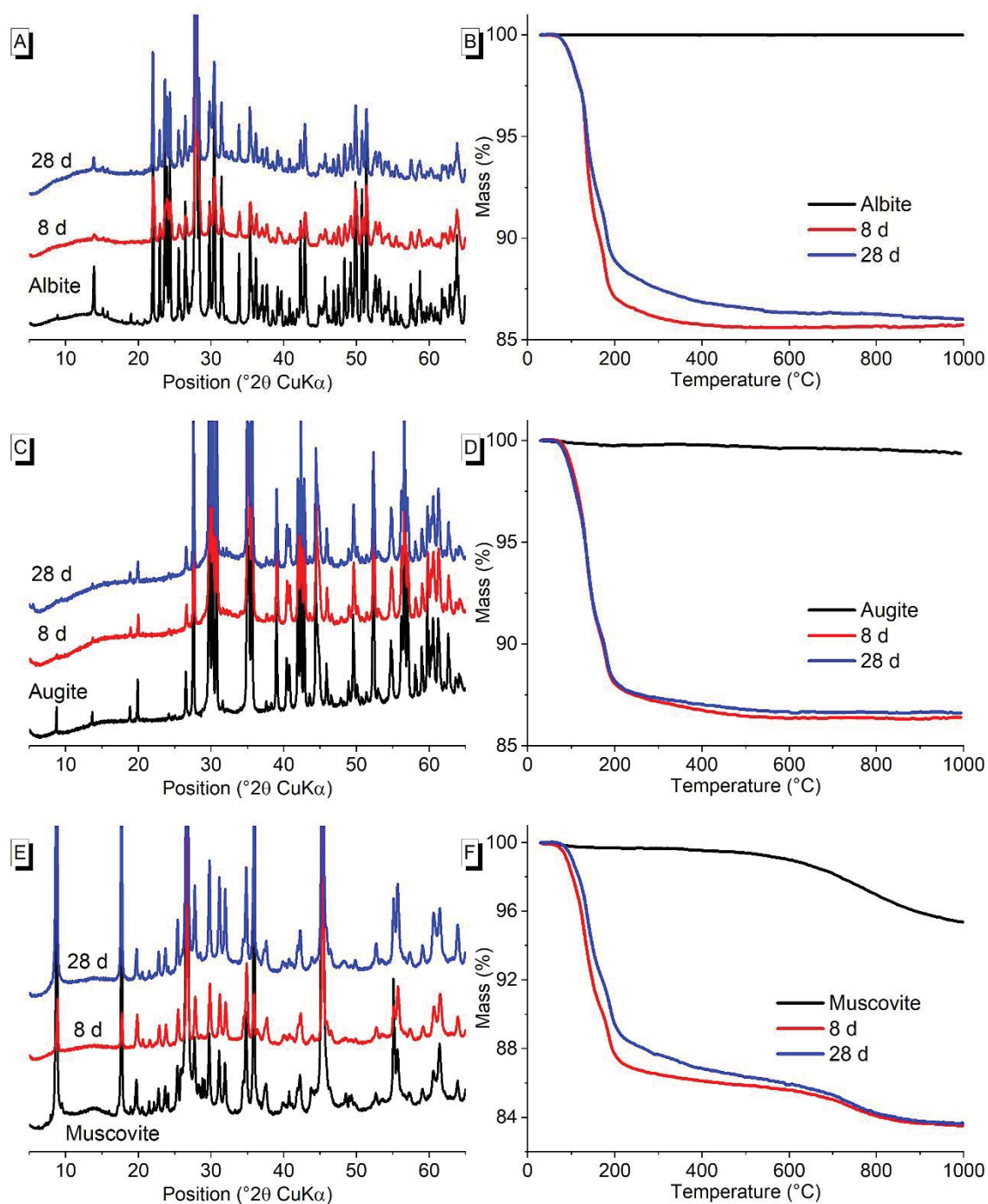
Fig. 3.5. (A), (C), (E) XRD, (B), (D), (E) TGA of the raw albite, augite, muscovite and their reacted samples at 8 and 28 d.

3.2.2. Reactivity of minerals with sodium hydroxide solution

The calorimetric study made on all the mineral phases showed that each mineral has a distinct behaviour. All the mineral phases showed an exothermic reaction. The reaction of most mineral phases (including albite, augite, biotite, clinochlore, glass phase, sanidine,

kaolinite, leucite, larnite, muscovite, montmorillonite, nepheline) is associated with one exothermic peak, which occurs within the first few minutes of mixing of mineral powder and alkaline solution and is assigned to first wetting and dissolution (Fig. 3.6). This is followed by deceleration of the reaction rate, where the deceleration rate was different for each mineral. This indicates that each mineral has different reaction kinetics. Thereafter, the reaction attains a steady state and continues over a longer time.

Some of the mineral phases such as calcite, chabazite and phillipsite exhibited distinct behaviour (Fig. 3.6A, Fig. 3.6B and Fig. 3.6D). The reaction of calcite with NaOH (Fig. 3.6A) is also associated with a first exothermic peak and the deceleration phase, followed by a second broad exothermic event. This second exothermic event starts after approx. 40 h and the heat flow continues to increase till the end time of experiment. Similarly, in the chabazite and phillipsite, a second exothermic peak was observed (Fig. 3.6B, Fig. 3.6D). In chabazite, this peak starts at approx. 42 h and reaches its maximum after approx. 56 h (Fig. 3.6B). While phillipsite exhibited a sudden reaction starting approx. 9 h and it reached maximum after approx. 12 h (Fig. 3.6D).
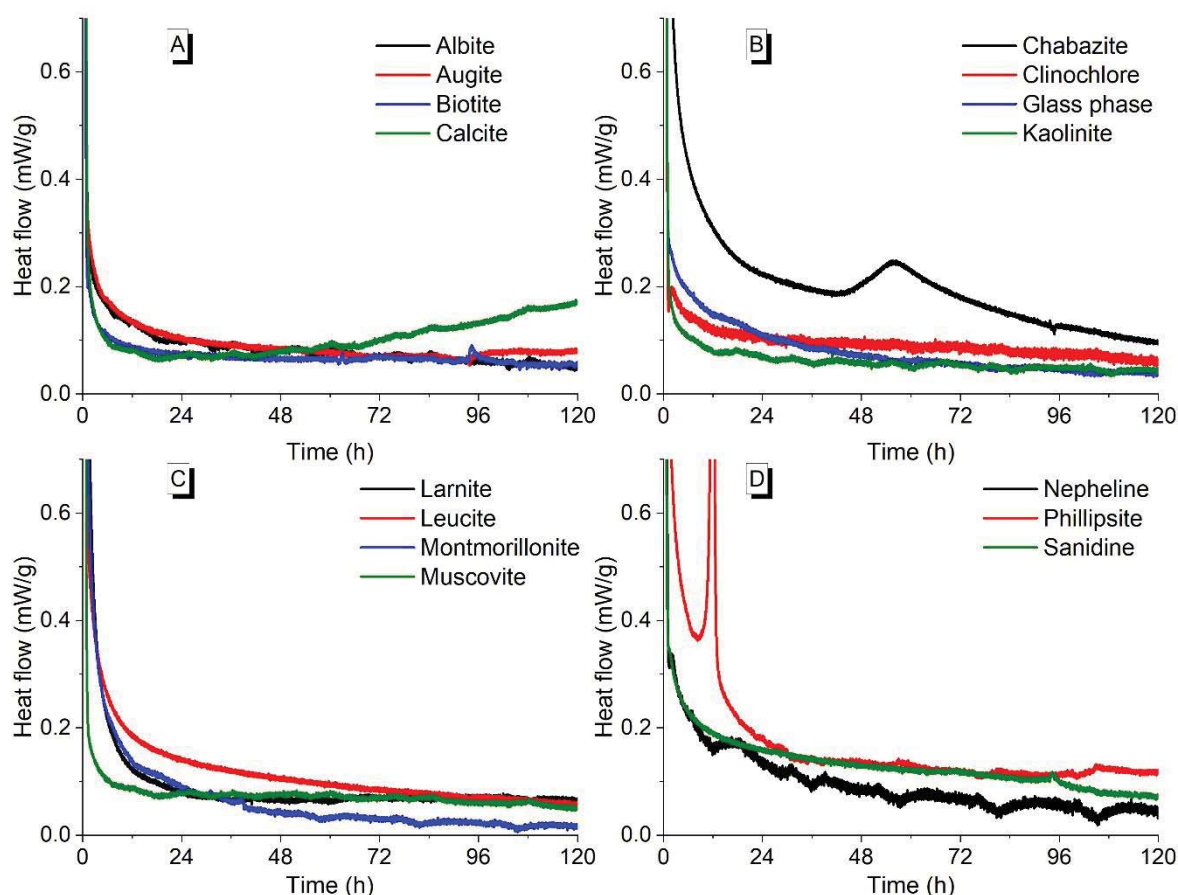

Fig. 3.6. Calorimetric heat evolution curves for all mineral samples with NaOH solution. The heat flow is normalized to weight of mineral sample.

On the one hand, occurrence of a second exothermic event in these three samples clearly indicates that these samples are reacting with NaOH solution. However, it does not mean that the other samples are not reacting, as not every reaction is attributed to a measurable heat formation or consumption. Therefore, further investigations about the reaction of all minerals with NaOH solution are carried out by thermogravimetric analysis and X-ray diffraction analysis. The findings of each mineral are individually presented in the text below.

It is important to mention here, that XRD detected often natrite (sodium carbonate) or thermonatrite (sodium carbonate monohydrate). The actual phase formed in all the samples was most likely thermonatrite which upon the implementation of freeze-drying process dehydrated to natrite. However, perhaps in some samples this conversion was not fully achieved, therefore, traces of thermonatrite are also observed.

i. Albite

The XRD analysis on the albite sample showed that it has similarity with albite which contains not only Na but also some Ca. In XRD (Fig. 3.7A), upon reaction of albite, formation of thermonatrite was observed, which can form by reaction of Na^+ ions from alkaline solution with CO_2 from air. Apart from that, a slight increase in the semi-crystalline or amorphous phase was observed by increase in background around $15° – 50°$ 2θ.
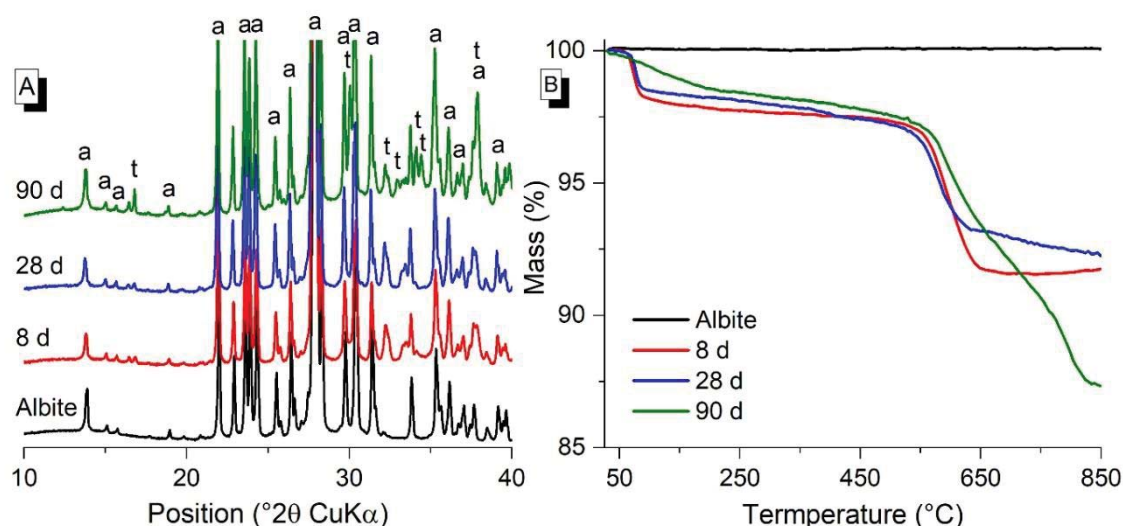

Fig. 3.7. (A) XRD, (B) TGA of the raw albite and its reacted samples at 8, 28 and 90 d. For the symbols used refer to Table 3.2.

The TGA (Fig. 3.7B) of raw albite showed no mass loss, while after reaction two to three distinct mass losses were observed. The first mass loss around 80 °C can be attributed to

174

liberation of physically bound water which is introduced from NaOH solution. The second mass loss is observed around 530 – 680 °C in 8, 28 and 90 d samples. The 90-d sample shows additionally a mass loss around 720 – 850 °C. These mass loss events cannot be assigned with surety, as the XRD showed formation of no new crystalline phases whose decomposition temperature is in this range. In literature the decomposition temperature of sodium carbonate has been reported to be higher than 1200 °C [1]. The possible explanation of the mass losses seen in albite samples can be the formation of a new phase which is still too low in crystallinity to be observed by XRD. However, this could not be further explained with the used experimental methods.

ii.   Augite

The raw augite as characterised with XRD contained majorly augite and a minor amount of mica matching to phlogopite. In XRD (Fig. 3.8A) of the reacted samples, formation of sodium carbonate in form of natrite and thermonatrite was observed. While at 90 d, additionally, a minor amount of sodium hydrogensilicate pentahydrate was also observed. Furthermore, the reflexes corresponding to phlogopite are not observed in reacted samples, indicating that this phase may have also contributed to the reaction. The reduction in peak intensity of augite in reacted samples compared to raw sample can be due to its participation in the reaction or due to lesser amount of augite in the mineral-activator samples.
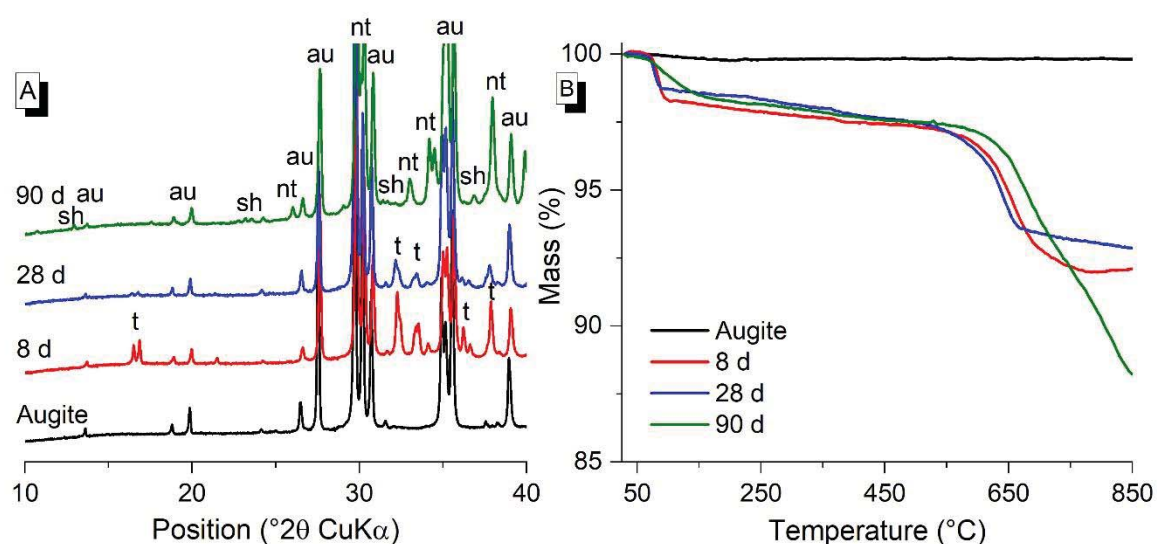

Fig. 3.8. (A) XRD, (B) TGA of the raw augite and its reacted samples at 8, 28 and 90 d. For the symbols used refer to Table 3.2.

In TGA (Fig. 3.8B), raw augite showed no mass loss, while all the reacted samples showed a mass loss around 100 °C likely corresponding to physically bound water. Moreover, like in albite, mass losses in temperature range of 540 – 740 °C were observed for all reacted samples, while a mass loss in temperature range of 740 – 850 °C was observed only for the 90-d sample. The dehydration and dehydroxylation of sodium hydrogensilicate pentahydrate is till 600 °C [2]. Therefore, it cannot be said with surety which other phases are decomposing till 850 °C. Moreover, as mentioned above, the decomposition of sodium carbonate is also not in the temperature range of 850 °C, as seen in literature [1].

iii.   Biotite

The raw biotite used in this study, in addition to biotite also contained a minor amount of clinochlore. In XRD (Fig. 3.9A) of the reacted sample, the major phase formed is sodium carbonate, while no other major crystalline phases are observed. The TGA (Fig. 3.9B) of the reacted sample showed similar characteristics as albite, where the physically bound water mass loss is observed around 100 °C and a second mass loss around 600 °C. This second mass loss could not be defined clearly as the only crystalline phase observed in XRD exhibits mass loss at higher temperature than 600 °C. Therefore, mass loss can be attributed to destabilisation of some X-ray amorphous phase as also indicated by a slight increase in background intensity in XRD.
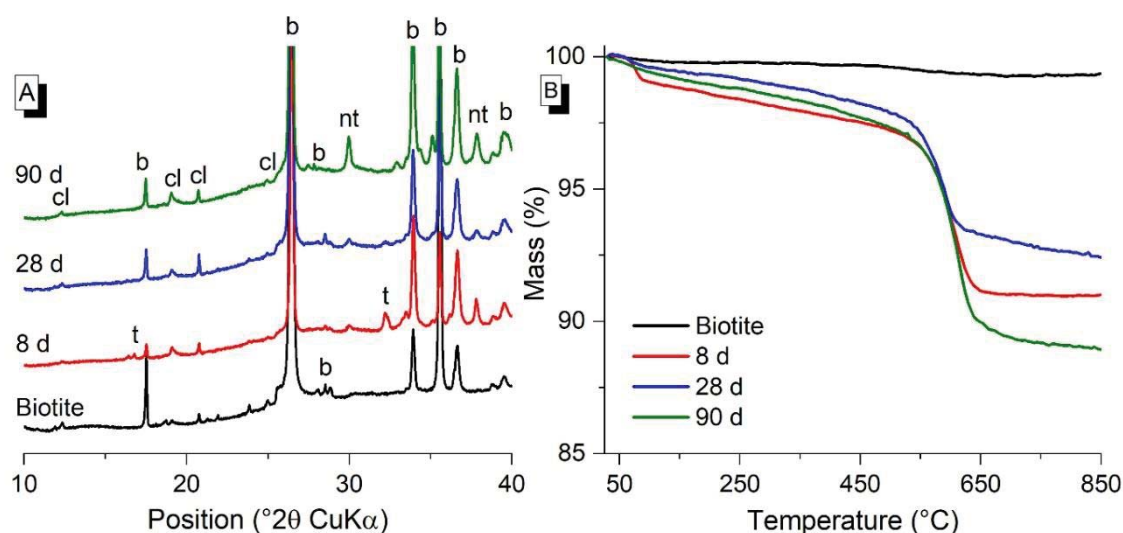

Fig. 3.9. (A) XRD, (B) TGA of the raw biotite and its reacted samples at 8, 28 and 90 d. For the symbols used refer to Table 3.2.

iv. Calcite

The obtained calcite sample from Chihuahua (Mexico) contained no minor phases as characterised by XRD. In XRD (Fig. 3.10A), upon its reaction with NaOH solution, formation of several new phases is observed. These phases include gaylussite, pirssonite, portlandite and sodium carbonate. The intensity of the XRD reflexes of these phases increased successively with the age showing that the reaction continued over long time. Formation of these phases under comparable conditions is also observed in literature [3]. In TGA (Fig. 3.10B), the distinct mass losses corresponding to each phase are observed. A mass loss around 100 °C is corresponding to liberation of physically or loosely bound water. A mass loss around 170 °C may correspond to dehydration of gaylussite and pirssonite [4]. Thereafter, a mass loss around 380 °C can be attributed to destabilisation of portlandite. The literature decomposition temperature of portlandite is slightly higher than the temperature observed here. However, the current XRD investigation and the literature clearly indicate the formation of portlandite in such systems. Furthermore, the signal around 380 °C is the only mass loss out of all observed mass losses, which is close to the dehydroxylation temperature of portlandite as reported in literature [5]. Therefore, it is likely that this mass loss is attributed to portlandite dehydroxylation. The last mass loss is attributed to decomposition of carbonate from unreacted calcite.
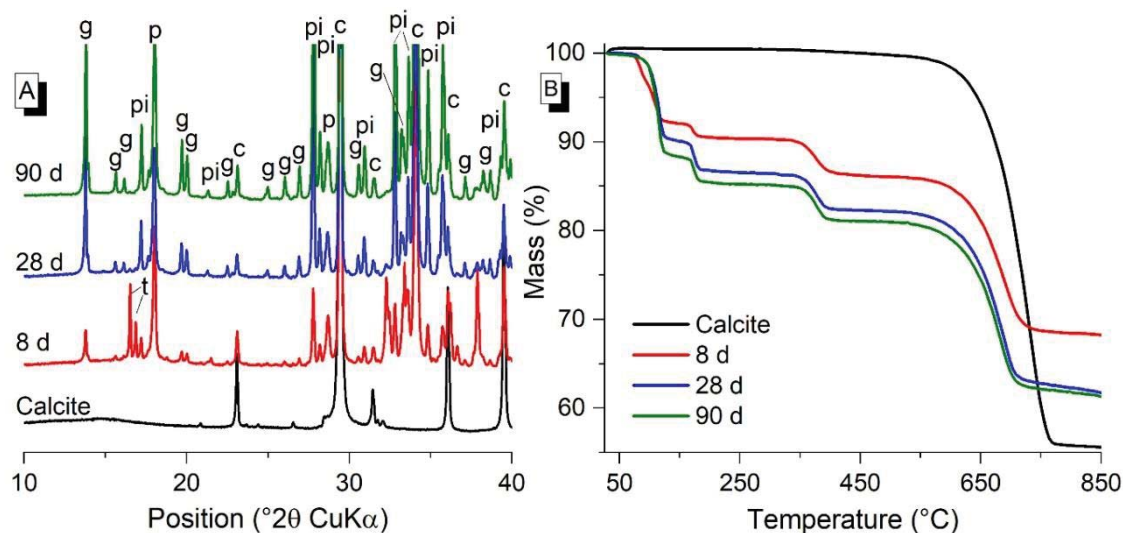

Fig. 3.10. (A) XRD, (B) TGA of the raw calcite and its reacted samples at 8, 28 and 90 d. For the symbols used refer to Table 3.2.

v. Chabazite

Raw chabazite obtained from Nordpfälzer Bergland in Germany contained only chabazite as characterised by XRD (Fig. 3.11A). The TGA (Fig. 3.11B) of raw chabazite showed a broad mass loss starting from approx. 50 °C till 200 °C. This is likely attributed to dehydration of chabazite [4,6]. In XRD, after reaction of chabazite with NaOH, the amorphous hump successively increased with the age of the sample (Fig. 3.11A), indicating that there are one or more new X-ray amorphous phases forming. Moreover, a slight change in the 2θ position of the reflexes showed the formation of Na-rich chabazite potentially through ion exchange. The TGA (Fig. 3.11B) on the reacted samples had similar mass losses as the raw chabazite, indicating that the new phases formed have likely similar structural characteristics as unreacted chabazite.
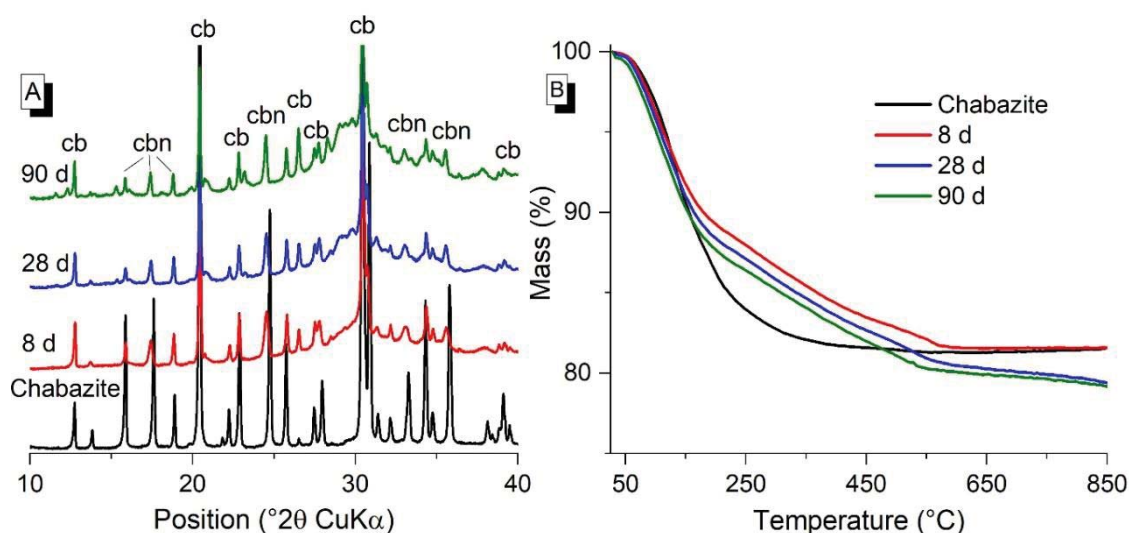

Fig. 3.11. (A) XRD, (B) TGA of the raw chabazite and its reacted samples at 8, 28 and 90 d. For the symbols used refer to Table 3.2.

vi. Clinochlore

From the chlorite group, clinochlore is tested in this study. Its atomic structure can be divided in an interlayer and a mica layer, and both layers contain hydroxyl groups. Therefore, the raw sample (Fig. 3.12B) showed two mass loss events: a mass loss event between 470 °C and 670 °C which may correspond to the dehydroxylation of the interlayer hydroxide. While the second mass loss around 800 °C is due to dehydroxylation of the mica layer [4]. Upon its reaction with NaOH solution, the XRD analysis (Fig. 3.12A) showed formation of only sodium carbonate, while the changes observed in clinochlore are minor. The formation of sodium carbonate is attributed to reaction of Na^+ with CO_2 from air. In TGA

(Fig. 3.12B), an additional mass loss related to physically bound water liberation is observed around 100 °C. While the mass losses around 600 °C is changing for samples at various age. However, these findings do not provide enough justification about the reactivity of clinochlore in used system.
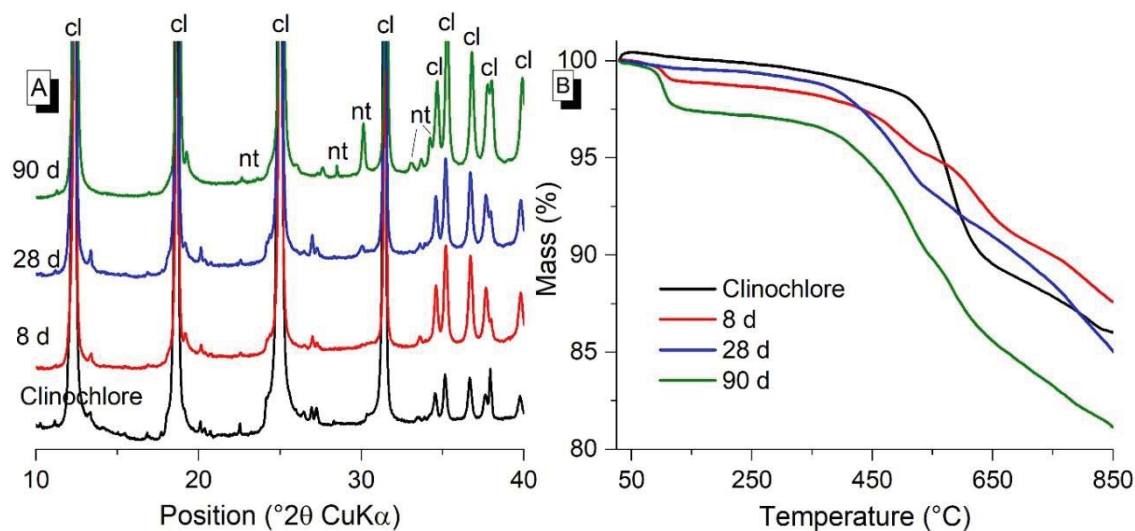

Fig. 3.12. (A) XRD, (B) TGA of the raw clinochlore and its reacted samples at 8, 28 and 90 d. For the symbols used refer to Table 3.2.

vii.   Glass phase

One of the examined phases was pumice stone found in Pozzolan Flegrea (PF). As PF was received unground, there was possibility to sort out this mineral physically and examine it separately. This pozzolan showed high content of glass phase in XRD but nevertheless, the reactivity of this pozzolan was low, as presented in chapter 2, section 2.5. Hence to examine this, the most likely glassy phase (pumice stone) of the pozzolan was collected and ground in lab. Fig. 3.13A and Fig. 3.13B show the XRD and TGA curves, respectively, for raw glassy phase and upon its reaction products with NaOH solution. After the reaction of this glassy phase with NaOH solution, by physical observations, the sample remained firstly a paste at early ages and became a thicker paste at later ages. This is comparable to the behaviour of geopolymer samples of the natural pozzolan PF (chapter 2, section 2.5).

The raw glass phase showed a wide amorphous hump in XRD with its centre approx. around 27° 2θ. After its reaction with NaOH solution, the centre of the amorphous hump shifted to a higher 2θ value (approx. 32° 2θ) at 8 d and remained same for 28 and 90 d age. Such a shift is attributed to formation of new X-ray amorphous phase or phases [7]. Additionally, at all ages, several new crystalline phases were observed. At 8 d, formation of thermonatrite was recognized, which is a sodium carbonate phase and can form because

179

of reaction between mobile Na^+ and CO_2 from air. With further progress of the reaction, formation of hydrosodalite at 28 d and clinotobermorite at 90 d is observed. Hydrosodalite (also known as hydroxysodalite hydrate) is a zeolite mineral and can also be synthesised by reaction of kaolinite and NaOH under hydrothermal conditions [8–10]. It is observed here that the formation of hydrosodalite is very slow at room temperature. Possibly, the processes of nucleation and/or growth are slow. Therefore, firstly the reactive sodium is taken up by a phase which can form fast at room temperature (thermonatrite) and with age hydrosodalite is forming. Furthermore, the formation of clinotobermorite is observed at 90 d only. The broad peaks in XRD indicate a substantial structural disorder of clinotobermorite. Highly disordered C-S-H phases can also be found for example in Portland cement reacted at room temperature conditions [11].
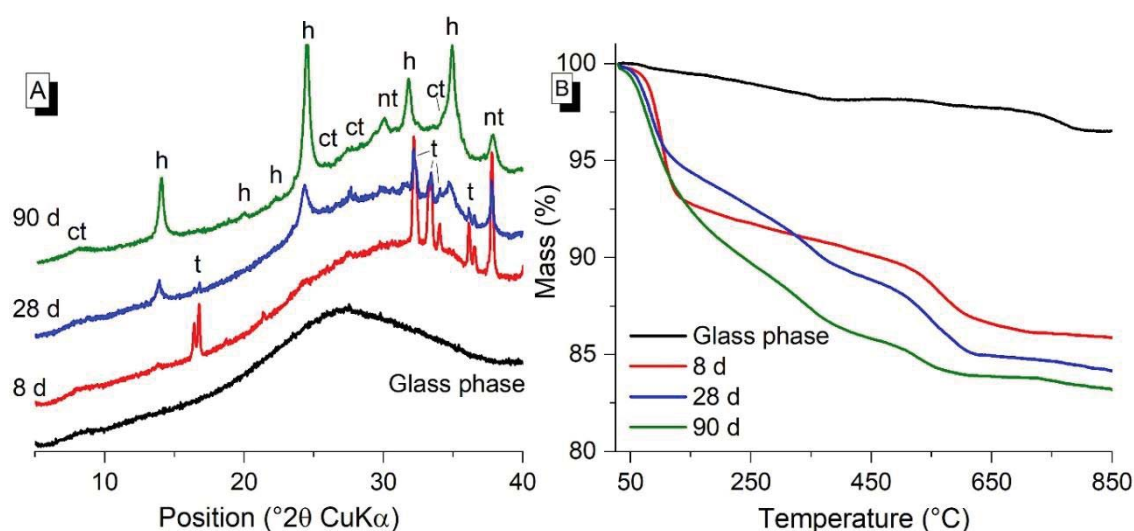

Fig. 3.13. (A) XRD, (B) TGA of the raw glass phase and its reacted samples at 8, 28 and 90 d. For the symbols used refer to Table 3.2.

In TGA of the raw sample, multiple gentle mass losses which form together a mostly continuous mass loss are observed till approx. 700 °C, this follows a better definable slight mass loss step around 760 °C. The likely explanation of this is a continuous dehydroxylation/dehydration of the glass phase and maybe decarbonation or dehydroxylation at 760 °C. After reaction, the overall mass loss is increased, and three new mass loss events are observed. The first mass loss event occurring around 100 °C can correspond to liberation of physically bound water and water in clinotobermorite. The continuous mass loss till 600 °C can be attributed to dehydroxylation of hydrosodalite as also shown in [8,12]. While the mass loss steps around 300 – 400 °C and 500 – 600 °C reflect the presence of unreacted glass phase. In 8 d sample, the mass loss curve till 600

°C is less steep compared to 28 and 90 d sample, indicating that either the amount of hydrosodalite is low or there is no hydrosodalite in 8 d sample. This is also in accordance to XRD findings. The findings of TGA and XRD correspond well to each other and confirm that this glass phase present in PF is indeed reactive but the reaction is slow as the first crystalline reaction products in tiny amount are observed after 28 d. Therefore, PF showed poor strength formation in the measured timeframe as seen in chapter 2, section 2.5.

viii. Kaolinite

The raw kaolinite is characterised with XRD (Fig. 3.14A), in addition to kaolinite, it contained minor amount of muscovite and quartz. In TGA (Fig. 3.14B) a broad mass loss around 500 °C was observed because of dehydroxylation of kaolinite's octahedral sheets [8]. In XRD of the reacted samples (Fig. 3.14A), formation of hydrosodalite and thermonatrite (sodium carbonate monohydrate) was observed. Hydrosodalite is a zeolite mineral and is in industry synthesised hydrothermally by reaction of kaolinite with NaOH solution [8]. While these findings show that the same reaction product can also be expected at ambient conditions of reaction. Furthermore, the reflexes of muscovite and quartz did not change in height indicating that these phases may not have reacted in the given conditions. Nevertheless, the reactivity of muscovite will also be determined individually later.

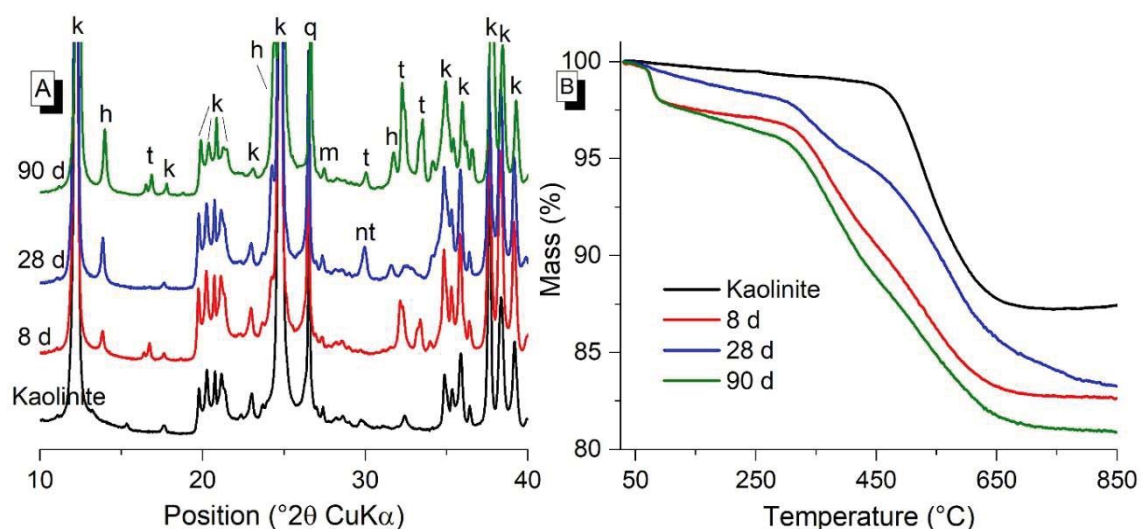**Fig. 3.14.** (A) XRD, (B) TGA of the raw kaolinite and its reacted samples at 8, 28 and 90 d. For the symbols used refer to Table 3.2.

The TGA of the reacted samples (Fig. 3.14B) correlate well the findings of XRD. The mass loss of physically bound water is observed around 80 – 90 °C. Thereafter the mass loss of hydrosodalite and unreacted kaolinite is observed till 600 °C, which is in accordance to

[8,12]. As the decomposition of sodium carbonate is happening at very high temperatures, therefore, its mass loss is not observed within the measured temperature range of the experiment [1].

ix.　Larnite

The larnite sample as characterised by XRD (Fig. 3.15A) contained no minor phases. While the raw larnite showed nearly no mass loss in TGA (Fig. 3.15B). Formation of several new phases is observed in XRD upon reaction of larnite with NaOH (Fig. 3.15A). These phases included an increase in amorphous hump with centre around 32° 2θ indicating formation of a new X-ray amorphous phase which can be likely a calcium silicate hydrate. Calcium silicate hydrate can also sorb sodium [13], which seems likely also for the system presented here. Furthermore, the crystalline phases formed included thermonatrite (sodium carbonate monohydrate) and clinotobermorite. In TGA (Fig. 3.15B), a mass loss observed around 100 °C is assigned to liberation of physically bound water or water retained in clinotobermorite and semi-crystalline phase. This is followed by a continuous mass loss till 750 °C which may indicate a continuous dehydration/dehydroxylation. In temperature range of 750 – 870 °C, a mass loss step is observed which can be assigned to destabilisation of possibly formed calcium silicate hydrates [14].
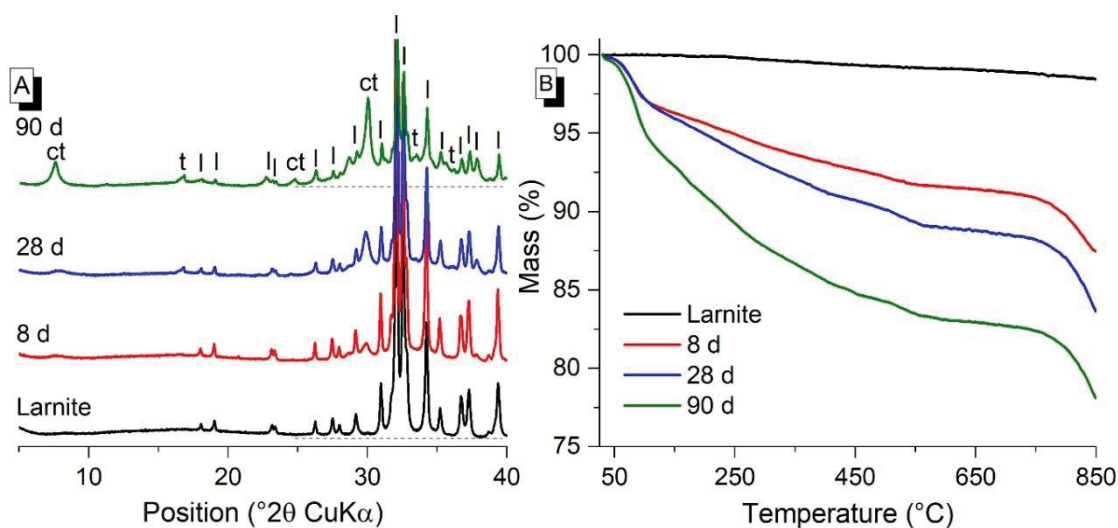

Fig. 3.15. (A) XRD, (B) TGA of the raw larnite and its reacted samples at 8, 28 and 90 d. For the symbols used refer to Table 3.2.

x.　Leucite

The raw leucite as characterised by XRD contained no minor phases (Fig. 3.16A). In TGA (Fig. 3.16B), no mass loss is observed for the raw sample. Upon its reaction, formation of

hydrosodalite and sodium carbonate / sodium carbonate monohydrate is observed (Fig. 3.16A). Formation of hydrosodalite was also observed in kaolinite and glass phase of PF after their reaction. Perhaps, the chemical composition of leucite can also favour this formation. In TGA (Fig. 3.16B), a continuous mass loss till 500 °C followed by a mass loss step which can be attributed to destabilisation of hydrosodalite [8]. This mass loss step may correspond to a carbonated hydrosodalite showing decomposition at this temperature as reported by [8,15] and also observed here. A mass loss around 100 °C can be because of liberation of physically bound water.
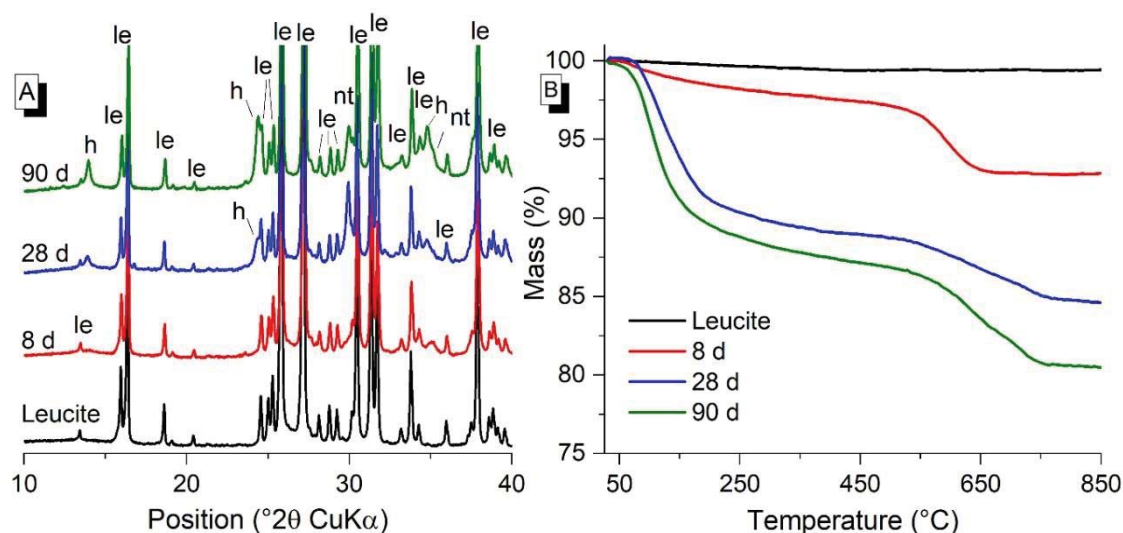

Fig. 3.16. (A) XRD, (B) TGA of the raw leucite and its reacted samples at 8, 28 and 90 d. For the symbols used refer to Table 3.2.

xi.   Montmorillonite

Raw montmorillonite as characterised by XRD consisted of montmorillonite with no minor phases (Fig. 3.17A). The TGA (Fig. 3.17B) of the raw sample showed two mass loss events, firstly a dehydration step is observed around 100 – 200 °C. While, a second mass loss event is observed around 800 °C which may correspond to dehydroxylation [4]. Upon the reaction with NaOH, the formation of sodium carbonate and hydrosodalite (Fig. 3.17A) is observed. The TGA (Fig. 3.17B) of the reacted sample showed a continuous mass loss till 500 °C which may correspond to dehydroxylation of hydrosodalite followed by a mass loss step. As mentioned above the mass loss of hydrosodalite at higher temperature could indicate presence of carbonated hydrosodalite [8,15]. Furthermore, a mass loss around 100 °C is representative of physically bound water in the system.

Fig. 3.17. (A) XRD, (B) TGA of the raw montmorillonite and its reacted samples at 8, 28 and 90 d. For the symbols used refer to Table 3.2.

xii.   Muscovite

Raw muscovite as characterised by XRD contained no other phases (Fig. 3.18A). The TGA (Fig. 3.18B) showed a mass loss in temperature range of 600 – 850 °C which is attributed to dehydroxylation of muscovite [4,16].
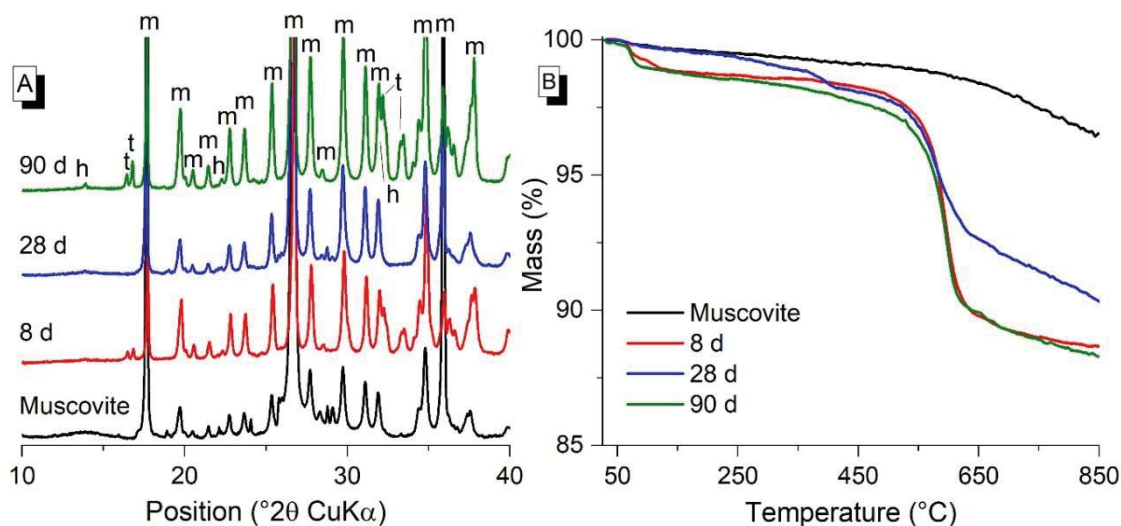
Fig. 3.18. (A) XRD, (B) TGA of the raw muscovite and its reacted samples at 8, 28 and 90 d. For the symbols used refer to Table 3.2.

Upon its reaction with NaOH, in XRD (Fig. 3.18A), formation of sodium carbonate and its monohydrate is observed. A minor amount of hydrosodalite is also observed in these samples. The TGA (Fig. 3.18B) showed a mass loss for physically bound water (around 100 °C) and a mass loss till 600 °C which may correspond to the dehydroxylation of

hydrosodalite. A mass loss step around 600 °C may also correspond to decomposition of carbonated hydrosodalite but owing to the low reflex intensity of hydrosodalite in XRD, it is possible that this mass loss belongs to another phase which is not detected by XRD.

xiii.   Nepheline

The raw nepheline sample is characterised as nepheline with a minor amount of analcime (Fig. 3.19A). In TGA (Fig. 3.19B), the raw sample showed a continuous mass loss which can be partially from dehydration of analcime or from other sources, which could not be determined with used experimental methods. Upon its reaction with NaOH, in XRD (Fig. 3.19A), several new crystalline phases were observed. These phases included sodium carbonate monohydrate and hydrosodalite. Moreover, the peaks corresponding to analcime successively reduced in their height with progress of the reaction. In TGA (Fig. 3.19B), a mass loss event corresponding to physically bound water liberation is observed around 100 °C. A continuous mass loss till 550 °C followed by a mass loss step can be attributed to hydrosodalite dehydroxylation and decomposition of carbonated hydrosodalite [8,15].
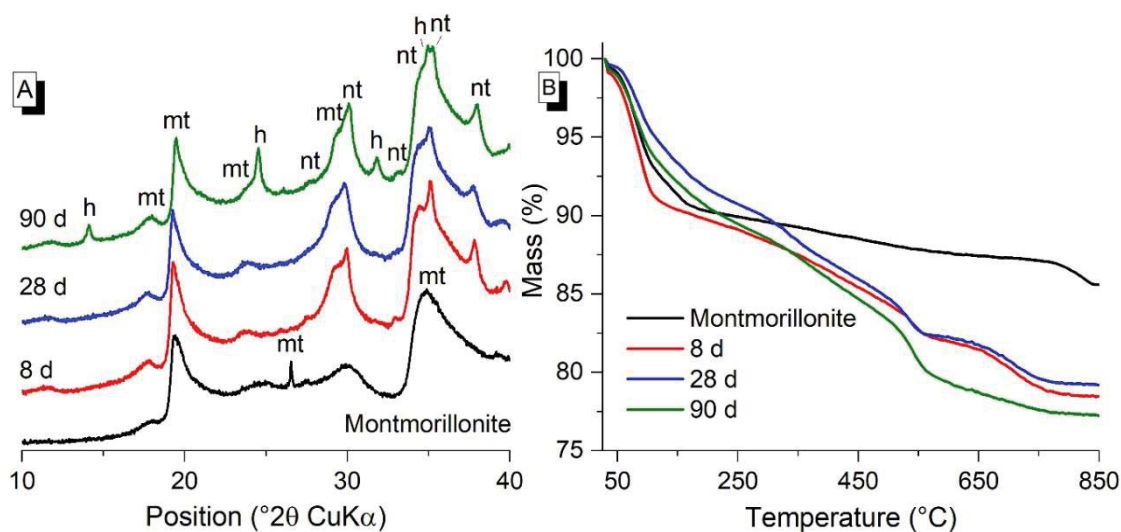

**Fig. 3.19.** (A) XRD, (B) TGA of the raw nepheline and its reacted samples at 8, 28 and 90 d. For the symbols used refer to Table 3.2.

xiv.   Phillipsite

Raw phillipsite was characterised by XRD (Fig. 3.20A) and it contained calcite as minor phase. In TGA (Fig. 3.20B), the raw phillipsite exhibited a continuous mass loss till 400 °C with a mass loss step around 100 °C. This can be attributed to liberation of water from phillipsite [4]. Upon its reaction with NaOH, formation of hydrosodalite and sodium

carbonate monohydrate is observed (Fig. 3.20A). Moreover, a continuous increase in the amorphous hump shows formation of new X-ray amorphous phase with its centre around 32° 2θ. Additionally, broadening of the peaks around 29° 2θ is also observed. TGA results also support the findings of XRD (Fig. 3.20B), as a mass loss till 600 °C is attributable to hydrosodalite dehydroxylation. Moreover, a mass loss corresponding to release of physically bound water around 100 °C is also observed.

Although calcite also reacted in the given system, the phases observed in the calcite sample reacted with NaOH (section 3.2.2. (iv)) are not observed here. This can be because of different reaction mechanism since phillipsite is the main reacting phase here and calcite is present only in minor amount. Possibly, the calcium ions from calcite are incorporated in the X-ray amorphous phase.
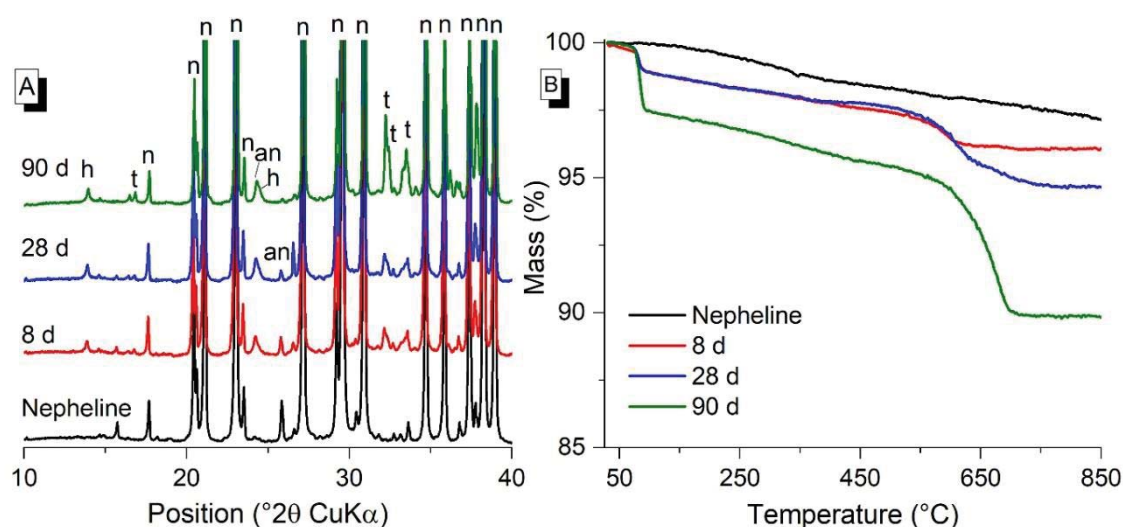

Fig. 3.20. (A) XRD, (B) TGA of the raw phillipsite and its reacted samples at 8, 28 and 90 d. For the symbols used refer to Table 3.2.

xv.   Sanidine

The raw sanidine as characterised by XRD contained no minor phases (Fig. 3.21A). In TGA (Fig. 3.21B), sanidine showed no mass loss. Upon its reaction with NaOH formation of sodium carbonate monohydrate and sodium carbonate is observed (Fig. 3.21A). Moreover, formation of a minor amount of hydrosodalite and at 90 d formation sodium hydrogensilicate pentahydrate is observed. In TGA (Fig. 3.21B), a mass loss of physically bound water is observed around 100 °C. Thereafter, a mass loss till 600 °C and a mass loss step around 600 °C can be due to hydrosodalite, and sodium hydrogensilicate pentahydrate at 90 d. Nevertheless, the low intensity of these two phases in XRD indicates that the two mass

loss events may originate not only from these two phases but also reflect presence of other phases.

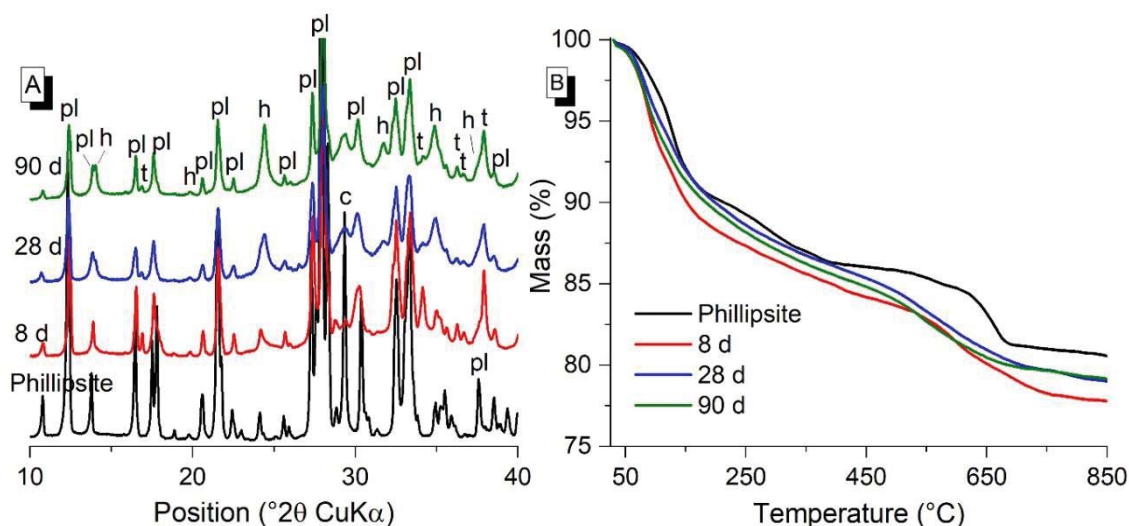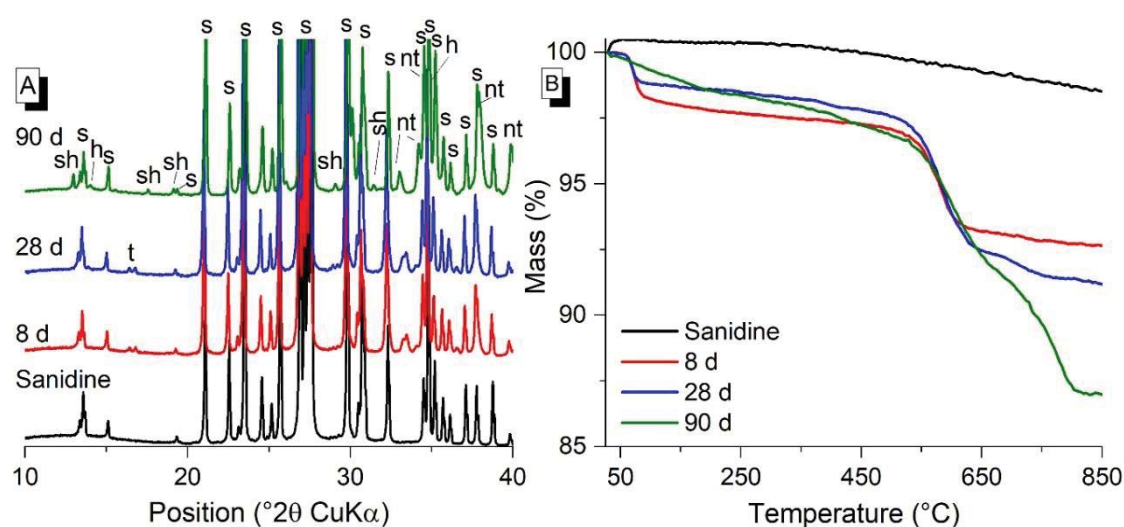**Fig. 3.21.** (A) XRD, (B) TGA of the raw sanidine and its reacted samples at 8, 28 and 90 d. For the symbols used refer to Table 3.2.

3.3. Conclusions

Based on this study, it can be confirmed that several crystalline minerals react with NaOH solution (16 mol/kg) and sodium silicate solution (Ms = 1.061). After reaction they form new phases which are crystalline to amorphous. The newly formed crystalline phases observed for several minerals included hydrosodalite, sodium hydrogensilicate pentahydrate, clinotobermorite and sodium carbonate upon reaction with sodium hydroxide. Furthermore, none of the mineral phases reacted completely in the used system. In most of the mineral samples, the share of new crystalline phases increased with the time and in most cases, the new crystalline phases can be clearly recognised only at 90 d of reaction. This emphasises that reaction of most of these minerals under used conditions is gradual. However, some minerals like kaolinite, chabazite, phillipsite and especially calcite showed a considerable amount of reaction products already after 8 d showing that these minerals have higher reaction degree compared to other investigated minerals. The reaction products of calcite are unique, indicating that calcite behaves different than other studied minerals, which will be mainly because it is a carbonate mineral and all others are silicate minerals.

A summary of the reaction of minerals with sodium silicate and sodium hydroxide solution is presented in Table 3.3 and 3.4, respectively. The reactivity of each mineral for each

method is characterised by high, medium, or low. Based on the results of each method the reactivity of each mineral is interpreted with respective solutions. The results show that chabazite showed high reactivity with sodium silicate solution. While, calcite, chabazite, kaolinite, larnite and phillipsite showed higher reactivity with sodium hydroxide solution.

Table 3.3. Summary of the reactivity of minerals with sodium silicate solution.

Sr. no.	Mineral sample	Calorimetry (first 24 h)	TGA (after 28 d)	XRD (after 28 d)	Overall intensity of reaction
1	Albite	+	Ø	Ø	Ø
2	Augite	+	Ø	Ø	Ø
3	Chabazite	Ø	++	++	++
4	Clinochlore	Ø	++	Ø	Ø
5	Muscovite	Ø	Ø	Ø	Ø
6	Sanidine	+	+	Ø	Ø

++ high, + medium, Ø low

Table 3.4. Summary of the reactivity of minerals with sodium hydroxide solution.

Sr. no.	Mineral sample	Calorimetry (first 120 h)	TGA (after 90 d)	XRD (after 90 d)	Overall intensity of reaction
1	Albite	Ø	++	+	Ø
2	Augite	Ø	++	+	Ø
3	Biotite	Ø	++	+	Ø
4	Calcite	++	++	++	++
5	Chabazite	++	++	++	++
6	Clinochlore	Ø	++	Ø	Ø
7	Glass phase	+	++	+	+
8	Kaolinite	Ø	++	++	++
9	Larnite	Ø	++	++	++
10	Leucite	+	++	+	+
11	Montmorillonite	Ø	++	+	+
12	Muscovite	Ø	++	+	Ø
13	Nepheline	Ø	++	+	+
14	Phillipsite	++	++	++	++
15	Sanidine	+	++	+	+

++ high, + medium, Ø low

References

[1] Kim J-W, Lee H-G. Thermal and carbothermic decomposition of Na_2CO_3 and Li_2CO_3. Metall. Mater. Trans. 2001;32B(1):17–24. https://doi.org/10.1007/s11663-001-0003-0.

[2] Schmid RL, Felsche J. Thermal studies on sodium silicate hydrates. I. Trisodium hydrogensilicate pentahydrate, $Na_3HSiO_4·5H_2O$; thermal stability and thermal decomposition reactions. Thermochim. Acta 1983;71:359–64.

[3]   Ortega-Zavala DE, Santana-Carrillo JL, Burciaga-Díaz O, Escalante-García JI. An initial study on alkali activated limestone binders. Cem. Concr. Res. 2019;120:267–78. https://doi.org/10.1016/j.cemconres.2019.04.002.

[4]   Földvári M. Handbook of thermogravimetric system of minerals and its use in geological practice. Budapest: Geological Inst. of Hungary; 2011.

[5]   Scrivener K, Snellings R, Lothenbach B (eds.). A Practical Guide to Microstructural Analysis of Cementitious Materials. Boca Raton: CRC Press; 2016.

[6]   Bordeneuve H, Wales DJ, Physick AJW, Doan HV, Ting VP, Bowen CR. Understanding the AC conductivity and permittivity of trapdoor chabazites for future development of next-generation gas sensors. Microporous Mesoporous Mater. 2018;260:208–16. https://doi.org/10.1016/j.micromeso.2017.10.032.

[7]   Sun Z, Vollpracht A. Isothermal calorimetry and in-situ XRD study of the NaOH activated fly ash, metakaolin and slag. Cem. Concr. Res. 2018;103:110–22. https://doi.org/10.1016/j.cemconres.2017.10.004.

[8]   Marsh A, Heath A, Patureau P, Evernden M, Walker P. A mild conditions synthesis route to produce hydrosodalite from kaolinite, compatible with extrusion processing. Microporous Mesoporous Mater. 2018;264:125–32. https://doi.org/10.1016/j.micromeso.2018.01.014.

[9]   Luger S, Felsche J, Fischer P. Structure of hydroxysodalite $Na_8[AlSiO_4]_6(OH)_2$, a powder neutron diffraction study at 8 K. Acta. Crystallogr. Sec. C Cryst. Struct. Commun. 1987;43(1):1–3. https://doi.org/10.1107/S0108270187097233.

[10] Provis JL, van Deventer JSJ (eds.). Geopolymers: Structure, processing, properties and industrial applications. Boca Raton, Fla.: CRC; Oxford Woodhead; 2009.

[11] Hewlett PC, Lea FM (eds.). Lea's chemistry of cement and concrete. 4th ed. Oxford: Elsevier Butterworth-Heinemann; 2004.

[12] Engelhardt G, Felsche J, Sieger P. The hydrosodalite system $Na_{6+x}[SiAlO_4]_6(OH)_x \cdot nH_2O$: formation, phase composition, and de- and rehydration studied by ^{1}H, ^{23}Na, and ^{29}Si MAS-NMR spectroscopy in tandem with thermal analysis, X-ray diffraction, and IR spectroscopy. J. Am. Chem. Soc. 1992;114(4):1173–82.

[13] Lothenbach B, Kulik DA, Matschei T, Balonis M, Baquerizo L, Dilnesa B et al. Cemdata18: A chemical thermodynamic database for hydrated Portland cements and alkali-activated materials. Cem. Concr. Res. 2019;115:472–506. https://doi.org/10.1016/j.cemconres.2018.04.018.

[14] Tajuelo Rodriguez E, Garbev K, Merz D, Black L, Richardson IG. Thermal stability of C-S-H phases and applicability of Richardson and Groves' and Richardson C-(A)-S-

H(I) models to synthetic C-S-H. Cem. Concr. Res. 2017;93:45–56. https://doi.org/10.1016/j.cemconres.2016.12.005.

[15] Buhl J-C. The properties of salt-filled sodalites: Part 3. Synthesis and thermal behaviour of basic and non-basic carbonate enclathrated sodalites. Thermochim. Acta 1993;219:205–14.

[16] Gaines GL, Vedder W. Dehydroxylation of Muscovite. Nature 1964;201(4918):495. https://doi.org/10.1038/201495a0.

Chapter 4

Main results and discussion

This chapter presents the discussion on the major results presented in chapter 2 and chapter 3 and aims to summarise the major findings.

4.1. Raw material processing and preliminary work

The first step of the study included the processing of raw materials in order to obtain homogenous samples with comparable Blaine fineness measured in accordance to EN 196-6 [1]. This method was chosen for the specific surface area determination as it is in common practice in cement industry. Later, particle size distribution was also measured with laser granulometry. For obtaining homogeneous samples with comparable Blaine fineness, a grinding methodology was defined which included drying of the samples followed by crushing of big stones to size < 1 mm. After that, samples were homogenized according to EN 932–2 [2] in order to obtain equal representative portions. These portions were ground in a planetary ball mill. This methodology enabled a better comparison of the reactivity of the raw pozzolans as geopolymer precursor. The six pozzolans used as raw materials for geopolymer synthesis included Rhenish trass (RT), Bavarian trass (BT2/BT and BT1), pozzolan Laziale red (PLR), pozzolan Laziale black (PLB) and pozzolan Flegrea (PF). Their chemical and mineralogical compositions are presented in chapter 2, section 2.2, Table 1 and Fig. 1, respectively. A summary of the mineralogical phases present in each pozzolan is shown in Table 4.1. *(Note: It is worth to mention here that BT2 in section 2.2 and BT in section 2.3 & 2.4 are two different abbreviations used for same material. However, in this chapter abbreviation BT will be used.)*

The second step was to determine the type of alkaline solution for better mechanical performance. Therefore, trial samples were made with sodium hydroxide solution, potassium hydroxide solution and sodium silicate solution of varying concentrations. The compressive strength results for all natural pozzolans showed that the best mechanical strength is achieved using sodium silicate solution as the alkaline activator. Therefore, mostly sodium silicate solutions were used in the further study.

Table 4.1. Mineralogical composition of all natural pozzolans

Mineral Group	Natural pozzolan sample					
	BT1	BT	RT	PLB	PLR	PF
Feldspars	Sanidine, albite	Sanidine, albite	Sanidine, albite	--	--	Sanidine, albite, anorthite
Foids	--	--	Nepheline, leucite	Nepheline, leucite	Nepheline, leucite	--
Zeolites	--	--	chabazite, phillipsite, analcime	Analcime	Analcime	Analcime
Micas	Biotite	Biotite	Muscovite, biotite	Muscovite	Muscovite	Muscovite
Pyroxenes	Augite	Augite	Augite	Augite, diopside (ferrian)	Augite, diopside (ferrian)	--
Soro-silicates	--	--	--	Akermanite	Akermanite	--
Neso-silicates	--	--	Larnite	Chloritoid	--	--
Carbonates	Calcite	Calcite	Calcite	--	--	--
Oxides	Quartz	Quartz	Quartz	Quartz, magnetite, hematite	Quartz, magnetite, hematite	Quartz

4.2. Silica modulus, age and compressive strength

The first objective was to investigate the effect of silica modulus of silicate solution and curing time on compressive strength of the six pozzolans. For the purpose, sodium silicate solutions of 16 various silica moduli were used, and samples were tested at various ages.

In compressive strength measurements, all the raw samples used had a distinct behaviour. Precursors including PLB, PLR, PF and BT1 did not exhibit significant reactivity in used alkaline system. While RT and BT showed significant compressive strength at all tested ages. The reason of such differences in the reactivity was assigned to the chemical composition and mineralogy of the pozzolan itself, as the other influencing factors (Blaine surface area, curing conditions, activator solutions) were kept constant. Therefore, the further investigations about effect of silica modulus and age were conducted only for RT and BT.

From results presented in chapter 2, section 2.2 and 2.3, it can be concluded that for both natural pozzolans, there is a range of silica modulus in which the highest compressive strength can be achieved. However, this range of silica modulus, called optimum silica modulus, is different for both natural pozzolans. For RT geopolymers, this range was

recorded as 0.946 – 1.272, while for BT geopolymers this range was recorded as 0.707 – 0.797 till 28 d age. Additionally, the BT samples made with silica moduli of 0.946 and 1.061 exhibited also better performance than the other samples outside optimum range. The optimum silica modulus ranges for both pozzolans differ likely because of the chemical and mineralogical characteristics of the natural pozzolans. With further increase or decrease of silica modulus beyond the optimum, the compressive strength significantly decreased for both natural pozzolan-based geopolymers. The rate of reduction of compressive strength was found to be higher for the samples on the lower silica modulus side. For increasing concentration of alkalis in the system (lower silica modulus), such a reduction in compressive strength was assigned to high amount of free alkali in the system [3]. While for the higher silica modulus, the reduction in compressive strength was assigned to lower pH of the solution, high degree of polymerization of silicate species and high viscosity of alkaline solution [4,5].

Furthermore, the rate of strength gain with age is depended on the silica modulus of alkaline solution used (chapter 2, section 2.3, Fig. 2 and 3). It was observed that with the age of the sample, the samples in optimum silica modulus range showed increase of the strength. However, the samples laying outside the optimum range of silica modulus exhibited loss of strength with age or relatively lower rate of strength increase. Such a loss of strength with age can be attributed to a possible weakening of the geopolymer structure with age, due to depletion of alkalis or unstable geopolymer gel formation [6,7].

Moreover, it was found that not only the silica modulus of alkaline solution but also the H_2O/Na_2O molar ratio of alkaline solution effects the rate of reaction. For alkaline solution with H_2O/Na_2O molar ratio higher than 19, a significant drop in compressive strength was observed (chapter 2, section 2.2, Fig. 2). This was assigned to the diluting effect of water and lower relative amount of Na_2O to efficiently dissolve the reactive phase. Therefore, while designing a binder to achieve higher compressive strength, attention must be given to both silica modulus and H_2O/Na_2O.

For BT geopolymer samples with higher share of alkalis, formation of alkali carbonate remained a problem (chapter 2, section 2.3, Fig. 3). In some samples, alkali carbonate was observed only on the surface of the sample. While in samples made with silica modulus of 1.158 and 1.272, the extended alkali carbonate development under the surface of the sample or in macropores caused complete destruction of the samples (as shown in Fig. 3b of chapter 2, section 2.3). On one hand, this can be attributed to the low reactivity of these samples, where the free alkalis can cause formation of alkali carbonate. On the other hand, it can be because of the mineralogical composition of the pozzolan. This pozzolan

contained calcite, which was largely consumed while geopolymerization (chapter 2, section 2.3). The reaction of calcite in the sample liberates carbonate, which may form sodium carbonate. Furthermore, calcite also provides calcium which can be incorporated in the gel phase and reducing the binding of alkalis from the alkaline solution in the gel. These alkalis which does not incorporated in the gel can additionally contribute to alkali carbonate formation. These findings were further investigated and will be summarised here in section 4.7.2. Alkali carbonates formed from the reaction of mobile alkalis with environmental carbon dioxide are referred to as efflorescence [7,8]. However, the results indicate that also carbonate from calcite in the sample can be source for formation of alkali carbonate. Possibly, the definition of efflorescence should be extended to this mechanism or a new term should be introduced. Irrespective of the reason for alkali carbonate formation within the binder, the development of alkali carbonate can cause internal crystallization pressure, generating inner tensile stresses and therefore weakening the structure and/or causing complete destruction.

Looking at both RT and BT geopolymers, it was found that the rate of efflorescence development depends on the reactivity of natural pozzolan (which in turn depends on the mineralogical and chemical composition of the natural pozzolan). RT had higher reactivity in the used alkaline solutions in comparison to BT as shown by higher compressive strength for RT geopolymers. Consequently, RT geopolymers were less affected by formation of alkali carbonate compared to corresponding BT geopolymers. The lower reactivity of BT, the higher calcite content and higher alkali mobility in BT geopolymers, resulted in formation of alkali carbonates comparable to sub- or efflorescence, which can in turn cause depletion of alkalis and water in the system [6], and thus further reducing the rate of strength development and can cause strength loss.

4.3. Implementation of reactivity enhancement methods

Owing to the low reactivity of PLB, PLR, PF and BT1, reactivity enhancement methods were applied on some of these pozzolans. This included implementation of heat curing on PLB- and PF-based geopolymers. Furthermore, as BT contained high amount of calcite, which was thought to be responsible for alkali carbonate formation in its geopolymer samples and consequent damage of the structure. This precursor was subjected to heat treatment and mechanical activation for reactivity enhancement followed by its use in geopolymer production. The details of these studies are discussed in the sections below.

4.3.1. Heat treatment and mechanical activation applied on BT

Several BT geopolymer samples exhibited a substantial formation of alkali carbonate. In order to improve the reactivity and reduce the alkali carbonate development in BT geopolymer samples, the raw sample was subjected to whether mechanical activation or heat treatment. The determination of the optimum conditions for mechanical activation and heat treatment was not in the scope of this study, rather a comparative study was made between the influence and effectiveness of these two reactivity enhancement methods. A method of mechanical activation between the subcategories mechanical dispersion and surface activation as defined by [9,10] was chosen. The mechanical activation was performed by milling the material at two milling durations (5 and 10 min) and speed of 200 rpm with constant media to material ratio (1:0.16). With the applied mechanical activation methodology, the d_{50} particle size was reduced by 23% or 43% for 5- or 10-min milling, respectively.

In contrast, calcination was applied as a heat treatment methodology. As the results presented in chapter 2, section 2.3 showed that one of the reasons for alkali carbonate development in BT geopolymers was the higher calcite content. Therefore, heat treatment methodology was designed to reduce the calcite content i.e. burning BT in muffle furnace at 700 °C for 3 h followed by cooling to room temperature in a desiccator with silica gel. As a result of heat treatment (calcination), calcite was partially converted to lime. The mechanically activated as well as the heat-treated raw materials were subjected to react with sodium silicate solution of silica modulus 0.707, 0.797 and 1.061.

Results of compressive strength (chapter 2, section 2.4, Fig. 3) showed that for heat-treated BT, the compressive strength increased significantly, while for mechanically activated samples only a marginal increase in the compressive strength was recorded (chapter 2, section 2.4, Fig. 4). Moreover, for heat treated raw material, the alkali carbonate formation decreased significantly. While, for mechanically activated sample, no significant improvement in this was observed. From the visual observation of the samples presented in Table 2 of section 2.4, the alkali carbonate formation reduced significantly in the samples prepared with silica modulus of 0.797 and 1.061 while using BTC (calcined BT). However, for sample prepared with silica modulus of 0.707 using BTC, the alkali carbonate increased. For samples BTC-0.797 and BTC-1.061 compressive strength also increased significantly in comparison to not-treated samples, while for sample BTC-0.707 the increase in compressive strength was marginal. This shows that the samples BTC-0.797 and BTC-1.061 precipitate enough geopolymer gel to incorporate most of alkalis and therefore lesser

alkali carbonate formed. While, for sample BTC-0.707 alkaline concentration was too high to be incorporated in geopolymer gel. Hence this sample exhibited high alkali carbonate content.

For mechanically activated samples i.e. BT5 (BT milled for 5 min) and BT10 (BT milled for 10 min), no appreciable changes in alkali carbonate and compressive strength were observed. Table 4.2 shows visual observations of alkali carbonate in BT, BT5 and BT10 samples prepared with silica modulus of 0.707 after 14 d. Comparing both reactivity enhancement methods applied on BT, it can be concluded that for this precursor the heat treatment is the more effective method. Furthermore, looking at the particle size distribution curves (chapter 2, section 2.4, Fig. 1a), BTC had higher fraction of coarser particles as compared to BT5 and BT10. However, the heat treatment in BTC imparted higher reactivity than reduced particle size in BT5 and BT10. Such a behaviour indicated that heat treatment or partial conversion of calcite to lime had higher impact as compared to reduced particle size.

Table 4.2. Visual observation of BT, BT5 and BT10 samples at 14 d age.

Sample	BT-0.707	BT5-0.707	BT10-0.707
Alkali carbonate development after 14 d			

4.3.2. Effect of heat curing on PLB- and PF-based geopolymers

As mentioned in the above section, the pozzolans PLB, PLR, PF and BT1 had low reactivity in used alkaline system. Therefore, a heat curing regime was used on the prepared geopolymer samples to evaluate its impact on the geopolymerization activity. For the purpose, PLB and PF were chosen as the precursor. Geopolymer samples were prepared using sodium hydroxide, potassium hydroxide and sodium silicate solutions with two concentrations/silica moduli of each solution. For comparison, two heat curing methods were simultaneously used: a) curing at 22 °C for all test ages and b) curing at 40 °C for first 28 d followed by room temperature curing till 90 d.

Results showed that PLB showed better reactivity in comparison to PF at ambient curing conditions (chapter 2, section 2.5, Fig. 1). While PF samples showed a comparatively

negligible reactivity for all types of solutions used. With implementation of heat curing for first 28 d, the compressive strength increased for both geopolymer systems, showing that higher temperature helps in increasing the dissolution of reactive phase and thus the geopolymer reaction accelerates. However, for all PLB samples, loss of strength was observed after 28 d. Such a loss of strength can be assigned to change of curing condition i.e. samples were moved from 40 °C to 22 °C. This can be attributed to possible formation and then collapse of an unstable geopolymer gel microstructure [7].

4.4. Silica modulus and reaction kinetics

4.4.1. Relationship between silica modulus and reaction kinetics

Reaction kinetics for RT- and BT-based geopolymers were studied by isothermal conduction calorimetry for first 7 d of reaction (chapter 2, section 2.2, Fig. 3 and 4). Samples were mixed outside the device. The results showed that geopolymer reaction is an exothermic reaction for all natural pozzolan-based geopolymers. For all samples, the calorimetric curves showed a first exothermic peak which is because of the first wetting and dissolution of reactive phase(s) and occurred within first few minutes of mixing. This peak was followed by lower heat evolution and decrease of dissolution rate associated to the polycondensation of the geopolymer product [11–14]. It was found that the time span of the deceleration phase is depended on the silica modulus of alkaline solution used. The rate constant (k) was determined by implementation of pseudo-first order kinetics on the calorimetric data. The correlation between silica modulus and rate constant showed that the rate constant decreases with increase of silica modulus (chapter 2, section 2.2, Fig. 5). However, the absolute concentration of Na_2O and SiO_2 have significant impact. Samples rich in Na_2O and SiO_2 content showed higher rate constant at early age. Therefore, it was concluded that in addition to silica modulus, higher concentration of Na_2O and SiO_2 can be used to accelerate the reaction at early age.

4.4.2. Second exothermic peak in calorimetric study of BT

BT geopolymers made with silica modulus of 0.707, 0.797 and 1.061 additionally exhibited a second exothermic event in calorimetry (chapter 2, section 2.2, Fig. 4). The possible reaction at this peak could be connected to its calcite content. This finding was confirmed by the calorimetric study of BT batches which were heat-treated (BTC) or mechanically activated (BT5 & BT10) (chapter 2, section 2.4, Fig. 5 and 6). As a result of heat treatment, the calcite was converted to lime, consequently, in calorimetric study, this second

exothermic peak shifted to earlier time or was not observed. Such a shift in reaction time was attributed to presence of lime in the system. As the reaction of lime with water can lead to rise in the pH of the system [15] and thus the rate of reaction increased and therefore, this peak shifted to earlier time, showing that the reaction occurring at this peak is related to its calcite content.

For mechanically activated BT samples, the reason for low improvement in reactivity and reaction occurring at second peak was also investigated by a calorimetry study. For this purpose, the BT, BT5 and BT10 samples were fractionated in order to obtain a fine fraction (< 40 µm) and a coarse fraction (> 40 µm). Such a portioning was made to split the bimodal particle size distribution curve. The XRD study on these samples (chapter 2, section 2.4, Fig. 7) showed that the lower fraction was rich in calcite, while the coarser fraction was rich in minerals with higher Mohs scale hardness. Whereas, as a result of further grinding, the agglomeration of calcite particles caused a successive increase in the calcite content of coarser fraction.

Calorimetric study on these separated fractions showed that the fraction < 40 µm had higher reactivity compared to the coarser fraction. The second exothermic peak was observed only for the fraction < 40 µm in samples BT and BT5. Whereas in sample BT10, both fractions exhibited this peak. With increasing fineness, this peak shifted to earlier time, peak height reduced and time span on which reaction occurred increased. Such a behaviour was correlated to the calcite content of the samples. Because of the agglomeration of calcite and subsequent decrease in the calcite content of BT5 < 40 µm and BT10 < 40 µm, the peak height decreased. Meanwhile, the calcite content increased in BT5 > 40 µm and BT10 > 40 µm, and in BT10 it reached to the limit that both fractions exhibited a second exothermic peak. Such separation of BT, BT5 and BT10 resulting in calcite separation gave additional indication that the second exothermic peak in these samples is related to their calcite content. Moreover, the results showed that the grinding in a planetary ball mill is mostly effective in reducing the size of larger particles, while the reactive fraction of BT was already smaller than 40 µm. This is indicated by twice as much heat production for this fraction compared to the coarser fraction (chapter 2, section 2.4, Fig. 6). Because of this, the improvement in reactivity for BT5 and BT10 was only marginal.

4.5. Silica modulus, age and extent of geopolymer reaction

The effect of silica modulus and age on extend of geopolymerization was studied by thermogravimetric analysis (TGA) and selective dissolution. Samples of 28 d age were

used for determining the effect of silica modulus on extend of geopolymer reaction. While to determine the effect of age, selected silica modulus samples were tested at 7, 28 and 90 d age.

Mass loss in TGA in the temperature range of 30 – 600 °C is characteristic of bound water in the geopolymer gel. The bound water in geopolymer gel can be characterised as physically bound water, chemically bound water molecules (zeolitic water) and OH groups [7,16]. The loss of physically bound water is considered till 150 °C. This water is released during condensation of the geopolymer gel and does not take part in the dissolution of aluminosilicate species [11,17–20]. While the chemically bound water molecules come from the dissolution of aluminosilicate species to form aluminate and silicate species and remain after condensation. The OH groups are present at the surface and edges of geopolymeric chains [16,20]. The mass loss of chemically bound water molecules is considered from 150 – 300 °C and the mass loss from OH groups is considered from 300 – 600 °C [16,20]. To determine the effect of silica modulus on the extend of geopolymerization, the mass losses of chemically bound water molecules and OH groups were considered separately for 28 d old samples. The results of chemically bound water molecules and OH groups for RT and BT geopolymers plotted against silica moduli showed a close relation with the compressive strength (chapter 2, section 2.2, Fig. 8). A higher amount of chemically bound water molecules showed the formation of more condense geopolymer gel thus generating higher compressive strength. The mass loss of OH groups is not just representative of the extend of dissolution but is also affected by the polymerization degree. A higher OH mass loss for BT geopolymers indicates a lower degree of polymerization in these samples as compared to RT geopolymers. Combing these results with findings of selective dissolution (chapter 2, section 2.2, Fig. 6), RT geopolymers have higher amount of reaction product and the reaction product formed is more condensed thus giving higher compressive strength.

The degree of reaction determined by selective dissolution (chapter 2, section 2.2, Fig. 6) decreased with increase of silica modulus for both pozzolans. The RT-based geopolymers exhibited higher degree of reaction for all silica moduli compared to BT-based geopolymers. However, for RT geopolymers prepared with lower silica modulus, selective dissolution showed formation of higher amount of reaction product formed, while TGA showed higher OH content (chapter 2, section 2.2, Fig. 8) which may indicate lower degree of polymerization. This can be a possible reason for lower compressive strength of samples prepared with lower silica modulus of alkaline solution in comparison to the optimum

samples of RT geopolymers. Furthermore, the depletion of excess alkalis because of efflorescence can have detrimental effect [3,6,21].

For RT geopolymers with the age of sample, the overall amount of bound water increased. However, the rate of increase showed dependence on the silica modulus (chapter 2, section 2.3, Fig. 6). The sample RT-1.272 exhibited higher compressive strength at 90 d, while the bound water content was nearly same as for other samples. Though, the degree of reaction as measured by selective dissolution was nearly 18% lesser than for other samples (chapter 2, section 2.3, Fig. 7). Such a behaviour was thought to be because of unreacted activator, as the activator (sodium silicate) in liquid or dried form showed no dissolution in the acidic medium used for selective dissolution.

For BT geopolymers, both the bound water and degree of reaction decreased with age of sample (chapter 2, section 2.3, Fig. 6). The loss of bound water with age is attributable to the alkali carbonate formation in these samples, as the mobile Na^+ and OH^- can react with atmospheric CO_2 or CO_3^{2-} from the sample to form sodium carbonate monohydrate, thus depleting the geopolymer matrix in alkalis and water [21]. Such depletion of alkalis is a potential reason for lower rate of strength development and reduction of strength at later ages. Similarly, sample BTC-0.707 exhibited excess alkali carbonate and the mass loss of bond water decreased with the age of the sample (chapter 2, section 2.4, Table 3). This once again confirmed that alkali carbonate in these samples is cause of depletion of alkalis and water, thus causing reduction in the rate of strength development. Alternatively, in samples BTC-0.797 and BTC-1.061, the bound water increased with the age and these samples also exhibited less alkali carbonate and improvement in compressive strength (chapter 2, section 2.4, Fig. 3 and Table 2).

Furthermore, it was found that the selective dissolution method cannot be accurately applied on the low reactive natural pozzolans prone to form sodium carbonate monohydrate in geopolymer samples, as this phase dissolved completely in the used acidic solutions, thus giving false indication about the degree of reaction.

In TGA, two additional thermal events were observed in the BTC samples (chapter 2, section 2.4, Fig. 8), where the first signal observed between 160 – 300 °C was assigned to dehydration of C-S-H. While the presence of C-S-H was confirmed by the second thermal event at around 795 °C which showed destabilization of C-S-H to wollastonite. Such conversion has been also observed in the literature [22,23] and was also confirmed here by conducting XRD on the decomposed residue as shown in Fig. 4.1. Formation of C-S-H in these samples was attributed to conversion of calcite to lime as result of applied

calcination process which imparted more reactive calcium. The presence of combeite in the decomposed residue may indicate the presence of sodium calcium silicate hydrate in the geopolymer gel [24].
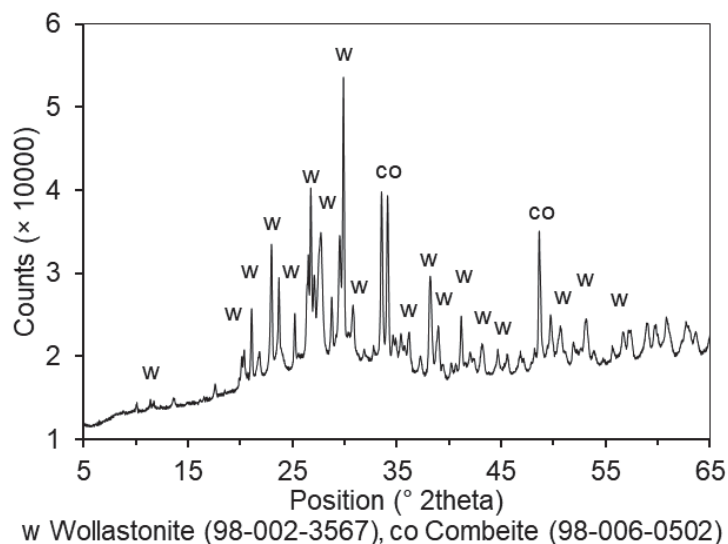

w Wollastonite (98-002-3567), co Combeite (98-006-0502)

Fig. 4.1. Sample BTC-0.797-28 d after burning at 850 °C for 5 h showing formation of wollastonite and combeite.

4.6. Silica modulus, age and phase composition of geopolymers

Phase composition of RT- and BT-based geopolymers was studied by X-ray diffraction analysis (XRD). Study was made for all silica modulus samples at 28 d age and selected samples additionally at 7 and 90 d age. The results gave insight about the reactivity of several crystalline as well as the amorphous phases. The composition of the amorphous phase for different natural pozzolans used was considered to be different. However, an accurate quantification of these crystalline and amorphous phases was not possible, because of the high number of phases and relatively complex composition of some phases. Nevertheless, the changes observed in amorphous phase (as discussed below and presented in chapter 2, section 2.2, 2.3 and 2.4) gave indication about its participation in geopolymer reaction, which is in accordance to the reported literature [25].

XRD study on RT geopolymers for various silica moduli and ages (chapter 2, section 2.2, Fig. 9; and section 2.3, Fig. 4 and Fig. S1) showed that several crystalline minerals may partially participate in geopolymer reaction, which include calcite, phillipsite, larnite and chabazite, as indicated by reduction of their peak height. While crystalline phases such as sanidine, leucite, biotite, muscovite and nepheline were superimposing in their reflexes with the above-mentioned phases and consequently, no clear statement about their behaviour

can be made. The main amorphous hump in RT moved its centre to higher 2θ values (from approx. 27° to 31° 2θ) as a result of geopolymerization. This indicates the changes in amorphous phase composition or formation of new amorphous phase or phases [26,27]. Furthermore, the area of amorphous hump increased for RT geopolymer samples in comparison to the raw sample, showing that the amount of semi-crystalline phase has increased because of geopolymer reaction. The results of XRD for various silica moduli and ages were in good agreement with the results of compressive strength, TGA and selective dissolution. As a result of geopolymerization in RT samples, formation of a semi-crystalline geopolymer gel was also indicated by increase of reflex intensity at 29.8° 2θ which displayed similarity to zeolite Y structure. Moreover, the broadening of reflexes around 35° and 37.8° 2θ was also indicative of formation of aluminosilicate gel structure in RT geopolymers [28].

Similarly, for BT the results presented in chapter 2, section 2.2, Fig. 10; and section 2.3, Fig. 4, S2 and S3 showed presence of two amorphous humps ranging 5.5° – 8.5° 2θ and 24° – 34° 2θ in raw BT. The first amorphous hump was assigned to presence of some clay mineral or zeolite phase. As a result of geopolymerization, the centre of this hump moved, which indicates the participation of this phase in geopolymer reaction and likely also the formation of aluminosilicate gel [28]. Like RT geopolymers, for BT geopolymers the centre of main amorphous hump (24° – 34° 2θ) also shifted to higher 2θ value, indicating formation of a new amorphous phase (aluminosilicate gel). Alkali carbonate formation in these samples was reflected by observation of a new phase named natrite (γ-Na_2CO_3). Natrite is the dehydrated alkali carbonate as the originally formed alkali carbonate, thermonatrite ($Na_2CO_3 \cdot H_2O$), converted to natrite as consequence of applied freeze-drying methodology. Such a conversion of thermonatrite to natrite was advantageous for accurate determination of extent of reaction. Moreover, formation of aragonite (a polymorph of calcium carbonate) was also observed in samples with high alkalinity of activating solution. Formation of this phase under high alkaline conditions was also observed in literature [29,30]. Moreover, this phase has also been observed to form due to carbonation in alkali activated materials [31,32]. However, because of the lower stability of this phase at ambient conditions, it was not observed in all samples at all ages [33]. In several samples, some new reflexes were observed, though these reflexes showed characteristics of low crystallinity and could not be identified clearly.

As a result of heat treatment of BT (preparation of BTC sample), the first amorphous hump was not recorded anymore, and formation of lime was observed (chapter 2, section 2.4, Fig. 9 and 10). The calcite present in BT partially decomposed to lime and carbon dioxide

as consequence of calcination. However, other than this BTC geopolymers showed similar characteristics as BT geopolymer samples. In BTC geopolymers, lime was completely utilized as indicated by the absence of lime peaks in BTC geopolymer samples. While calcite peaks only reduced in height. In BT and BTC geopolymer samples, reflex intensities were reduced for some crystalline phases such as calcite, biotite and sanidine, indicating that these phases may also be partially participating in the reaction. The scanning electron microscopic study (chapter 2, section 2.4, Fig. 12 and 13) showed that the geopolymer gel in BT- and BTC-based geopolymers is a combination of N-A-S-H and C-N-A-S-H, though K, Mg and Fe were also found as cations. While it possessed zeolite-like structure in RT geopolymers (chapter 2, section 2.2, Fig. 9; and section 2.3, Fig. 4). Furthermore, the participation of calcite (discussed in detail in section 4.7.2) showed that presence of calcite promotes availability of Ca for gel phase.

4.7. Reactivity of minerals under alkaline conditions

In the context of results presented so far, it was concluded that the reactivity of different natural pozzolans in alkaline medium was greatly affected by the differences in mineralogical and chemical composition of these pozzolans. While the results of XRD showed that not only X-ray amorphous phases but also crystalline phases may participate in the geopolymer reaction. Further, a better assessment about the reactivity of natural pozzolan can be made if the reactivity of each mineral phase is known. Therefore, further work was carried out on the reactivity of crystalline mineral phases in sodium silicate and sodium hydroxide solution.

For this purpose, one amorphous and fourteen crystalline mineral phases were collected in the natural state (14 natural minerals and 1 synthetic phase) and were milled in lab to comparable Blaine fineness. These minerals included albite, augite, biotite, calcite, chabazite, clinochlore, glass phase of PF, kaolinite, larnite, leucite, montmorillonite, muscovite, nepheline, phillipsite and sanidine. These samples represent nearly all the mineral phases present in RT and BT. The reactivity of these minerals was tested with sodium silicate (silica modulus, Ms = 1.061) and sodium hydroxide (16 mol/kg) solutions. The higher initial pH of sodium hydroxide solution can give better indication about the reactivity of minerals; therefore, samples were not only tested in silicate solution but also in hydroxide solution. However, for their reactivity in sodium silicate solution only selected minerals including muscovite, clinochlore, sanidine, chabazite, calcite, augite and albite were tested. On the one hand, this mineral selection was made such that at least one mineral of each representative group is tested with sodium silicate solution, while on the

other hand the low available amount of some minerals hindered the experiments for all minerals. Moreover, out of the minerals tested with sodium silicate solution not all were included in the results, as they formed a stiff paste consistency which obstructed grinding and accurate sample preparation for the applied experiments. However, all minerals were tested with sodium hydroxide solution. The summary of mineral reactivity with sodium silicate solution and sodium hydroxide solution is as presented below.

4.7.1. Reactivity of minerals in sodium silicate solution

The above-mentioned mineral samples were reacted with sodium silicate solution of silica modulus 1.061 ($\approx$ 1.1). The isothermal conduction calorimetry on the paste samples (chapter 3, Fig. 3.1) showed that, like in natural pozzolan geopolymers, the reaction is associated with a single initial exothermic peak followed by deceleration of heat evolution and attaining a steady state of reaction. Muscovite and clinochlore exhibited highest deceleration rate after the first peak, showing least heat formation. While other samples such as sanidine, albite and augite evolved heat in deceleration zone. XRD study on chabazite and its reacted samples (chapter 3, Fig. 3.2) showed that as a result of reaction, X-ray amorphous product was formed. Moreover, the crystalline peaks showed tendency of Na-rich chabazite formation (ion exchange of chabazite). TGA on these samples (chapter 3, Fig. 3.2) supported the XRD results as the mass loss of reacted chabazite and raw samples exhibited similar behaviour. Similarly, clinochlore also showed formation of an X-ray amorphous phase and reduction of basal reflex heights and increase of other reflexes (chapter 3, Fig. 3.3). Clinochlore has a layered structure because of which during the sample preparation for powder XRD, preferred orientation occurred. However, a possible reason can be that after reaction with sodium silicate solution the clinochlore particles may dissolve from edges towards centre, thus the preferred orientation of the particles is disturbed, therefore the basal reflexes are less pronounced. Furthermore, the particles of formed reaction products could disable the clinochlore platelets to orientate. The TGA results (chapter 3, Fig. 3.3) at 8 d showed presence of unreacted sodium silicate (mass loss curve similar to mass loss curve of sodium silicate solution presented in Fig. 4.2), but at 28 d age a continuous mass loss was observed. This also indicates that maybe a new reaction product is formed. Thus, showing that clinochlore may have participated in the reaction. Comparable TGA characteristics were also observed for sanidine, which gave indication about reactivity of sanidine (chapter 3, Fig. 3.4). TGA of muscovite, albite and augite (chapter 3, Fig. 3.5) showed presence of unreacted sodium silicate solution with only slight reduction of peak intensities in XRD. Therefore, it was considered that these minerals

do not react considerably with sodium silicate solution. An overall assessment of the reactivity of these minerals with sodium silicate solution is given in chapter 3, Table 3.3.
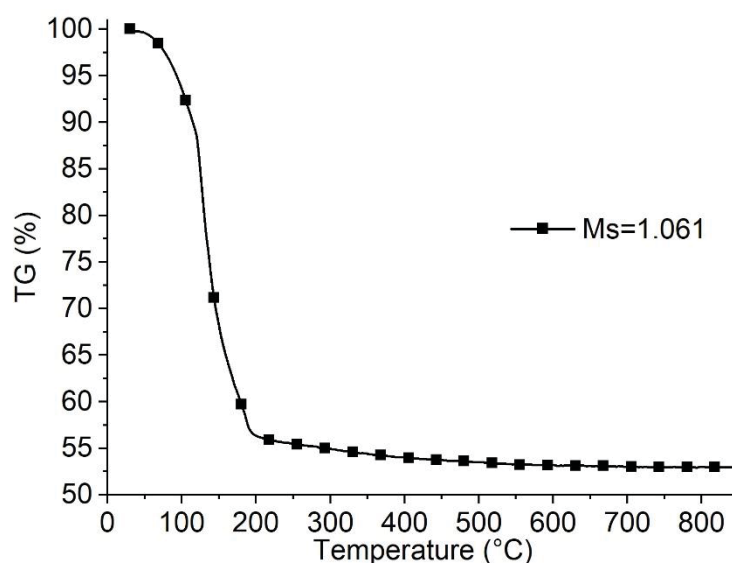

Fig. 4.2. TGA of the sodium silicate solution (Ms = 1.061)

The reaction of calcite with sodium silicate solution (chapter 2, section 2.3, Fig. 8) was most interesting out of all. In TGA of reacted samples, three distinct stages were observed, first being the dehydroxylation, followed by decarbonation of calcite and last mass loss can be because of formation of wollastonite from material which was originally C-S-H. While, in XRD, natrite was observed. Natrite was formed as result of freeze-drying of thermonatrite. Formation of natrite also confirmed the previous findings of BT geopolymers, where formation of efflorescence-like phases was assigned to its calcite content. To explore these findings in more detail, further work was conducted on reactivity of calcium carbonates in sodium silicate solution and is presented in following section.

4.7.2. Reactivity of calcium carbonates in sodium silicate solution

The first comprehensive study about reactivity of calcite in sodium silicate system (chapter 2, section 2.3) gave indications about the possible formation of C-S-H-like phases. This finding was further explored in detail (chapter 2, section 2.6) for seven natural calcium carbonates by its two polymorphs, calcite and aragonite, and for one synthetic calcium carbonate sample. The reaction products and reaction kinetics at early and later age were investigated by several methods such as isothermal conduction calorimetry, in-situ & ex-situ X-ray diffractometry (XRD), in-situ Fourier transform infrared spectrometry (FTIR), thermogravimetric analysis-differential scanning calorimetry-mass spectrometry (TGA-DSC-MS) and thermodynamic calculations. The reaction of calcium carbonates with

sodium silicate solution (Ms = 1.1) is associated with two exothermic events (chapter 2, section 2.6, Fig. 1), the first peak occurred within first few minutes of mixing powder and solution, followed by a deceleration phase. Afterwards, a second exothermic peak is observed for several calcium carbonate samples at different times of reaction. The possible factors such as mineralogical impurities in the samples and particle size distribution were found not to influence the time of second exothermic peak in calorimetry. The in-situ XRD showed the precipitation of natron ($Na_2CO_3 \cdot 10H_2O$) as only crystalline phase at this time of reaction (chapter 2, section 2.6, Fig. 2). While, combining with in-situ FTIR results (chapter 2, section 2.6, Fig. 3), formation of poorly crystalline C-S-H phase was observed. Thus, it can be said that nucleation of C-S-H could be the pivotal factor for the observed sudden reaction in calorimetry.

At the later age reaction (8 and 90 d), XRD (chapter 2, section 2.6, Fig. 4) showed presence of thermonatrite ($Na_2CO_3 \cdot H_2O$) and poorly crystalline phase around 30° 2θ which indicates the formation of C-S-H. For the simultaneous thermal analysis including TGA-DSC-MS, the sample was freeze-dried in order to remove the water in thermonatrite, which excludes the water from the only crystalline water-containing phase in the sample. Thus, the water from the non-crystalline phases can be determined. Therefore, the first mass loss around 100 °C and associated OH and H_2O signals in MS can be anticipated from C-S-H (chapter 2, section 2.6, Fig. 6). Another mass loss in temperature range of 800 – 950 °C accompanied by detection of H_2 in MS can be originating from destabilisation of C-S-H into wollastonite ($CaSiO_3$) (chapter 2, section 2.6, Fig. 6) [23,34]. The thermodynamic analysis gave insight about the reaction products formed with the extend of calcite reaction and the results showed similarity with the experimental findings. Thermodynamic calculations showed the formation of Na-containing C-S-H (chapter 2, section 2.6, Fig. 7).

Moreover, it is observed that aragonite irrespective of different crystal structure reacts in similar way as calcite and forms same reaction products as calcite. Therefore, it can be said that calcium carbonates in general promote availability of calcium for formation of aluminosilicate gel and also form the phases which are generally expected from efflorescence formation. In other words, presence of calcium carbonate can result in a phenomenon which could be called as self-florescence.

Combining the results of this part and the findings about the second peak in calorimetric study of BT geopolymers, it can be said that the second peak observed in BT based-geopolymer is related to its calcite content and possibly consequent nucleation of C-S-H, which can be major reason for sudden change in the reaction kinetics. However, this claim should be further investigated. These results also strengthen the previous findings of BTC

geopolymers, where the lime content enhanced the reaction kinetics and hence the C-S-H precipitation may occur at an earlier time.

Moreover, these findings also confirm the results presented in chapter 2 section 2.3, where the calcite content of BT was found responsible for sodium carbonate formation and eventually cause of compressive strength loss along with lower rate of strength gain. The Ca^{2+} from calcite can replace the alkalis in the gel structure. This leaves free alkalis in the matrix which can react with CO_3^{2-} from calcite and OH^- from alkaline solution to form alkali carbonate. This alkali carbonate can precipitate within the gel binder thus causing weakening of the gel structure by alkalis and water depletion as well as internal crystallization pressure.

4.7.3. Reactivity of minerals in sodium hydroxide solution

The reactivity of 15 mineral samples was tested with NaOH solution (16 mol/kg) by using isothermal conduction calorimetry for first 5 d and, thermogravimetric analysis and X-ray diffraction analysis at 8, 28 and 90 d age (chapter 3, section 3.2.2). Out of all the tested minerals, several showed formation of new crystalline or semi-crystalline reaction products. The minerals, their reaction products and intensity of reaction are listed below in Table 4.3.

Table 4.3. Tested mineral samples, their reaction products and intensity of reaction (++ high, + medium, Ø low) after 90 d of reaction with NaOH solution (16 mol/kg).

Sr. No.	Mineral sample	Reaction product	Intensity of reaction
1	Albite	Semi-crystalline phase, thermonatrite	Ø
2	Augite	Sodium hydrogensilicate pentahydrate, natrite	Ø
3	Biotite	Semi-crystalline phase, natrite	Ø
4	Calcite	Gaylussite, pirssonite, portlandite, thermonatrite	++
5	Chabazite	Semi-crystalline phase, Na-rich chabazite,	++
6	Clinochlore	Natrite	Ø
7	Glass phase	Semi-crystalline phase, hydrosodalite, clinotobermorite, natrite	+
8	Kaolinite	Hydrosodalite, thermonatrite	++
9	Larnite	Semi-crystalline phase, clinotobermorite, thermonatrite	++
10	Leucite	Hydrosodalite, natrite	+
11	Montmorillonite	Hydrosodalite, natrite	+
12	Muscovite	Hydrosodalite, thermonatrite	Ø
13	Nepheline	Hydrosodalite, thermonatrite	+
14	Phillipsite	Semi-crystalline phase, hydrosodalite, thermonatrite	++
15	Sanidine	Hydrosodalite, sodium hydrogensilicate pentahydrate, natrite	+

The most frequently observed phases included thermonatrite or natrite, which is likely to form because of reaction of Na^+ ions from the alkaline solution with the CO_2 from air (or carbonate from sample in case of calcite). The actual phase formed is indeed thermonatrite (sodium carbonate monohydrate) which upon freeze-drying dehydrated to natrite (sodium carbonate). This dehydration was on the one side beneficial for natural pozzolan geopolymer samples, as the degree of reaction cannot be overcalculated by the water entrapped in this carbonate phase. On the other hand, this dehydration in the samples of minerals with NaOH solution was not every time fully attained, therefore, a mixture of these two phases is observed here.

Hydrosodalite, also known as hydroxysodalite hydrate [35], is most commonly produced by reaction of kaolinite with alkaline solution under hydrothermal conditions and is used in several applications in fields of selective adsorption, ion-exchange and thermal stability [36,37]. In the context of alternative binders, hydrosodalite was observed in high temperature resistance geopolymer binders derived from fly ash and metakaolin precursors [7,16]. The results presented in this chapter showed that this phase can be obtained by reaction of several minerals with NaOH solution (Table 4.3) at room temperature conditions, where only a minor amount of this phase forms after up to 90 d of reaction. The silicate mineral phases containing sodium or potassium mostly resulted in formation of hydrosodalite. Whereas calcium-containing silicate minerals exhibiting high reactivity resulted in formation of clinotobermorite. The formation of clinotobermorite and sodium hydrogensilicate pentahydrate emphasizes the likelihood of presence of C-(N)-S-H-like phases in the resultant binder. These findings can be used as first indication about expected phases to form while using precursors rich in studied minerals under these conditions.

The study of the mineral reactivity with sodium hydroxide and sodium silicate solution showed that higher reactivity of RT can be in addition to X-ray amorphous phase mainly attributed to presence of zeolites (chabazite, phillipsite) and larnite. While the formation of sodium carbonate from calcite and partly because of environmental CO_2 affected the reactivity of BT.

References

[1]   EN 196-6. Methods of testing cement – Part 6: Determination of fineness. Brussels: CEN; 2010.

[2]   EN 932-2. Test for general properties of aggregates - Part 2: Method for reducing laboratory samples; 1999.

[3] Bondar D, Lynsdale CJ, Milestone NB, Hassani N, Ramezanianpour AA. Effect of type, form, and dosage of activators on strength of alkali-activated natural pozzolans. Cem. Concr. Compos. 2011;33(2):251–60. https://doi.org/10.1016/j.cemconcomp.2010.10.021.

[4] Gharzouni A, Joussein E, Samet B, Baklouti S, Pronier S, Sobrados I et al. The effect of an activation solution with siliceous species on the chemical reactivity and mechanical properties of geopolymers. J. Sol-Gel Sci. Technol. 2015;73(1):250–9. https://doi.org/10.1007/s10971-014-3524-0.

[5] Duxson P, Fernández-Jiménez A, Provis JL, Lukey GC, Palomo A, van Deventer JSJ. Geopolymer technology: The current state of the art. J. Mater. Sci. 2007;42(9):2917–33. https://doi.org/10.1007/s10853-006-0637-z.

[6] Zhang Z, Provis JL, Ma X, Reid A, Wang H. Efflorescence and subflorescence induced microstructural and mechanical evolution in fly ash-based geopolymers. Cem. Concr. Compos. 2018;92:165–77. https://doi.org/10.1016/j.cemconcomp.2018.06.010.

[7] Provis JL, van Deventer JSJ (eds.). Geopolymers: Structure, processing, properties and industrial applications. Boca Raton, Fla.: CRC; Oxford Woodhead; 2009.

[8] Shi C, Krivenko PV, Roy D. Alkali-Activated Cements and Concretes. London, New York: Taylor & Francis; 2006.

[9] Juhász Z. Mechano-chemical activation of kaolin minerals. Acta Mineral.-Petrogr;XXIV 1980, Supplementum Proceedings of the 10th Kaolin Symposium in Budapest, 3 September 1979, IGCP Project No. 23:121–45.

[10] Mucsi G. Mechanical activation of power station fly ash by grinding – A review. Epitoanyag - J. Silic. Compos. Mater. 2016;68(2):56–61. https://doi.org/10.14382/epitoanyag-jsbcm.2016.10.

[11] Firdous R, Stephan D, Djobo JNY. Natural pozzolan based geopolymers: A review on mechanical, microstructural and durability characteristics. Constr. Build. Mater. 2018;190:1251–63. https://doi.org/10.1016/j.conbuildmat.2018.09.191.

[12] Djobo JNY, Elimbi A, Tchakouté HK, Kumar S. Volcanic ash-based geopolymer cements/concretes: The current state of the art and perspectives. Environ. Sci. Pollut. Res. 2017;24(5):4433–46. https://doi.org/10.1007/s11356-016-8230-8.

[13] Kani EN, Allahverdi A, Provis JL. Calorimetric study of geopolymer binders based on natural pozzolan. J. Therm. Anal. Calorim. 2017;127(3):2181–90. https://doi.org/10.1007/s10973-016-5850-7.

[14] Djobo JNY, Elimbi A, Tchakouté HK, Kumar S. Mechanical activation of volcanic ash for geopolymer synthesis: Effect on reaction kinetics, gel characteristics, physical and

mechanical properties. R. Soc. Chem. (RSC Adv.) 2016;6(45):39106–17. https://doi.org/10.1039/C6RA03667H.

[15] Černý R, Rovnaníková P. Transport processes in concrete. London: Spon Press, Taylor & Francis Group; 2002.

[16] Davidovits J. Geopolymer Chemistry and Applications. Saint-Quentin, France: Institut Géopolymère; 2008.

[17] Djobo JNY, Elimbi A, Tchakouté HK, Kumar S. Reactivity of volcanic ash in alkaline medium, microstructural and strength characteristics of resulting geopolymers under different synthesis conditions. J. Mater. Sci. 2016;51(22):10301–17. https://doi.org/10.1007/s10853-016-0257-1.

[18] Weng L, Sagoe-Crentsil K. Dissolution processes, hydrolysis and condensation reactions during geopolymer synthesis: Part I—Low Si/Al ratio systems. J. Mater. Sci. 2007;42(9):2997–3006. https://doi.org/10.1007/s10853-006-0820-2.

[19] Firdous R, Stephan D, Jin Y. Investigation of Rhenish and Bavarian Trass as Geopolymer Precursor. 20th International Conference of Building Materials - Ibausil 2018, 12 – 14 September 2018, Weimar, Germany 2018;Book 2:617–624.

[20] Tchakouté HK, Rüscher CH, Kong S, Kamseu E, Leonelli C. Comparison of metakaolin-based geopolymer cements from commercial sodium waterglass and sodium waterglass from rice husk ash. J. Sol-Gel Sci. Technol. 2016;78(3):492–506. https://doi.org/10.1007/s10971-016-3983-6.

[21] Zhang Z, Provis JL, Reid A, Wang H. Fly ash-based geopolymers: The relationship between composition, pore structure and efflorescence. Cem. Concr. Res. 2014;64:30–41. https://doi.org/10.1016/j.cemconres.2014.06.004.

[22] Scrivener K, Snellings R, Lothenbach B (eds.). A Practical Guide to Microstructural Analysis of Cementitious Materials. Boca Raton: CRC Press; 2016.

[23] Tajuelo Rodriguez E, Garbev K, Merz D, Black L, Richardson IG. Thermal stability of C-S-H phases and applicability of Richardson and Groves' and Richardson C-(A)-S-H(I) models to synthetic C-S-H. Cem. Concr. Res. 2017;93:45–56. https://doi.org/10.1016/j.cemconres.2016.12.005.

[24] MA T. Low-Temperature Preparation of β-C_2S from Sand/Lime Mixture: Influence of Sodium Hydroxide. Ann. Chem. Sci. Res. 2019;1(3). https://doi.org/10.31031/ACSR.2019.01.000512.

[25] Djon Li Ndjock BI, Elimbi A, Cyr M. Rational utilization of volcanic ashes based on factors affecting their alkaline activation. J. Non-Cryst. Solids 2017;463:31–9. https://doi.org/10.1016/j.jnoncrysol.2017.02.024.

[26] Zhang Z, Provis JL, Wang H, Bullen F, Reid A. Quantitative kinetic and structural analysis of geopolymers. Part 2. Thermodynamics of sodium silicate activation of metakaolin. Thermochim. Acta 2013;565:163–71. https://doi.org/10.1016/j.tca.2013.01.040.

[27] Sun Z, Vollpracht A. Isothermal calorimetry and in-situ XRD study of the NaOH activated fly ash, metakaolin and slag. Cem. Concr. Res. 2018;103:110–22. https://doi.org/10.1016/j.cemconres.2017.10.004.

[28] Bakharev T. Geopolymeric materials prepared using Class F fly ash and elevated temperature curing. Cem. Concr. Res. 2005;35(6):1224–32. https://doi.org/10.1016/j.cemconres.2004.06.031.

[29] van Deventer JSJ, San Nicolas R, Ismail I, Bernal SA, Brice DG, Provis JL. Microstructure and durability of alkali-activated materials as key parameters for standardization. J. Sustain. Cem. Mater. 2015;4(2):116–28. https://doi.org/10.1080/21650373.2014.979265.

[30] Komnitsas K, Zaharaki D, Perdikatsis V. Geopolymerisation of low calcium ferronickel slags. J. Mater. Sci. 2007;42(9):3073–82. https://doi.org/10.1007/s10853-006-0529-2.

[31] Bernal SA, Provis JL, Walkley B, San Nicolas R, Gehman JD, Brice DG et al. Gel nanostructure in alkali-activated binders based on slag and fly ash, and effects of accelerated carbonation. Cem. Concr. Res. 2013;53:127–44. https://doi.org/10.1016/j.cemconres.2013.06.007.

[32] Bernal SA, Provis JL, Brice DG, Kilcullen A, Duxson P, van Deventer JSJ. Accelerated carbonation testing of alkali-activated binders significantly underestimates service life: The role of pore solution chemistry. Cem. Concr. Res. 2012;42(10):1317–26. https://doi.org/10.1016/j.cemconres.2012.07.002.

[33] Albright JN. Mineralogical notes: Vaterite stability. Am. Miner. 1971;56:620–4.

[34] Myers RJ, L'Hôpital E, Provis JL, Lothenbach B. Composition-solubility-structure relationships in calcium (alkali) aluminosilicate hydrate (C-(N,K-)A-S-H). Dalton Trans. 2015;44(30):13530–44. https://doi.org/10.1039/c5dt01124h.

[35] Luger S, Felsche J, Fischer P. Structure of hydroxysodalite $Na_8[AlSiO_4]_6(OH)_2$, a powder neutron diffraction study at 8 K. Acta. Crystallogr. Sec. C Cryst. Struct. Commun. 1987;43(1):1–3. https://doi.org/10.1107/S0108270187097233.

[36] Marsh A, Heath A, Patureau P, Evernden M, Walker P. A mild conditions synthesis route to produce hydrosodalite from kaolinite, compatible with extrusion processing. Microporous Mesoporous Mater. 2018;264:125–32. https://doi.org/10.1016/j.micromeso.2018.01.014.

[37] Zong Y-b, Zhao C-y, Chen W-h, Liu Z-b, Cang D-q. Preparation of hydro-sodalite from fly ash using a hydrothermal method with a submolten salt system and study of the phase transition process. Int. J. Miner. Metall. Mater. 2020;27(1):55–62. https://doi.org/10.1007/s12613-019-1904-8.

Chapter 5

Conclusions and future recommendations

The study shows the potential of various European natural pozzolans for geopolymer synthesis. The properties of the resultant geopolymers are largely depended on the mineralogical and chemical composition of the natural pozzolans. The highest compressive strength can be achieved by using an optimum silica modulus range. Beyond each side of the optimum, the compressive strength increases at a relatively slow rate with the age of the sample or even decreases. The degree of reaction determined by selective dissolution decreases with increase of silica modulus; however, a higher early reaction kinetics can be obtained by using higher initial concentration of Na_2O and SiO_2. A higher initial concentration of alkalis in the mixture can lead to formation of efflorescence (formation of sodium carbonate by environmental CO_2), which can affect the mechanical properties of the geopolymer binder. The mineralogical composition of pozzolans affects its reactivity. Presence of calcite in the pozzolan leads also to formation of sodium carbonate in the binder gel thus generating inner tensile stresses and depleting the gel structure in alkalis and water, causing weakening of structure or complete destruction. Formation of efflorescence as well as participation of calcite in reaction were reflected by formation of thermonatrite. The geopolymer gel formed in these natural pozzolans is mostly semi-crystalline to amorphous where the more crystalline parts corresponded to zeolite structure. The possible composition of this geopolymer gel can be N-A-S-H and C-N-A-S-H, though K, Mg and Fe can also be present as cations.

The attempts to improve the reactivity of natural pozzolans and to reduce the sodium carbonate formation in geopolymer system show that heat treatment is more efficient method than mechanical activation for the studied natural pozzolan. Calcination of calcite to lime imparts higher reactivity and lowers the sodium carbonate formation. Moreover, the calorimetric analysis of these samples showed that the sudden change of reaction kinetics observed in BT geopolymers is associated with its calcite content.

Study on the reactivity of minerals in sodium hydroxide and sodium silicate solutions showed that not only X-ray amorphous phases but also crystalline mineral phases partially

react under used alkaline conditions. The reaction can result in formation of new semi-crystalline to crystalline phases. Minerals such as kaolinite, leucite, montmorillonite, muscovite, nepheline, phillipsite and sanidine upon their reaction with sodium hydroxide solution can form the zeolite phase "hydrosodalite" in small amount. Formation of sodium hydrogensilicate pentahydrate and clinotobermorite in augite, sanidine and larnite shows the possible participation of these minerals in formation of calcium- and/or sodium-rich aluminosilicate hydrates. The calcium carbonate present in the natural pozzolans promotes availability of calcium for the formation of aluminosilicate gel while the carbonate ion can result in formation of phases similar to efflorescence products. The results of this part combined with the calorimetric study of BT geopolymer showed that the sudden change of reaction kinetics of BT geopolymer is likely connected to its calcite content.

Based on this study, following recommendations for future work are proposed:

In the attempt to generalize the synthesis conditions for natural pozzolan-based geopolymers, the potential of other natural pozzolans can be determined. These natural pozzolans may include the pozzolans of sedimentary origin. As the reactivity of natural pozzolans in alkali activated systems is not only depended on its glass phase composition but also depends on crystalline phase composition, a detailed study on the reaction mechanism of glass phases and other crystalline phases can be made. The minerals investigated in the present study where based on the phases present in the two most reactive pozzolans of this study. Other minerals and phases occurring in natural pozzolans or available in large quantity in nature or industry should also be tested. The current minerals were mainly silicates. Minerals with other chemical composition should also be evaluated especially as calcium carbonate showed distinct behaviour in comparison to the silicates. The effect of different quenching methods, composition of glass phase and its particle size distribution can be studied. As the current investigation focused on the reactivity of single mineralogical phases, a next step could be to explore mixtures of two or more mineralogical phases. This will enable to study the interactions in their reaction mechanisms. The reaction of calcium carbonate in the presence of other mineralogical phases can be further explored under alkaline conditions. This detailed study will help to give first predictions about the reactivity of various natural pozzolans for geopolymer synthesis. The effect of incorporation of other supplementary cementitious materials in natural pozzolan-based geopolymers can be studied such as ground granulated blast furnace slag, metakaolin etc. Furthermore, the durability of these binders is an open question and needs extensive work.

Bibliographic information

- Rafia Firdous, Dietmar Stephan, Jean Noël Yankwa Djobo (2018): Natural pozzolan based geopolymers. A review on mechanical, microstructural and durability characteristics. In Construction and Building Materials, 190, 1251 – 1263.
  Publisher's version added in chapter 2, section 2.1.
  DOI: https://doi.org/10.1016/j.conbuildmat.2018.09.191.

- Rafia Firdous, Dietmar Stephan (2019): Effect of silica modulus on the geopolymerization activity of natural pozzolans. In Construction and Building Materials, 219, 31 – 43.
  Publisher's version added in chapter 2, section 2.2.
  DOI: https://doi.org/10.1016/j.conbuildmat.2019.05.161

- Rafia Firdous, Dietmar Stephan (2020): Impact of the mineralogical composition of natural pozzolan on properties of resultant geopolymers. In Journal of Sustainable Cement-Based Materials, Manuscript number: TSCM-2020-0075.
  Preprint version added in chapter 2, section 2.3.

- Rafia Firdous, Dietmar Stephan (2019): Influence of heat treatment and mechanical activation on reactivity of natural pozzolan for geopolymer synthesis. Accepted in the peer-reviewed conference "2nd International Conference of Sustainable Building Materials, ICSBM 2019, August 12 – 15 2019, Eindhoven, The Netherlands". Proceedings ICSBM 2019, Volume 2, ID 057, Pages 138-155, In-press. ISBN (print): 978-90-386-4911-5
  Preprint version added in chapter 2, section 2.4.

- Rafia Firdous, Dietmar Stephan (2019): Factors effecting the properties of alkali activated natural pozzolan based geopolymers. Published in the conference "Tagung Bauchemie der Fachgruppe Bauchemie, 30 September – 2 October 2019, Aachen, Germany" Tagung Bauchemie, GDCh-Monographie, Volume 54, Pages 100-106. ISBN: 978-3-947197-13-2.
  Preprint version added in chapter 2, section 2.5.

- Rafia Firdous, Tamino Hirsch, Detlef Klimm, Barbara Lothenbach, Dietmar Stephan (2021): Reaction of calcium carbonate minerals in sodium silicate solution and its role in alkali-activated systems. In Minerals Engineering, 165 (3), p. 106849.
  Preprint version added in chapter 2, section 2.6.
  DOI: https://doi.org/10.1016/j.mineng.2021.106849